9th INTERNATIONAL ENGINEERING SYMPOSIUM – IES2020

Faculty of Engineering (Building No.2)

Kumamoto University

March 3-5, 2020

Kumamoto University

Conveners

Shuichi TORII

Professor, Department of Mechanical & Mathematical Engineering

Kumamoto University, Japan

&

Katta VENKATARAMANA

Professor, Department of Civil Engineering

NITK, Surathkal, India

Organized by

Graduate School of Science & Technology

Kumamoto University, Japan

In association with

National Institute of Technology Karnataka,

Surathkal, Mangalore, India

PROCEEDINGS OF

9th INTERNATIONAL ENGINEERING SYMPOSIUM – IES2020

Venue

Faculty of Engineering (Building No.2)
Kumamoto University

Date

March 3-5, 2020

Conveners

Shuichi TORII
Professor, Department of Mechanical & Mathematical Engineering
Kumamoto University, Japan
&
Katta VENKATARAMANA
Professor, Department of Civil Engineering
NITK, Surathkal, India

Organized by

Graduate School of Science & Technology
Kumamoto University
Kumamoto City, Japan

In association with

National Institute of Technology Karnataka
Surathkal, Mangalore, India

PREFACE

The 1st International Engineering Symposium (IES2011), the 2nd International Engineering Symposium (IES2012), the 3rd International Engineering Symposium (IES2013), the 4th International Engineering Symposium (IES2015), the 5th International Engineering Symposium (IES2016), the 6th International Engineering Symposium (IES2017), the 7th International Engineering Symposium (IES2018) and the 8th International Engineering Symposium (IES2019) were organized very successfully at Kumamoto University with more than 100 participants each time from India, Japan, Indonesia, Thailand, Taiwan, Vietnam and other countries. With the objective of continuing the interaction between the researchers during these symposia, the 9th International Engineering Symposium (IES2020) has been organized in the month of March, 2020. This symposium provides a common platform for bringing together researchers for expanding academic collaboration.

As part of this symposium, the researchers and the students from abroad have been invited to visit Kumamoto University and get exposed to its educational and research activities. The event focuses on the current R&D of the participating institutions on topics of mutual interest, with a special emphasis on "Science & Technology". The emerging technology and scientific advancements are discussed during the symposium. Presentations feature new and innovative technologies in the relevant fields.

This proceedings volume contains the technical papers presented at the symposium. The topics include a wide spectrum of themes covering major disciplines of science and engineering. The effort put in by the faculty, the staff and the students of Kumamoto University in organizing this event are greatly appreciated.

We sincerely hope that you will find the contents of this proceedings volume useful and productive. We look forward to more intense academic collaborations and research interactions in the coming days, to achieve the common goal of technological advancement for global peace and prosperity.

Shuichi Torii
Katta Venkataramana
Conveners

Contents

Keynote Lectures

Mechanical Engineering & Related Fields

Physics, Electrical, Electronics, Computer Science & Related Fields

Civil Engineering, Environment & Related Fields

KEYNOTE LECTURES

9th International Engineering Symposium - IES 2020
March 3-5, 2020, Kumamoto University, Japan

Study of Biomass Gasification and Torrefaction as Alternative Source of Energy in Indonesia

Priyambodo Nur Ardi Nugroho
Shipbuilding Institute of Polytechnic Surabaya
Jl. Teknik Kimia, Kampus ITS Sukolilo, Surabaya 60111, Indonesia.
Email: priyambodo@ppns.ac.id

ABSTRACT: People prosperity could be determined by the quality and quantity of energy usage since energy is currently being used every day as one of the necessities for human. Many countries like Indonesia currently still rely on fossil fuel like oil, coal and gas to fulfil their energy demand. Carbon emission reduction techniques has been performed by using the renewable source of energy to replace conventional fossil fuel. Biomass is one of the most promising method of renewable energy because it is carbon neutral fuel, or no net carbon emitted from biomass usage. Palm oil tree (Elaeis guineensis) is one of the main non-oil and gas commodity in Indonesia.

Since biomass in original shape is bulky and inconvenient for storing, transportation and feeding into engine, biomass need to be converted into another form of energy. There are two main path of biomass conversion, i.e. biochemical and thermochemical path. In biochemical conversion, biomass molecules are cracked down into much smaller molecules using bacteria or enzymes. This process does not require much external energy, but biochemical takes a longer process compared to thermochemical conversion. Anaerobic and aerobic digestion, fermentation, and hydrolysis are some processes in the biochemical conversion. Thermochemical conversion is much faster but requires much external energy. Some process belongs to thermochemical, are pyrolysis, liquefaction, combustion, gasification, and torrefaction.

Gasification is one of the most promising biomass conversions and consist of four steps. The first process is drying at 200 to 300^{0}C, it is needed to increase the gasification efficiency because raw solid biomass always contains a certain amount of water moisture. The second process is pyrolysis or thermal decomposition at 300 to 700^{0}C. Pyrolysis vaporizes the volatile components of biomass as it is heating the volatile vapor produced as a combination chemical, like tar and water vapor. The third step is oxidation or partial combustion of some gases, vapours, and char at 700 – 1500^{0}C. Oxygen, carbon dioxide, and water react with char and releasing heat because the chemical reactions are exothermic. The last step is reduction or gasification of decomposition products (char), at 800 – 1100^{0}C without the presence of oxygen. Reduction is naturally endothermic, and the energy needed is supported by the previous oxidation process. Reduction yields useful combustion gas like hydrogen, carbon monoxide, and methane during some series of reactions.

Torrefaction is being considered for effective utilization of biomass as a clean and convenient solid fuel. Biomass is slowly heated to 200-300^{0}C without or very little presence of oxygen. Torrefaction reshape the chemical structure of biomass hydrocarbon and increase its carbon content while reducing oxygen content. Energy density also increased significantly and makes biomass hygroscopic or tends to absorb moisture from the environment. As a result, torrefaction improve the commercial value of the biomass, either for energy production or transportation. Other advantages are improved energy density, water resistance and grindability of biomass.

9th International Engineering Symposium - IES 2020
March 3-5, 2020, Kumamoto University, Japan

Bio-inspired Materials & Surfaces - Methods and applications -

Yoshitaka Nakanishi, Prof., Dr.Eng.
Faculty of Advanced Science & Technology,
Kumamoto University, Japan
Email: y-naka@mech.kumamoto-u.ac.jp

ABSTRACT:
The author innovates "bio-inspired materials" and "bio-inspired surface", which are considered from microscopic to macroscopic structures. In this lecture, the methods of creations are explained, and the various possible applications for our daily lives are showcased.

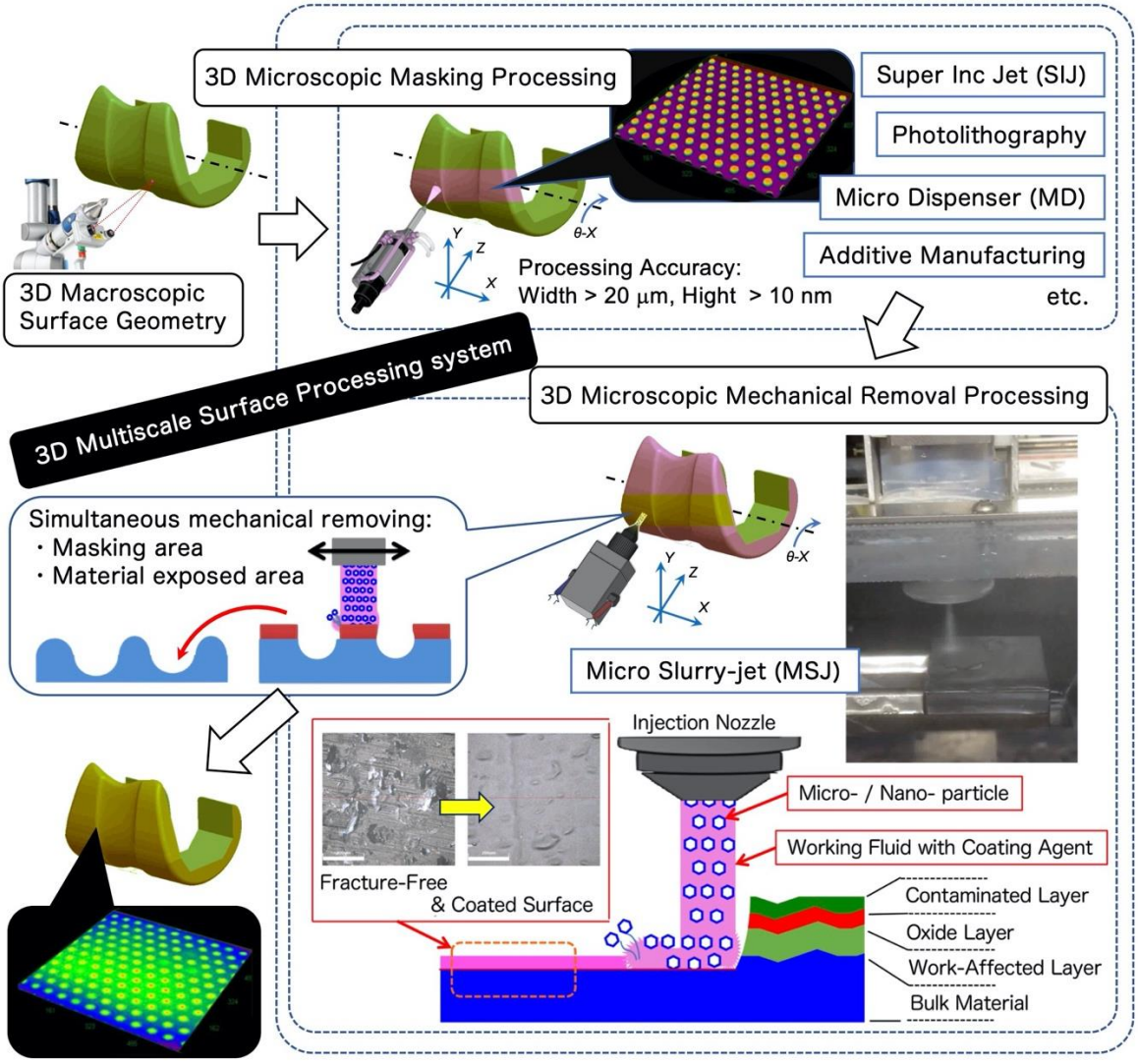

3D Macroscopic Surface + Micro-/Nano-surface Structure

Machining Accuracy: Width > 20 μm, Hight > 1 nm, Surface Roughness > 1 nm (Ra)

MECHANICAL ENGINEERING
&
RELATED FIELDS

9th International Engineering Symposium - IES 2020
March 3-5, 2020, Kumamoto University, Japan

Study of Stable Biodiesel Emulsion Fuel Using Soybean Oil

Christie Yurie Yokoyama[1], Shuichi Torii [2] and Takumi Iwanaga[3]

1 *Research Scholar, Department of Mechanical System Engineering, Kumamoto University, Kurokami, 2-39-1, Kumamoto 860-8555, Japan. e-mail: christie.yurie@gmail.com*
2 *Professor, Department of Mechanical System Engineering, Kumamoto University, Kurokami, 2-39-1, Kumamoto 860-8555, Japan. e-mail:torii@mech.kumamoto-u.ac.jp*
3 *Master Course Student, Department of Mechanical System Engineering, Kumamoto University, Kurokami, 2-39-1, Kumamoto 860-8555, Japan. e-mail: 181d8453@st.kumamoto-u.ac.jp*

ABSTRACT: Due to oil depletion and environmental problems, researchers are seeking renewable alternatives to fossil fuel. Biodiesel is a suitable fuel to replace it on account of it similar characteristics. In this study, biodiesel were produced by transesterification reaction, using soybean oil, methanol and potassium hydroxide. However, biodiesel emits higher NOx than diesel, so emulsification were conducted to reduce it. In experiment 1, the surfactant CR-310 showed better results, hence used for experiment 2 and 3. In experiment 2, the surfactant content were varied, while in experiment 3, 20wt.% water content sample (W4) displayed higher stability. When W4 were compared to diesel and SOME, NOx emission were reduced. The SOME fuel consumption increased when compared to diesel, however after the emulsification, it slightly improved.

***Keywords**: soybean biodiesel, food surfactant, W/O emulsion fuel, NOx emission, PGPR*

INTRODUCTION

Population growth, technological development and industrialization effect have all contributed to the energy demand increase. In past years, energy crisis happened due to the significant decline of untenable source, especially of fossil fuel that represents 80% of global energy usage Alalwan et al (2019). In addition, the world is suffering from oil depletion and environmental problems mainly caused by burning fossil fuels, such as global warming and changing rainfall patterns, Ozener et al (2014) and Reham et al (2015). Carbon monoxide (CO), carbon dioxide (CO2), sulfur oxides (SOx), nitrogen oxides (NOx), and particulate matter (PM) are gases emitted by this burning in diesel engine, in which NOx and PM are the two primary pollutants Lin and Lin (2006).

In order to minimize these problems, several studies are being conducted worldwide, seeking renewable alternative sources capable of replacing fossil fuels. Biofuel is one of the promising one between the options, considered economically viable due to its improved emission characteristics, Ozener et al (2014). Among biofuels, biodiesel is one of the most suitable to replace the standard fuel due to its similar characteristics to diesel with no engine modifications, Elkelawy et al (2019). It is estimated that 4 to 7% of the fossil fuel total global consumption are going to be replaced for biodiesel by 2030, Cesar et al (2019). Biodiesel is oxygenated, possesses low emission profiles, biodegradable, non-toxic, environmentally friendly, Ramadhas et al(2004) and Sinha et al (2008).

There are several methods to produce biodiesel, among them transesterification is the

most conventional one, as it results in characteristics close to the standard fuel Demirbas (2008). Through the reaction of animal fat or vegetable oils with an alcohol, results in the formation of esters and glycerin. Among alcohols, methanol and ethanol are the most commercially used, due to their low cost and their physical and chemical advantages. As the cheapest catalysts sodium or potassium hydroxide are used to improve and accelerate the reaction, Ramadhas et al (2004) and Rathore et al (2016).
Although biodiesel improves the burning efficiency and reduces the emissions of carbon monoxide (CO) due to the high content of oxygen, it also produces 10% higher NOx emissions than the same amount of diesel Koc and Abdullah (2013), Qi et al (2010) and Gülüm and Bilgin (2015) .
Nitrogen oxide (NO) and nitrogen dioxide (NO2) are the main reactive gases that composes group known as NOx. When it react in the atmosfere forms ozone and acid rain, causing the acidification of water resources and being harmful to public health. Emulsified fuel were an effective way to decrease NOx emissions at a reduced cost without significant change of design nor adverse effect on the engine reliability, Koc and Abdullah (2013) and Fernando et al (2006).

MATERIAL AND METHODS

Materials

Soybean oil were selected as the feedstock (purchased from the Riken Kako Co., Ltd.) in the transesterification process to prepare the biodiesel, methanol (CH3OH; 99.8%) as alcohol, and potassium hydroxide pallets(KOH;85.0%) as the catalyst. Acid acetic were used to neutralize the mixture in the first washing process after the transesterification reaction. Sorbitan Monooleate (Span 80), Rheodol AO-15V (Span 83) and Tetraglycerin ester (CR-310) were the three types of surfactants used in the emulsion, the produced biodiesel were used as the oily phase while distilled water were used as aqueous phase.

Biodiesel preparation

The transesterification reaction was used to produce biodiesel as described in Fig. 1. Firstly the soybean oil was preheated to a temperature of 60 °C for 15 min. While, 1% of catalyst, KOH pallets, was stirred in the methanol alcohol on a magnetic plate until forming a homogeneous methoxide solution. The solution was stirred at a speed of 650 rpm in the preheated oil to a temperature of 60 °C under atmospheric pressure for 30 min. Finally, the solution was decanted for the separation of crude biodiesel and glycerol, crude biodiesel consist in the upper phase while glycerol decanted to the bottom of the container. In this case, the most often used molar ratio of 1:6 were selected for the proportion between oil and alcohol Stojković et al (2014).
In order to neutralize any unreacted hydroxide or methoxide, the crude biodiesel is treated with acetic acid. Followed by water washing to remove soluble impurities, such as unreacted alcohol or glycerol particles. The heating process ensures the removal of all water particles mixed in the biodiesel. In the first washing process, 30wt.% of water and 1wt.% of acetic acid are stirred with the crude biodiesel for 30 min, then for decanting process for 2 days. In the following second and third process, 50wt.% of water are stirred with the crude biodiesel for 30min. After the After the mixture separation, the biodiesel is removed and heated for 10min at 150C while stirring, resulting in the final biodiesel, in this case, Soybean methyl ester (SOME).
Heating value and viscosity of SOME were measured and compared to diesel, as shown in Figure 2 and 3, respectively. When compared to diesel, SOME heating value reduced 13%, while the viscosity increased 28%. The heating value were measure using the calorimeter (Shimadzu autocalculating bomb calorimeter C4-4AJ, Shimadzu Co.), in which 0.7g of the sample heating value were measured 3 times and averaged. While the viscosity were done by using the Brookfield viscometer, 0.5ml of the sample were measured 3 times at 40C and averaged.

Emulsion Fuel Preparation

Emulsions are mixtures of immiscible liquids composed of two phases, one dispersed phase and another continuous phase Nadeem et al (2006). Emulsions are commonly used in the food industry. For instance, milk is an oil-in-water emulsion (water: continuous phase) and margarine is a water-in-oil emulsion (oil: continuous phase), Taneja et al (2013) and Okuro et al (2019). According to Lin and Wang (2004), most emulsions require the use of functional chemicals called emulsifiers, to stabilizes the suspension of small droplets and prevents them from growing together into large droplets. The driving force of coalescence is the reduction of the interfacial area, and the emulsifier forms a physical barrier, preventing the droplets from combining, Nadeem et al (2006).

The emulsion fuel homogenization was made using the rotary homogenizer (Model AHG-160A, shaft HT1018, AS ONE company, Japan), rotation number set in 12,000 rpm during 10min. Three experiments were conducted, varying the surfactant type, surfanctant content and water content.

Experiment 1 was performed with different types of surfactants. The three surfactants used were Span 80 and Span 83, surfactants commonly used in diesel and CR310 used for biodiesel emulsion, Pagano et al (2018).The experiment objective were to evaluate which surfactants are more stable in soy-based biodiesel emulsions. The surfactants types are as shown in Table 1. All sample were made using 75wt.% of SOME, 20wt.% of distilled water and 5wt.% of surfactant. Based in experiment 1 results, CR-310 were selected as the surfactant for experiment 2 and 3.

Experiment 2 were made by using different surfactant concentrations, varying between 0.5wt.% to 4.0wt.%, distilled water was fixed at 20wt.%. The purpose is to evaluate the minimum amount required to ensure acceptable stability of the emulsion. Samples composition is as showed in Table 2.

In Experiment 3, the moisture content was changed between 5 to 20wt.%, surfactant concentration was fixed at 5wt.%.The purpose of this experiment is to evaluate the stability of the sample by changing the concentration of distilled water. Table 3 display the samples composition.

The engine test was performed with a small Yanmar diesel engine (382cc), the exhaust gas was measured using a Testo-350 (TESTO K.K.). The engine speed were set in 2000 rpm, in each engine speed, it was measured during 5min and averaged. NOx emission and fuel consumption were measured.

RESULTS AND DISCUSSION

The separation results were obtained by visual observation. In the experiment 1, one day after the sample production, separation of the samples S1 and S2 occurred, as indicated by the red circle in Figure 4. However, one month later, no separation occurred in the CR310 sample S3, indicating that CR310 has higher stability than the others .

As a result for Experiment 2 separation, one day after the sample was manufactured, the E1 sample with 0.5wt.% surfactant showed separation. One week after production, the E2 sample with 1wt.% surfactant also displayed separation. One month after sample production, the E3 sample showed separation. In the Figure 5, the separation were highlighted in red. However, there is no separation in the 4wt.% sample, suggesting that the lowest concentration required for the sample stability is 4wt.%.

The experiment 3 results showed that the prepared sample was stable at all moisture contents even after one month (Figure 6), indicating that CR310 has high stability.

In engine tests, NOx gas emission and fuel consumption were measured from a sample with a water content of 20%. Among the samples produced, sample W4 was selected because of its low price and high stability.

When comparing the W4 sample with diesel, the NOx emission was reduced by about 49%, and by comparing with SOME, the emission was reduced by about 68%. In other words, although SOME emits higher NOx when compared to diesel, by emulsifying SOME it were possible to reduce NOx emission, as shown in Figure 7.

In this study, instead of considering water and biodiesel as total fuel, the exact amount of biodiesel was evaluated for the fuel consumption. It shows that the SOME fuel consumption is 24% higher than that of diesel, but it has been found that the emulsification of SOME improves fuel consumption by 2% resulted by the micro-explosion phenomena improvement Vellaiyan et al (2018). The micro-explosion improve the air–fuel mixture atomization and formation , improving the combustion and resulting in slightly lower fuel consumption, Qi et al (2013). Figure 8 compares the fuel consumption of Diesel, SOME and SOME emulsion (sample W4).

CONCLUSIONS

The following conclusions are deduced from this study:

- ☐In experiment 1, 3 surfactants were used to produce SOME emulsion. One day after producing the samples, S1 and S2, using the surfactants span 80 and 83, respectively showed separation, while when CR310 was applied , it was able to maintain stability for 1 month. In other words, CR-310 were more stable than the others surfactants.
- ☐In experiment 2, CR-310 were selected as surfactant and it content were varied between 0.5 to 4wt.%, in which all samples except 4wt.% content separated before 1 month after it production. The moisture content were fixed at 20wt.%, while SOME content varied according to the surfactant content.
- ☐In experiment 3, the moisture content were varied from 5 to 20wt.%. The surfactant CR-310 content were fixed at 5wt.%, while the SOME content varied according to the distilled water content. In this experiment all the samples were stable for 1 month, indicating that CR-310 has high stability.
- The emulsion fuel with 20wt.% water content (W4) were selected to the engine test. W4 reduced NOx by about 49% and about 68% compared to diesel and SOME, respectively. The SOME fuel consumption increased by 24% if compared to diesel, but after emulsification reduced the fuel consumption by 2%.

REFERENCES

Alalwan, Hayder A. et al (2019), Promising evolution of biofuel generations. Subject review. Renewable Energy Focus 28, pp.127-139.

Cesar, Aldara da Silva et al (2019),Competitiveness analysis of "social soybeans" in biodiesel production in Brazil, Renewable Energy 133, pp.1147-1157

Demirbas, Ayhan (2008), Comparison of transesterification methods for production of biodiesel from vegetable oils and fats, Energy Conversion and Management 49, pp.125–130

Elkelawy, Medhat et al (2019), Experimental studies on the biodiesel production parameters optimization of sunflower and soybean oil mixture and DI engine combustion, performance, and emission analysis fueled with diesel/biodiesel blends, Fuel 255, 115791

Fernando, Sandun (2006), NOx Reduction from Biodiesel Fuels, Energy & Fuel 20, pp. 376-382

Gülüm, Mert and Bilgin, Atilla (2015), Density, flash point and heating value variations of corn oil biodiesel–diesel fuel blends, Fuel Processing Technology 134, pp.456–464
Lin, Cherng-Yuan and Lin, Hsiu-An (2006), Diesel engine performance and emission characteristics of biodiesel produced by the peroxidation process, Fuel 85, pp.298–305

Koc, A. Bulent and Abdullah, Mudhafar (2013), Performance and NOx emissions of a diesel engine fueled with biodiesel-diesel-water nanoemulsions, Fuel Processing Technology 109, pp.70-77

Lin, Cheng-Yuan and Wang, Kuo-Hua (2004), Effects of an oxygenated additive on the emulsification characteristics of two- and three-phase diesel emulsions, Fuel, Vol. 83, pp. 507-515

Nadeem, M et al (2006), Diesel engine performance and emission evaluation using emulsified fuels stabilized by conventional and gemini surfactants, Fuel 85, pp. 2111-2119

Okuro, Paula K. et al (2019), Formation and Stability of W/O-high internal phase emulsion (HIPEs) and derived O/W emulsion stabilized by PGPR and lecithin, Food Research International 122, pp.252-262

Ozener, Orkun et al (2014), Effects of soybean biodiesel on a DI diesel engine performance, emission and combustion characteristics, Fuel 115, pp.875–883

Pagano, Ana Paula Eskildsen et al (2018), Microencapsulation of betanin in monodisperse W/O/W emulsions, Food Research International, vol. 109, pp. 489-496

Qi, D.H. et al (2010), Combustion and emission characteristics of ethanol–biodiesel–water micro-emulsions used in a direct injection compression ignition engine, Fuel 89, pp.958–964

Qi, D.H. et al (2013), Combustion and emission characteristics of a direct injection compression ignition engine using rapeseed oil based micro-emulsions, Fuel 107, pp. 570-577

Ramadhas , A.S. et al (2004), Use ofvegetable oils as I.C. engine fuels—A review, Renewable Energy 29, pp.727–742

Rathore, Vivek et al (2016), Processing of vegetable oil for biofuel production through conventional and non-conventional routes, Energy for Sustainable Development 31, pp.24–49

Reham, S. S. et al (2015), Study on stability, fuel properties, engine combustion, performance and emission characteristics of biofuel emulsion, Renewable and Sustainable Energy Reviews 52, pp.1566–1579

Sinha, Shailendra et al (2008), Biodiesel development from rice bran oil: Transesterificationprocess optimization and fuel characterization, Energy Conversion and Management 49, pp.1248–1257

Stojković, Ivan J. et al (2014), Purification technologies for crude biodiesel obtained by alkali-catalyzed transesterification, Renewable and Sustainable Energy Reviews, vol. 32, pp. 1-15

Taneja, A. et al (2013), Behaviour of oil droplets during spray drying of milk-protein-stabilisedoil-in-water emulsions, International Dairy Journal 28, pp.15-23

Vellaiyan, Suresh et al (2018), Combustion, performance, and emission analysis of diesel engine fueled with water-biodiesel emulsion fuel and nanoadditive, Environmental Science and Pollution Research, vol. 25, pp. 33478-33489

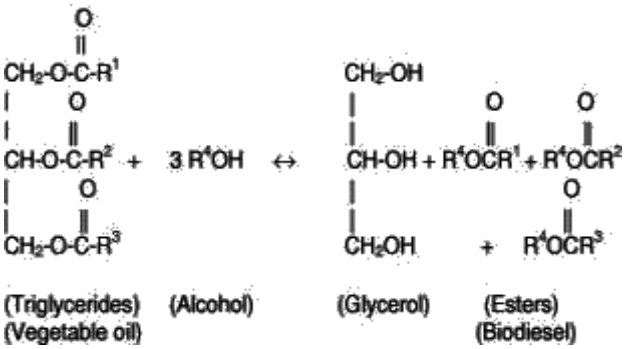

Fig. 1: Vegetable oil transesterification reaction, Sinha et al (2008)

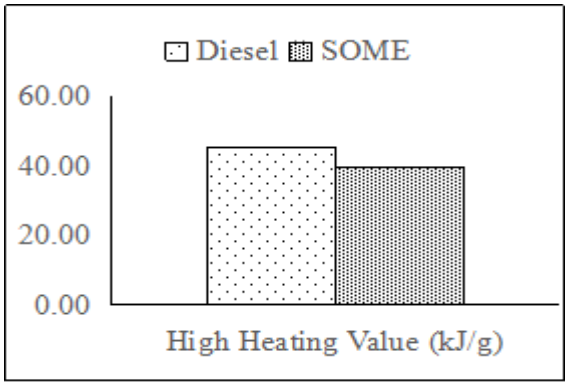

Fig. 2: High heating value comparison

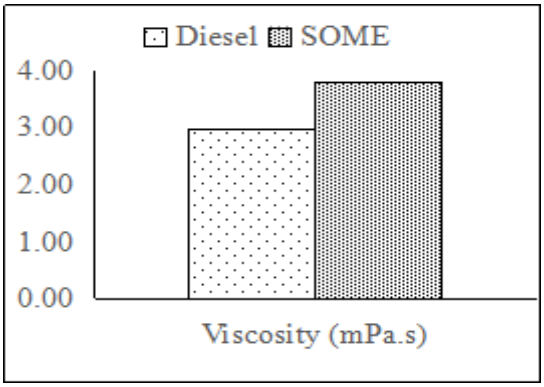

Fig. 3: Viscosity comparison

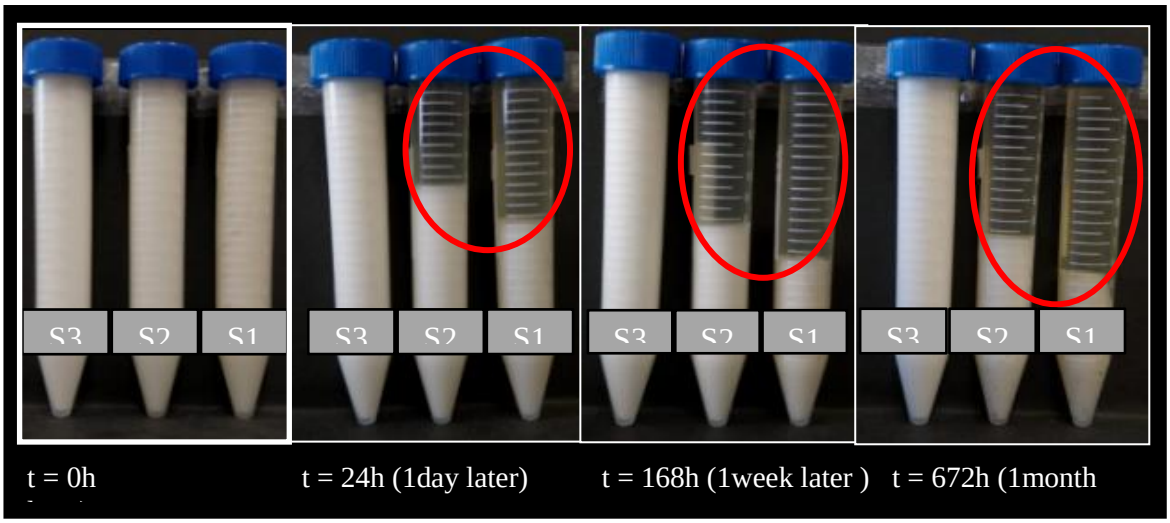

Fig. 4: Experiment 1 visual observation

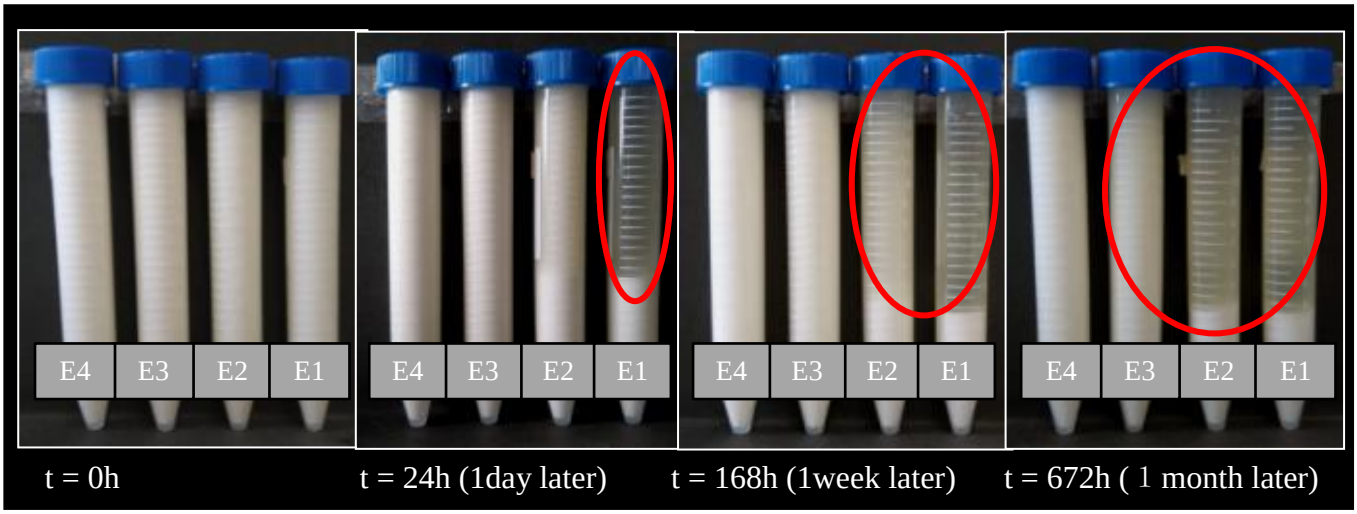

Fig. 5: Experiment 2 visual observation

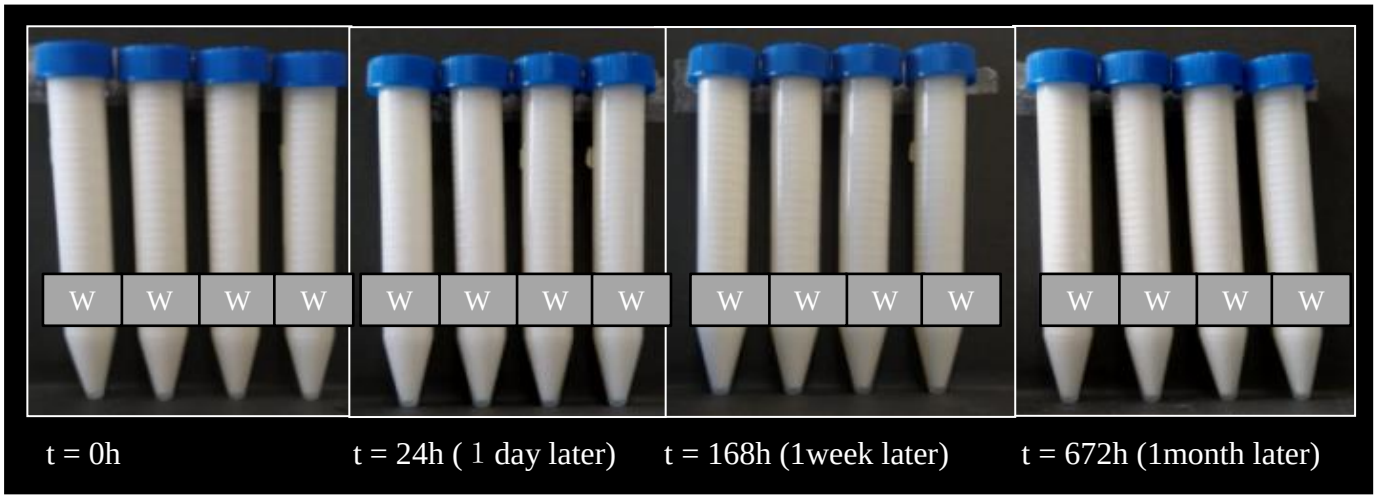

Fig. 6: Experiment 3 visual observation

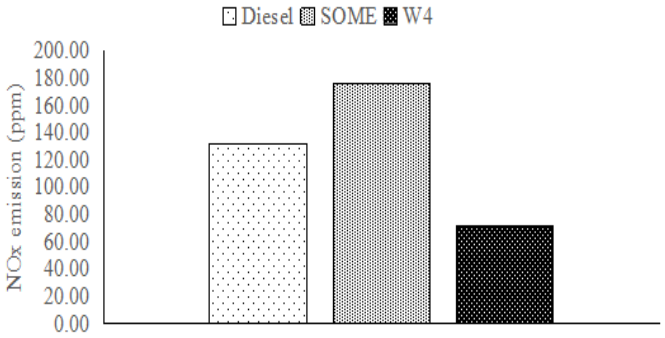

Fig. 7: NOx emission comparison

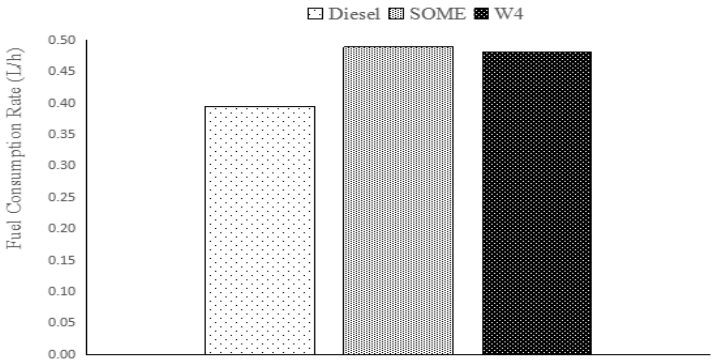

Fig. 8: Fuel consumption comparison

Table 1: Experiment 1 surfactants types

Sample	Surfactant
S1	Span 80
S2	Span 83
S3	CR-310

Table 2: Experiment 2 samples compositions

Sample	SOME (wt.%)	Distilled Water (wt.%)	Surfactant (wt.%)
E1	79.5%	20.0%	0.5%
E2	79.0%	20.0%	1.0%
E3	78.0%	20.0%	2.0%
E4	76.0%	20.0%	4.0%

Table 3: Experiment 3 samples composition

Sample	SOME (wt.%)	Distilled Water (wt.%)	Surfactant (wt.%)
W1	90.0%	5.0%	5.0%
W2	85.0%	10.0%	5.0%
W3	80.0%	15.0%	5.0%
W4	75.0%	20.0%	5.0%

9th International Engineering Symposium - IES 2020
March 3-5, 2020, Kumamoto University, Japan

Heat transfer enhancements by using a copper porous microstructure inside heat pipe's evaporator section

Yang Dong Ling [1], Shuichi Torii [2]

1 *Graduate student, Department of Mechanical System Engineering, Kumamoto University, Kurokami, 2-39-1, Kumamoto 860-8555, Japan. email:tony81129@gmail.com*
2 *Professor, Department of Mechanical System Engineering, Kumamoto University, Kurokami, 2-39-1, Kumamoto 860-8555, Japan. e-mail:torii@mech.kumamoto-u.ac.jp*

ABSTRACT: In this study, a surface modification of heat pipe was studied to enhance the heat transfer performance of heat pipe. The surface was coated by hydrogen codeposition of copper electrodeposits to modify the surface's porosity and roughness. Hydrogen codeposition of copper electrodeposits is an electroplating method that hydrogen bubbles will be generated during the process and create porous microstructure on the surface. There are two samples prepared from different temperature in this experiment, one is 15°C, the other is 30°C. This surface modification result in enhancement on heat pipe's thermal resistance from 5.4% to 11.7% for sample 1; 6.4% to 14.6% for sample 2. The surface modification successfully enhance the performance of heat pipe, especially for low heat flux.

***Keywords**: Heat pipe, Porous microstructure, Electrodeposition, Hydrogen evolution*

INTRODUCTION

A heat pipe is a heat exchanging device which combines both thermal conductivity and phase transition. The working fluid at the evaporator inside the pipe boils and turns into a vapor by absorbing heat from that surface, then travels along the heat pipe to the condensor and condenses into a liquid by releasing the heat. At last, the liquid will back to the evaporator by capillary force or gravity. For the working fluid of the heat pipe, most heat pipes use water as their working fluid. Recently, a significant amount of research has been conducted on nanofluids as a working fluid and has proved that a nanofluid is able to enhance the heat transfer performance of the heat pipe.

S.Venkatachalapathy et al.,[1] studied about the thermal performance of a cylindrical heat pipe using CuO nanofluids with copper mesh wick under different tilt angles. The thermal resistance is reduced 26.88%, and 10.25% when the tilt angle is 60° ,and 90° . They concluded that this phenomenon happens due to the formation of a thin porous layer on the mesh, which would cause the increase of the surface wettability. Kyu HyungDo et al.,[2] studied about screen mesh wick heat pipes's thermal perforance by using 1.0vol% and 3.0vol% Al2O3 nanofluids. The experiment results show that the thermal resistance decreased in both different kinds of concentration's nanofluids, and it even decreased more in the 3.0vol% nanofluid. By using 3.0vol% nanofluids, the thermal resistance is reduced by about 40%. They concluded that the formation of the nanoparticle deposition at the screen mesh wick of the evaporation region which becomes a porous layer is the principal reason for the thermal performance enhancement in this experiment. MadhusreeKole et al.,[3] investigated the thermal

resistance of screen mesh wick heat pipes by using differnet kinds of working fluid, such as distilled water, and several different weight concentration Cu-distilled water nanofluid. The results showed that 0.5wt% nanofluid has the best thermal performance. The vertically heat pipe with 0.5wt% Cu-distilled water nanofluid reduced the thermal resistance for 27% compared with a distilled water heat pipe. The enhancement is explained by the deposition happened on the mesh wick in the evaporator section. A.Brusly Solomon et al.,[4] studied about the thermal performance of a heat pipe with a wick which is already coated by nanoparticles. This experiment coated the heat pipe by keeping the wick in the copper nanofluids for 5 min and then exposing it to hot air until it dries. Consequently, the thermal resistance is reduced by 19%, 15%, and 14% at 100W, 150W, and 200W, respectively. When the power input is lower than 100W, the coated wick heat pipe even has a better thermal performance than the heat pipe operated with nanofluid directly. This experiment also found that the thermal resistance in the condensor section is slightly increased because of the layer coated on the condensor section. Kyu Hyung Do et al.,[5] developed a mathematical model for evaluating the thermal performance of a grooved heat pipe with Al_2O_3 nanofluid as working fluid. They considered both the thermophysical properties of nanofluids and the porous surface characteristics formed by nanoparticles. They concluded the thin porous layer formed by nanoparticles is the key factor of the heat transfer enhancement happened in a heat pipe using nanofluids as working fluid. Nandy Potra et al.,[6] studied about using several kinds of nanofluids as working fluid in a mesh wick heat pipe. The thermal resistance of the heat pipe is reduced in all kinds of nanofluids successfully. They concluded that the coating on the mesh wick produced a good capillary structure which could increase the surface roughness and the wettability. Consequently, the surface structure leads to the reduction in thermal resistance. M.M.Sarafraz et al.,[7] studied about fouling formation of a TiO2 nanofluid mesh wick thermosyphon. They concluded that if the operation time is short, the porous structure formed on the surface will provide more nucleation sites and reduce the thermal resistance, however, if the operation time is long, too many nanoparticles deposition will be formed on the surface and cause blocking of small cavities on the wick. Sang M. Kwark el al.,[8] studied about the pool boiling of nanofluids over a flat heater. They discovered that microlayer evaporation is the main reason for the nanoparticle coating formed on the heater surfaces during nanofluid boiling. As the vapor grows, the nanoparticles will be left behind and assemble at the base of the bubble. After the microlayer evaporates, the nanoparticles will leave behind and bond on the heater surface.

For the surface characteristics of evaporator, several studies have revealed the influence of surface roughness on nucleate boiling heat transfer. M.Jakob [9] reported that the surface roughness can considerably affect the boiling heat transfer's behavior. The theory that boiling bubbles are generated from the cavities by entrapping air or vapor was presented. Kang [10] studied about the pool boiling heat transfer for a tubular heat exchanger with different surface roughness to understand the effect of it. They concluded that the rough surface could provide more cavities and have better thermal performance than a smooth surface. Stephan Kotthoff et al.,[11] made a copper tube surface with some cavities on it. They concluded that the nucleate boiling heat transfer was increased because of the increase of nucleation sites.

Many researches about boiling heat transfer enhancement by using nanofluid-coated surface were also conducted. Hyungdae Kim et al.,[12] studied about the CHF enhancement in nanofluid pool boiling. They showed that the CHF enhancement by using pure water as working fluid on a nanoparticle-coated surface was almost the same as using nanofluid as working fluid. They concluded that the main reason of this enhancement is because of the nanoparticle coated on the surface. Srinivas Vemuri et al.,[13] studied about pool boiling of alumina oxide nanoporous surface on a heater with FC-72 as working fluid. They discovered that the incipient superheat decreased by 30% when compared with a smooth surface. Steven B. White et al.,[14] studied about a surface modification of using electrophoretic deposition of nanoparticles to enhance the

boiling transfer performance of the heater. The experiment results showed that the heat transfer coefficient increased by 200% due to the increase in active nucleation site density. Yong et al.,[15] [16] studied about pool boiling for a nanoporous metallic surface. They concluded that the surface wettability and the increase of nucleation sites density enhance the boiling heat transfer performance, especially when the heat flux is very low. Biao Tang et al.,[17] studied about the thermal performance of a copper nanoporous surface. They concluded that the porous structure could promote the occurence of boiling and enhance the boiling heat transfer, especially when the heat flux is very low. The bubbles departed from the surface were smaller and with higher frequency. The vapor or air trapped in the porous promote the occurence of bubbles at low heat flux. Chi Young Lee et al.,[18] studied about the thermal performance of alluminum oxide nanoporous surface. They concluded that the porous surface has higher heat transfer coefficient than the plain surface. D.Saeidi et al.,[19] studied about pool boiling on nanostructured alluminum surface made by anodization. The results showed that the heat transfer coefficient in this experiment was increased by 159% compared with untreated surface.

All the previous research has been conducted for using nanofluid as working fluid in a heat pipe concluded that the principal reason for the thermal performance enhancement is the porous layer formed by nanoparticle deposition at the evaporator which will provide more nucleation sites. Also, many research has been conducted for surface modification concluded that provide more nuceation sites could enhance the boiling heat transfer which could be explained by trapped vapor theory, when microstructure ordefects are presented on the surface of evaporator.

HEAT TRANSFER ENHANCEMENT OF VIA POROUS MICROSTRUCTURE

Porous microstructure can be made by hydrogen codeposition of copper electrodeposits which was published by N.D.Nikolić et al. in 2006 [20][21]. They concluded that the morphologies of copper electrodeposits were correlated with the hydrogen evolution rates. When the overpotential is large, lots of hydrogen will be emitted and the dominant form becomes a crater which could subsequently become the nucleation sites. Copper is electroplated on the cathode surface by Eq.(1). Hydrogen is generated by Eq.(2).

$$Cu^{2+} + 2e^{-} \rightarrow Cu \quad (1)$$

$$2H^{+} + 2e^{-} \rightarrow H_2 \quad (2)$$

The sample used here is a stainless pipe with a diameter of 10 mm and thickness of 0.5 mm. The pipe was used as the cathode and the copper tube was used as the anode.

SAMPLE PREPARATION

The electrodeposition process was completed in a solution of 0.15M CuSO4 and 1M H2SO4. The temperature of the solution is 15°C for sample 1, and 30°C for sample 2. A DC power supply was attached on both the stainless pipe and the copper tube. The electroplating apparatus is shown in Fig.1, and procedure is shown in Fig.2. The copper surface was made by the following process:

(1) The inside of the stainless pipe was first covered with a thin copper film under 0.2 mV overpotential for 3 mins. This process is necessary as the force between the copper and the stainless is very small when the overpotential is large. We need to do this process to make a foundation for the second process.

(2) Change the overpotential to 5000 mV and electroplate it for 20 mins. During this process, many hydrogen bubbles will be codeposited with copper and some micro cavities will form at the top of the copper surface. After this process, the porous copper structure was made.

(3) Switch the overpotential back to 0.2 mV and electroplate it for 3 mins. Since the structure made in the second process is very weak, we need to perform this process to make a dense film to cover the cavities made in the second process in order to protect it.

EXPERIMENT METHOD

The heat pipe we used in this experiment is 300mm, 10mm, and 0.5mm, as length, diameter, and thickness, respectively. The experiment schematic is shown in Fig.3, and device is shown in Fig.4.

In this experiment, a thermostatic bath, volt slider, data logger, pump, vacumum pump, pressure gauge, water tank, stainless pipe, insulated material, and thermocouples were used. The 120mm from the top of the pipe is a condenser section which is cooled by water in the water jacket, the 100mm from the bottom of the pipe is evaporator section and covered by the insulated material, and the middle part between them is an adiabatic section which is also covered by the insulated material.

The test section of this experiment, the material of the pipe is stainless steel. The length of the heat pipe is 300mm, and the diameter of the pipe is 10mm with 5mm thickness. The connection of the power supply is achieved by soldering at both ends of the evaporator section. The evaporator section is 100mm, the adiabatic section is 80mm, and the condenser section is 120mm. 9 thermocouples are attached to the heat pipe: four thermocouples (T1, T2, T3, T4) on the evaporator section, two thermocouples (T5, T6) on the adiabatic section, and three thermocouples (T7, T8, T9) on the condenser section. The test section is shown at the Fig.5. Since the evaporator section is heated by electricity, the thermocouples at the evaporator is covered by Teflon.

For experiment procedure, at first, turn on the pump, set the thermostatic bath to 20°C and wait until stable. Second, fill 5ml distilled water (26% filling ratio) in and decrease the pressure to 0.01 Mpa. At last, covered the pipe with insulation material and set the power input at 20W, 30W and 40W.

EXPERIMENT RESULT

In this experiment, the thermal performance will be compared by thermal resistance and heat transfer coefficient calculated by Eq.(3) and Eq.(4).

$$R = \frac{\Delta T}{Q} = \frac{\overline{T_{eva}} - \overline{T_{con}}}{Q} \tag{3}$$

$$h = \frac{q}{\overline{T_{eva}} - \overline{T_{con}}} = \frac{\frac{Q}{A}}{\overline{T_{eva}} - \overline{T_{con}}} \tag{4}$$

Fig.7 and Table1 shows the thermal resistance of this experiment. Fig.8 and Table2 shows the heat transfer coefficient of this experiment. Compare with uncoated heat pipe, the thermal resistance is reduced for 11.7%, 5.4%, and 5.9% for sample 1; 14.6%, 8.2%, and 6.4% for sample 2.

For heat transfer coefficient, the sample 1 has improved the heat transfer coefficient for 12.8%, 5.4%, and 6.3% compared with uncoated heat pipe. The sample2 has improved the heat transfer coefficient for 17.1%, 8.9%, and 6.9% compared with uncoated heat pipe.

The coated surface measured by scanning electron microscope are shown in Fig.6. Both sample 1 and sample 2 successfully make a copper porous microstructure inside the heat pipe's evaporator section. The porous structure made for sample 2 consists bigger, deeper and denser holes because of the higher electroplating temperature. When the temperature of the solution is higher, the solution will dissociate more ion and cause the current to increase. Due to the increase of the current, more copper and more hydrogen are generated and coated on the stainless pipe. That's why the porous of sample 2 are bigger, deeper and denser.

CONCLUSION

To improve the efficiency of a heat pipe, the effect of applying copper porous microstructure formed by electroplating was studied. The thermal resistance was reduced sucessfully by applying copper porous microstructure coating.

- The copper porous surface was formed inside the pipe by electroplating successfully.
- Compare with uncoated heat pipe, the thermal resistance of the heat pipes are improved from 5.4% to 11.7% for sample 1 by applying a copper porous microstructure which provided more nucleation sites, especially for low heat flux.
- For sample 2, the thermal performance are even better than sample1. The porous structure on sample 2 has bigger, deeper, and denser holes on the surface because of higher electroplating temperature. Compare with uncoated heat pipe, the thermal resistance of the heat pipes are improved from 6.4% to 14.6%.

Though hydrogen codeposition copper electroplating has proved as a successful method to improve the thermal performance of heat pipe, the ideal electroplating condition still remains unknown. In the future, electroplating time, thickness of the electroplatng film and the current for electroplating are also worth looking forward to.

REFERENCE

[1] S.Venkatachalapathy, G.Kumaresan, S.Suresha
Performance analysis of cylindrical heat pipe using nanofluids – An experimental study
International Journal of Multiphase Flow Volume 72, June 2015, Pages 188-197

[2] Kyu Hyung Do ,Hyo Jun Ha, Seok Pil Jang
Thermal resistance of screen mesh wick heat pipes using the water-based Al2O3 nanofluids
International Journal of Heat and Mass Transfer Volume 53, Issues 25–26, December 2010, Pages 5888-5894

[3] Madhusree Kole, T.K.Dey
Thermal performance of screen mesh wick heat pipes using water-based copper nanofluids
Applied Thermal Engineering Volume 50, Issue 1, 10 January 2013, Pages 763-770

[4] A. Brusly Solomon, K.Ramachandran, B.C.Pillai
Thermal performance of a heat pipe with nanoparticles coated wick
Applied Thermal Engineering Volume 36, April 2012, Pages 106-112

[5] Kyu Hyung Do, Seok Pil Jang
Effect of nanofluids on the thermal performance of a flat micro heat pipe with a rectangular grooved wick
International Journal of Heat and Mass Transfer Volume 53, Issues 9–10, April 2010, Pages 2183-2192

[6] Nandy Putra, Wayan Nata Septiadi, Haolia Rahman, Ridho Irwansyah
Thermal performance of screen mesh wick heat pipes with nanofluids
Experimental Thermal and Fluid Science Volume 40, July 2012, Pages 10-17

[7] M.M.Sarafraza, F.Hormozi, S.M.Peyghambarzadeh
Role of nanofluid fouling on thermal performance of a thermosyphon: Are nanofluids reliable working fluid?
Applied Thermal Engineering Volume 82, 5 May 2015, Pages 212-224

[8] Sang M.Kwark, Ratan Kumar ,Gilberto Moreno, Jaisuk Yoob, Seung M.Youa
Pool boiling characteristics of low concentration nanofluids
International Journal of Heat and Mass Transfer Volume 53, Issues 5–6, February 2010, Pages 972- 981

[9]Max Jakob
Heat transfer in evaporation and condensation
Mech. Eng. 58(1936) 643–660 u.

[10]Myeong-Gie Kang
Effect of surface roughness on pool boiling heat transfer
International Journal of Heat and Mass Transfer Volume 43, Issue 22, 15 November 2000, Pages 4073-4085

[11]Stephan Kotthoff, Dieter Gorenflo, Elisabeth Danger, Andrea Luke
Heat transfer and bubble formation in pool boiling: Effect of basic surface modifications for heat transfer enhancement
Heat transfer and bubble formation in pool boiling: Effect of basic surface modifications for heat transfer enhancement

[12]Hyungdae Kim, Jeongbae Kim, Moo Hwan Kim
Effect of nanoparticles on CHF enhancement in pool boiling of nano-fluids
International Journal of Heat and Mass Transfer Volume 49, Issues 25–26, December 2006, Pages 5070-5074

[13]Srinivas Vemuri ,Kwang J.Kim
Pool boiling of saturated FC-72 on nano-porous surface
International Communications in Heat and Mass Transfer Volume 32, Issues 1–2, January 2005, Pages 27-31

[14]Steven B. White ,Albert J. Shih ,Kevin P. Pipe
Boiling surface enhancement by electrophoretic deposition of particles from a nanofluid
International Journal of Heat and Mass Transfer Volume 54, Issues 19–20, September 2011, Pages 4370-4375
[15]Yong Tang, Biao Tang, Jianbo Qing, Qing Li, Longsheng Lu
Nanoporous metallic surface: Facile fabrication and enhancement of boiling heat transfer
Applied Surface Science Volume 258, Issue 22, 1 September 2012, Pages 8747-8751
[16]Yong Tang, Biao Tang, Qing Li, Jianbo Qing, Longsheng Lu, Kangping Chen
Pool-boiling enhancement by novel metallic nanoporous surface
Experimental Thermal and Fluid Science Volume 44, January 2013, Pages 194-198
[17]Biao Tang, Rui Zhou, Longsheng Lu, Guofu Zhou
Augmented boiling heat transfer on a copper nanoporous surface and the stability of nano-porosity in a hydrothermal environment
International Journal of Heat and Mass Transfer Volume 90, November 2015, Pages 979-985
[18]Chi Young Lee ,Bong June Zhang ,Kwang J.Kim
Morphological change of plain and nano-porous surfaces during boiling and its effect on nucleate pool boiling heat transfer
Experimental Thermal and Fluid Science Volume 40, July 2012, Pages 150-158
[19]D.Saeidi ,A.A.Alemrajabi
Experimental investigation of pool boiling heat transfer and critical heat flux of nanostructured surfaces
International Journal of Heat and Mass Transfer Volume 60, May 2013, Pages 440- 449
[20]N.D.Nikolić ,K.I.Popov ,Lj.J.Pavlović ,M.G.Pavlović
The effect of hydrogen codeposition on the morphology of copper electrodeposits. I.The concept of effective overpotential
Journal of Electroanalytical Chemistry Volume 588, Issue 1, 1 March 2006, Pages 88-98
[21]N.D.Nikolić ,G.Branković ,M.G.Pavlović ,K.I.Popov
The effect of hydrogen co-deposition on the morphology of copper electrodeposits. II.Correlation between the properties of electrolytic solutions and the quantity of evolved hydrogen
Journal of Electroanalytical Chemistry Volume 621, Issue 1, 1 September 2008, Pages 13-21

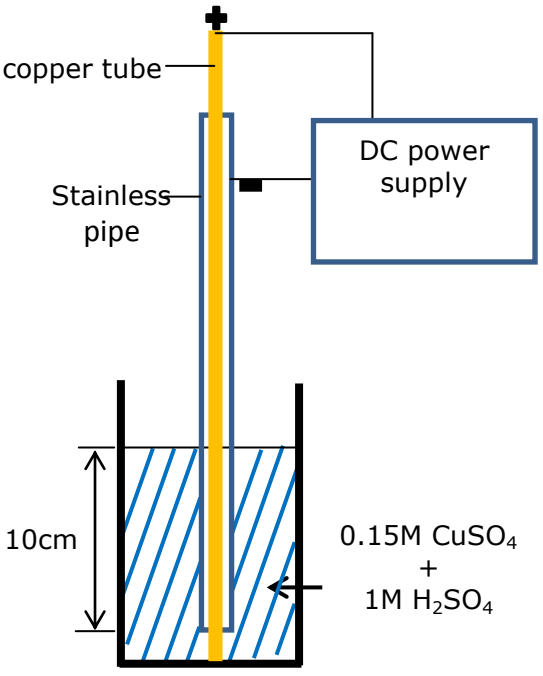

Fig.1 Electroplating apparatus

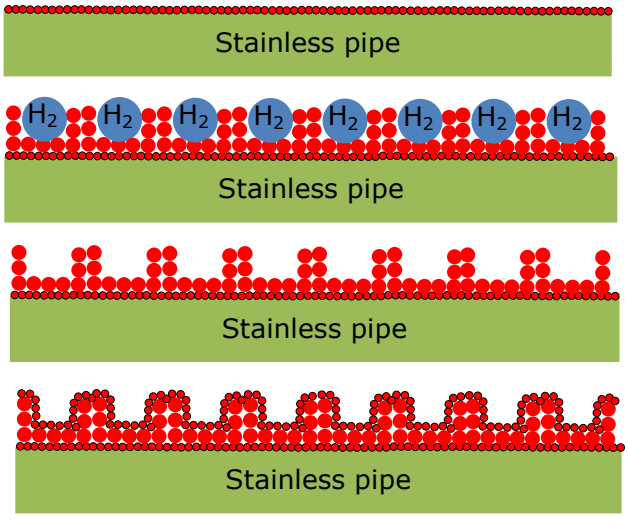

Fig.2 Electroplating procedure

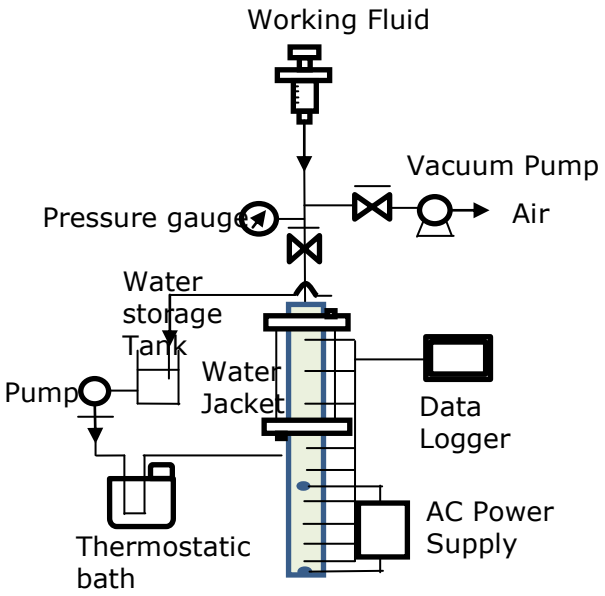

Fig.3 Experiment apparatus

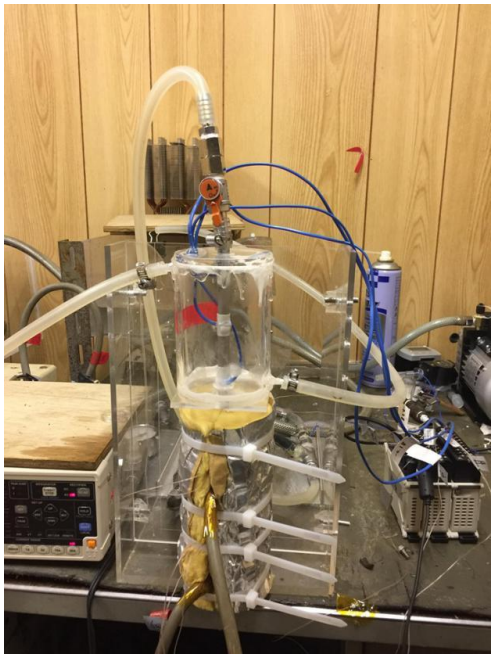

Fig.4 Experiment device

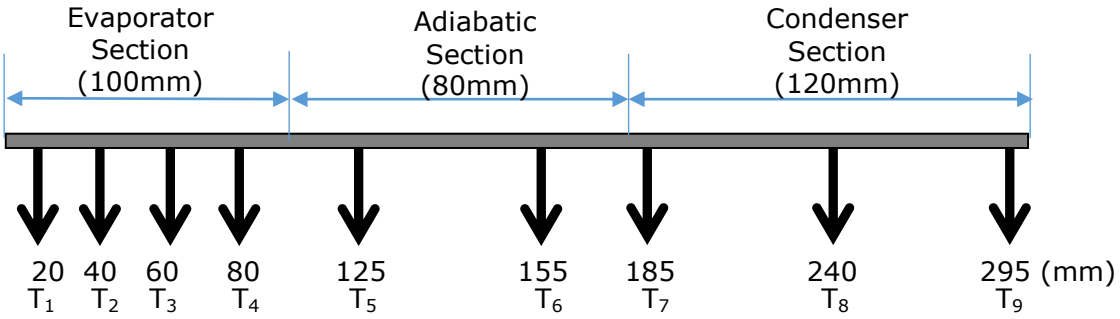

Fig.5 Test section

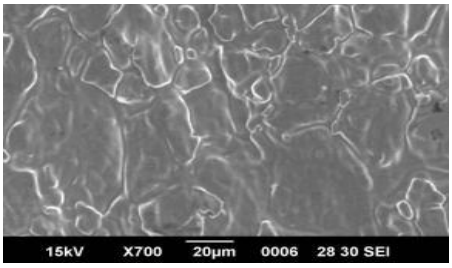

Uncoated heat pipe

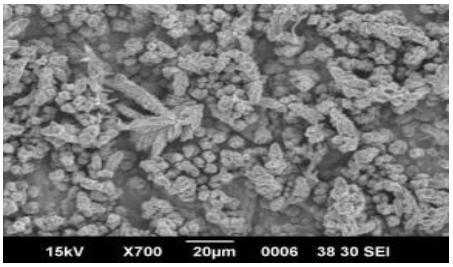

Sample 1

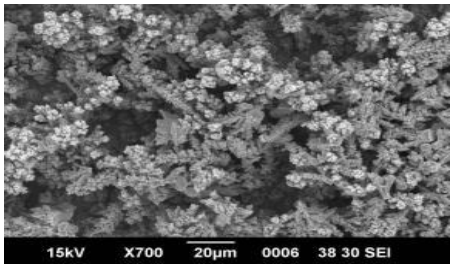

Sample 2

Fig.6 Surface condition

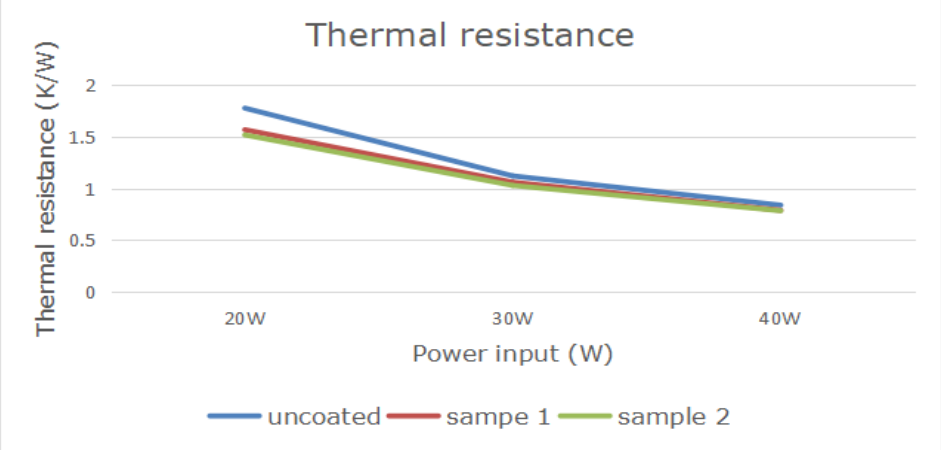

Fig.7 Thermal resistance

Power	20W	30W	40W
Uncoated	1.777	1.121	0.838
Sample 1	1.575	1.063	0.788
Sample 2	1.518	1.029	0.784

Table 1 Thermal resistance [K/W]

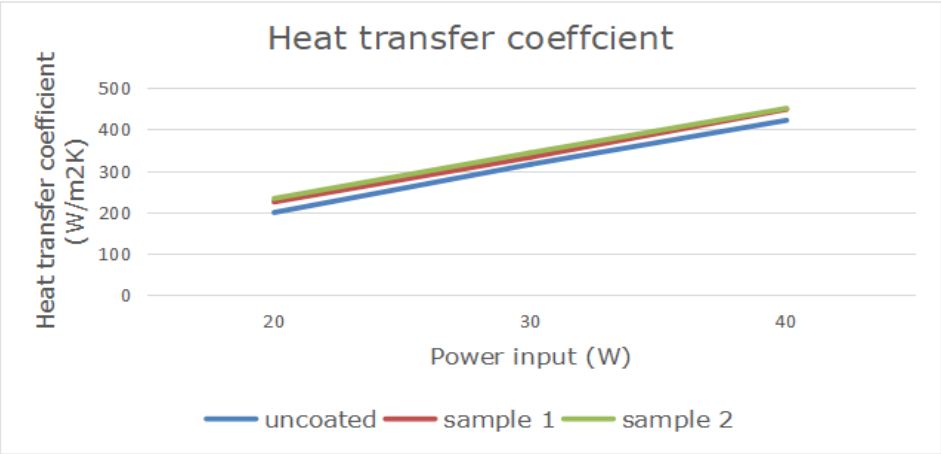

Fig.8 Heat transfer coefficient

Power	20W	30W	40W
Uncoated	199.020	224.520	233.039
Sample 1	315.512	332.614	343.612
Sample 2	422.109	448.675	451.164

Table 2 Heat transfer coefficient [W/m^2K]

9th International Engineering Symposium - IES 2020
March 3-5, 2020, Kumamoto University, Japan

DEVELOPMENT OF SURFACE MICROMACHINING METHOD FOR LARGE AREA AND 3D CURVED SURFACE

Yusuke HIRATA [1], Kazuma SHIBATA [2], Yuta NAKASHIMA[3], Yoshitaka NAKANISHI[4]

1 *Faculty of Engineering, Kumamoto University, Kurokami 2-39-1, Chuo-ku, Kumamoto 860-8555, Japan*
E-mail : 166t3814@st.kumamoto-u.ac.jp
2 *Graduate School of Science and Technology, Kumamoto University, Kurokami 2-39-1, Chuo-ku, Kumamoto 860-8555, Japan*
E-mail : 183d8460@st.kumamoto-u.ac.jp
3 *Faculty of Advanced Science and Technology, Kumamoto University, Kurokami 2-39 Chuo-ku, Kumamoto 860-8555, Japan*
E-mail : yuta-n@mech.kumamoto-u.ac.jp
4 *Faculty of Advanced Science and Technology, Kumamoto University, Kurokami 2-39 Chuo-ku, Kumamoto 860-8555, Japan*
E-mail : y-naka@mech.kumamoto-u.ac.jp

ABSTRACT: Proposes processing methods for large area, various surfaces and materials. The important micro-masking process is also discussed. As a processing method, a micro-masking process do, and fine particles are directly ejected to remove material. Photolithography is one method of masking. However, it has many processes and the processing area is limited. So, method that resin was directly masked on surface was suggested. Two methods were tested to resolve these problems. One is resin was dropped by an ink jet. Another is pushed out from a uniaxial polarization screw pump.
Ink jet and screw pumps differ in dropping stability and speed. By using MSJ(Micro Slurry Jet) as a removal method, direct processing on the surface and application to any material becomes possible. In this study, the compatibility of the masking method and MSJ was verified to establish a processing method.

***Keywords**: Micro Slurry-Jet, Masking Plate, Micro Dispenser, Micro-Masking Process*

INTRODUCTION

In an effort to fabricate a microstructure existing in the natural world on the surface of an artificial material, it has been proposed that the material be mechanically removed to cut the material and produce microfabrication. In this study, we explored the possibility of creating fine structures on large-scale 3D surfaces by combining fine masking with machine removal.

MATERIALS AND METHODS

MSJ (Micro Slurry Jet) processing was used as the mechanical removal process. Fig. 1,2 shows the MSJ processing method. The MSJ method is a technique for generating microstructures using alumina particles as a polishing medium together with compressed air and water. It has ultra-precision machining capability on the order of nano-meters on the material. In the MSJ method, the processing accuracy in the parallel direction was less than sub-milli-meter due to the size limitation of the slurry jet injection nozzle. Therefore, by preparing a mask that is finer than the MSJ nozzle size, finer processing with higher precision was performed.
In addition, there are two methods: a method of placing a masking plate on a

workpiece, a method of extruding and solidifying the resin from a uniaxially polarized screw, and a method of hanging and solidifying the resin by an inkjet method. In this study, we tried three simpler masking methods. Figure 3 shows the respective patterns. For each masking, the resist pattern on the surface after MSJ processing and the processed surface were analysed using a three-dimensional laser measurement microscope and a laser microscope.

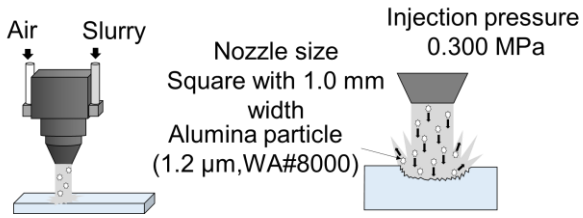

Fig. 1 Schematic of MSJ processing

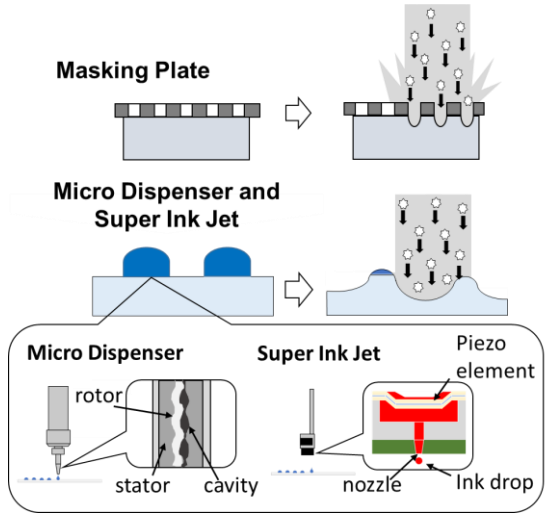

Fig. 2 Schematic of creation of microstructure by Masking process and MSJ processing

RESULTS AND DISCUSSION

Although the target depth could be dug with the masking plate, it was found that the plate itself became a consumable, and that the concave could be processed but the convex could not. Resin masking made with a uniaxial polarizing screw and ink-jet method causes variations in resin size and requires adjustment when bonding the resin. Showed that it was compatible with MSJ.

CONCLUSION

This time, only the scanning of MSJ is performed, but the curved surface processing is also performed. It is considered that any microstructure can be more easily applied to artificial materials by combining the working examples of masking and curved surface processing in this study. This processing mechanism seems to have a wide range of applications.

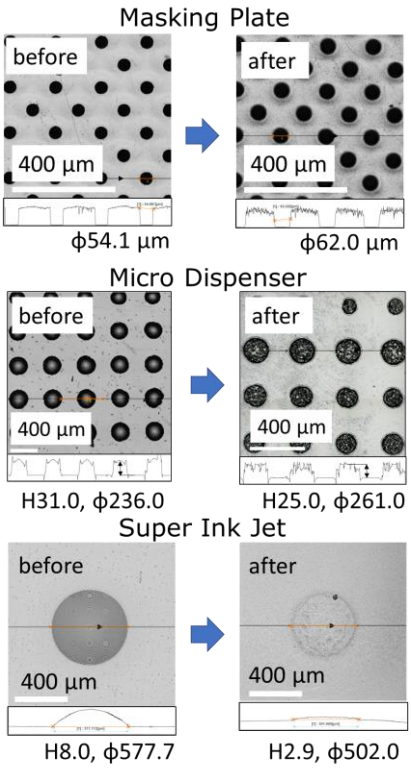

Fig. 3 Before and after MSJ processing of each masking (unit; μm) (H; Height) (φ; masking diameter)

REFERENCES

[1] Chen, Jang F., and James A. Matthews. "Mask for photolithography." U.S. Patent No. 5,242,770. 7 Sep. 1993.
[2] Marmur, Abraham. "The lotus effect: superhydrophobicity and metastability." Langmuir 20.9 (2004): 3517-3519.
[3] Nakanishi, Yoshitaka, et al. "Textured bearing surface in artificial joints to reduce macrophage activation." Surface Topography: Metrology and Properties 3.4 (2015): 044005.
[4] Nouraei, H., et al. "Characteristics of abrasive slurry jet micro-machining: a comparison with abrasive air jet micro-machining." Journal of Materials Processing Technology 213.10 (2013): 1711-1724.
[5] SHIBATA, Kazuma, Yuta NAKASHIMA, and Yoshitaka NAKANISHI. "Anti-fingerprint glass surface created by mechanical removal process." Journal of Biomechanical Science and Engineering 14.4 (2019): 19-00388.

9th International Engineering Symposium - IES 2020
March 3-5, 2020, Kumamoto University, Japan

Influence of geometric surface of Co-28Cr-6Mo alloy on wear characteristics of ultra-high molecular weight polyethylene (UHMWPE)

Nana Motojima[1], Hajime Yamaguchi[2], Yuta Nakashima[3], Yoshitaka Nakanishi[4]

1 *Graduate School of Science and Technology, Kumamoto University, Japan, Kurokami, 2-39-1, Kumamoto 860-8555, Japan.*
Email:188d8530@st.kumamoto-u.ac.jp
2 *Graduate School of Science and Technology, Kumamoto University, Japan, Kurokami, 2-39-1, Kumamoto 860-8555, Japan.*
Email:163t3841@st.kumamoto-u.ac.jp
3 *Associate Professor, Faculty of Advanced Science and Technology, Kumamoto University, Japan, Kurokami, 2-39-1, Kumamoto 860-8555, Japan.*
Email: yuta-n@smech.kumamoto-u.ac.jp
4 *Professor, Faculty of Advanced Science and Technology, Kumamoto University, Japan, Kurokami, 2-39-1, Kumamoto 860-8555, Japan.*
Email: y-naka@mech.kumamoto-u.ac.jp

ABSTRACT: Wear particles generated from artificial joints are considered to be factor in osteolysis, which affects the service life of the artificial joint. In this study, the influence of the geometric surface of Co-28Cr-6Mo alloy processed with micro slurry-jet (MSJ) on the wear characteristics of an ultra-high molecular weight polyethylene (UHMWPE) was investigated experimentally. It was elucidated that the surface processed with MSJ reduced the total wear of UHMWPE, however, the surface processed was thought to make the size of UHMWPE wear particles smaller. Influence of the particle size on immune system was also investigated using a microdevice. It was revealed that the cytokine production was remarkable in a sample with a high percentage of particles less than 1.0 μm in size. Those results lead to the further discussion for the ideal geometric surface which avoid the osteolysis.

***Keywords**: Artificial joints, UHMWPE, Surface processing, Surface profile, Microdevice*

INTRODUCTION

Artificial joints are widely used in the world. There are sliding parts that combine metal as a hard material and ultra-high molecular weight polyethylene (UHMWPE) as a counter material. The micron- or submicron-polyethylene wear particles generated from the sliding parts lead to a problem for service life of the joint, because the macrophage which is one of the immune cells phagocytoses the wear particles as foreign substance. The macrophage produces inflammatory cytokines such as TNF-α and IL-6, which induce osteolysis eventually. The osteolysis leads to loosening of the artificial joint, so that the service life of joint has been in about 20 years yet.

Numerous researchers have reported that the UHMWPE wear particle, which is about 1.0 μm or less than 1.0 μm, induced biological reaction significantly. It can be concluded that not only the reduction of UHMWPE wear but also the enlargement of UHMWPE wear particle should be realized in order to avoid the osteolysis and prolong the service life of artificial joint.

In this report, influence of geometric surface of Co-28Cr-6Mo alloy on wear characteristics of ultra-high molecular weight polyethylene (UHMWPE) was investigated.

MATERIALS AND METHODS

Figure 1 shows the pin-on-disc wear testing device. The pin made of UHMWPE was pressed onto the disc (Co-28Cr-6Mo alloy) in the liquid bath set on the table. The table moved on a horizontal plane by using actuators. It has been reported that a multi-directional friction between the pin and the disc is important in order to prevent the reorientation of the polymer chain of UHMWPE, which is approximately the same frictional behaviour *in vivo*. Diameter in a centre of wear truck was 10 mm, the sliding speed was 20 mm/s, and the total sliding distance was 50 km. The contact surface pressure was set at 7.0 MPa. Fetal bovine serum was used for a lubricating liquid. The liquid was adjusted to 37 ° C (the human body temperature), and it was replaced every 72 hours (about 5.0 km) in order to avoid the deterioration of protein in the fetal bovine serum.

Fig. 1 Pin-on-disc wear testing device

Micro-slurry jet (MSJ) was used as a mechanical removal process to adjust the surface geometry of Co-28Cr-6Mo alloy disc. Figure 2 shows a schematic illustration of the MSJ. The MSJ is a kind of wet-blasting, in which alumina particles (WA #8000, average particle size of 1.2 μm) as an abrasive medium was used. A water solution of 3.0 wt% alumina particles (slurry) was sprayed with compressed air of 0.30 MPa onto the disc surface. By controlling the movement of the spray nozzle, it is possible to obtain a highly accurate surface geometry with a high reproducibility.

Three types of surface geometry processed by the MSJ were prepared. A mirror-finished surface by using a conventional lapping method was also prepared. Figure 3 shows the surface geometries. A non-contact three-dimensional surface profiler (NewView 7000, Zygo) was used.

After test, the UHMWPE pin was removed. The pin was cleaned in an ultrasonic bath sonicator with an aqueous solution of 5 vol% poly-oxyethylene-octylphenyl-ether for 10 min, with deionised water for 10 min, and with ethanol for 10 min. The pin was dried for 24 h in a vacuum dryer at a temperature of 60 °C. The gravimetric wear of the UHMWPE pin was measured. The wear particles were separated and collected from the lubricating liquid.

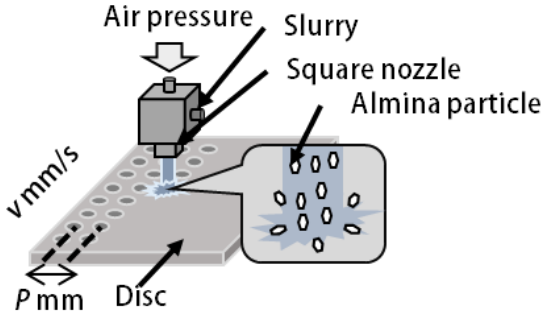

Fig. 2 Micro-slurry jet (MSJ) for adjusting surface geometry of Co-28Cr-6Mo alloy disc

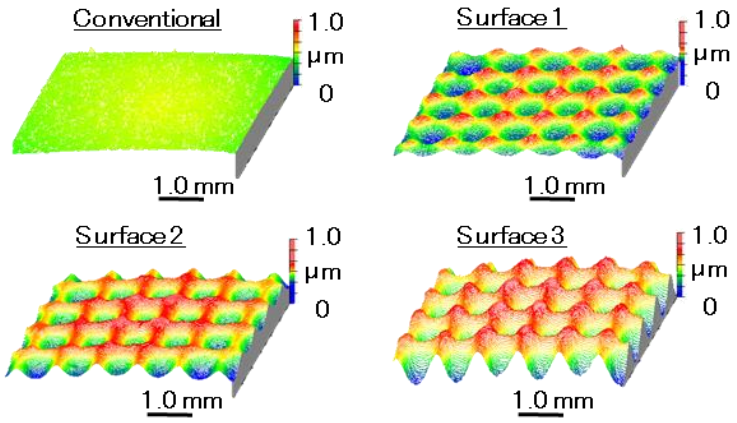

Fig. 3 Surface geometry processed by Micro-slurry jet (MSJ)

The isolated wear particles were observed using a scanning electron microscope (JSM-6390LV, manufactured by JEOL Ltd.). The length in the major axis direction (*Ll*) and the minor axis direction (*Ls*) were measured. The equivalent circular diameter (*L*) was calculated from *Ll* and *Ls* by the following equation (1).

$$L = \sqrt{(Ll \times Ls)} \qquad (1)$$

Figure 4 shows the culture environment of macrophages in a micro device in order to assess the influence of the particle size on immune system. Figure 5 shows procedure for creating a micro device. The glass was ultrasonically cleaned using methanol, acetone, and ultrapure water. Next, the organic compounds and other contaminants on the glass surface were removed using piranha solution (a mixture of 3:1 sulfuric acid, 30% hydrogen peroxide, and up to 40% HF). The SU-8 photocurable resin was used as a photoresist. The surface of the glass was coated with SU-8. It was irradiated with ultraviolet rays through a photomask after drying for 12 h at room temperature (20 to 25 °C). The nonirradiated parts were removed through immersion in 2-acetoxy-1-methoxypropane. The irradiated parts were retained, and the patterns were created.

The glass pattern was placed in a square styrene case were hydrophobic treated. Polydimethylsiloxane (PDMS) was poured. After degassing and curing, the PDMS was removed from the glass pattern. The surface of the PDMS and the new glass substrate were irradiated with an excimer lamp for 1.0 minute, and they were joined and cured to complete the micro device.

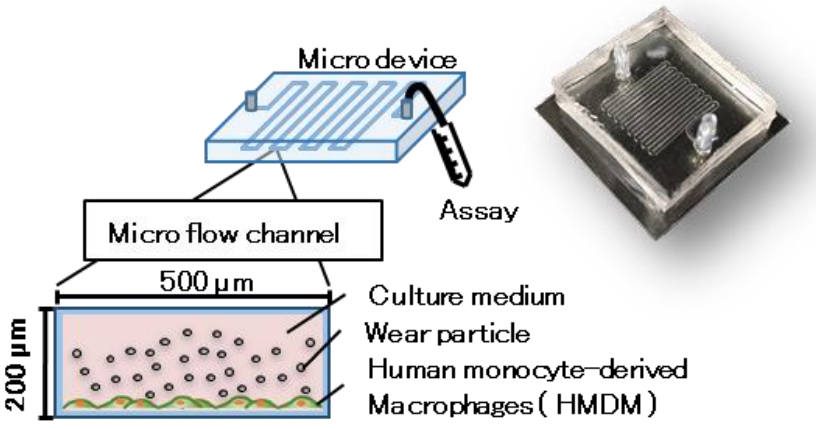

Fig. 4 Culture environment of macrophages in micro device

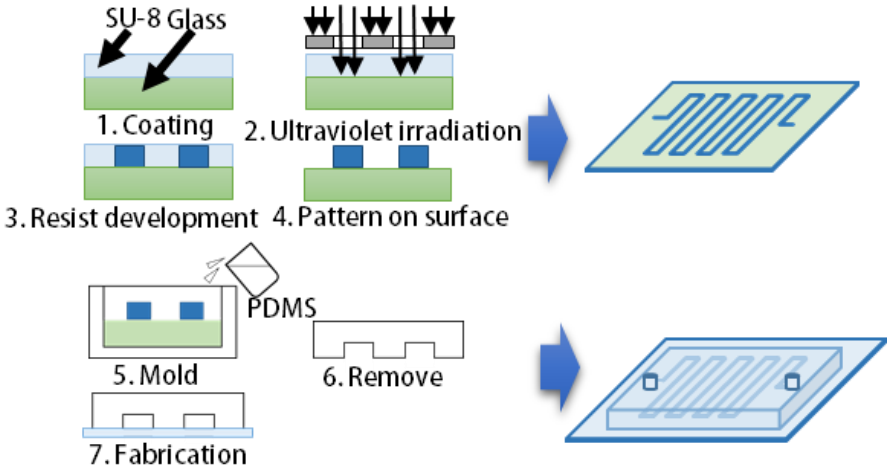

Fig. 5 Procedure for creating a micro device

Micro flow channels fabricated in the micro device were washed with ethanol and ultrapure water. The flow channels were substituted with D-MEM (Dulbecco's Modified Eagle's Medium). A medium containing 5.0 μg / ml of fibronectin diluted with D-MEM was placed in the device. Then it stored 12h over at room temperature. Cells adjusted to a predetermined cell density were introduced into the device. The device was placed on a hot plate set at 37 ° C. 1.0mL sample with or without the UHMWPE particles was sent through the micro flow channels for 4 hours at a speed of 0.694mm/s. The wear particles collected with a cellulose membrane filter was extricated into ethanol using ultrasonic waves, and the concentration was adjusted to 5.0×10^4 particles/device. A normal culture without the particles were also conducted as a negative control, and as a positive control with lipopolysaccharide (0.1 μg/mL LPS). Culture supernatant through each the micro flow channel was recovered and the production amount of inflammatory cytokine IL-6 was measured using the sandwich method of ELISA.

RESULTS AND DISCUSSION

Figure 6 shows the total wear of UHMWPE and the number of wear particles, respectively. The conventional surface produced much higher wear weight than surface 1, 2, and 3. Figure 7 shows the friction coefficient at each surface. The conventional surface recorded a higher coefficient of friction than the other three surfaces. Conventional surface has a mirror-finished surface by lapping and polishing. Therefore, it is probable that an unlubricated state occurred at the contact surface between pin and disc. From the surface observation shown in figure 8, it was estimated that the adhesive wear was predominant in the conventional surface at early stage of the testing. However, the lubrication mode would be moderated in accordance with the testing time (sliding distance). The other surfaces, processed by the MSJ, had the concave areas. The geometrical structure might improve the lubrication between two surfaces, so that the total wear would be reduced. Table 1 shows percentage of wear particles less than 1.0 μm size at each surface. It was elucidated that the MSJ surfaces produced the small size of wear particles in comparison with the conventional surface. The concave areas might improve the lubrication between two surfaces, so that the mixed or full-fluid lubrication would be predominant. In those lubrication modes, the particle size generated would be smaller than that in the adhesive wear mode.

Figure 9 shows the results of IL-6 production. As shown in table 1, it was supporsed that the production of IL-6 have a high correlation to the concentration of small particles. Significant progress has been made in verifying the usefulness of micro devices.

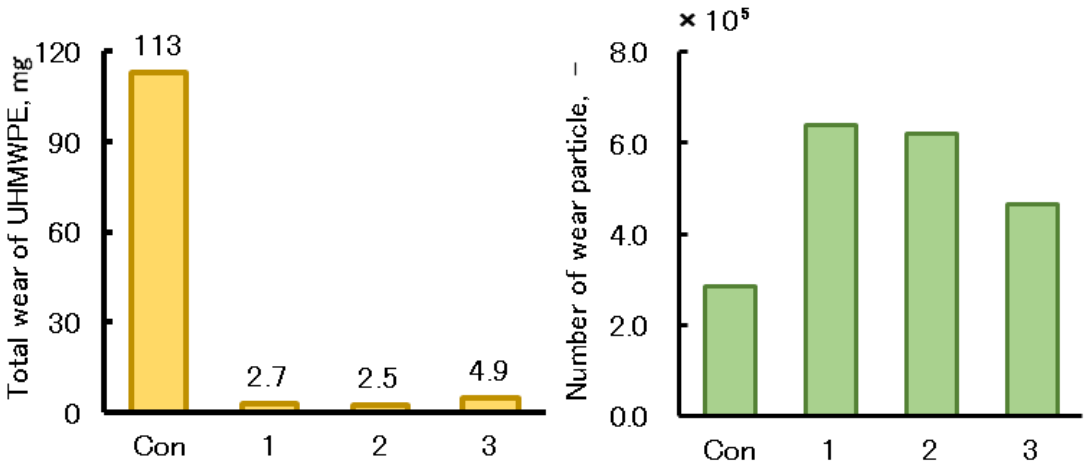

Fig. 6 Total wear and number of wear particles at each surface

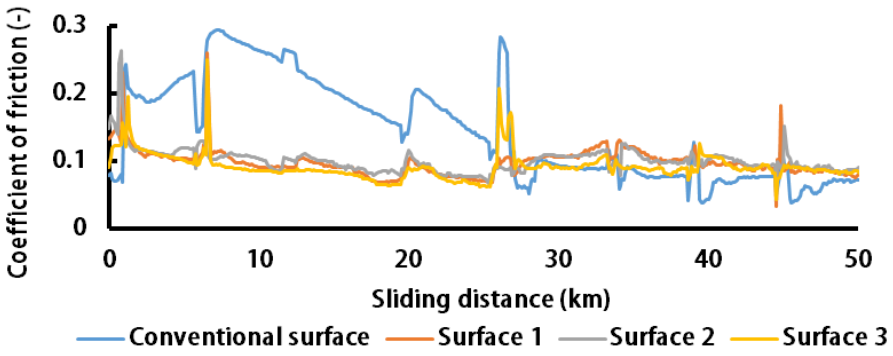

Fig. 7 Friction coefficient at each surface

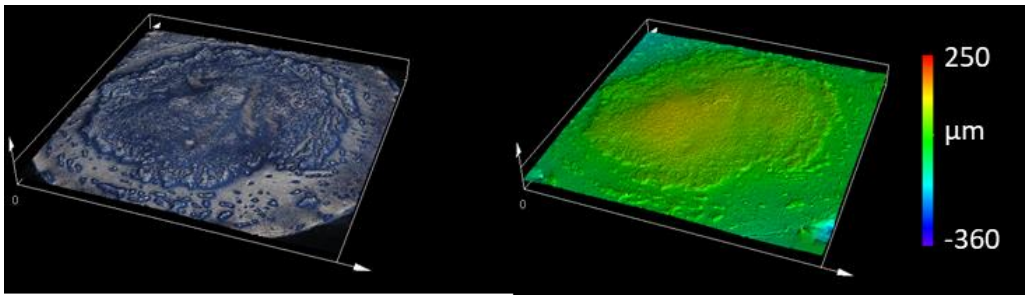

Fig. 8 Pin surface after the test (Counter surface: conventional surface)

Table.1 Percentage of wear particles less than 1.0 μm size

	Conventional surface	Surface 1	Surface 2	Surface 3
< 1.0 μm	1.81%	8.33%	12.77%	12.63%

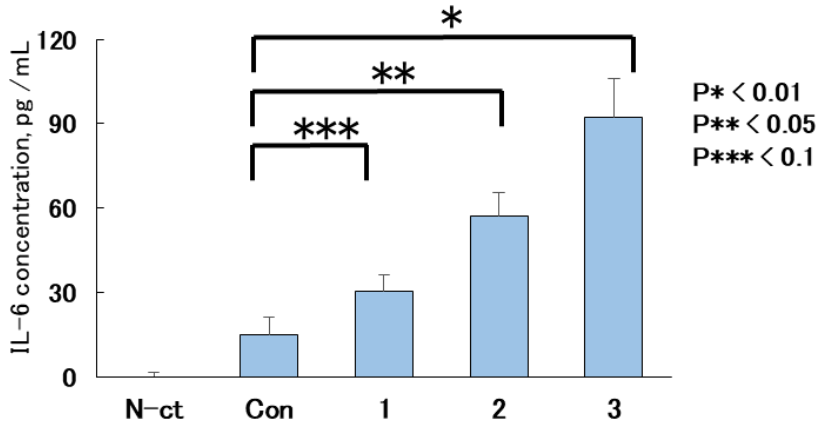

Fig. 9 Concentration of IL-6 secretion

CONCLUSIONS

Influence of geometric surface of Co-28Cr-6Mo alloy on wear characteristics of ultra-high molecular weight polyethylene (UHMWPE). The surface of Co-Cr-Mo alloy with concave areas decreased the wear of UHMWPE and the wear particle size. It was confirmed that the morphological behavior of particle could be detected by using the macrophage culture with micro flow channels.

REFERENCES

Chen-Ying Su, et al, "Optimization of biomolecular additives for a reduction of friction in the artificial joint system", Tribology International, Volume 111 (2017), pp 220-225.
J.Bridget Matthews, et al. "Evaluation of the Response of Primary Human Peripheral Blood Mononuclear Phagocytes to Challenge with In Vitro Generated Clinically Relevant UHMWPE Particles of Known Size and Dose.", Journal of Biomedical Materials Research, 52 (2000), pp 296-307.
Koseki H, Matsumoto, T et al., "Analysis of polyethylene particles isolated from periprosthetic tissue of loosened hip arthroplasty and comparison with radiographic appearance." J Orthop Sci. Vol. 10, No. 3 (2005), pp 284-290.
Mobuko Yamamoto, et al., "Dependence of the phagocytic uptake of polystyrene microspheres by differentiated HL60 upon the size and surface properties of the microspheres", Colloids and Surfaces B: Biointerfaces, Vol. 25, Issue 2(2002), pp. 157-162.
Tipper J L, Ingham E, Hailey J L, Besong A A, Fisher J, Wroblewski B M, Stone M H. Quantitative analysis of polyethylene wear debris, wear rate and head damage in retrieved Charnley hip prostheses. J Mater Sci Mater Med 2000; 11: 117–24.

9th International Engineering Symposium - IES 2020
March 3-5, 2020, Kumamoto University, Japan

STUDY ON THE STABILITY OF BIODIESEL EMULSION FUEL USING CRUDE GLYCERIN AS EMULSIFIER

Junpei Kanmura[1], *Shuichi Torii[2]
Department of Mechanical Systems Engineering, Kumamoto University,Japan
[1] Kumamoto University, Chuo-Ku, Kurokami 2-39-1, Kumamoto, 860-8555 Japan
161t3730@st.kumamoto-u.ac.jp
[2]Kumamoto University, Chuo-Ku, Kurokami 2-39-1, Kumamoto, 860-8555 Japan

†Presenter: **Junpei Kanmura**
*Corresponding author's e-mail: *torii@mech.kumamoto-u.ac.jp*

ABSTRACT: in recent years, air pollution has become serious due to the rapid promotion of industrialization. One way to reduce such air pollution is to use an emulsion fuel in which fuel oil and water are mixed using an emulsifier.
In this study, crude glycerin was used as an emulsifier, and several conditions were changed when preparing biodiesel emulsion fuel, and the stability was observed visually. The biodiesel used was rapeseed oil washed with ethanol after transesterification (ROEE) and unwashed (UROEE). In addition, a pH 7.0 buffer was used for the aqueous phase. Good results were obtained when the oil phase was 73.0 wt.%, the aqueous phase was 25.0 wt.%, and the crude glycerin was 2.0 wt.%. When the oil phase was UROEE, no separation was observed even after 4 hours.

***Keywords**:* Biodiesel emulsion fuel, Stability, Crude glycerine

1. INTRODUCTION

On the planet today, the total consumption of fossil fuels is rapidly increasing with the development of industry in developing countries, leading to global warming and environmental problems such as rising temperatures and rising sea levels.
As a countermeasure for such a problem, use of an emulsion fuel is considered.
Emulsion fuel is a fuel made by mixing insoluble liquids such as fuel oil and water. It can greatly reduce substances such as nitrogen oxides and carbon dioxide contained in exhaust gas at the time of combustion as compared with the case where fuel oil is used as it is. [5] [4]
Furthermore, in recent years, the use of biofuels, particularly biodiesel fuels, [1] has become popular from the viewpoint of limited resources and environmental impact during combustion. Therefore, research on biodiesel emulsion fuel, which is an emulsion of biodiesel fuel, is also being conducted. [2]
In this study, we used biodiesel fuel as the oil phase, and used crude glycerine as an emulsifier with the production of biodiesel fuel. The observation was made as to whether or not to hold without separating.
This is one of the methods for treating crude glycerine, and it can be said that relatively inexpensive emulsifiers are not

purchased, so that a less expensive emulsion fuel can be produced.

2. Materials and method

2.1 Constituent materials of emulsion fuel

In this experiment, a phosphate buffer (ph7.0, 0.1 M) was used for the aqueous phase, and biodiesel fuel derived from rapeseed oil was used for the oil phase. The rapeseed oil used is from Nisshin Oillio Group of Japan. As the production method, a transesterification method using an alkali catalyst was selected.

In addition, a comparison was made between the unpurified rapeseed oil ethyl ester(UROEE) which was omitted the washing step in the process of producing biodiesel fuel and the purified rapeseed oil ethyl ester(ROEE) which had been washed.

2.2 method of creation emulsion fuel

In preparing the emulsion fuel, emulsification was performed using a rotary homogenizer. The rotating homogenizer used was AHG-160A of ASONE Corporation. The stirring conditions were 8000 rpm for 5 minutes in all experiments.

The state of emulsification is shown in Fig.1.

Fig.1 State of emulsification

2.3 Emulsion fuel observation method

Emulsion fuel was evaluated by visual observation in all experiments.

The sample was collected by preparing an emulsion fuel and using a dropper near the center of the beaker. Thereafter, the emulsion fuel was added so that air could not enter the centrifuge tube as much as possible, and stored in the room.

Follow-up photographs were taken immediately after the preparation of the emulsion fuel. If the difference in stability was not immediately evident immediately after the preparation, a picture was taken one day later.

3. Experimental results and discussion

3.1 Effect of surfactant concentration on emulsion fuel

The effect of the concentration of the crude glycerine, which is a surfactant, on the stability of the emulsion fuel was examined. In 3.1.1, the stability of the sample when unpurified ethyl ester (UROEE) is used for the oil phase and when the purified ethyl ester (ROEE) is used for the oil phase are evaluated in 3.1.2.

3.1.1 Emulsion fuel using unpurified ethyl ester (UROEE) for oil phase

The stability of the emulsion fuel was observed using UROEE in the oil layer while changing the ratio of crude glycerine.

Table.1 shows the sample conditions.

Fig.2 shows the results.

Looking at the state of each emulsion after stirring, it was found that they were all separated and the stability could not be secured. It is considered that saponification was caused by alcohol (KOH) remaining in UROEE and crude glycerine, and the stability was reduced.

Samples 3 and 4 also had a color similar to that of rapeseed oil in the oil layer, and their stability was quite low. It is considered that when the amount of glycerine added increases, the difference in specific gravity between the aqueous phase and the oil phase increases, so that

coalescence of the emulsified particles becomes easier [3].

From the color of the emulsion, Sample 2 is the most cloudy and has a small grain size, so it is considered that Sample 2 gave the best results.

Table.1 Condition of each sample in 3.1.1

	UROEE [wt.%]	Phosphate buffer [wt.%]	Crude Glycerine [wt.%]
Sample 1	79	20	1
Sample 2	78	20	2
Sample 3	75	20	5
Sample 4	70	20	10

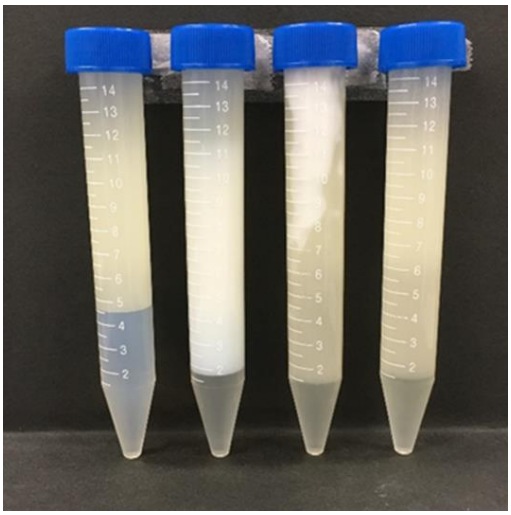

Fig.2 Picture of each emulsion immediately after stirring (Sample1, 2, 3, 4)

3.1.2 Emulsion fuel using purified ethyl ester (ROEE) for oil phase

The stability of the emulsion fuel was observed by changing the ratio of crude glycerine using ROEE in the oil layer.

Also, based on the result of 3.1.1, the ratio of the water layer was set to 25 wt.%, And the stability was improved.

Table.2 shows the sample conditions.

Fig.3 shows the results.

Immediately after stirring, the samples were stable except for sample 4, but one day later, all samples were separated. The oil phase was separated, and the separation of the aqueous phase could not be confirmed. This is considered to be due to the fact that glycerine is soluble only in the aqueous phase, so that the oil film is weak and the oil phase is easily separated.

Table.2 Condition of each sample in 3.1.2

	ROEE [wt.%]	Phosphate buffer [wt.%]	Crude Glycerine [wt.%]
Sample 1	74	25	1
Sample 2	73	25	2
Sample 3	70	25	5
Sample 4	65	25	10

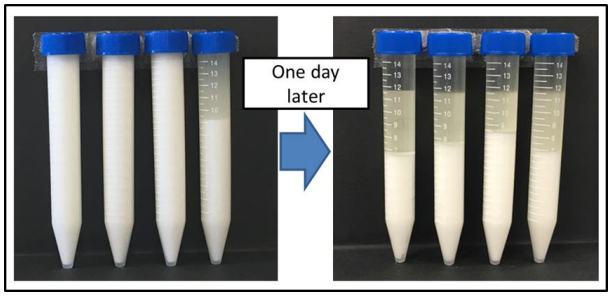

Fig.3 Picture of each emulsion immediately after stirring and one day after (Sample1, 2, 3, 4)

3.2 Effect of water phase proportion on emulsion fuel

In 3.1.1, it was considered that when the amount of glycerine added increased, the difference in specific gravity between the aqueous phase and the oil phase increased, so that coalescence of emulsified particles became easier. As a countermeasure, the ratio of the water layer was increased and the stability of emulsion fuel using UROEE for the oil phase was improved. The ratio of crude glycerine is set to 2 wt.% With reference to the sample having the best result in 3.1.1.

Table.3 shows the sample conditions.

Fig.4 shows the results.

Four hours after stirring, the oil layers had separated except for Sample 1. Therefore, it can be said that the ratio of the aqueous phase is most preferably 25 wt.%.

One day later, the separation of Sample 1 also occurred. Therefore, when crude glycerine was used as a surfactant, low emulsification was an issue.

Table.3 Condition of each sample in 3.2

	UROEE [wt.%]	Phosphate buffer [wt.%]	Crude Glycerine [wt.%]
Sample 1	73	25	2
Sample 2	68	30	2
Sample 3	63	35	2

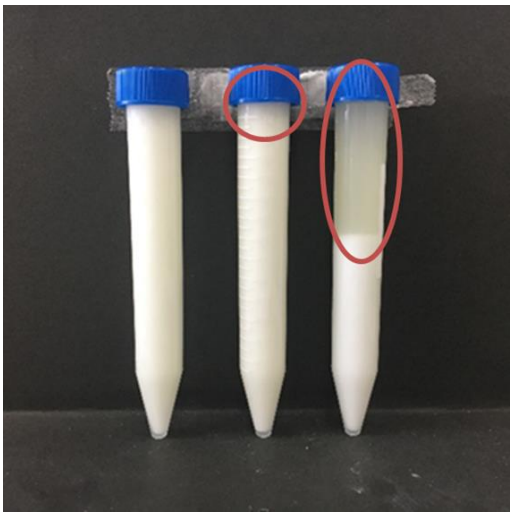

Fig.4 Picture of each emulsion immediately after stirring (Sample1, 2, 3, 4)

CONCLUSIONS

The following conclusions were drawn from this study.

- When unpurified ethyl ester (UROEE) was used for the oil phase, the emulsion fuel prepared with the ratio of UROEE 73 wt.%, Phosphate buffer 25 wt.%, Crude Glycerin 2 wt.% was most stable.
- There was no significant difference in stability depending on whether the oil phase was UROEE or ROEE.
- Due to the low emulsifying action of crude glycerin, it is difficult to ensure stability when used alone as an emulsifier.

REFERENCES

[1] A.S.Ramadhas, S.ayaraj, C.Muraleedharan, (2004), Use of vegetable oils as I.C. engine fuels-A review, Renewable Energy, 29, pp.727-742

[2] Manpreet Singh Sidhu, Murari Mohon Roy, Wilson Wang, (2018), Glycerine emulsions of diesel-biodiesel blends and their performance and emissions in a diesel engine, Applied Energy, 230, pp.148-159

[3] Motoi Hayase, (2010), Characteristic formulation and stability control, J. Soc. Cosmet. Chem. Jpn, 44(4), pp.269-277

[4]M.Senthil Kumar, M.Jaikumar, (2014), A comprehensive study on performance, emission and combustion behavior of a compression ignition engine fuelled with WCO (waste cooking oil) emulsion as fuel, Journal of the Energy Institute, 87, pp.263-271

[5] S.S.Reham, H.H.Masjuki, M.A.Kalam, I.Shancita, I.M.Rizwanul Fattah, A.M.Ruhul, (2015), Study on stability,fuel properties, engine combustion, performance and emission characteristics of biofuel emulsion, Renewable and Sustainable Energy Reviews, 52, pp.1566-1579

9th International Engineering Symposium - IES 2020
March 3-5, 2020, Kumamoto University, Japan

A BASIC STUDY ON BIODIESEL SPRAY COMBUSTION

Shuhei Kadowaki[1], *Shuichi Torii[2]
Department of Mechanical Systems Engineering, Kumamoto University,Japan
[1] Kumamoto University, Chuo-Ku, Kurokami 2-39-1, Kumamoto, 860-8555 Japan
167t3724@st.kumamoto-u.ac.jp
[2]Kumamoto University, Chuo-Ku, Kurokami 2-39-1, Kumamoto, 860-8555 Japan

†Presenter: **Shuhei Kadowaki**
*Corresponding author's e-mail: *torii@mech.kumamoto-u.ac.jp*

ABSTRACT: In recent years, biodiesel has become popular around the world as the fuel said to be an alternative fuel to replace a conventional type of fuel, which is diesel fuel. The alarming environmental hazard that occurs such as climate change, heat island, melting of ice blocks at the South and North poles has increases the concerns to reduce the production of carbon dioxide gas (a greenhouse gas) from vehicles.

Benefits of biodiesel fuel are carbon neutral, that it is biomass, that emission gas can reduce soot and SOx rather than diesel fuel. Biodiesel fuel is attracting attention as an alternative energy to diesel fuel.

The final goal of this experiment is to develop a biodiesel-fuelled torch.
***Keywords**:* Biodiesel fuel, Spray combustion, torch, SOx, Particle size

INTRODUCTION

First, biodiesel fuel are described. The main raw materials and production method are as follows. Methanol is added to a vegetable oil such as corn oil, sunflower oil, rapeseed oil, etc. as a raw material, and methanol is added. It is to remove such by-products. Biodiesel whose kinematic viscosity has been reduced to about twice that of light oil is called biodiesel. The biodiesel used in this study is a biodiesel fuel from Kumamoto prefecture named ReESEL. I was very surprised to see this mark on the changed oil container at my part-time job. As a result of analysis by the Japan Maritime Inspection Association, ReESEL has cleared all 26 JIS-K2390 standards. The content of methyl ester, which is necessary for fuel, is 99-8%, which is much higher than JIS standard value. (As of December 2013)

Next, the advantages of biodiesel fuel are described.

The first point is a renewable energy. Japan originally relies on imported rapeseed oil and soybean oil. Therefore, in Japan biodiesel fuel cannot be made from pure rapeseed oil or soybean oil unlike overseas. Therefore, a method that is often used is to recycle and use waste oil generated in daily life. For this reason, it is a resource-recycling type familiar energy that can be locally produced and

consumed at the same time as renewable energy.

The second point is diesel engines can be used as an alternative fuel to light oil. Biodiesel and light oil are used in a diesel engine, and the mileage and fuel efficiency were compared. Another advantage, it is not necessary to modify the diesel engine to use biodiesel.
Another point is that using biodiesel can reduce emissions of carbon monoxide, Hydrocarbons and SOx.

The third point is carbon neutrality by balancing carbon emissions with carbon removal. For example, plants that are the raw material of biodiesel absorb carbon dioxide in the air while growing and cancel the carbon dioxide emitted when burning it to zero. Biodiesel can also apply to this concept.

The fourth point is that by burning biodiesel almost no sulphur oxides are produced like gas oil.

In this study, the final goal is to create a torch using biodiesel. In order to achieve the purpose, it is necessary to carry out flame holding, and the main purpose of the experiment is to find out the conditions. In conducting this experiment, searched for previous research, but could not find any previous research. Most of them were spray combustion under high temperature and high pressure. Therefore, it was necessary to try many times. There were times when the experimental results were not as expected, but based on the results, I was able to consider and connect to the next experiment. Until now, flame torches ignited gaseous fuel to form a flame. However, the biodiesel used in this experiment is of course a liquid fuel, and it is necessary to atomize it to ignite them. Atomization increases the area of contact of fuel particles with air, leading to better combustion processes. The use of biodiesel as fuel for the flame torch can also be a catalyst for spreading clean energy to the world.

Materials and Methods

The outline of the experiment is shown in Fig. 1.

Last year failed to successfully spray upward. The reason was considered to be ignition timing and ignition time. The ignition timing and the ignition position can be controlled by changing the proportion of ethanol mixed with biodiesel from the reference[1].

The experiments were performed with different ethanol contents of 20%, 40% and 60%.

The experimental method is as follows.

Turn on the air compressor. Accumulate a higher pressure than desired in the compressor tank. Adjust the pressure regulator to determine the pressure of the supplied air. Open the outlet valve of the pressure regulator and supply air into the spray tank. The fuel inside the spray tank is pushed out by the compressed air and comes out of the nozzle. The flame is ignited by a gas match with the nozzle facing vertically upward, and the state of the flame is photographed and observed.

CONCLUSIONS

Figure 2 shows the experiment.

Before conducting the experiment, ethanol was mixed to control both the ignition position and the ignition time, but before that, an attempt was made to vertically stabilize the flame using only biodiesel. But didn't work.

Next, a mixture of biodiesel and ethanol at three different concentrations was sprayed and ignited according to the procedure described in the experimental method. As a result, at all concentrations, the flame was kept better than biodiesel. Among them, the mixture with a concentration of 40%, which was placed on top in Fig. 2, was the most stable and stable.

As an impression, it can be said that the ignition position was too far as it was hypothesized and that it took a long time to ignite, which was the reason that the flame was not successfully held.

REFERENCES

[1] Effect of Viscosity on the Size of Droplets of Vegetable Oil
Chiyuki TOGASHI, Kazuhiro MATSUMORI, Jun-ichi KAMIDE

[2] Effect of Biodiesel Fuel Mixed with Ethanol on Spray, Ignition and Combustion Characteristics
Yasuhiro INOUE, Takashi MATSUURA and Jiro SENDA

[3] Combustion Characteristics of Biofuels: Utilization of Raw Plant Oils in Diesel Engines
Tomohisa DAN

[4] Particle Size of Injected Deacidified Rapeseed Oil Spray
Chiyuki TOGASHI, Jun-ichi KAMIDE

[5] Atomization Technologies for Liquid Fuel
Takashi SUZUKI

[6] Effect of the Cavitation in a Nozzle on the Liquid Breakup (3rd Report, Pressure Variation Inside 2D Nozzle)
Masatoshi DAIKOKU, Hitoshi FURUDATE, Takao INAMURA

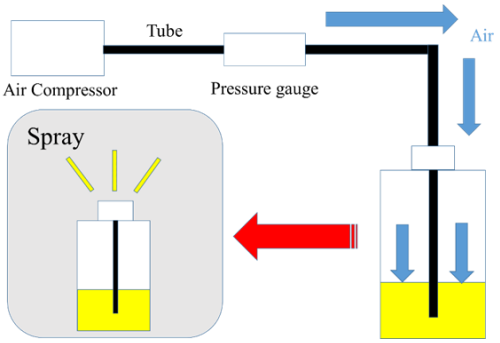

Fig.1 Experimental apparatus

Fig.2 Experiment

9th International Engineering Symposium - IES 2020
March 3-5, 2020, Kumamoto University, Japan

A BASIC STUDY ON BIOFUEL COMBUSTION

Tetsushi Kataoka[1], *Shuichi Torii[2]
Department of Mechanical Systems Engineering, Kumamoto University,Japan
[1] Kumamoto University, Chuo-Ku, Kurokami 2-39-1, Kumamoto, 860-8555 Japan
169t3723@st.kumamoto-u.ac.jp
[2]Kumamoto University, Chuo-Ku, Kurokami 2-39-1, Kumamoto, 860-8555 Japan

†Presenter: **Tetsushi Kataoka**
*Corresponding author's e-mail: *torii@mech.kumamoto-u.ac.jp*

ABSTRACT: In recent years, the introduction of biofuels has been rapidly promoted worldwide as part of measures to combat global warming. It is thought that there are various factors behind the rapid spread of such biofuels, such as the response to global warming and the instability of crude Oil prices. Aspects of regional promotion are also behind the spread of biofuels. For this reason, the introduction of biofuels is expected to affect various aspects of the local economy and the global environment, and it is necessary to comprehensively evaluate these effects.

One way to support the introduction of biofuels is to create biofuels using undeveloped biomass. The end goal of this experiment is to use waste oil to produce biofuels and burn them in burners
***Keywords**: Biofuel, waste oil, combustion,* viscosity

INTRODUCTION

Waste biomass refers to biomass such as paper, livestock excreta, food waste, wood from construction, black liquor (pulp mill effluent), and sewage sludge.As it contributes to global warming countermeasures by reducing greenhouse gas emissions as well as forming a recycling-based society, it has been selected from treatment methods such as feed, composting methane gasification (biogasification), and BDF conversion. It is necessary to promote appropriate recycling, etc. according to the characteristics of the region, including the combination of these [3].

Next, Waste biomass is limited in the method of treatment and is not energy that can be used in various ways like gas oil. Therefore, in this study, we tried to develop a liquid fuel that can be used in high-efficiency energy equipment using solid waste oil and high-viscosity liquid waste oil, which are waste biomass. In this study, we used solid waste oil and highly viscous liquid waste oil obtained from an experimental facility in Mashiki-cho, Kumamoto Prefecture. The goal in the experiment is to reduce the viscosity to the level of heavy oil while maintaining a high calorific value, and to make the liquid fuel capable of stable combustion. Furthermore, in view of the problem of global warming, the greenhouse effect on the combustion gas components requires that the combustion gas components be clarified for the study. In this study, we developed a liquid fuel using solid waste oil and high-viscosity liquid waste oil, analyzed the combustion gas components of the liquid material, and evaluated combustion.

Laws related to waste

Waste is classified into general waste and industrial waste in the Waste Management and Public Cleansing Law (Waste Management Law) [2]. Waste biomass waste oil used in this experiment is classified as industrial waste. As a law on biomass in Japan, there is the "Basic Act on Promotion of Utilization of Biomass" [1], in which the following basic concepts are defined.

(1) Comprehensive, integrated and effective promotion of biomass utilization.
(2) Promotion of prevention of global warming.
(3) Promotion of the formation of a recycling-oriented society.
(4) Contribution to industrial development and strengthening of international competitiveness.
(5) Promotion that contributes to the revitalization of fishing villages, etc.
(6) Maximum use according to the characteristics of each type of biomass.
(7) Diversification of energy supply sources.
(8) Promotion of community-based initiatives.
(9) Fostering social momentum.
(10) Stable supply of food Security.
(11) Consideration of environmental conservation.

Experimental conditions

The calorific values of solid waste oil and high-viscosity liquid waste oil before the production of liquid fuel were measured and recorded, and this data was used to compare how the values changed between the waste oil and the fuel produced. The average value of the calorific value before fabrication is shown in Table 1.
Fig 1 Shows the appearance of waste oil.

Table 1 Calorific Value

Calorific Value [j/g]
33025

Fig 1

Waste oil

Experimental procedure

The experimental procedure for liquid fuel production in this experiment is shown below.

1. Add alcohol to the waste oil, find out which alcohol mixes with the waste oil in the least amount, and adopt it.
2. Mix vegetable oil or biodiesel with the mixture of alcohol and waste oil mixed in the least amount in step 1.
3. Determine which of the two samples prepared in step 2 can reduce the viscosity with less amount of vegetable oil or biodiesel and use it.
4. If the sample prepared in step 3 has a high viscosity, mix with a small amount of glycerin or sorbitan monooleate and adjust.

Ethanol, propanol, butanol, and pentanol were used as the alcohol in step 1.
The reason for mixing in a small amount is to not reduce the calorific value.
Glycerin or sorbitan monooleate was used in step 4 because both were considered to be excellent in lipophilicity and easy to mix with waste oil.

Experimental result

The results of the first experimental procedure are shown in Table 2, which shows the amount of alcohol added to 1 g of waste oil until it becomes a completely mixed liquid. Table 3 shows the results of Experimental Procedure 3. Table 3 shows the amount of vegetable oil and biodiesel added to the mixture of waste oil 1 [g] and butanol 1 [g] until the viscosity was measured.

Table 2 Alcohol ratio

Waste Oil[g]	Ethanol[g]	Propanol[g]	Butanol[g]	Pentanol[g]
1	-	5	3.5	4

Table 3 Ratio of vegetable oil and biodiesel

Waste oil[g]	Butanol[g]	Vegetable oil[g]	Biodiesel[g]
1	1	5	4

In Table 2, ethanol could not be measured because it was not mixed with the waste oil, but it can be seen that butanol is the most easily mixed with the waste oil.

Table 3 shows that biodiesel is easier to mix than vegetable oil. The viscosity measured by mixing waste oil 1 [g], butanol 1 [g] and biodiesel 4 [g] is 56.1 [mPa · s].

Although the viscosity could be lowered until it could be measured, the viscosity was still a little high, and the drawback was that butanol and biodiesel were added in excess.

Next, the results of Experimental Procedure 4 are shown in Table 4, which is the ratio of glycerin and sorbitan monooleate mixed with the liquid prepared in Experimental Procedure 3 while adjusting the ratio. The viscosity of the manufactured liquid was 40.5 [mPas].

Table 4 Mixing ratio

Waste oil[g]	Butanol[g]	Biodiesel[g]	Glycerin[g]	Sorbitan monooleate[g]
1	1	1.5	0.2	0.1

Fig 2 shows how the liquid fuel produced in step 4 changes in viscosity with temperature, and Fig 3 shows a comparison between the calorific value and the calorific value of the waste oil.

Hereinafter, the liquid fuel produced in step 4 is referred to as a sample.

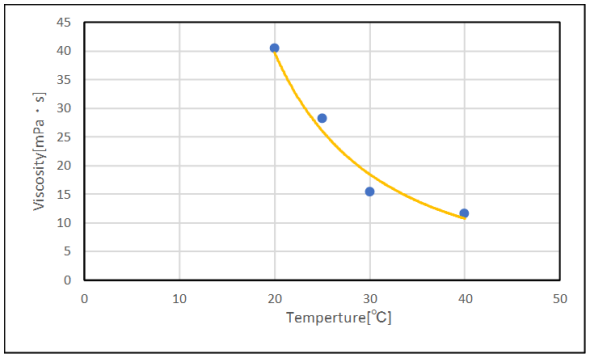

Fig 2 Viscosity with temperature

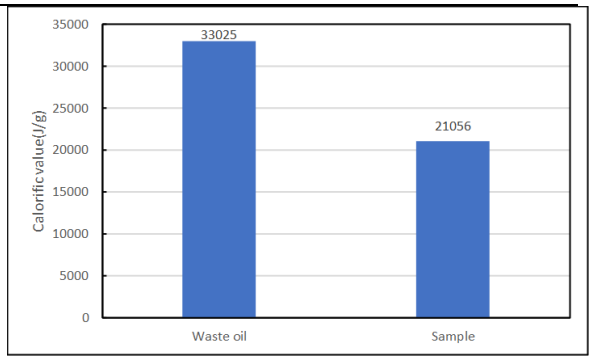

Fig 3 Calorific value

It can be seen that the viscosity decreased in inverse proportion to the temperature rise. At 40 ° C, the viscosity decreased to 11.6 [mPas], which seems to have achieved the task of lowering the viscosity. If the amount of biodiesel can be reduced and the low viscosity can be maintained, it is considered to be a highly practical fuel. This is probably due to excessive mixing of non-waste oil to reduce the viscosity.

CONCLUSIONS

- The waste oil used in the experiment is compatible with butanol and biodiesel.
- Adding glycerin and sorbitan monooleate made mixing easier.
- Although the viscosity decreased, the calorific value decreased, and it lacked practicality.

REFERENCES

[1] House of Representatives (2020-1-6), Basic Act on Promotion of Utilization of Biomass Website: http://www.shugiin.go.jp/internet/itdb_housei.nsf/html/housei/17120090612052.htm

[2] House of Representatives (2020-1-6), Waste Disposal and Public Cleansing Law Website: http://www.shugiin.go.jp/internet/itdb_housei.nsf/html/houritsu/06419701225137.htm

[3] Ministry of Agriculture, Forestry and Fisheries (2020-1-6), Utilization of waste biomass, Website: http://www.env.go.jp/recycle/waste/biomass>

9th International Engineering Symposium - IES 2020
March 3-5, 2020, Kumamoto University, Japan

Microstructures on glass surface through mechanical removal processing

Kazuma SHIBATA [1], Yuta NAKASHIMA [2] and Yoshitaka NAKANISHI [3]

1 *Graduate School of Science and Technology, Kumamoto University, Kurokami 2-39-1, Chuo-ku, Kumamoto 860-8555, Japan*
E-mail : 183d8460@st.kumamoto-u.ac.jp
2 *Faculty of Advanced Science and Technology, Kumamoto University, Kurokami 2-39 Chuo-ku, Kumamoto 860-8555, Japan*
E-mail : yuta-n@mech.kumamoto-u.ac.jp
3 *Faculty of Advanced Science and Technology, Kumamoto University, Kurokami 2-39 Chuo-ku, Kumamoto 860-8555, Japan*
E-mail : y-naka@mech.kumamoto-u.ac.jp

ABSTRACT: It has been elucidated that surface processing for creating microstructures on glass was difficult. Because of its brittle material characteristic, the mechanical removable process such as a milling process is not suitable. Because of its chemically stable characteristics, the chemical etching is not excellent method. This study shows a new processing method of microstructures on the glass surface by mechanical removal processing. The processing method was micro slurry-jet (MSJ) of mechanical removal method. In addition, a masking process was used to create microstructures. As an example, we evaluated the glass created by these processing methods. Microstructures were created on the glass surface through the combination of the masking process and MSJ processing.

***Keywords**: Micro slurry-jet,* Microstructures, Masking process, Photolithography

INTRODUCTION

There is a characteristic microstructure in nature. As an examples, water repellency exhibited on the surface of a lotus leaf, and light reflection suppression exhibited by moth-eye. There are attempts to reproduce the microstructures in artificial materials. However, it has been elucidated that surface processing for creating microstructures on glass was difficult. Because of its brittle material characteristic, the mechanical removable process such as a milling process is not suitable. In general, nanoimprinting is one of the methods for making microstructures. Although microstructures based on a mold can be produced, the cost of preparing the mold is high. And, this method creates microstructures by adding resin to the substrate surface. Another example is a method of chemically removing a substrate to create a microstructure. The substrate surface is removed and microstructures are created with the substrate material. However, such chemical removal processing is limited by materials because chemical solutions are used
This study has explored a processing method that can solve these problems. Therefore, we attempted to change the surface shape by processing a material surface directly. The processing method was MSJ processing, which is a mechanical removal method. MSJ processing, which is a mechanical removal method, was considered because it can be applied to numerous materials, it can be processed on the order of nanometers in the vertical direction, and it provides a continuous curved surface after MSJ processing. In addition, a masking process was used to create the microsurface structures. Exploring

the possibility of creating microstructures in various materials by mechanical removal of MSJ processing and masking process as an alternative to chemical removal processing.

Materials and methods

Micro slurry-jet processing

MSJ processing was used instead of the chemical removal process (Figure 1). MSJ processing allows for precise texture processing. When switching to mechanical removal such as MSJ, surface processing can be performed on various materials that are difficult to etch. It has ultraprecise machining capability of nanometer order in the orthogonal direction on a material. It is a wet blasting technique that uses alumina particles as an abrasive medium with compressed air and water to produce microstructures. A slurry consisting of pure water with 3.2 wt% alumina particles was prepared. Micropolyhedral alumina particles were used, and their average diameter was 1.2 μm (WA # 8000). The slurry was sprayed vertically on the glass surfaces through an injection nozzle with a square shape of 1 mm width, with compressed air at 0.3 MPa. The injection nozzle could be moved parallel to the processed surface using a numerical control system. MSJ processing conditions can be changed by controlling the injection nozzle speed and processing pitch. After finishing a reciprocal movement on a surface, the movement direction of the nozzle was changed by 90° to finish another reciprocal movement on the surface (Figure 2).

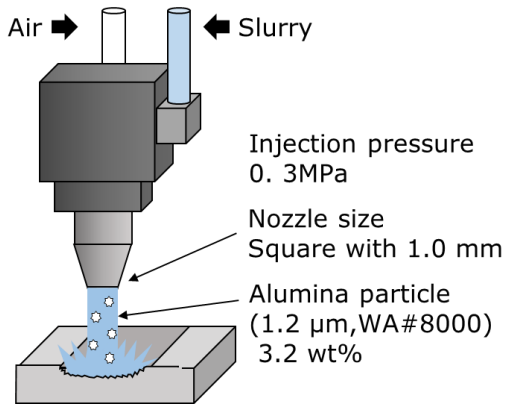

Fig.1 Schematic of MSJ processing

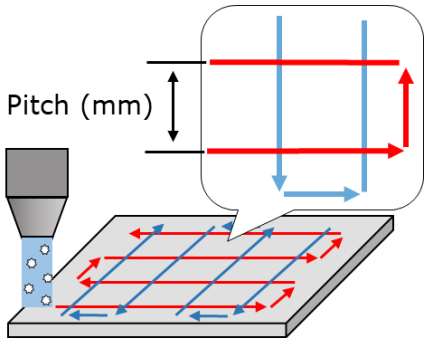

Fig.2 Schematic of MSJ movement for glass surface processing

Covering mask

The MWB processing has a precision processing capability on nanometer order in the direction perpendicular to the material surface. Injection nozzle size is 1mm square. Therefore, the processing accuracy in the horizontal direction is sub-millimeter. A cover mask was used between the glass surface and the injection nozzle to improve the horizontal processing accuracy. An aluminum plate with a thickness of 0.5 mm was used for the cover mask. The plate has 500 μm holes with a 1000 μm pitch (Figure 3). The cover mask was fixed on glass and processed by MSJ procesing. The processing conditions of the MSJ were controlled in a grid pattern at a processing pitch of 0.1 mm.

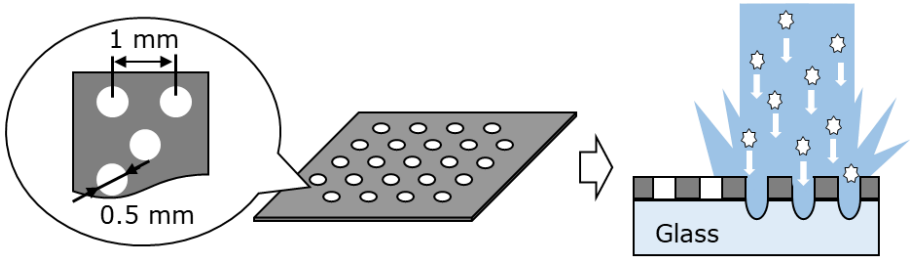

Fig.3 Image of covering mask and MSJ processing

Micro masking process

A concave pattern can create according to the design by the covering mask. However, when creating a convex microstructure, separate masks were required. A micro masking process based on the photolithography technology was adopted to create the glass with various microstructures. Micro masking process was used to increase the horizontal processing accuracy with the MSJ processing and to create a convex shape on the processed glass (Figure 4). Before the masking process, the glass was ultrasonically cleaned using methanol, acetone, and ultrapure water. Next, the organic compounds and other contaminants on the glass surface were removed using piranha solution (a mixture of 3:1 sulfuric acid, 30% hydrogen peroxide, and up to 40% HF). The SU-8 photocurable resin was used as a photoresist. It was dipped in silane coupling material (kbm 403) for 30 min to increase the bonding strength of glass (inorganic material) and SU-8 (organic material). The silane coupling agent contains two or more different reactive groups. One reactive group is capable of chemically bonding with an inorganic material, and the other is capable of chemically bonding with an organic material. The surface of the processed glass was coated with SU-8. It was irradiated with ultraviolet rays through a photomask after drying for 12 h at room temperature (20 to 25 °C). The nonirradiated parts were removed through immersion in 2-acetoxy-1-methoxypropane. The irradiated parts were retained, and the patterns were created. After, the glass was processed by MSJ processing. The processing conditions of the MSJ were a processing pitch of 0.1 mm, and the nozzle speed was 30 mm/s, which was operated in a grid pattern.

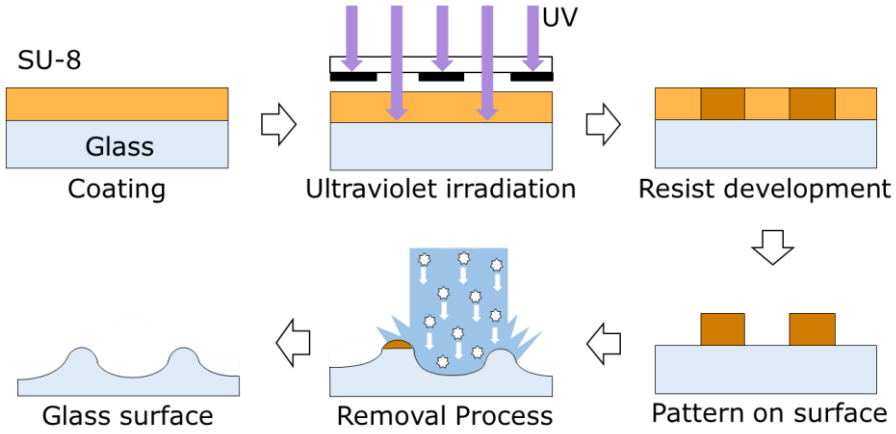

Fig.4 Method of creating microstructures on glass by masking process and micro slurry-jet processing.

RESULTS AND DISCUSSION

Micro Slurry-Jet processing

These glasses were processed by the MSJ processing (Figure 5). These surfaces was processed into a lattice shape, creating an uneven shape. Figure 5a was processed at a processing pitch of 1.0 mm, and Figure.5b was processed at a processing pitch of 0.5 mm. Both glasses were processed at a processing nozzle speed of 1.5 mm/s. The height difference of glass with a processing pitch of 1 mm was about 160 nm. The height of a processing pitch of 0.5 mm was about 30 nm. Reducing the processing pitch also reduced the processing depth. It was thought that the size of the injection nozzle had an effect. When the processing pitch is smaller than the size of the nozzle, the processing portions overlap. Therefore, it is considered that the processing depth decreases. It is thought that smaller uneven shape cannot be produced only by MSJ processing. The processing accuracy in the horizontal direction was required.

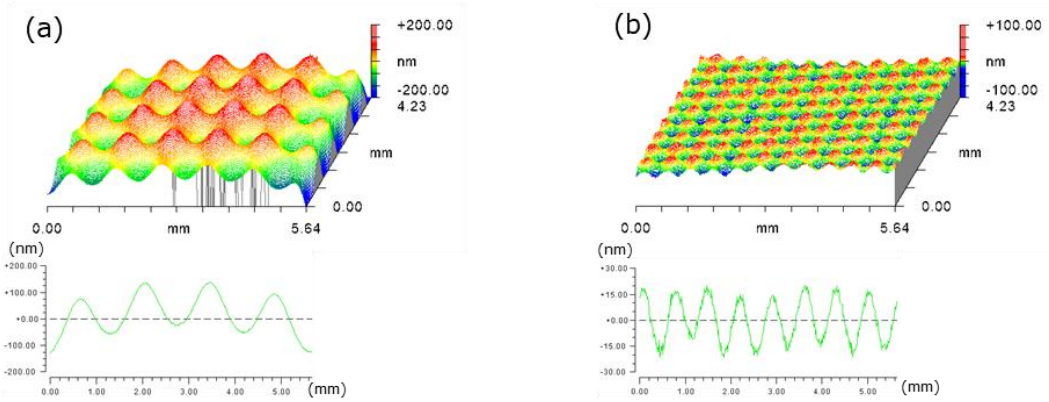

Fig. 5 Observation results of the glass after and the MSJ processing :(a) Pitch of processing 1.0 mm, (b) Pitch of processing 0.5 mm

Covering mask

A covering mask was used between the glass surface and the injection nozzle to improve the horizontal processing accuracy. The processing conditions of the MSJ were a processing pitch of 0.1 mm, and the nozzle speed was 3 mm/s, which was processed in a grid pattern. This glass was processed seven times under these conditions. The processed glass had a concave shape with a diameter of 495 μm. This glass processed according to mask design. This glass pattern was created with a depth of about 5 μm (Figure 6).

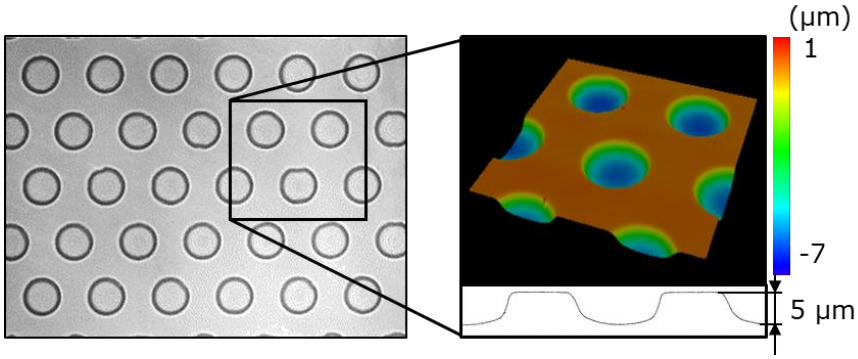

Fig.6 Observation results of the glass after covering mask and the MSJ processing

Micro masking process

Three patterns (30, 60, and 90 μm) in diameter were prepared to examine the size limit of the microstructure. Pattern pitch was prepared at twice the diameter. In addition, three target heights of photomask (15, 30, and 60 μm) were prepared to examine the height that can be created. A total of nine glasses were prepared. Figure 7 shows an observation image with target heights of 60 μm. These glasses after MWB processing is shown in Figure 8. Conical microstructures were created on surface of (b') and (c'). No uniform microstructure was created for (a'). Photomask peeled off during MSJ processing. This is because the diameter of the photomask is small and the height is high, so it was peeled off by the pressure of MSJ processing.

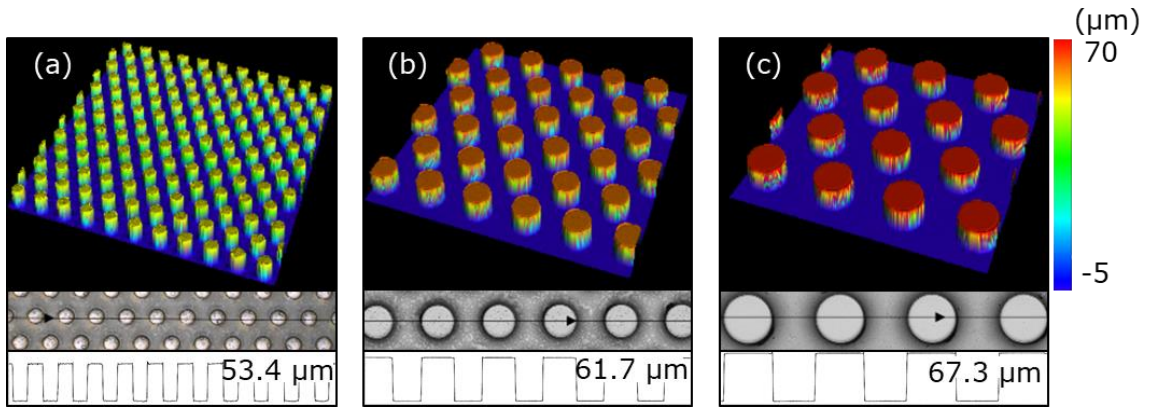

Fig.7 Observation results of the glass after the micro masking process :(a)Diameter 30 μm, (b)Diameter 60 μm, (c)Diameter 90 μm

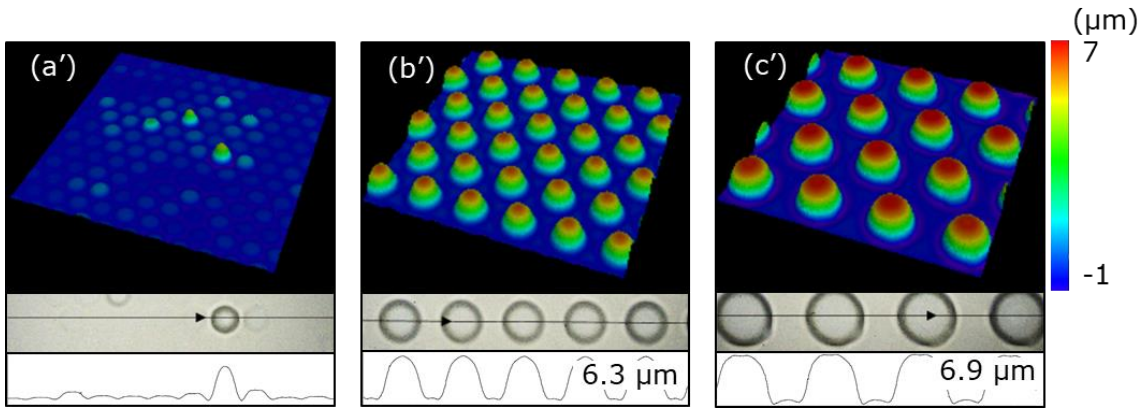

Fig.8 Observation results of the glass after the MSJ processing :(a')Diameter 30 μm, (b')Diameter 60 μm, (c')Diameter 90 μm

CONCLUSIONS

Glass surface was processed in nanometer order in the vertical direction of material surface by MWB processing. Furthermore, the surface was processed according to the mask design by using the covering mask. Various designs can be processed by changing the design of the cover mask. A convex structure was created by using photolithography technology in the masking process. Microstructure on glass surface created by MWB processing and micro masking process. The processing examples in this study show the possibility of creating microfabrication on the surface of artificial materials without using chemical removal processing or nanoprints that require molds. Furthermore, this shows that it can be a technology that enables a wide range of processing including curved surfaces and direct creation on limited-quantity product surfaces. The mechanism of this processing is relatively simple, the width of the material that can be processed is very wide, and it seems to have a wide range of applications.

REFERENCES

Al-Milaji, K. N. and Zhao, H., (2017), Fabrication of superoleophobic surfaces by mask-assisted electrospray, Applied Surface Science, Vol.396, pp.955–964.
Baba, T et al (2019), Micro slurry-jet for surface processing of dental ceramics, Biosurface and Biotribology, Vol.5, No.1, pp.8–12.
D.Ko,J.R.Tumbleston, et al, Biomimetic microlens array with antireflective moth-eye surface, Soft Matter, Vol.7, pp. 6404-6407
Ginestra, P. S., Madou, M. and Ceretti, E., (2019), Production of carbonized micro-patterns by photolithography and pyrolysis, Precision Engineering, Vol.55, pp.137–143.

Hussain, M et al (1996), Effects of coupling agents on the mechanical properties improvement of the TiO2 reinforced epoxy system, Materials Letters, Vol.26, No.6, pp.299–303.
Jheng, Y.-S, Lee, Y.-C (2016), Fabrication of micro/nano hierarchical structures with analysis on the surface mechanics, Applied Surface Science, Vol.384, pp.393‐399.
J. Zhang et al (2001), Characterization of the polymerization of SU-8 photoresist and its applications in micro-electro-mechanical systems, Journal of Polymer Testing, Volume 20, Issue 6 , pp 693-701
Nakanishi, Y et al, (2018) Influence of surface profile of Co-28Cr-6Mo alloy on wear behaviour of ultrahigh molecular weight polyethylene used in artificial joint, Tribology International, Vol.118, pp.538–546.
Psoma, S. D et al (2010), A novel enzyme entrapment in SU-8 microfabricated films for glucose micro-biosensors, Biosensors and Bioelectronics, Vol.26, No.4, pp.1582–1587.
Saito, Y et al (2008), Fabrication of microstructure on glass surface using micro-indentation and wet etching process, Applied Surface Science, Vol.254, pp.7243–7249.
Takashi Matsumura, Mitsuto Kakishita (2013), Parametric glass milling with simultaneous control, Journal of Manufacturing Processes, Vol 15, pp 1-7
Tokuhisa, H et al (2017), Fabrication of micro-textured surfaces for a high hydrophobicity by evaporative patterning using screen mesh templates, Applied Surface Science, Vol.400, pp.64–70.
Wei-Hsuan Hsu et al (2013), A method for in situ measurement of residual layer thickness in nano-imprint lithography, Microelectronic Engineering, Vol 110, pp 132-140
Yilian Xi et al (2018), A facile synthesis of silicon nanowires/micropillars structure using lithography and metal-assisted chemical etching method, Journal of Solid State Chemistry, Vol. 258, pp. 181-190
Zhang, M., Feng, S., Wang, L.Zheng, Y, (2016), Lotus effect in wetting and self-cleaning, Biotribology, Vol 5, pp. 31-43,

9th International Engineering Symposium - IES 2020
March 3-5, 2020, Kumamoto University, Japan

Experimental analysis of emission gas and fuel characteristics of diesel engine fueled by waste cooking oil biodiesel

Takumi Iwanaga [1] and Shuichi Torii[1]

1 *Department of Mechanical System Engineering, Kumamoto University, Kurokami, 2-39-1, Kumamoto 860-8555, Japan.*
email:181d8453@st.kumamoto-u.ac.jp

ABSTRACT: Biodiesel have higher NOx emissions than diesel but can be solved by emulsification. The objective of this study was the development of W/O emulsion fuel using CR-310. Emulsions were prepared using WOME (waste cooking oil methyl ester), CR-310 (tetraglycerin ester) alone for water-in-oil (W/O) emulsions. Samples containing 0.5 and 1% of surfactant concentration, separation occurs in one day, but at 2% or more, it is stable for over 1 month. If the water content is between 5 and 20%, it did not separate for over 1 month. In engine tests, NOx was reduced by up to 70%. With the increase of water content, CO emission also increases.

Keywords*: Emulsion fuel, Diesel engine, Biodiesel, Vegetable oil, Food science*

INTRODUCTION

Diesel engines are widely used as various power sources such as car and others, H. An (2018). However, CO, PM, and NOx emissions from diesel engines are causing damages in the global environment and ecosystems. In addition, the escalating cost of fossil fuels has become a serious problem. In this regard, the technical researchers are questing for alternative fuels resource, M. Senthil Kumar(2014). Vegetable oil is one of the alternative fuels. It is renewable, sustainable and carbon neutral energy, YOSHIMOTO Yasufumi(2009). It has most of the properties that is close to diesel and less polluting than fossil fuels. However, vegetable oils have high viscosity, and if used directly in an engine, combustion failure may occur, YOSHIMOTO Yasufumi(2009). The methods applying directly for diesel engine include preheating and transesterification. When the vegetable oil is heated to about 80 ℃, it has the same viscosity and performance as diesel fuel, Narayan LalJain(2017). Transesterification changes characteristics of vegetable oil. Viscosity is reduced by 90% and cetane number is promoted, Toshiya okazima(2015). Biodiesel is also biodegradable like vegetable oils and can reduce harmful emissions compared to fossil fuels. However, higher NOx emissions than fossil fuels have also been reported, Zhiqing Zhang(2019). Various studies have been conducted to reduce emissions, L. Wei(2018), S. Manigandan(2019) , Kim-Bao Nguyen(2014). Biodiesel-butanol blends produce 2 to 16% lower NOx emissions. While biodiesel-ethanol blends produce 5 to 46% lower NOx emissions, L. Wei(2018). Biodiesel-pentanol blends have lower combustion temperatures. Therefore, NOx emissions are lower than biodiesel, S. Manigandan(2019). It was found that the addition of water was effective in reducing both PM and NOx, Zhiqing Zhang(2019). The 15% water content in the rapeseed oil methyl ester emulsion reduces about 23% of NOx emission, Kazunori Hamasaki(2001). According to Zhiqing Zhang et al(2019)., NOx can be reduced even at low water content, though emulsion fuels usually increase CO emissions. While adding 6% water to biodiesel can reduce CO emissions by about 67%. However, these papers do not have information on the formation of emulsion fuel. Nor the data of long period stability of emulsion fuel. Therefore, this study focused on

surfactants used in food science, where many studies on emulsification were conducted. In the food science, PGPR is extensively used as a hydrophobic emulsifier, Jiahong Su(2006). Tetraglycerin Ester (CR-310) is one of the components of PGPR, R. WILSON(1988). Although it has been used as food science emulsifier for W/O emulsions, the effects of incorporating it in the biodiesel does not appear to have been previously reported. As Tetraglycerin Ester is commercially available and relatively cost-effective emulsifier, it may be possible to replace synthetic hydrophobic emulsifiers such as Sorbitan in the W/O emulsions. The objective of the present study was to investigate the conditions related to the effective of Tetraglycerin Ester as a hydrophobic emulsifier in biodiesel emulsions in which Waste cooking Oil Methyl Ester (WOME) was used as the oil phase. Furthermore, the emulsion was used to investigate the characteristics of exhaust gas.

Materials and Methods

The emulsion fuel of this study consists of three components and those were purchased from commercial sources with the highest available purity. Oil phase used in this experiment was commercial biodiesel, which was purchased from Nature and Future Inc., Japan. Tetraglycerin ester used in this experiment as surfactant (CR-310) was purchased from Sakamoto Yakuhin Kogyo Co., Japan. CR-310 is shown in Table 2 and Fig. 1. Distilled water was used as water phase. The ratio of experiments condition was carried out with varied ratio of oil, surfactant and water. Emulsion fuel was made by rotary homogenizer. Homogenization of the composed liquid is done by the using of rotary homogenizer (Model; AHG-160A, shaft; HT1018, AS ONE Company, Japan). The viscosity was measured by the viscometer of the BROOKFIELD. 0.5 mL of each samples were taken, and the viscosity were measured three times at 40 ℃ which it was used to obtain the average. Evaluation of emulsion was carried out by visual observation and heating value. In the visual observation, samples were fixed in the motionless environment and the separation between WOME and water were observed. Heating value was measured by calorimeter (SHIMADZU AUTO-CALCULATING BOMB CALORIMETER CA-4AJ, SHIMADZU Co.). Engine tests were conducted on a small engine (Yanmar, TF70V-E, 382cc, Yanmar Holdings Co., Ltd.). The gas emission was measured by Testo350 (Testo K.K.). WOME was used as the oil phase. Distilled water was used as the inner aqueous phase. The W/O mixture (150g) with a weight fraction of the inner aqueous phase of 5–20% was emulsified with a rotary homogenizer (12,000 rpm, 10 min, room temperature). Experiment A, B and C condition were shown in the Table 3, 4 and 5.

Results and discussion

Experiment A

Fig. 2 shows the sample after stirring (left) and the sample after one day (right). Separation (oil phase) is occurred in the sample 0.5 and 1.0 wt.% in which the concentration of the surfactant is low, and it can also be confirmed the separation range widened. On the other hand, samples with high concentration 2.0 and 4.0 wt.% show good stability for over 1 month. Al. Viktorija Eisinaite (2018) reported the condensed Ricinoleate Ester concentrations >1.5 wt.% emulsion was stable, and no macroscopic phase separation was observed after 1 week of storage. It is considered that by increasing the concentration of the surfactant, it was possible to increase the packing density of the amphiphilic substance (surfactant) at the interface, which promotes the reduction of the interfacial tension between the water and the oil creating good stability. In this result, it was possible to obtain good stability by adding at least 2.0% of CR-310 as an emulsifier using biodiesel fuel generated from waste cooking oil.

Experiment B

The homogenization temperature is one factor that determines the quality of emulsification. Fig. 3 is shown the comparison of homogenization temperature results.

The higher the temperature, the faster the separation speed while the lower the temperature, the slower the separation speed. When the emulsification temperature is high, the stability is lowered because the particles are unstable. However, when the surfactant concentration is high, due to the particles becoming stronger, the temperature effect is lost, allowing the emulsion to become stable, al. Yoshimasa Yamano.

Calculated water content

Water content and Heating value do not change greatly for 1 month. From this result, the water particles in the fuel are dispersed uniformly and stable for over 1 month. Fig. 5 show the results of water content and heating value. It is natural that as the water content increases, the heating value decreases. When the water content increases by 5%, the heating value decreases by about 20 kJ /g. The heating value decreases by up to 19%. However, although biodiesel have a lower heating value than pure diesel, oxygen content in biodiesel promotes thermal efficiency. It increased with the additional water content in emulsion fuel, al. Osama Ahmed Elsanusi.

Measurement of viscosity Fig. 6 shows the results of viscosity measurement. In this result, as the water content increases, the viscosity also increases. In both, O / W emulsions and W / O emulsions, the viscosity raised with increasing internal phase content, al. Yoshimasa Yamano. Alternatively, as the water content raised the water particle size decreased, the smaller the dispersed particle size, the higher the viscosity. The reason is that the smaller the particle size, the larger the interface area between water and oil, making the interaction between particles stronger, al. Kyoko Ohashi(2002). This result considers that as the water content increases, the particle size decreases. That reduction causes the increase of the interface between the water particles, as it increases, the viscosity also raises.

Engine test

NOx emission

The formation of NOx during the fuel combustion greatly depended upon the temperature and high activation energy. The high activation energy due to high temperature converted the atmospheric nitrogen into oxides of nitrogen, al. Suresh Vellaiyan(2019). The NOx emission (ppm) variation of all test fuels under different engine speed conditions is shown in Fig. 7. As shown in the figure, the water inclusion in WOME significantly reduces the formation of NOx, and an increase in the water concentration directly proportional to the drop in NOx emission. Water content over 15% reduces the combustion chamber temperature, allowing the greatly decrease in NOx gas emission. The sample as containing water 5% promotes a drop of 4.7% in NOx emission at 2000rpm engine speed condition compared to pure Straight Biodiesel (SB), whereas the sample as containing water 20% exhibits a drop of 73.2%. At higher engine speed, the micro explosion occur more often, therefore those are probably the reason why NOx emissions and combustion chamber temperature decrease. These results prove that water in fuel is effective in reducing the harmful emissions of NOx. Increasing water concentrations in emulsion fuel reduced NOx emissions significantly compared to WOME NOx emissions measured.

At high water content, relative of NOx gas emission decreases as engine speed increases. A. Bulent Koc. reported it is because of water droplets on the combustion that the peak ignition temperature was reduced, decreasing the NOx formation, al. A. Bulent Koc(2013).

CO emission

The formation of CO in the diesel engine is due to insufficient oxygen supply and combustion duration to completely convert the CO into CO2. The CO emission variation of all test fuels 2000rpm conditions is depicted in Fig. 8. The CO emission became low at

reduced water content in WOME emulsion, and a remarkable increase is observed at high water content. As the water content increases, the cooling effect increases, due to this effect, the CO which was supposed to turn into CO2, remain unchanged. Another explanation for the CO increase is the water gas shift reaction occurrence, when the water reacts with the free carbon, al. Kazunori Hamasaki. However, even the maximum concentration of CO is within the regulatory limits of Japan (1,100pp). H. An reported that the trends of CO emission and engine speed were significantly affected by the engine load. If the load on the engine is increased, CO emission decrease. This is because with further increase in the engine load, the fuel injection pressure also increases so that the viscosity effect of biodiesel becomes less dominant.

Fuel consumption

The Brake Fuel Consumption (BFC) of all test fuels is represented in Fig. 9. The consumption of emulsion fuel is higher when comparing biodiesel. However, in order to evaluate the fuel consumption in emulsion fuel, the exact amount of biodiesel is considered as total fuel consumption in the present work, instead of considering water + biodiesel as a total fuel. Therefore, there is no considerable difference in the fuel consumption in this experiment. The sample with 20% water content is slightly higher at 1000 and 1500 rpm but is similar to the other samples at 2000 rpm. From relative BFC, there is no difference in it. On the other hand, Brake Specific Fuel Consumption (BSFC) decreases as the water content increases. The reason why the micro-explosion occur during the secondary atomization is the rapid evaporation of water particles that are initially contained in the oil drop and slashing up the droplet into fine particles [23].

Conclusion

In this study, the stability and exhaust gas of WOME emulsions using Tetraglycerin Ester have been evaluated. Biodiesel emulsions containing various water concentrations have been prepared and tested for their engine performance and exhaust gas.

1. The surfactant concentrations were 0.5 - 5%. The water concentration varied between 5 - 20%. It was possible to obtain satisfactory stability by adding at least 2.0% of CR-310 as an emulsifier in the biodiesel fuel generated from waste cooking oil.
2. Emulsion fuels using CR-310 stabilize at a water content between 5 - 20% for over 1 month.
3. The water content held by the emulsion fuel did not change for more than 1 month.
4. Since there was no load applied in this experiment, it is going to be applied in the future.

References

[1] H. An, W.M. Yang, S.K. Chou, K.J. Choa, Combustion and emissions characteristics of diesel engine fueled by biodiesel at partial load conditions, ELSEVIER, Contents lists available at SciVerse ScienceDirect, Applied Energy, Volume 99, November 2012, Pages 363-371

[2] M. Senthil Kumar, M. Jaikumar, A comprehensive study on performance, emission and combustion behavior of a compression ignition engine fuelled with WCO (waste cooking oil) emulsion as fuel, Journal of the Energy Institute, Volume 87, Issue 3, August 2014, Pages 263-271

[3] YOSHIMOTO Yasufumi, KINOSHITA Eiji, Applied Technology of Vegetable Oils for Diesel Engines -Use of Biodiesel Fuel-, Journal of Japan Society of Combustion Research, Volume 51, 2009, Pages 121-128

[4] Narayan LalJain S. L. Soni M. P. Poonia DilipSharma Anmesh K. Srivastava HardikJain, Performance and emission characteristics of preheated and blend thumba vegetable oil in a compression ignition engine, Applied Thermal engineering, Volume 113, 25, February 2017, pp.970-979

[5] Toshiya okazima and Takeru shima. (2015)On the Difference of the Reactivity of Ester-exchange reaction by the Number of Carbon atoms of Alcohols,Fac. Saga Univ. Vol19, No2 pp.235-243
[6] Zhiqing Zhang, Jiaqiang E, Jingwei Chen, Hao Zhu, Xiaohuan Zhao, Dandan Han, Wei Zuo, Qingguo Peng, Jinke Gong, Zibin Yin, Effcts of Low-level water addition on spray, combustion and emission characteristics of a medium speed diesel engine fueled with biodiesel fuel, ELSEVIER, Fuel, Volume 239, 1 March 2019, Pages 245-262
[7] L. Wei, C.S. Cheung, Z.Ning, Effect of biodiesel-ethanol and biodiesel-butanol blends on the combustion, perfoemance and emission of diesel engine, ELSEVIER, Energy, Volume 155, 15 July 2018, Pages 957-970
[8] S. Manigandan, P.Gunasekar, JDevipriya, S.Nithya, Emission and injection characteristics of biodiesel blends in diesel engine, ELSEVIER, Fuel, Volume 235, 1 January 2019, Pages 723-735
[9] Kim-Bao Nguyen, Tomohisa Dan, Ichiro Asano, Combustion, performance and emission characteristics of direct injection diesel engine fueled by jatropha hydrogen peroxide emulsion, ELSEVIER, Energy, Volume 74, 1 September 2014, Pages 301-308
[10] G.R. Kannan, R. Anand, Experimental investigation on diesel engine with distro water micro emulsion, ELSEVIER, Energy, Volume 36, Issue 3, March 2011, Pages 1680-1687
[11] Orkun Özener, Levent Yüksek, Alp Tekin, Ergenç, Muammer Özkan, Effects of soybean Biodiesel on a DI diesel engine performance, emission and combustion characteristics, ELSEVIER, Fuel, Volume 115, January 2014, Pages 875-883
[12] K.A.Abed, A.K.El Morsi, M.M.Sayed, A.A. ElShaib, M.S.Gade, Effect of waste cooking oil biodiesel on performance and exhaust emissions of a diesel engine, ELSEVIER, Egyptian Journal of Petroleum, Volume 27, Issue 4, December 2018, Pages 985-989
[13] Sahar, Sana Sadaf, Javed Iqbal, Inam Ullah, Haq Nawaz, Bhatti, Shazia Nouren, Habib-ur-Rehman, Jan Nisar, Munawar Iqbal,Biodiesel production from waste cooking oil: An efferent technique to convert waste into biodiesel, ELSEVIER, Sustainable cities and Society, Volume 41, August 2018, Pages 220-226
[14] Kazunori Hamasaki, utilization of Emulsified Vegetable Oil Methyl Esters for Diesel Fuel, Transactions of the Japan Society of Mechanical Engineers, Volume 67, Pages 2001-2011
[15] Jiahong Su, John Flanagan, Yacine Hemar, Harjinder Singh, Synergistic effect of polygycerpl ester of polyricinoleic aicid and sodium caseinate on the stabilization of water-oil-water emulsion, ELSEVIER Food Hydrocolloids, Volume 20, Issues 2-3, March-May(2006), Pages 261-268
[16] R. WILSON, B. J. Van SCHIE and D. HOWES, Overview of the preparation, Useand biological studies on Polyglycerol Polycinolate, ELSEVIER, Fodd and chemical Toxicology, Volume 36, Issue9-10, September-October(1998), Pages711-718
[17] Viktorija Eisinaite, Patricia Duque Estrada, Karin Schroën, Claire Berton-Carabin, Tayloring W/O/W emulsion composition for effective encapsulation: The role of PGPR in water transfer-induced swelling, ELSEVIER Food Research International 106(2018), Pages 722-728
[18] Yoshimasa Yamano, Kazuhiko Ueda, Eiko Mki, Effect of Emulsifing Conduction on Emulsification with Soybean Lecithin, Yoshimasa Yamano, Kazuhiko Ueda, Eiso Miki, Nippon shokuhin kogyo Gakkai, Volume 30, No. 2, Pages 73-78
[19] S.S.RehamaH.H.MasjukiaM.A.KalamaI.ShancitaaI.M.Rizwanul FattahbA.M.Ruhul, Study on stability, fuel properties, engine combustion, performance and emission characteristics of biofuel emulsion, ELSEVIER Renewable and Sustainable Energy, Volume 52, December 2015, Pages 1556-1579
[20] Osama Ahmed Elsanusi, Murari Mohon Roy, Manpreet Singh Sidhu, Experimental Investigation on a Diesel Engine Fueled by Diesel-Biodiesel Blends and

their Emulsions at Various Engine Operating Conditions, ELSEVIER Applied Energy, Volume 203, 1 October 2017, Pages 582-593
[21] Yoshimasa Yamano, Toshiyuki Tsuru, Shiro Sugihara, Stability and Viscosity of Monoglyceride Emulsion, Nippon Shokuhin Kogyo Gakkaishi Vol. 29, NO. 3, Pages 137-142.
[22] Kyoko Ohashi, Atsuko Shimada, Emulsifying Properties of Diacylglycerol in a Concentrated Oil-in-water Emulsion System, Journal of the Japan Cooking Association, Volume 35(2002), Pages 132-138.
[23] Suresh Vellaiyan, Enhancement in combustion, performance, and emission characteristics of a biodiesel – fueled diesel engine by using water emulsion and nanoadditive, ELSEVIER Renewable Energy, Available online 30 July 2019
[24] A. Bulent Koc, Mudhafar Abdullah, Peformance and NOx emission of a diesel engine fueled with biodiesel-diesel-water nanoemulsions, ELSEVIER Fuel Processing Technology, Volume 109, May 2013, Pages 70-77
[25] Kazunori Hamasaki, Ayako Hirotsu, Choesnul JAQIN, Koji Takasaki, Takayuki Oyama, Utilization of Emulsified Vegetable Oil Methyl Esters for Diesel Fuel, Transaction of the Japn ociety of Mechanical Engineers(B), Volume 67, Issue 663, Pages 2001-2001.

Table 1 Detail of Wome

Test items	Unit	Result
Ester content	wt.%	99.6
Density@15℃	g/cm^3	0.8824
Kinematic viscosity@40℃	mm^2/s	4.238
Heating value	J/g	39,636
Flash point	℃	180
Sulfur content	wt.%	0.0001
Cetane number	---	51.0
water content	mg/kg	110
Aicid number	mgKOH/g	0.08
Lodine value	gI2/100g	113
Pour point	℃	-7.5

Table 2 Detail of CR-310

	Composition	HLB number
CR-310	Tetraglycerin ester	1.5±0.5

Table 3 Experiment A condition

	WOME (wt.%)	DW (wt.%)	S (wt.%)
Sample 1	79.5	20	0.5
Sample 2	79	20	1
Sample 3	78	20	2
Sample 4	76	20	4

Table 4 Experiment B condition

	Temperature (℃)
Sample 1	10
Sample 2	30
Sample 3	50

Table 5 Experiment C condition

	WOME (wt.%)	DW (wt.%)
Sample 1	90	5
Sample 2	85	10
Sample 3	80	15
Sample 4	75	20

Fig. 1 CR-310

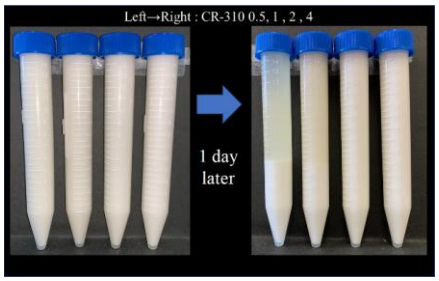

Fig. 2 Comparison of several surfactant content

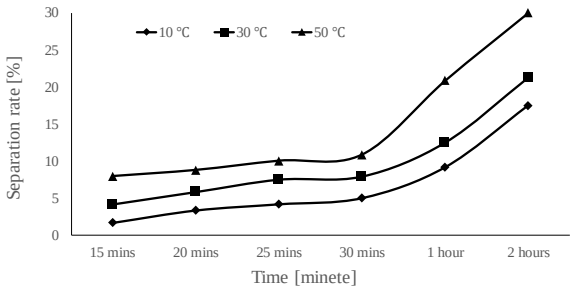

Fig. Comparison of homogenized temperature

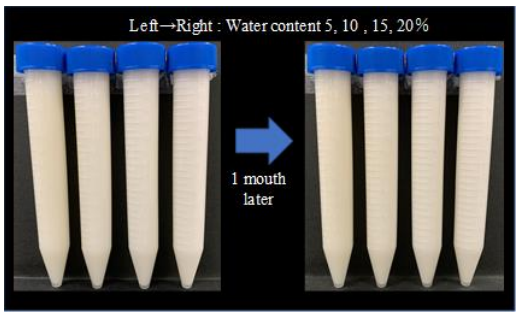

Fig. 4 Comparison of water content

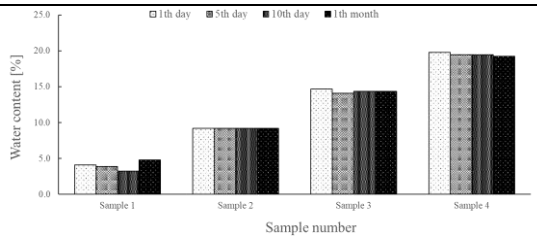

Fig. 5 Heating value

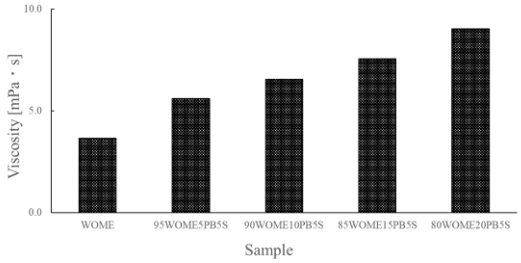

Fig. 6 Viscosity

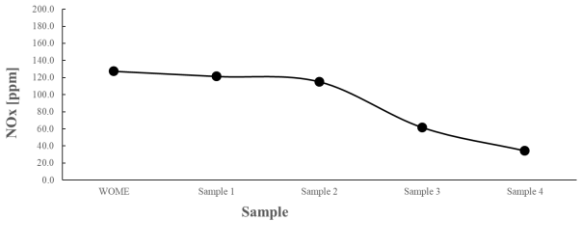

Fig. 7 NOx emission

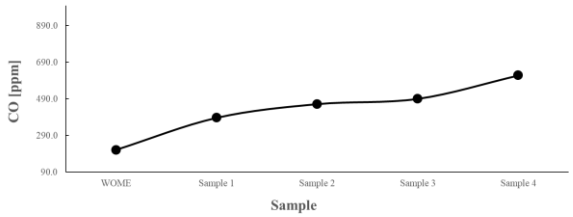

Fig. 8 CO emission

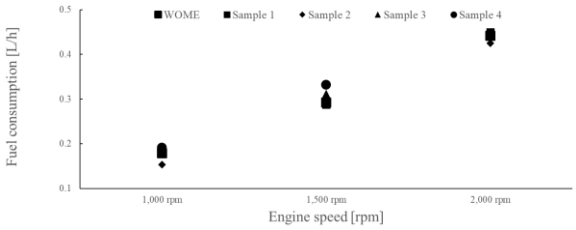

Fig. 9 fuel consumption

9th International Engineering Symposium - IES 2020
March 3-5, 2020, Kumamoto University, Japan

Influences of microplastics on living tissue of aquatic organism

Keisuke NOGUCHI [1], Yuta NAKASHIMA [2] and Yoshitaka NAKANISHI [3]

1 *Faculty of Engineering Kumamoto University, Kumamoto University, Kurokami 2-39-1, Chuo-ku, Kumamoto 860-8555, Japan*
E-mail : 161t3808@st.kumamoto-u.ac.jp
2 *Faculty of Advanced Science and Technology, Kumamoto University, Kurokami 2-39 Chuo-ku, Kumamoto 860-8555, Japan*
E-mail : yuta-n@mech.kumamoto-u.ac.jp
3 *Faculty of Advanced Science and Technology, Kumamoto University, Kurokami 2-39 Chuo-ku, Kumamoto 860-8555, Japan*
E-mail : y-naka@mech.kumamoto-u.ac.jp

ABSTRACT: In recent years, it has become a problem that microplastics are found in the sea. Microplastics have been accumulated in aquatic organisms, finally are thought to affect ecosystems. In particular, particles smaller than 1 mm may move from the digestive system to the vascular system. In this study, fine particles were given to arthropods in an environment similar to ecosystems, how fluorescent plastic fine particles migrated and accumulated in tissues, and their effects were observed on paraffin tissue sections, etc. It was revealed by histological observation. This research has contributed to clarifying the effects of microplastics and the chemical substances contained in them on aquatic organisms.

***Keywords**: Microplastic, Aquatic organisms, Tissue*

INTRODUCTION

In recent years, microplastics in the ocean have been attracting attention as major environmental problems worldwide. First, what is microplastic? Microplastics are plastic particles less than 5mm in diameter that result from the decomposition of plastic products into small pieces by mechanical action, UV radiation, or thermal oxidation. Until now, research on microplastics has attracted much attention to macro-sized plastics. However, it has been found that micro-sized plastics are present, and the effect on small organisms of lower trophic levels, which has not received much attention until now, is regarded as dangerous. Therefore, we focused on the micro size among micro plastics. Microplastic additives and adsorbent chemicals have been shown to be a source of internal exposure in ingested organisms and have adverse effects. However, when the size of microplastic becomes micron, it is considered that it also acts as a physical foreign matter. Therefore, in this study, microplastics were given to aquatic organisms, and histologically revealed how microplastics migrate, accumulate in living tissues, and affect them.

MATERIALS AND METHODS

Polystyrene, a fluorescent particle, was used for the microplastic for testing. Tween 80, a surfactant, was applied to make the surface properties of the particles uniform. The animals used for the experiment were Caridina multidentata in view of size and other factors. In the experiment, five types of microplastics with particle sizes of 1.1 μm, 0.49 μm, 0.2 μm, 0.15 μm, and 0.046 μm were prepared, and 1.0×10^8 microplastics were used. Figure 1 shows the breeding protocol. Put the shrimp in the water left for one day and fast for two days to discharge the accumulated wastes. After that, the shrimp were transferred to water containing microplastic and observed for 3

days. Animals were checked for mortality once every 12 hours during particle exposure and mortality due to microplastic ingestion was estimated. Experimental and post-experimental animals that died during these three days were immediately stored in bottles containing 10% neutral buffered formalin solution. After that, paraffin fixation was performed, paraffin sections were prepared with a microtome, and the place where the microplastics migrated to the biological tissue was observed using an inverted microscope.

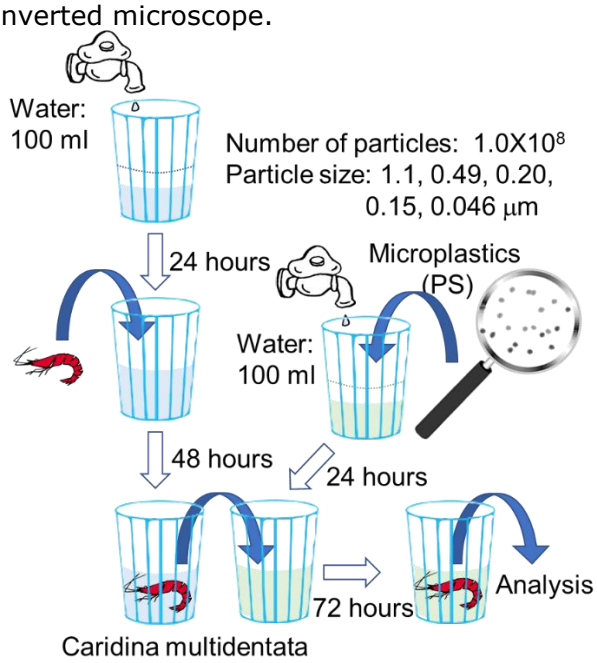

Fig.1 Breeding method of shrimp.

RESULTS AND DISCUSSION

As a result of this experiment, the digestive tract was clogged with only shrimp that gave 0.2 μm particles. Figure 2 shows micrographs of shrimp (1) with and without particles (2). Looking at Figure 2, you can see that the digestive tract is clogged with black material. Figure 3 shows the results of fluorescence observation of each area with an inverted microscope. You can see the fluorescence and you can see that the digestive tract is clogged with microplastic. No fluorescence was observed outside of the digestive tract of D.

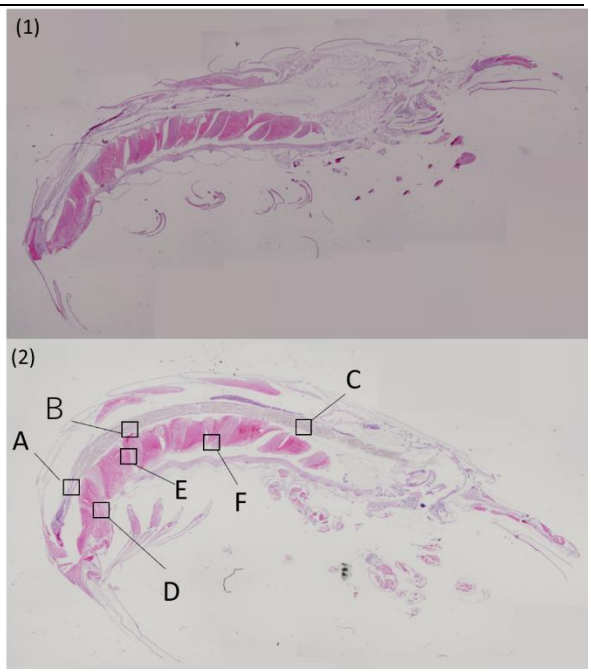

Fig.2 Tissue sections with and without particles.

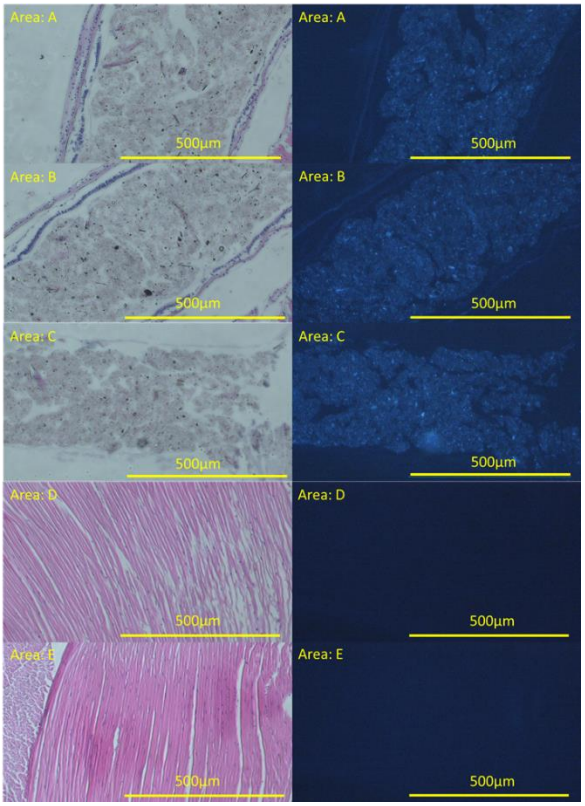

Fig.3 Enlarged view and fluorescence image of each area

REFERENCES

[1] Klingelhöfer, Doris, et al. "Research landscape of a global environmental challenge: Microplastics." *Water Research* 170 (2020): 115358.

9th International Engineering Symposium - IES 2020
March 3-5, 2020, Kumamoto University, Japan

Influences of microplastics on human immune system

Masaki Morita [1], Haruki Miyamoto [2] and **Yoshitaka Nakanishi[3]**

1 *Faculty of Engineering Kumamoto University,Kurokami 2-39-1, Chuo-ku, Kumamoto 860-8555, Japan*
e-mail;165t3837@st.kumamoto-u.ac.jp
2 *Graduate School of Advanced Science and Technology, Kumamoto University, Kumamoto 860-8555, Japan*
e-mail;193d8482@st.kumamoto-u.ac.jp
3 *Faculty of Advanced Science and Technology, Kumamoto University*
2-39-1 Kurokami, Cyuo-ku, Kumamoto, 860-8555, Japan
email;y-naka@mech.kumamoto-u.ac.jp

ABSTRACT: With the widespread use of plastic products, microplastics have become a problem. There are many microplastics in the sea. It is said that microplastic accumulates in the human body as humans eat marine organisms such as fish that have eaten microplastic. Microplastic may extend to the immune system. In order to investigate how plastic affects the human immune system, macrophages derived from human monocytes were seeded and phagocytosed by microplastics with different sizes. A channel device using microelectromechanical system (MEMS) technology was used to cause macrophages to phagocytose microplastic more. The amount of inflammatory cytokine produced when macrophages phagocytosed microplastic was investigated. This experiment shows the influence of the size of microplastic on the reactions that occur in the human body.

***Keywords**: Microplastic, Macrophages, MEMS, Proinflammatory cytokine, Immune response*

INTRODUCTION

In recent years, microplastics drifting in the ocean has come to be a problem. An estimated 8 million tons of plastic waste is expected to enter the ocean each year, with an additional single digit increase by 2025.
In the natural environment, plastic products are decomposed by mechanical action, UV radiation, or thermal oxidation, which results in a large number of small pieces. Thus, what plastic flowed out into the environment has become a small strips (5mm or less) by external factors it is said to be a secondary plastic.
The problem caused by microplastics that have been studied so far is often studied around the size of 5mm or less, most of which focused on the problem when chemicals adhering to the plastic has melted.
Therefore, we focused on the particles in microns among microplastics. When the size of the particles is several hundred micrometers or less, it is considered to act as a physical foreign body.
Specifically, the transition and accumulation of marine and terrestrial organisms to the body tissue is made, it is considered that phagocytosis by macrophages is performed. Macrophages phagocytosis foreign substances that have invaded the body, decomposition, is a cell to digest. This is thought to happen to human macrophages in the human body.

Marine life such as small fish sometimes mismakes microplastics floating in the sea for food. In fact, it has been reported that the zooplankton is eating microplastics mistaken for phytoplankton, and that microplastics have been found in the stomachs of small fish. By eating large fish and humans, microplastics accumulate in the human body, which can affect the human body.
Therefore, in this study, using a microdevice using Bio-MEMS technology, we exposed fine microplastics to macrophages derived from human monocytes and performcell tests, and the state of the phagocytosis of macrophages, Inflammatory cytokines generated during phagocytosis were investigated and the effects of microplastics on the human immune system were investigated..

MATERIALS AND METHODS

Fig. 1 shows a schematic diagram of the experimental apparatus. For the test microplastic, polystyrene, which is a fluorescent particle, was used. In order to make the surface characteristics of the particles uniform, Tween 80, a surfactant, was applied. Then, a microfluidic device was fabricated so that the particles could easily react with macrophages, and a liquid transfer experiment was performed under conditions close to the human body environment. The production of inflammatory cytokine IL-6 was evaluated using an ELISA sandwich method.

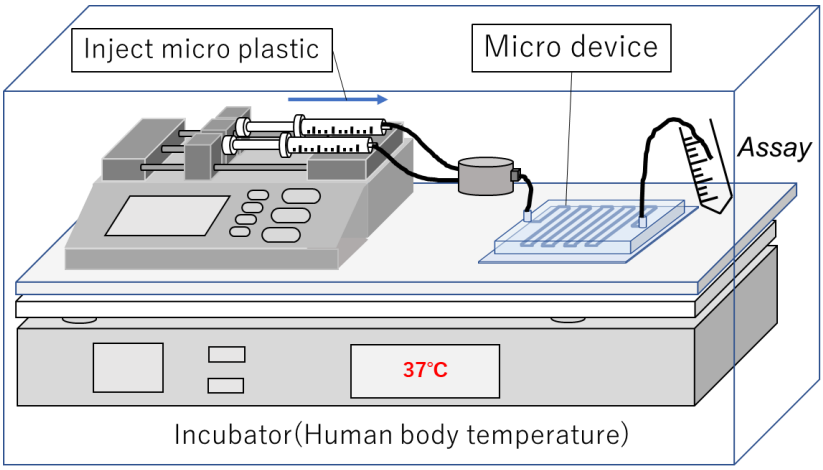

Fig.1 Schematic diagram of experimental equipment

RESULTS AND DISCUSSION

Fig. 2 shows microscopic observation photographs of macrophages before and after the experiment. The decrease in macrophages after the experiment may be due to the end of phagocytosis and detachment. It can be observed that the fluorescent particles are incorporated into the macrophages. The amount of inflammatory cytokine production is shown in Fig. 3. It was confirmed that the function of cells was produced by the micron-sized microplastic particle system.

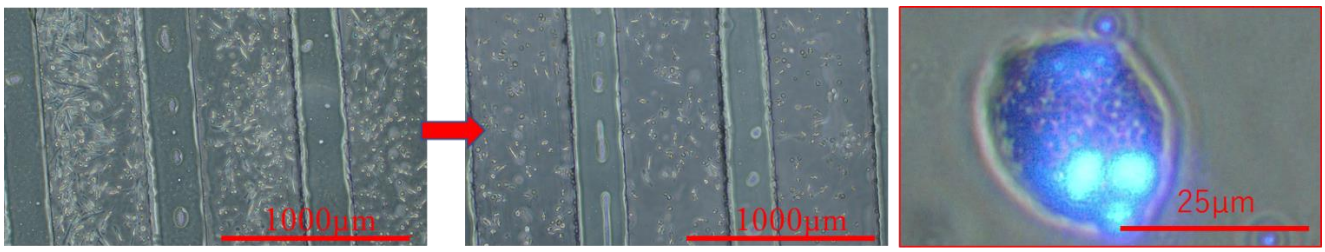

Fig.2 Macrophages before and after the experiment

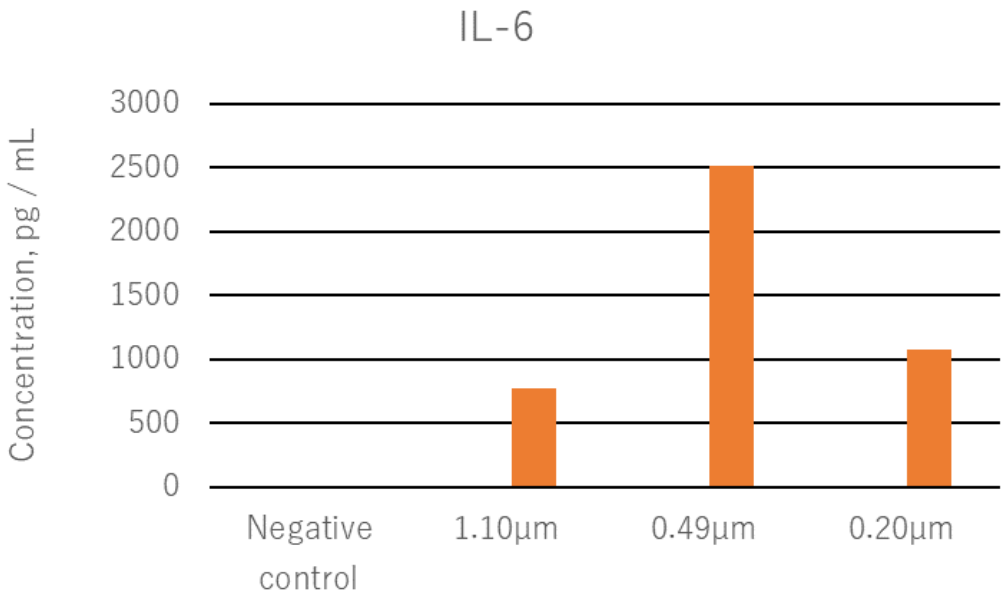

Fig.3 Cytokine production

CONCLUSIONS

When microplastics affect the human immune system, their particle size may be a significant factor.

REFERENCES

References should be given in alphabetical order. (font to be used: Verdana 8)
[1] Andrady, Anthony L. "Microplastics in the marine environment." Marine pollution bulletin 62.8 (2011): 1596-1605.
[2] Jambeck, Jenna R., et al. "Plastic waste inputs from land into the ocean." Science 347.6223 (2015): 768-771.
[3] Zhong-Min Wang. "SEM/EDS and optical microscopy analyses of microplastics in ocean trawl and fish guts", Science of The Total Environment, (2017): 616-626.

9th International Engineering Symposium - IES 2020
March 3-5, 2020, Kumamoto University, Japan

New brace for upper limb joint in order to improve tremor disorder

Hajime Yamaguchi [1], Haruki Miyamoto [2], Kazuhiko Tokuda[3], Wakana Togami[4], Eiichi Nakamura[5], Yuta Nakashima[6], Yoshitaka Nakanishi[7]

1 *Faculty of Engineering, Kumamoto University, 2-39-1 Kurokami, Chuo-ku, Kumamoto, 860-8555, Japan.*
Email:163t3841@st.kumamoto-u.ac.jp
2 *Graduate school of Science and Technology, Kumamoto University, 2-39-1, Kurokami, Chuo-ku, Kumamoto, 860-8555, Japan.*
Email:193d8482@st.kumamoto-u.ac.jp
3 *Tokuda artificial limbs factory, 6-27-20 OOe, Chuo-ku,Kumamoto, 862-0971, Japan.*
Email: kazuhiko.tokuda@tokuda-gishi.co.jp
4 *Faculuty of Life science, Kumamoto University, 1-1-1 Honjo, Chuo-ku, Kumamoto,860-8556, Japan.*
Email: wakana.desu@kuh.kumamoto-u.ac.jp
5 *Faculty of Life Advanced Science and Technology, Kumamoto University, 2-39-1 Kurokami, Chuo-ku, Kumamoto,860-8555, Japan.*
Email: ei.nakamura@reha-kaiseikai.or.jp
6 *Faculty of Life Advanced Science and Technology, Kumamoto University, 2-39-1 Kurokami, Chuo-ku, Kumamoto, 860-8555, Japan.*
Email: yuta-n@mech.kumamoto-u.ac.jp
7 *Faculty of Life Advanced Science and Technology, Kumamoto University, 2-39-1 Kurokami,Chuo-ku,Kumamoto,860-8555,Japan.*
Email: y-naka@mech.kumamoto-u.ac.jp

ABSTRACT: *A brace for upper limb joint in order to improve tremor disorder has been developed. The frictional torque at the joint in the brace could be adjusted by the screw-nut in order to moderate the patient's tremor disorder. The purpose of this study is to elucidate the frictional behaviour of the brace joint during the flection-extension movement. The durability test was also performed, and the service life of the brace was also discussed.*

***Keywords**: Surface engineering, Essential tremor, Wearable, Brace, Medical and engineering collaboration*

INTRODUCTION

Essential tremor is one of the most common involuntary movements in the elderly. It is the most commonly found in the upper limb. The American Academy of Neurology treatment guidelines and the standard neurotherapy "Essential tremor" provide the general treatment strategy. The standard neurotherapy "Essential tremor" describes three types of treatments, in which pharmacotherapy, botulinum toxin therapy, and surgery are explained.

The incidence rate at the elderly patients is high, and the elderly patients often have a complication of cardiac dysfunction and dementia, so that careful treatment is necessary when adapting to pharmacotherapy or surgical therapy. Adopting the brace is one of the mechanical system, which moderate the tremor by using externally forces. For example, wearable robots for eating were developed, in which pneumatic pressure controls the tremor.

The purpose of this study is to elucidate the frictional behavior of the brace joint during the flection-extension movement.

MATERIALS AND METHODS

The brace adopted was shown in Fig.1. At the joint area, the frictional torque controlling system was installed. The system composed of discs made of vinyl chloride and a Poly-Lactic Acid, and those discs were connected and tightened by using a screw-nut pair. The friction generated between these vinyl chlorides would adjust the patient's tremor disorder. Fig.2 shows a general view of experimental device. The brace was attached to the device in order to apply its flection-extension movement. A tightening torque was applied to the screw-nut pair in the range of 0.155~0.917[N・m], and the moving angle was 150° .

Then, the flection-extension movements were applied to the brace for 10 cycles. The frictional torque generated from the discs was measured by the strain gauges attached to the connecting bars between a motor and the brace.

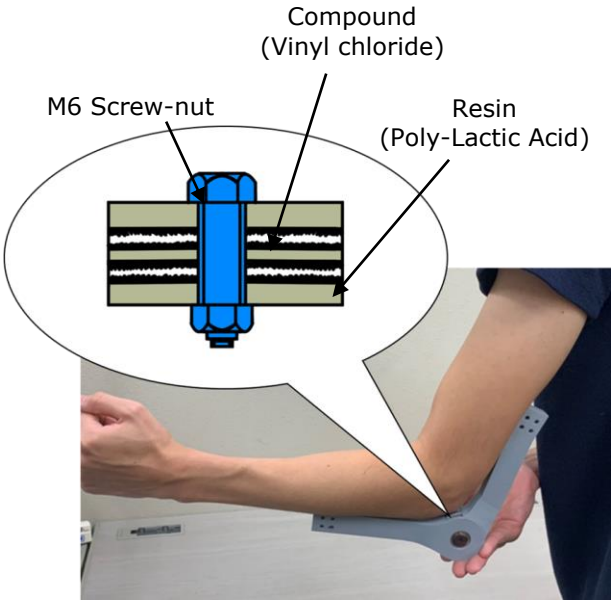

Fig.1 Brace and its friction mechanism

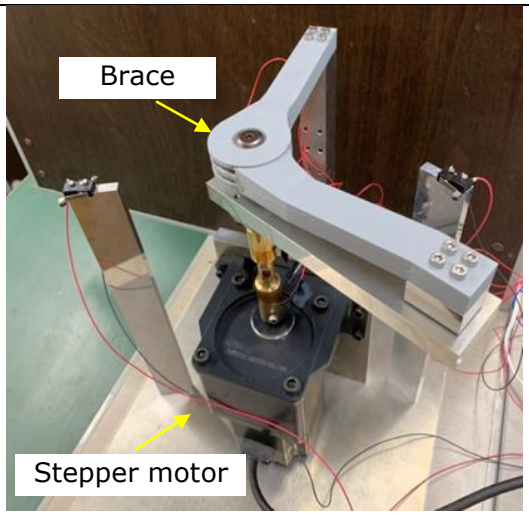

Fig.2 Experimental device and brace

RESULTS AND DISUCUSSION

Fig.3 shows the measured frictional torque. Extension side is over 0.0 N・m, flection side is under 0.0 N・m. The mean value of frictional torque during flection was not the same during extension. Frictional torque during the movement were not constant, and the higher value was recorded nearby the end of cycle. At the end of cycle, the speed of movement was lower, so that the frictional torque has influenced by the rotational speed. Fig.4 shows the relationship between the measured maximum frictional torque and the tightening torque to the screw-nut pair in flection direction. Non-liner correlation was detected, that was thought to adjust the frictional torque.

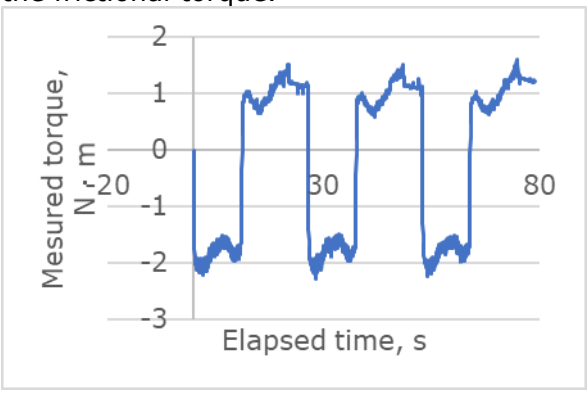

Fig.3 Relationship between elapsed time, measured torque and motor speed when tightened with any torque

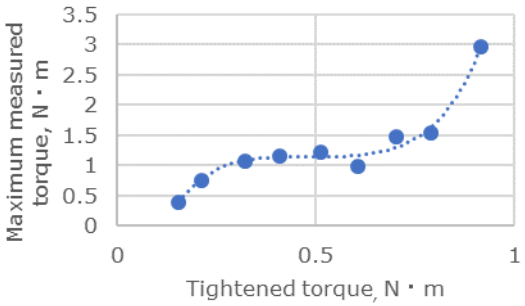

Fig.4 Relationship between the measured torque and the tightened torque in flection directions

REFERENCES

[1]Yssaku Nakamura. "Diagnosis and treatment of essential tremor." Neurotherapeutics. 34.4 (2018): 364-367.

[2] Yusaku Nakamura. "Standard Neurotherapy: Essential Tremor||| Treatment: General." Neurotherapy 28(2011):308312

[3] Yuya Matsumoto, et al."3P2-X07 Construction of a method for identifying the degree of freedom of tremor occurrence in essential tremor patients based on measurement of hand acceleration and posture of upper limb(nursing and mechatronics)." Abstracts of Robotics and Mechatronics 2014. The Japan Society of Mechatronics Engineers. 2014

[4] Yasutaka Nishioka, Kentaro Kojima, and Toshihiko Yasuda."2A1-H02 Development of a lightweight, compact, low-restraint pneumatic orthosis to support patients with essential tremor. "Proceedings of the Robotics and Mechatronics Conference 2015. General The Japan Society of Mechanical Engineers,2015.

[5] Zesiewicz, T. A., et al. "Practice parameter: therapies for essential tremor: report of the Quality Standards Subcommittee of the American Academy of Neurology." Neurology 64.12 (2005): 2008-2020.

9th International Engineering Symposium - IES 2020
March 3-5, 2020, Kumamoto University, Japan

Evaluation of emotional change by viscous liquid on palm skin

Sho Hosokawa [1], Nana Motozima[2]
Yuta Nakashima[3] and *Yoshitaka Nakanishi*[4]

1 *Faculty of Engineering, Kumamoto University, Kurokami 2-39-1, Chuo-ku, Kumamoto 860-8555, Japan*
E-mail: 167t3819@st.kumamoto-u.ac.jp
2 *Graduate School of Science and Technology, Kumamoto University, Kurokami 2-39-1, Chuo-ku, Kumamoto 860-8555, Japan*
E-mail: 188d8530@st.kumamoto-u.ac.jp
3 *Faculty of Advanced Science and Technology, Kumamoto University, Kurokami 2-39 Chuo-ku, Kumamoto 860-8555, Japan*
E-mail: yuta-n@mech.kumamoto-u.ac.jp
4 *Faculty of Advanced Science and Technology, Kumamoto University, Kurokami 2-39 Chuo-ku, Kumamoto 860-8555, Japan*
E-mail: y-naka@mech.kumamoto-u.ac.jp

ABSTRACT: Various effects have been observed when a viscus liquid is contacting on the skin, but there are few reports on changes in the emotional state (unpleasant, sensual, fun, etc.) The purpose of this study is to use psychophysiological indicators to elucidate the investigate emotional changes caused by viscous liquid on the skin. Newtonian liquid and Non-Newtonian liquid with various viscosities were prepared. The temperature of each liquid used was 33℃. The subjects were (eight males in their twenties,) blindfolded, and then touched the liquid. Frequency analysis was performed by using the recorded heart rate activations during the trial, and autonomic nervous activity was estimated. In this experiment, the activation of autonomic nerves was changed depending on the type of Newtonian characteristics, even when the temperature and viscosity were approximately the same.

***Keywords**: Viscous liquid, Emotion, Viscosity, Newtonian liquid, Non-Newtonian liquid*

INTRODUCTION

We constantly experience the presence of "slimy" viscous liquids in our hands. The purpose is to clean and moisturize the skin. Rubbing the viscous liquid between the palms provides "fun", "comfortable", "sensual", "unpleasant", or "disgust" feeling.

The purpose of this study is to investigate the relationship between viscous liquid and emotional change using a heart rate sensor and questionnaire**.**

MATERIALS AND METHODS

Fig.1 shows the experimental situation. The subjects were eight males in their twenties, and each subject was isolated in different place so that they did not interfere with each other. Newtonian fluids and non-Newtonian fluids were provided to their palms. The Newtonian fluid was a water solution of polyvinyl alcohol (PVA), and the Non-Newtonian fluid was of polyethylene glycol (PEG). The viscosity was adjusted, in three different viscosities, from the range of 0.01 to 100 Pa·s.

The questionnaire consisted of a semantic differential method was also performed, and the results were plotted it on an 8-axis circular layout extending radially from the center point. Emotional words were placed on each axis. The arrangement was based on Russell's circle of emotions (Emotional circle).

Fig. 1 Experimental situation

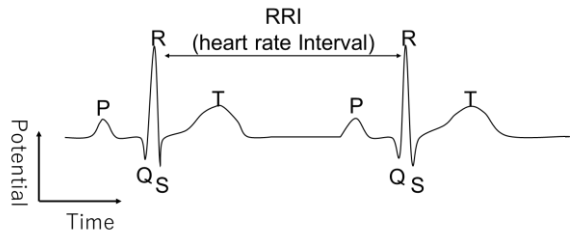

Fig. 2 Hear rate interval (RRI) diagram

Fig. 2 shows a heart rate interval (RRI). The RRI was measured using a heart rate sensor and the frequency analysis was performed to calculate the powers in high-frequency area (HF) and low-frequency area (LF). The LF indicates automatic nerve activitiy. The HF indicates parasympathetic nerve activity, and the LF/HF indicates sympathetic nerve activitiy. An increasing or decreasing rate (%) of the sympathetic and para-sympathetic nerve activities after the experiment was plotted.

RESUTLS AND DISCUSSION

The results after using Newtonian liquid and Non-Newtonian liquid are shown in Fig.3 and 4, respectively.

The emotional circles showed that the viscous liquids adopted in a series of tests provided the subjects to more nervous emotions than relaxed emotions. It was also revealed that the Newtonian liquid provided the subjects to more fun or surprised emotions.

In a series of tests, viscous liquid was found to affect sympathetic and parasympathetic activity. It is clear from Fig. 3 that the Newtonian fluid decreased the para-sympathetic nerve activity. Those results had high correlations to the results of emotional circles.

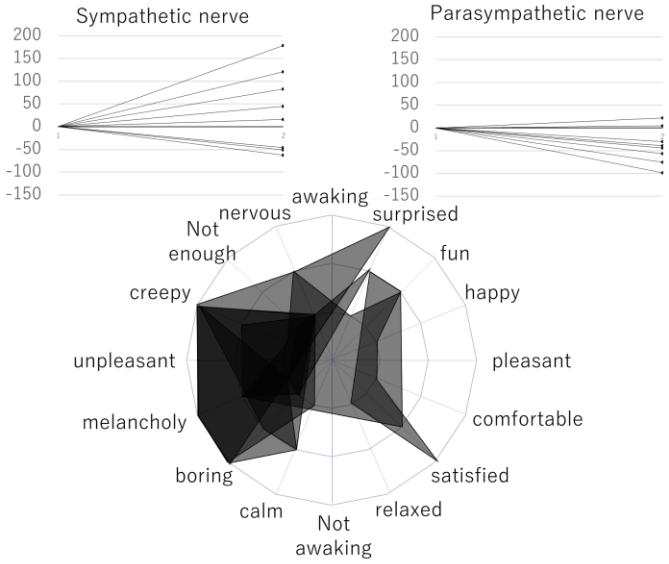

Fig. 3 Emotional change after using Newtonian liquid

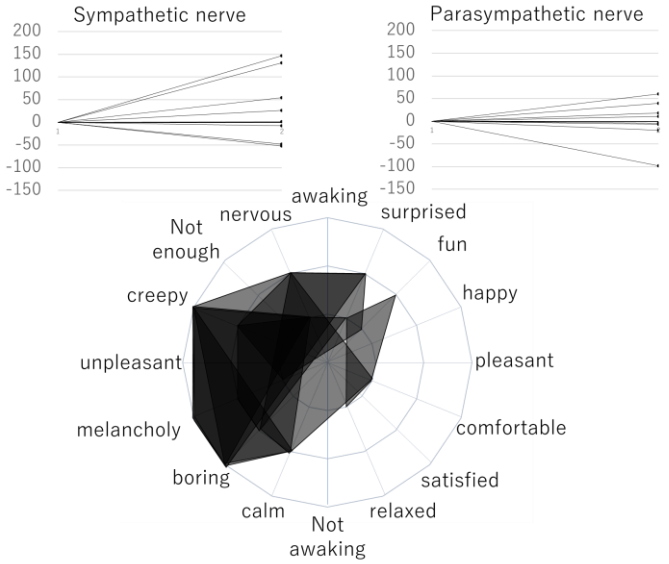

Fig. 4 Emotional change after using Non-Newtonian liquid

REFERENCES

[1] James A Russell: Circumplex Model of Affect, Journal of Personality and Social psychology, Vol.39, No.6, pp.1161-1178, (1980)

[2] Task Force of The European Society of Cardiology and The North American Society of Pacing and Electrocardiology: Heart rate variability —Standards of measurement, Physiological Interpretation, and Clinical Use—, European Heart J, 17, 354-381, 1996

9th International Engineering Symposium - IES 2020
March 3-5, 2020, Kumamoto University, Japan

Promoted Effect of Pool Boiling Heat Transfer by Diamond Particles Coated Heating Surface

Yuma Nakamura [1], Shuichi Torii [2] and Shigeru Tanaka[3]

1 *Student, Department of Mechanical System Engineering, Kumamoto University (GGST), Kurokami, 2-39-1, Kumamoto 860-8555, Japan. e-mail: 196d8472@st.kumamoto-u.ac.jp*
2 *Professor, Department of Mechanical System Engineering, Kumamoto University, Kurokami, 2-39-1, Kumamoto 860-8555, Japan. e-mail:torii@mech.kumamoto-u.ac.jp*
3 *Associate Professor, Institute of Pulsed Power Science (IPPS), Kumamoto University, Kurokami, 2-39-1, Kumamoto 860-8555, Japan. e-mail: tanaka@mech.kumamoto-u.ac.jp*

ABSTRACT: Boiling heat transfer is a heat transfer phenomenon in which boiling bubbles carry thermal energy on the heating surface by phase change. In recent years, heat transfer performance needs to be enhanced because of the heat generation of integrated circuits with improved performance of digital equipment. The microfabrication of heating surface is one of the ways to promote boiling heat transfer. In my study, I try to promote boiling heat transfer by diamond particles coated (DPC) heating surface. Diamond particles (8-20μm) are embedded in copper block surface by using the underwater shock wave of explosion. From the results of the boiling experiments, it is confirmed that the heat transfer coefficient of the DPC heating surface in the heat flux = 400 kW/m2 increase to 1.33 times as compare with smooth heating surface.

***Keywords**: Boiling heat transfer, Diamond particle, Underwater explosion shock wave*

INTRODUCTION

Boiling heat transfer is a heat transfer phenomenon in which boiling bubbles carry thermal energy on the heating surface by phase change. The boiling heat transfer is more effective than other heat transfer phenomenon. Many Industrial products such as air-conditioner use it. In recent years, heat transfer performance needs to be enhanced because of the heat generation of integrated circuits with improved performance of digital equipment. The microfabrication of heating surface is one of the ways to promote boiling heat transfer. And it is currently being actively studied [1]. In addition, there are other methods to promote boiling heat transfer, such as the use of nanoflows and alternative CFCs [2] [3]. Boiling bubbles usually generate from the cavity of scratches and cracks on a smooth surface.

Boiling bubbles are generated efficiently by increasing the number of artificial cavities with microfabrication of the heating surface and boiling heat transfer is promoted. In my research, I try to promote boiling heat transfer by diamond particles coated (DPC) heating surface. Diamond has high thermal conductivity and excellent mechanical properties such as wear resistance. In addition, it is considered that boiling heat transfer is promoted by providing the microstructure of diamond particles on the heating surface. Conventionally, it is difficult to manufacture a composite material of diamond and metal by heat treatment or bonding. Therefore, in my study, diamond particles (8-20μm) are embedded in copper block surface by using the underwater shock wave of explosion.

Fabrication of DPC Copper Block

In my study, diamond particles are embedded in copper block surface by using the underwater shock wave of explosion. Fig.1 shows the method of coating diamond particles on heating surface. This experimental apparatus is composed of explosive, electric detonator, copper block, diamond particles, stainless steel plate and a sealing vinyl tape. The underwater shock wave of explosion impinges on the steel plate, and the diamond particles is coated on the surface of upper part of the copper block. The experimental conditions as shown in table 1. The experiments are conducted with three explosive attachment distances (D=10, 20, 30mm) as the experimental conditions.

Observation results of DPC surface

The observation results of DPC copper block surface are shown in Fig.2. Fig. 2(b) shows that the diamond particles were adhered to each other without gaps indicating firm bonding. The distance of DPC surface of explosive attachment in this case was 10 mm. Fig. 2(c) and Fig. 2(d) illustrates that the diamond particles adherence at DPC surface of 20 mm and 30 mm respectively was less than that in 10 mm. Therefore, it is confirmed in fabrication of DPC surface by underwater shock wave that if the explosive attachment distance is smaller, the adhesion amount of the diamond particles on the copper surface increases. The relation between the explosive attachment distance and diamond particles adhesion density or peak pressure by underwater shock wave is shown in Fig.3. Where, particle adhesion density is the number of adhered diamond particles per unit area. From Fig.3, it is confirmed that the particle adhesion density and the peak pressure decreased exponentially in accordance with the increase of the value of the explosive attachment distance D.

Boiling Experimental Method

The boiling condition in this experiment were identical to saturated pool boiling under atmospheric pressure. The boiling experimental apparatus is shown in Fig.4. This experimental apparatus is composed of boiling container, plastic ball, auxiliary heater, DPC copper block, ceramic heater, insulation and voltage converter. In addition, K type thermocouple and data logger used for measurement. The DPC copper block and the ceramic heater are adhered with thermally conductive adhesive. Distilled water is boiled and well degas for 40 minutes using the auxiliary heater. And, thermal energy is transferred from the upper part of DPC copper block by heat input with the ceramic heater. At this time, the temperature of the saturated water and internal temperature of copper block are recorded using the K type thermocouple and the data logger. Furthermore, details of the experimental conditions are shown in Table 2.

Evaluation Value Equation

The detail of Heating surface is shown in Fig. 5. The heat flux q W/m^2 in boiling heat transfer is given by Eq.1.

$$q = -\lambda \frac{dT}{dx} \qquad (1)$$

Where, λ is the thermal conductivity [W/(m · K)] of the copper, T is the internal temperature [K] of copper block , and x is the arbitrary position [m] in the heat transfer direction.
The surface temperature T_W [K] of the heating surface is given by the Eq.2.

$$T_W = T_1 - \frac{q}{\lambda} l \qquad (2)$$

Where, T_1 is the internal temperature [K] of the copper block measured at the position closest to the heating surface and l is the length [m] of the thermocouple1 to the heating surface.

The degree of superheat ΔT [K] is given by Eq.3.

$$\Delta T = T_W - T_S \qquad (3)$$

Where, T_S is the saturation temperature [K] of water.
The heat transfer coefficient h [W/(m^2·K)] is given by Eq.4.

$$h = \frac{q}{\Delta T} \qquad (4)$$

Effect of DPC Surface on Boiling Heat Transfer

The relation between the degree of superheat ΔT and the heat flux q is shown in Fig.6. According to Fig.6, it is confirmed that boiling heat transfer is promoted by diamond particles coated on the heating surface. It is assumed that this result is got because the artificial cavity increased by diamond particles and boiling bubbles are generated efficiently. In addition, it is confirmed that boiling heat flux increased in accordance with the particle adhesion density increased. In the DPC heating surface (D=10mm), it can be considered that the saturated water is efficiently supplied to the boiling bubble generation point and boiling heat transfer is most promoted because the capillary force is improved by adhesion of diamond particles.
The relation between the heat flux q and the heat transfer coefficient h is shown in Fig.7. According to Fig.7, it is confirmed that the heat transfer coefficient of the diamond particles coated heating surface increase in 1.16 times at the q=200 kW/m^2, 1.27 times at the q=300 kW/m^2 and 1.33 times at the q=400 kW/m^2.

CONCLUSIONS

The following conclusions are deduced from this study:

- Diamond particles are adhered to each other without gaps and successfully bonded in the DPC surface of explosive attachment distance D=10mm.
- Fabrication of DPC surface by underwater shock wave that the explosive attachment distance is smaller, the adhesion amount of the diamond particles increase more on the copper surface.
- Boiling heat transfer is promoted by diamond particles coated on the heating surface.
- Boiling heat flux increase in accordance with the particle adhesion density more increase.
- Heat transfer coefficient of the diamond particles coated heating surface increases in 1.33 times at the q=400 kW/m2.

REFERENCES

[1] D. Eok et al., "Review of boiling heat transfer enhancement on micro/nanostructured surfaces", Experimental Thermal and Fluid Science, Vol.66, pp.173-196, 2015.
[2] D.W. Zhou, "Heat transfer enhancement of copper nanofluid with acoustic cavitation", *International Journal of Heat and Mass Transfer*, Volume 47, Issues 14–16, pp.3109-3117, July 2004.
[3] Hitoshi Matsushima and Takuya Saitou, "Heat transfer characteristics of pool boiling under low pressure condition", *Thermal Science & Engineering* Vol.26, No.1, 2018.

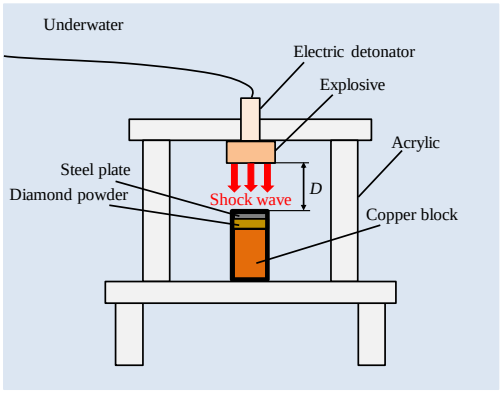

Fig.1 Fabrication method of DPC heating surface

Table 1 Fabrication conditions of DPC heating surface

Copper block size [mm]	15×15×25
Diameter of diamond particle [μm]	8~20
Diamond powder [g]	0.1
SEP explosive [g] (Manufactured by Asahi Kasei Co.)	3
Attachment distance of explosive *D* [mm]	10,20,30

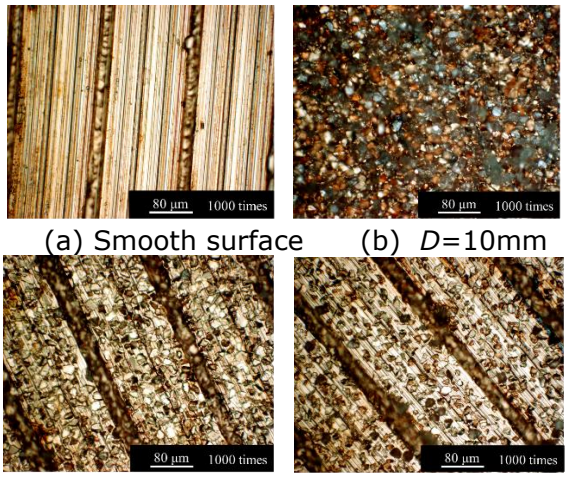

(a) Smooth surface (b) *D*=10mm

(c) *D*=20mm (d) *D*=30mm

Fig.2 Observation results of DPC surface

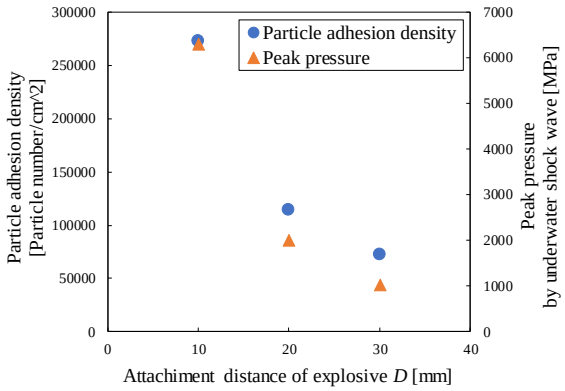

Fig.3 Relation between the explosive attachment distance and diamond particles adhesion density or peak pressure

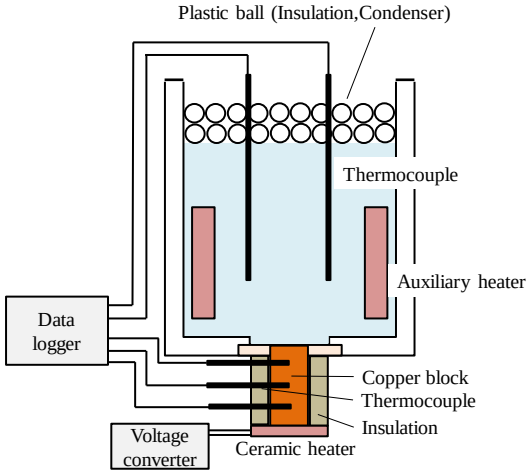

Fig.4 Boiling experimental apparatus

Table 2 Experimental conditions

Input power range [W]	10~90
Heat input of auxiliary heater [W]	200
Volume of saturated water [cm^3]	900~1100
Copper block size [mm]	10×10×17
Condition of heating surface *D* [mm]	10, 20, 30

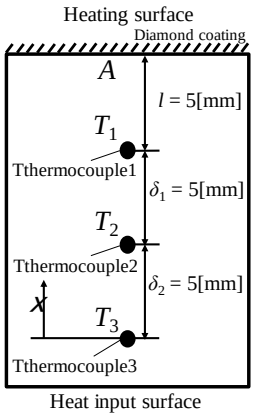

Fig.5 Detail of heating surface

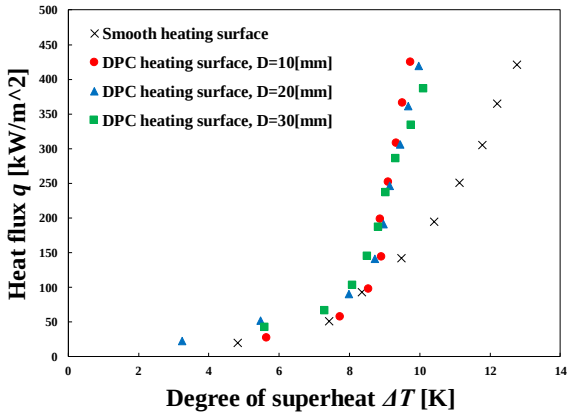

Fig.6 Relation between the degree of superheat and the heat flux

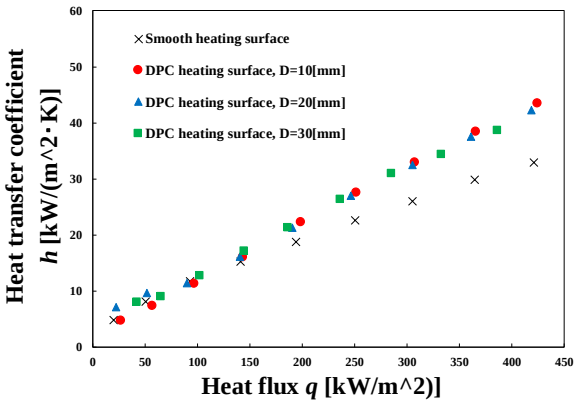

Fig.7 Relation between the heat flux and the heat transfer coefficient

9th International Engineering Symposium - IES 2020
March 3-5, 2020, Kumamoto University, Japan

Effect of Embrittlement on Microstructure, Mechanical and Wear Behaviour of Aged Duplex Stainless Steel

Mahesh Davanageri [1], Disha D[2], Narendranath.S[3] and **Ravikiran Kadoli[4]**

1 *Associate professor, Department of Mechanical Engineering, Sahyadri College of Engineering and Management, Mangaluru 575007 India. email: Mahesh.mech@sahyadri.edu.in.*
2 *Undergraduate Student, Department of Mechanical Engineering, Sahyadri College of Engineering and Management, Mangaluru 575007, India. email: dddisha7@gmail.com*
3 *Professor, Department of Mechanical Engineering, National Institute of Technology Karnataka, Surathkal, Mangalore 575025, India. email: snnath88@yahoo.co.in*
4 *Professor, Department of Mechanical Engineering, National Institute of Technology Karnataka, Surathkal, Mangalore 575025, India. email: rkkadoli@nitk.ac.in*

ABSTRACT: This paper presents the influence of embrittlement on the mechanical properties like microstructure, Impact energy, tensile, hardness and dry sliding wear of super duplex stainless (SDSS) AISI 2507. Prior to heat treatment the material has been solution treated. Further, heat treatment was carried out 475°C for 60 minutes, quenched in water and quenching oil at room temperature. Heat treatment at 475°C leads to embrittlement in duplex stainless steel (DSS) owing to ferrite phase decomposition by spinodal decomposition into two phases, Cr-rich (α') phase and Fe-rich (α) phase. Embrittlement of super duplex steel resulted in significant improvement in the ultimate tensile strength (UTS) and hardness. However, decrease in the impact energy was observed. Oil quenched specimens according to wear tests show better wear resistance compared to water quenched and solution treated specimens.

***Keywords**: Embrittlement, Microstructure, Hardness, Wear*

INTRODUCTION

In recent years, the use of duplex stainless steel increased owing to its widespread engineering application in pulp and paper, offshore oil, gas, , chemical, petroleum and power industries due to their high mechanical properties and excellent corrosion resistance (Olsson and Snis, 2007, Lasebikan et.al., 2013 and Vogt et al., 2002;). Duplex stainless steels are assemblage of two phase microstructure of ferrite and austenite. The approximately two equal phase microstructure of ferrite and austenite combines the effects of these two phases that are beneficial to make the DSS to obtain high strength of ferrite and toughness of austenite (Fargas et al. 2005, Weng, K. L., and Chen, H. R.).The DSS are exposed to a temperature range of 280-500ºC undergo embritllement and its rate to be highest at 475°C. It was observed that embrittlement alter the mechanical properties significantly and it limits the usage of duplex stainless steel below the temperature below the 280°C (Sahu et al., 2009, Hanninen et al., 2001, and Martins et al. 2005). Embrittlement results in decomposition of highly alloyed ferritic phase to iron rich (α) and chromium rich phase (α') and it was also noticed that ferrite is unstable within the miscibility gap and therefore, ferrite decomposes into two phases. Embrittlement concept is normally ascribed to spinodal decay of the ferrite, to be specific, the development of ferrite-advanced (α) stage and chromium-enhanced (α') stage, or the arrangement of chromium-improved (α') expedites installed in a ferrite-rich (α) lattice in the wake of maturing in the 250°C to 550°C temperature (Hwang et al.

2014).The embrittlementat 475°C significantly affects the properties like hardness, impact, tensile strength, toughness. However, very few researchers focused on effects of heat treatment at low temperatures on mechanical and wear behavior of duplex stainless steel. This research work is mainly focused on exploring the possibilities to enhance the wear properties of aged super duplex stainless steel AISI 2507, as in some of the application of super duplex stainless such as pumps, valves and bearings where in contact of metal surface exist.

MATERIAL AND EXPERIMENTATION

The commercially available as-cast SDSS AISI 2507 was selected for the present study. The chemical composition of the material was obtained through optical spectroscopy test after the solution treatment at the temperature of 1050°C for the duration 120 minutes and quenched in water at room temperature and results are shown in Table 1.

Table 1. Chemical composition weight (%) of solution treated material (AISI 2507 SDSS).

C	Cr	Ni	Mo	Mn	Si	N	Fe %
0.019	25.387	6.714	3.77	0.738	0.328	0.028	Bal

UTS and yield strength (YS) were determined via tensile tests. Room temperature experiments were executed using computer controlled TINIUS OLSEN H75KS (Tinius Olsen, UK) Universal Testing Machine and shown in Figure 1a. Specimen having gauge length (25 mm) was processed as per ASTM E8 standards (Figure 1b and 1c). The YS and UTS of the heat treated specimens were examined. An average of three reading was taken and reported for each test. The Charpy impact test was used to measures the fracture toughness. An impact testing machine was used to perform experiments on specimens with V-notch.

1(a)

1(b)

1(c)

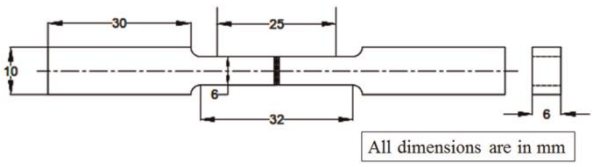

Fig.1a) Tensile test equipment.1b) Prepared tensile specimens as per ASTM E8 1c) Dimensions of the specimens as per ASTM E8.

Wear test examples of size of Ø10×30 mm were set up as per ASTM G99A (Davanageri et al., 2017). The samples of specimens which were prepared are exposed to heat treatment at 1050ºC for duration of 120 minutes. Further, quenched in water to obtain the balanced two phase microstructure of ferrite and austenite. Subsequently specimens are further heat treated to temperature 475ºC for 60 minutes and subsequently quenched in water and quenching oil. Dry sliding wear experiments were conducted on with the pin-on-disc wear test rig (Model: TR-20, DUCOM) as per ASTM G99A.

The samples are priorly cleaned, then it is subjected to experimentation and wear test process parameters are shown in the Table 2. Microstructure analysis was carried on the heat treated specimens using scanning electron microscope. The specimen's microscopic study was prepared using standard metallographic techniques (Davanageri et al. 2017 Davanageri et al., 2016).

Table 2. wear test process parameters

SL No	Operating conditions					
1	Load (N)	10	20	30	40	50
2	Velocity (m/s)	1	2	3	4	5
2	Distance (m)	200	400	600	800	1000
4	Relative humidity	70%				
5	Track diameter (mm)	140				
6	Temperature	Room temperature				
7	Surface condition	Dry				

RESULT AND DISCUSSION

Solution treatment and Microstructure

The solution treatment of DSS has significant effect on balance of the ferrite and austenite phase. At the temperature range of 1000-1400°C the solution heat treatment is carried out. The solution treatment is necessary, to dissolve any retained precipitates and thermal residual stress and assimilates the alloying elements in the solid solution of the cast material (Padilha et al.,2007). The specimens prepared for experimentation work are initially subjected to solution treatment at a temperature 1050ºC for 120 minutes and quenched in water at room temperature. The SEM and optical micrographs of solution treated was shown in Figure 2a and 2b. It was observed that only two phases were present and there is no evidence for existence of other phases. Further, to confirm the phase present in the microstructure the XRD analysis of solution treated specimen was carried out and only two peaks of austenite and ferrite were observed and shown in Figure.3.

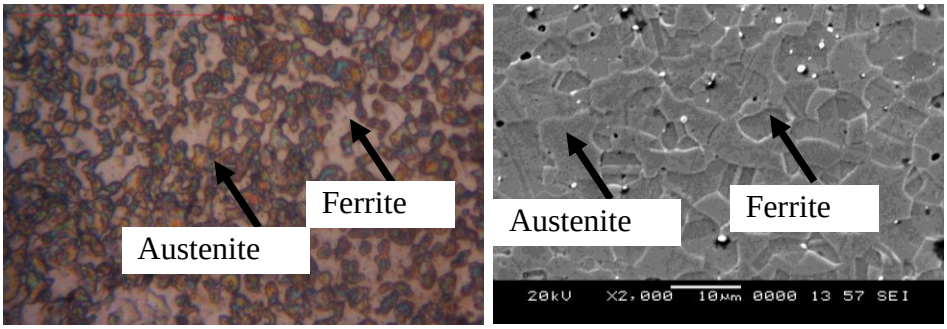

Fig.2 a and b Optical and SEM microscope image of AISI 2507 solution treated.

The volume fraction of austenite and ferrite phase in the microstructure was determined based on the measured area of each phase with help of optical image analyser software. The Optical image of solution treated (as-cast) is shown in Figure 4. The individual phases are shown with different colours in the optical micrograph. The volume fraction of

austenite and ferrite in the solution treated specimen was found and average volume fraction was observed to be 55% for the ferrite and 45% for austenite.

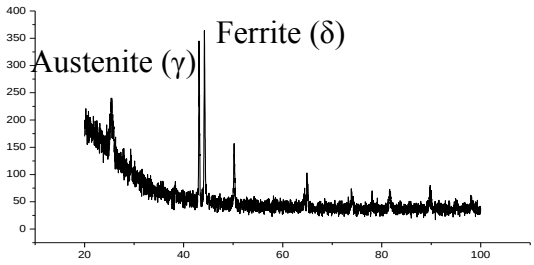

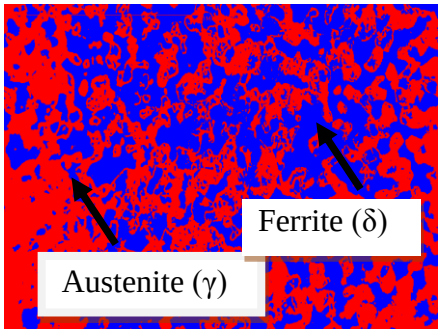

Fig.3. XRD analysis of solution treated specimen. **Fig.4** Volume fractions of austenite and ferrite.

Heat treatment and Microstructure analysis

The solution treated specimens were further exposed to a temperature of 475ºC for 60 minutes and subsequently quenched in water and oil. Microstructure are shown in Figure 5 and Figure 6.The embrittlement at 475ºC,formation of ferrite-enriched (α) phase and chromium-enriched (α') phase, or the formation of chromium-enriched (α') precipitates embedded in a ferrite-rich (α) matrix after aging and obtained results are in line with (Masayuki et al. 2011). The microstructures of heat treated specimens at 475ºC are observed to be mottled contrast in nature as seen in figure 5 and 6. This type contrast is observed in the spinodally decomposed materials and the darkish gray colour regions represent the Cr-rich zone, while dim gray zone represents the Fe-rich zone. This mottled regions significantly observed to be more in oil quenched specimens compared with the water quenched specimens.

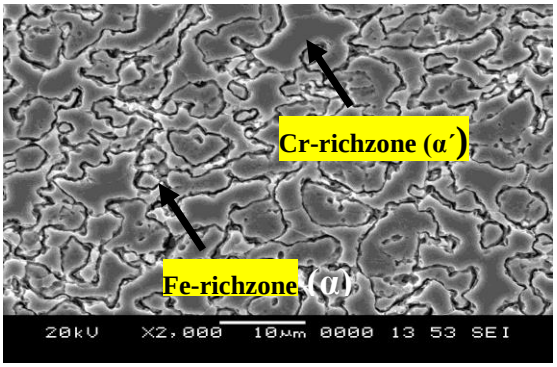

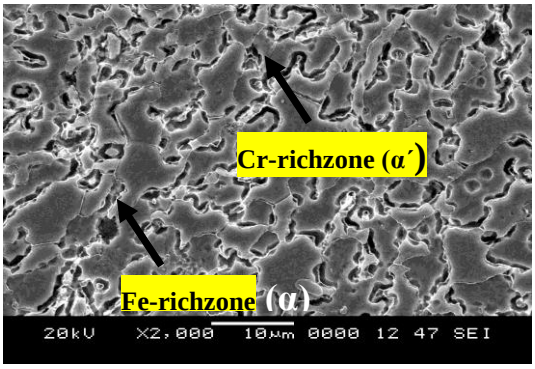

Fig.5 Microstructure of heat treated specimen 475ºC with water quenched.

Fig.5 Microstructure of heat treated specimen 475ºC with oil quenched

Tensile Test

Heat treatment was carried out at temperature 475°C for 60 minutes and further quenched in water and oil, to determine effect on tensile properties due to low temperature. All the results of yield and ultimate strength are presented in the Table 3. It was observed that there was increase in ultimate tensile and yield strength in both

water and oil quenched specimens. It is mainly due to embrittlement occurred during the heat treatment. The spinodal decomposition can obstruct the dislocation movement and affects the plasticity which leads to increase in yield and ultimate strength of the heat treated specimens. However, maximum yield stress and ultimate stresses were observed in the specimens with oil quench when compared to specimens of water quenched and solution treated. This is mainly due embrittlement , rate is high in oil quenched .

Table 3 Tensile properties of super duplex stainless steel at 475˚C.

Stresses (MPa)	Solution heat treatment at 1050˚C for 120 minutes.	Heat treated at 475 for 60 minutes. Water quenched	Heat treated at 475˚C for 60 minutes.Oil quenched
Yield stress	554	815	915
Ultimate stress	804	919	970

Hardness

Five hardness measurements were taken and the average values of hardness measurements of specimen were shown in Figure 7. A noticeable increase in the hardness was observed in the specimens with heat treated, quenched in oil and water. The heat treated specimens shows better hardness compared to solution treated due to formation hard phases of chromium-enriched (α') precipitates embedded in a ferrite-rich (α) matrix after aging due to spinodal decomposition of ferrite phase as seen in the Figures 5 and 6 which promote the hardening of the heat treated specimens.
.

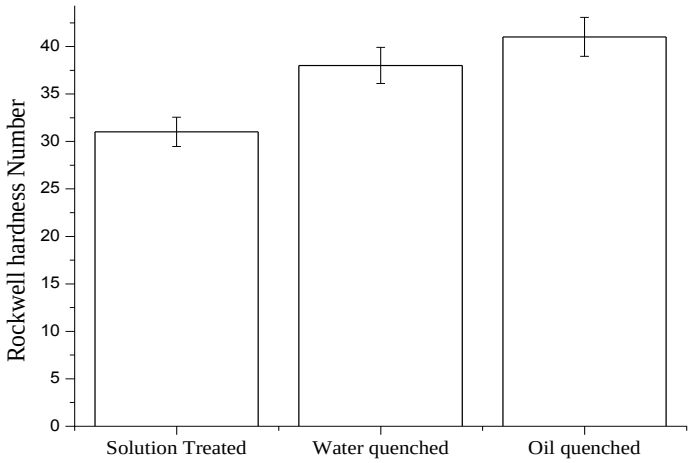

Fig.7 Rockwell hardness number of cone indenter (120º) for 150kgf.

Impact Charpy Test

The charpy tests were conducted as per ASTM standard and results are shown in the Figure 13.It was observed there is a significant reduction in the impact energy in both water and oil quenched specimens.

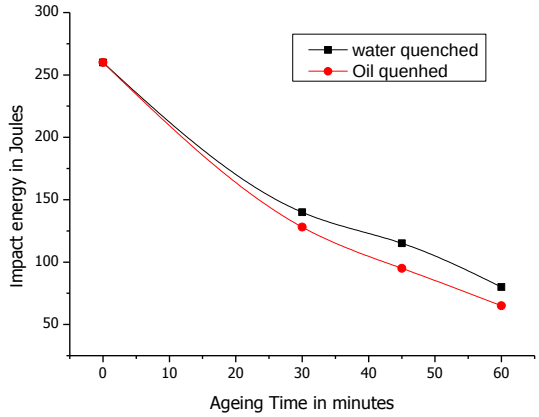

Fig.7 Variation of impact energy with time of ageing at 475°C.

The impact energy drops to 80 Joules in water quenched specimens and 65 Joules in oil quenched specimens in comparison with the solution treated impact energy of 260 Joules. The decrease in the impact energy of duplex stainless steel is mainly due to dislocation pinning caused by chromium, carbon and nitrogen atoms which aredue to spinodal decomposition occurred during the heat treatment. Spinodal decomposition can slow down the dislocation movement and further it stops the dislocation movement and it leads to plasticity inturn increasing the yield strength which is associated (refer Table 3) with decrease in toughness.

Effect of embrittlement on wear behaviour

The wear experiments were conducted in accordance with ASTM G99A and wear test conditions are selected depending on the some pilot experiments which was conducted in the laboratories and previous literature survey (refer Table 2)

Effect of Normal load

The material loss because of wear due to application of normal load on the differently treated specimens were shown in Figure 8, when load is varied in the range of 10 to 50 N in the step interval of 10N. Results reveal that wear behaviour is impacted due to applied load. Wear volume loss increases with increase in load and also increased in solution treated specimens as well as in heat treated specimens for the entire range of applied load. However, it had been observed that there is a significant improvement in wear resistance of heat treated specimens quenched with water and oil. Further, in particular the oil quenched specimens show better wear resistance when compared to solution treated and heat treated with water quenched specimens due to increase in hardness during the embrittlement. It was noticed that, as the load increases temperature at the interface of two rubbing surface due to the friction, which results in formation of debris, thermal softening and oxidation of debris of the material and causes enhancement of wear volume loss in solution treated specimens. The improvement in the wear resistance of heat treated specimens is mainly due to the formation of two phases' Cr-rich phase and Fe-rich phase because of embrittlement occurred during the heat treatment (refer Figure 5 and 10). Further enhancement in the hardness of heat treated specimens due to formation of these phases has significantly improved the wear resistance in the heat treated specimens.

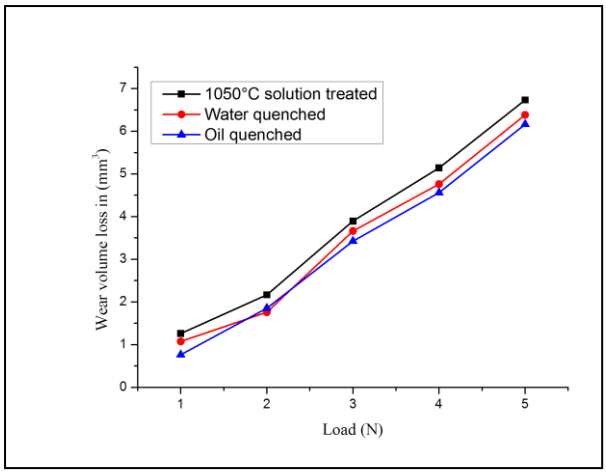

Fig.8 Variation of Load vs. wear volume loss.

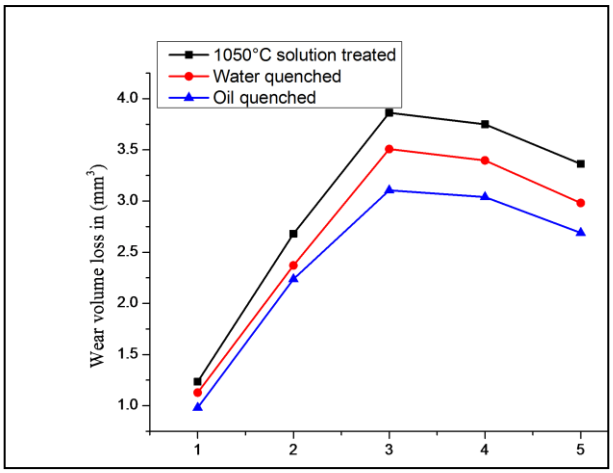

Fig.9 Variation of sliding velocity vs. wear volume loss.

Effect of sliding velocity

The Figure 9 shows wear loss with sliding velocity. The wear volume loss increases with increase in the sliding velocity. However, it was observed that the after 4m/s velocity the wear loss decrease in all the specimens. This is mainly due to the transition period during which the frictional force reduces as sliding velocity increases. The transition velocity will depend on material structure and there is a distinct transition velocity for each structure above which its wear loss starts decreasing as observed in the Figure 9. Further, the profundity of plastic disfigurement may increment and structures the Tribological layer and this layer watched more past speed 4m/s, accordingly separating the normal thickness of the debris. This diminishes the measure of entangled debris, which is to be divided and oxidized, accordingly prompting the progress.

CONCLUSIONS

The effect of embrittlement on mechanical, microstructural properties and wear behaviour were studied on the super duplex stainless steel AIS 2507. The following conclusions were made.

- The annealing at temperature of 1050°C for 60 minutes and subsequently quenched in water resulted in balanced microstructure of ferrite and austenite approximately in equal proportion.

- The low temperature heat treatment at 475°C leads to embrittlement and forms the Cr-rich phase (α') and Fe- rich phase (α) in the microstructure of the heat treated specimens with water and oil quenched and alter the mechanical properties.
- Increase in the hardness is observed to be associated with embrittlement phenomenon, Yield strength and Ultimate strength was increased with increase in ageing time and reduction in toughness of the material was observed.
- Based on the results observed in experiments, it was observed that heat treated specimens' shows the better wear resistance compared to solution treated specimens. The specimens heat treated at temperature 475°C for 60 minutes, the

oil quenched specimens shown the better wear performance as compared to a specimen that was solution treated and heat treated, water quenched specimens due to embrittlement the formation of Fe-rich (α) and Cr-rich (α') in the microstructure. It is mainly because of cooling rate and it is slow in oil compared to water quenching which provides the enough time for precipitation of sigma phase.

REFERENCES

Davanageri, M et el (2017). "Influence of ageing time on hardness, microstructure and wear behaviour of AISI2507 super duplex stainless steel, Materials Research Express, 4(8), 086506

Davanageri, M et al. (2016), Dry Sliding Wear Behavior of Super Duplex Stainless Steel AISI 2507: A Statistical Approach. Archives of Foundry Engineering, 16(4), 47-56.

Fargas, G et al (2013), Effect of Sigma Phase on the Wear Behavior of a Super Duplex Stainless Steel, Wear , 303(1–2), 584–90.

Hanninen et al (2001), Effects of processing manufacturing of high nitrogen-containing stainless steels on their mechanical, corrosion and wear properties, Journal of Material Processing and Technology. 117, 424-430.

Lasebikan, B.A., Akisanya, A.R. and Deans, W.F. (2013), The Mechanical Behaviour of a 25Cr Super duplex stainless steel at elevated temperature, Journal of Materials Engineering and Performance. 22(2), 598-606.

Martins, M., and Castelletti, L.C. (2005), Effect of heat treatment on the mechanical properties of ASTM A890 Gr6A super duplex stainless steel, Journal of ASTM International, 2, 1-14.

Olsson, J. and Snis, M. (2007). Duplex - A new generation of stainless steels for desalination plants; *Desalination*, *205*(1-3), 104–113.

Masayuki et al (2011). Microstructural changes of chromium ferritic stainless sreel subjected to cyclic loading in 475 ºC Embrittlement region, *Engineering* Procedia, 88.

Padilha et al (2007), Comparative study on sigma phase precipitation of three types of stainless steels: austenitic, super ferritic and duplex, Material . Science . Technology. 22, 1098–1104.

Sahu, J.K., Krupp, U., Ghosh, R.N., Christ, H. J. (2009), Affect of 475°C embrittlement on the mechanical properties of duplex stainless steel, Materials Science and Engineering, 508, 168–173.

Vogt, J.B., Massol, K., and Foct, J. (2002), Role of the microstructure on fatigue properties of 475°C aged duplex stainless steels, International Journal of Fatigue, 24, 627-633.

Weng, K. L., and Chen, H. R. (2004), The low temperature aging embrittlement in a 2205 duplex stainless steel, Material science and engineering, 379, 119-132.

9th International Engineering Symposium - IES 2020
March 3-5, 2020, Kumamoto University, Japan

Influence of Ageing Time on Microstructure, Hardness and Corrosion of UNS Zeron 100 Super Duplex stainless steel

D Disha [1], Mahesh Davanageri[2] and Narendranath.S[3]

1 *Undergraduate Student, Department of Mechanical Engineering, Sahyadri College Of Engineering And Management, Mangalore 575007,India.*
E-mail: dddisha7@gmail.com
2 *Associate professor, Department of Mechanical Engineering, Sahyadri College of Engineering and Management, Karnataka,India.*
E-mail address: Mahesh.mech@sahyadri.edu.in
3 *Professor, Department of Mechanical Engineering, National Institute of Technology Karnataka, Surathkal, Mangalore 575025, India. E-mail: snnath88@yahoo.co.in*

ABSTRACT: The present study is to investigate the influence of ageing time on the microstructure, hardness and corrosion properties of UNS Zeron 100 super duplex stainless steel. The material was solution treated at 1050°C and water quenched; further the ageing has been carried out at 850°C for 30, 60 and 90 minutes. Hardness test and corrosion test were carried out for both solution treated as well as aged specimens for different ageing period. Results of hardness test indicates an increase in hardness as the ageing period increased. Corrosion test results showed good resistance to corrosion as the ageing time increases. Changes in mechanical properties were observed due to sigma phase formation. Scanning electron microscope (SEM) analysis showed the sigma phase precipitation in duplex stainless steel. EDX analysis shows the consumption of ferrite and formation of chromium which indicates the formation of sigma phase. Optical image analysis showed the increment of sigma phase as the ageing time is increased.

Keywords: Microstructure, Hardness, Sigma phase.

INTRODUCTION

Duplex stainless steels (DSS) are called "duplex" as they have a assemblage of two phase of ferrite and austenite. Zeron 100 (DSS) has found wide industrial application in pharmaceutical, chemical, desalination, pulp, paper industries, power generation and mining industries. Alfred R. Akisanya et.al (2012) studied, the effect of ageing temperature and ageing time effects on a 25Cr-6.7Ni-0.32N-3.0Mo-2.5W (DSS).The ageing temperature of 600-900°C and ageing time of 1 to 240 minutes which resulted in formation of chi phase and sigma. Ageing significantly influenced on the mechanical properties due to precipitation of inter-metallic phases. Researchers Wang, Y Q et al (2013) reported that the sigma phase effects on Z3CN20M cast (DSS). At temperature of 600-900°C, formation of sigma phase occurs at ferrite phase boundaries. Further, authors have observed that for temperature range less than 700°C and aged for less than 4 hours yield strength and tensile strength was less when compared to aged specimens. Villalobos, D et al (2009) studied on SAF2507 Super duplex stainless steel (SDSS) at the temperature range of 200°C-700°C there was no significant change in mechanical properties. And at 800°C formation of sigma phase starts in SDSS. Chen T H, and Yang J R (2002), studied the effects of solution treatments (1020°C 1080°C 1200°C) and different continuous cooling rates (1, 0.5, 0.25 and 0.1°C/second) on 2205 DSS and reported that precipitation of sigma phase was obtained in lower cooling rates and at lower solution treated temperature. Magnabosco, R (2009), observed that the

sigma phase formation occurs at 850°C significantly high. Escriba, D M et al(2009), DSS was heat treated at 700°C and 750°C which resulted the inter-metallic phases which were formed in USN S31803 DSS. The formation of chi and sigma phase was noticed. It was found that chi phase precipitation was initiated at ferrite/ferrite grain boundaries and chi phase precipitation occurs before sigma phase precipitation. It was observed that the sigma phase after precipitating consumes the chi phase by surrounding it with secondary austenite phases. Davanageri, M B et al (2015), carried out an investigation on AISI 2507 SDSS where heat treatment was carried out for 850°C for 60 min and different quench media. The formation of a secondary inter-metallic sigma phase was observed due to which hardness increases and resistance to wear in heat treated super duplex stainless steel due to sigma phase formation. From the above literature it was observed that there is less focus on Zeron 100 SDSS. Hence the present study will give the insight to the influence of ageing on microstructure and mechanical properties of Zeron100 SDSS.

EXPERIMENTATION

The commercially available material Zeron 100 duplex stainless steel was selected to carry out the experiments to study effect of ageing on Microstructure, mechanical and Corrosion properties. The prepared specimens for these tests were polished with metallographic techniques. After the polishing the etching was carried out by 40% aqueous NaOH solution as shown in Figure 1. The material was initially solution treated at 1050°C for 120 minutes and quenched in water to obtain the balanced micro structure of austenite and ferrite. The aging was carried out at 850°C for 30 , 60 and 90 minutes and all the specimens were quenched in water. SEM as shown in Figure 2 was used to study the microstructure and the corresponding elemental analysis using EDX Analysis for identification of inter-metallic phases in Zeron 100 DSS. The hardness test was conducted by Rockwell hardness test rig. The depth of indentation of the indenter, the hardness value of the material is obtained by the 120° cone indenter. Optical image analyzer as shown in Figure 3 was used to study the volume fraction of the phases observed in the material after the ageing. To determine the corrosion resistance of the specimen Salt spray or fog test is conducted in corrosion analyzer as shown in Figure 4.

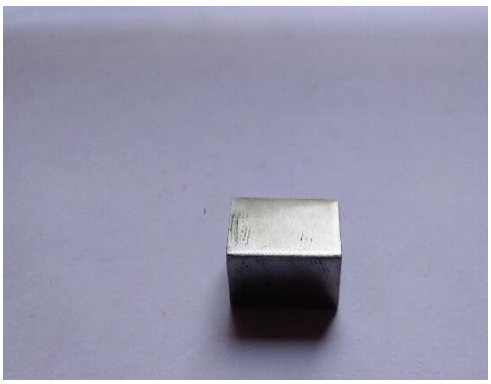

Fig.1 Specimen according to ASTM standards

Fig.2 Scanning electron microscope

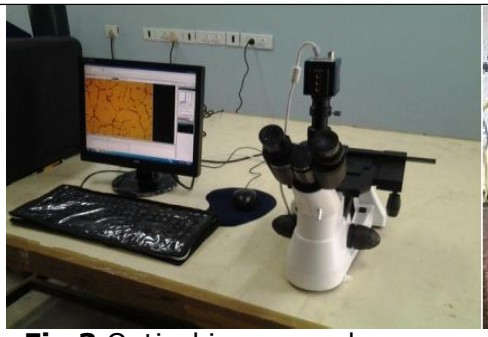

Fig.3 Optical image analyser

Fig .4 Corrosion Analyser

RESULT AND DISCUSSION

Solution treatment

The solution treatment was carried at 1050°C for 120 minutes. The Figure 5 and Figure 6 are the SEM and optical micrographs of solution treated specimens respectively. It was observed that all the precipitates which exist in the Zeron 100 DSS are dissolved and only equal phase microstructure of ferrite and austenite was obtained. The chemical composition after the solution treatment presented in the Table.1.The volume fraction analysis shown in Figure 7 resulted in 57% of ferrite and 43 % austenite for solution treatment.

Table 1 Chemical Composition of UNS Zeron100 SDSS

C	Mn	Si	S	P	Cr	Ni	Mo	Cu	W	Fe
0.30	0.476	0.494	0.009	0.027	25.378	7.153	3.437	0.598	0.620	61.778

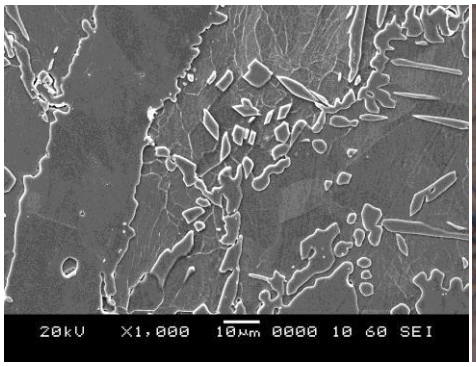

Fig.5 SEM image of solution treated specimen

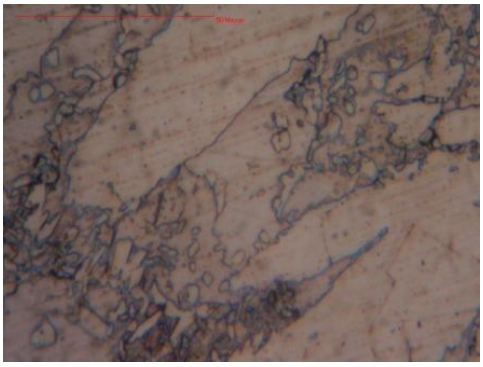

Fig.6 Optical Image of Solution treated specimen

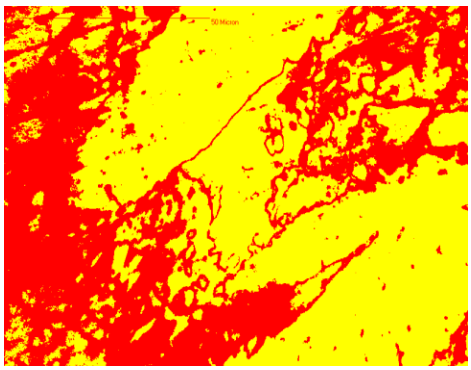

Fig. 7 Phase volume of solution treated

Heat treatment

The heat treatment was done at 850°C for 30, 60 and 90 minutes and quenched in water. The precipitation of secondary inter-metallic phases was observed. When A1SI ZERON 100 SDSS was heated to the formation of sigma phase precipitates could be observed in the microstructure of SDSS. It precipitates clearly at the austenite and ferrite boundary region and as the ageing time increases the ferrite phase of DSS is consumed and sigma phase precipitation increases as observed in the Figure 8, 9 and 10 respectively for 30, 60 and 90 minutes of ageing time.

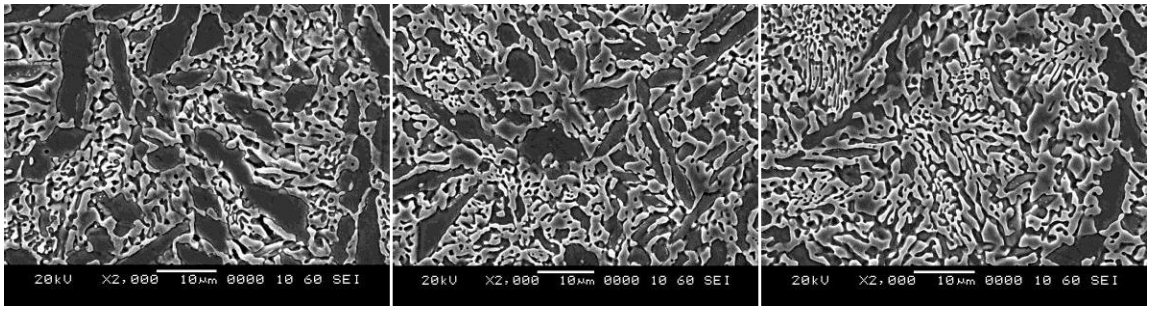

Fig.8 Heat treated specimen at 850°c Aged for 30min **Fig.9** Heat treated specimen at 850°c Aged for 60min **Fig.10** Heat treated specimen at 850°c Aged for 60min

The Figure 11, 13, 15 and the optical images of microstructure and Figure 12, 14, 16 the phase volume fraction of Zeron 100 duplex stainless steel at different ageing times. The heat treatment process introduces microstructural changes promoting inter-metallic changes. As the ageing time of heat treatment increases the phase volume of sigma phase increases. The phase volume fraction of all the three phases for different ageing time is given in the table 2

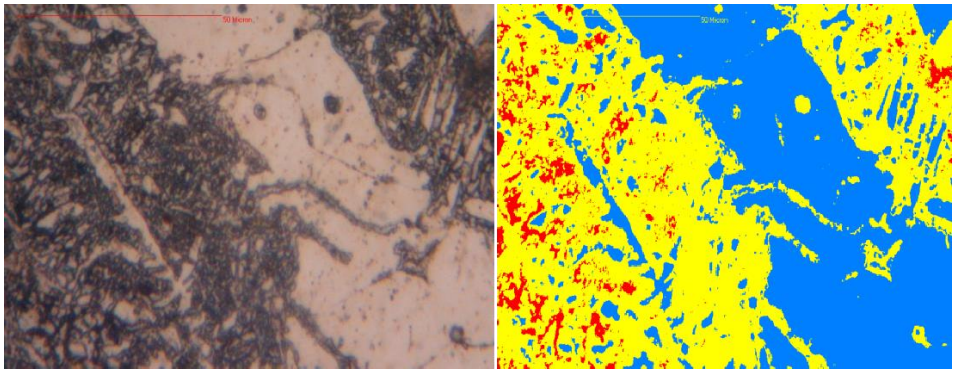

Fig.11 Optical Image of Heat Treated specimen at 850°c Aged for 30min **Fig.12** Phase volume of Heat Treated specimen at 850°c Aged for 30min

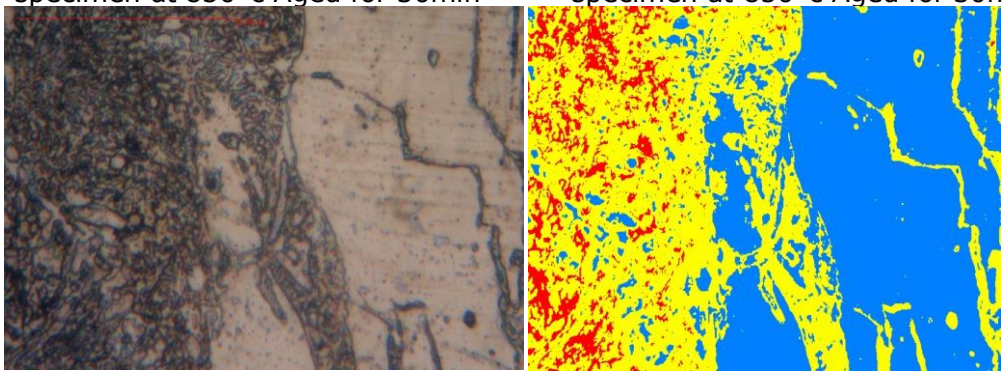

Fig.13 Phase volume of Heat treated specimen at 850°c Aged for 60min **Fig.14** Optical Image of Heat Treated specimen at 850°c Aged for 60min

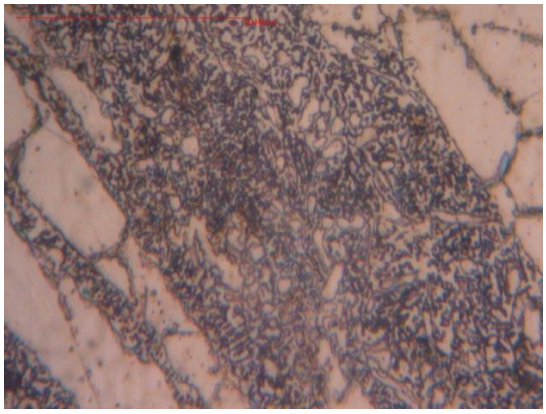

Fig. 15 Optical Image of Heat Treated specimen at 850°c Aged for 90min

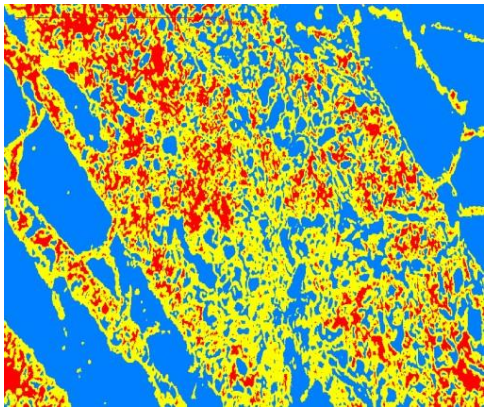

Fig.16 Phase volume of Heat Treated specimen at 850°c Aged for 90min

Table 2 Phase volume fraction of Zeron 100 SDSS at different ageing time

Heat Treatment Temperature 850° C	Phase Volume Fraction (%)		
Ageing Time(min)	Ferrite	Austenite	Sigma
0	56.62	43.38	0
30	53.84	40.85	5.31
60	46.65	45.48	7.87
90	43.07	42.40	14.53

EDX Analysis results indicated that there is increase of chromium as the ageing time is increased. Although the increment observed was not much but there was a decrement in ferrite**.** This is because the sigma phase nucleates at the ferrite phase by consuming chromium and molybdenum. Fig 17, 18, 19 and 20 shows the location on the material and the corresponding analysis results for different ageing times. The table 3 shows the chemical composition for different ageing times in terms of weight and atomic mass percentage. It clearly indicates the increase in chromium as the ageing time increases.

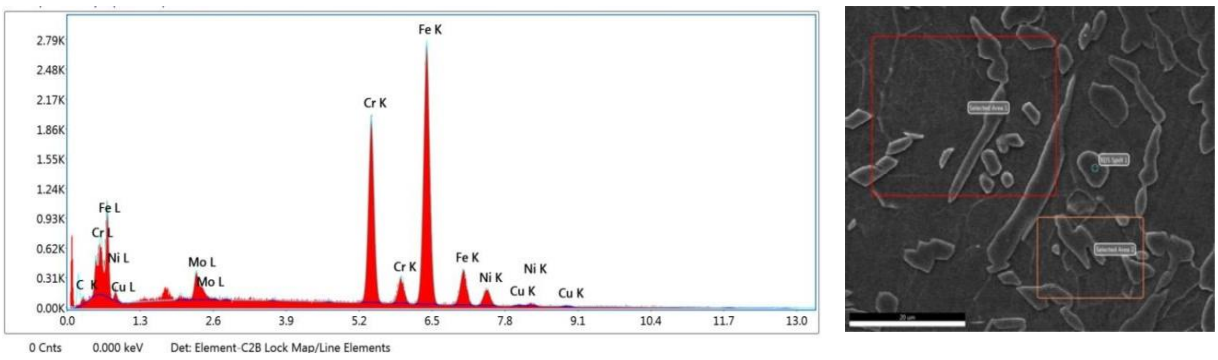

Fig.17 EDX Analysis of solution Treated specimen

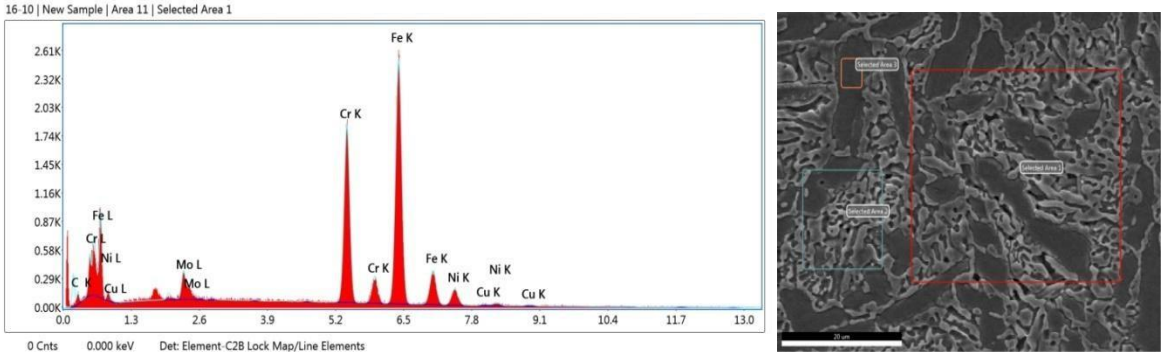

Fig.18 EDX Analysis of Heat Treated specimen at 850°c Aged for 30 min

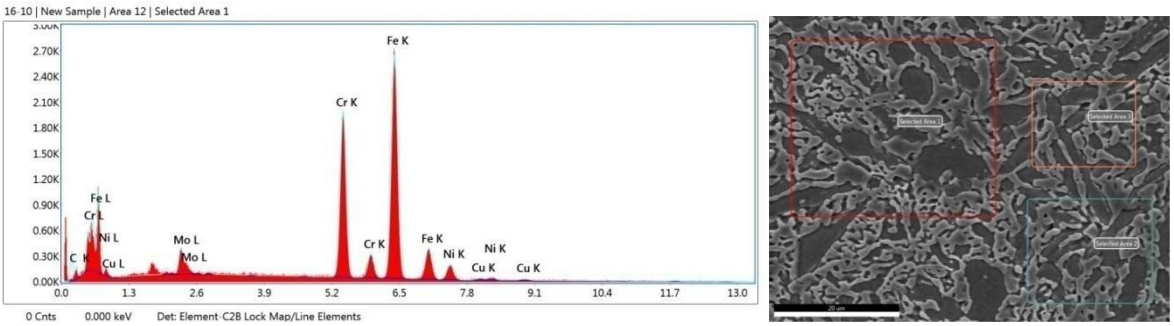

Fig.19 EDX Analysis of Heat Treated specimen at 850°c Aged for 60 min

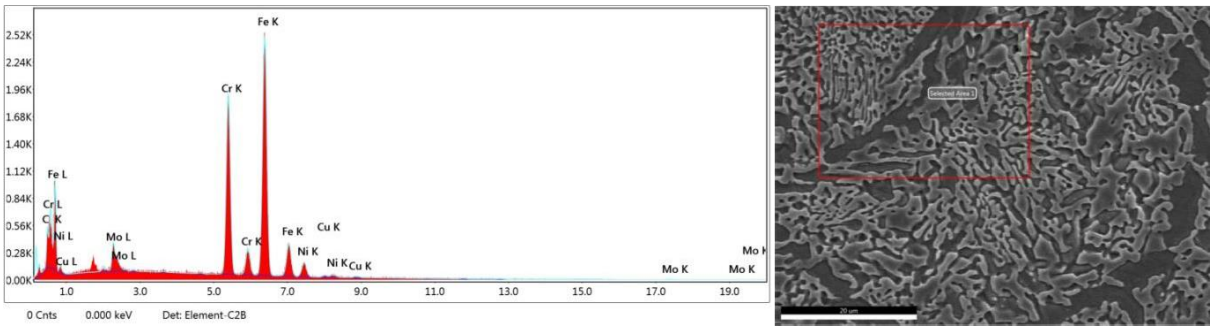

Fig.20 EDX Analysis of Heat Treated specimen at 850°c Aged for 90 min

Table 3 Mass percentage of different elements at different ageing time

Ageing Time(min)	0		30		60		90	
Element	Weight%	Atomic %	Weight %	Atomic %	Weight %	Atomic %	Weight %	Atomic %
Molybdenum	3.65	1.99	3.80	2.01	3.79	1.99	3.92	2.09
Chromium	28.18	28.36	28.35	27.70	28.62	27.81	29.12	28.59
Fe	60.06	56.28	58.94	53.63	58.05	52.53	58.63	53.59

Result obtained after Optical Image Analysis concludes that as the aging time increases the diffusion rate goes on increasing and hence we can see more ferrite promoting elements gets concentrated and hence sigma phase goes on increasing.

Hardness

Hardness value has a direct relationship with the sigma phase formation. Specimens were tested for Rockwell hardness value at 850°C for different ageing time. The aging time was taken as 0 min, 30 min, 60min and 90 min. Due to the precipitation of intermetallic phase called sigma phase, the Rockwell hardness value is found to be increasing as the aging time increases. There is no much difference in the Rockwell hardness number between the ageing times, but it is found to be increasing. Figure 21 shows us the Rockwell hardness value for different ageing time at 850° C.

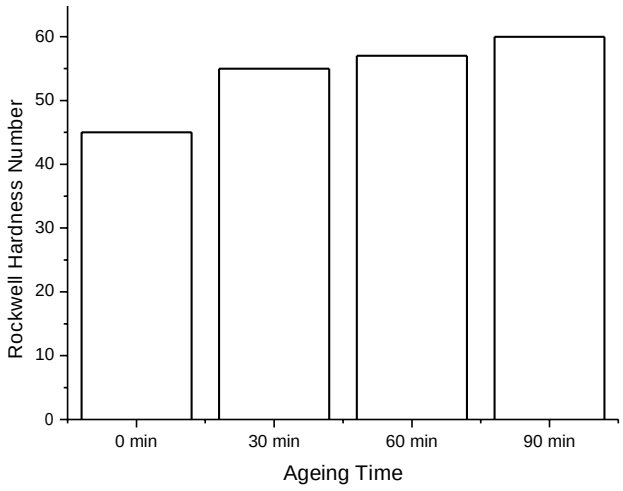

Fig.21 Rockwell hardness value for different aging time at 850° C.

Corrosion

The examinations of corrosion resistance have revealed that the ageing process after super saturation do not cause significant changes in the anti-corrosive properties. The σ phase precipitates occurring along the boundaries of primary solidification grains, according to the reaction δ ferrite→phase+γ' secondary austenite. The prolonged annealing time results in the ferrite decomposition hence improving the corrosion resistance. The test carried out here showed no formation of white and red rust after 90 mins of test as observed in Figure 22 and 23.

Fig.22 Before corrosion treatment

Fig.23 After corrosion treatment

Conclusion

- Solution treated Zeron 100 only showed austenite and ferrite phases, however after heat treatment bright sigma phases rich in chromium were formed at the interface of ferrite and austenite phases.
- SEM analysis showed the formation of sigma phase at the interface of ferrite and austenite phases. Optical image analysis revealed the increase in the formation of sigma phase as the ageing time of heat treatment was increased.
- EDX analysis showed the formation of chromium-molybdenum rich phase
- Due to the formation of sigma phase the hardness value was found to be increasing in the heat treated specimens as compared to the solution treated specimens, this also indicates the reduction in toughness and the brittle nature of Zeron 100.
- The chromium rich phase improved the localized corrosion resistance in heat treated Zeron 100.

REFERENCES

Akisanya A R, and Renton N C (2012), Effect of ageing on phase evolution and mechanical properties of a high tungsten super-duplex stainless steel, Materials Science and Engineering: A, Vol.535, pp.281-289.

Chen T H, and Yang J R (2002), Microstructural characterization of simulated heat affected zone in a nitrogen-containing 2205 duplex stainless steel, Materials Science and Engineering: A, Vol.338(1-2),pp.166- 181.

Davanageri, M et al (2016). Dry Sliding Wear Behavior of Super Duplex Stainless Steel AISI 2507: A Statistical Approach. Archives of Foundry Engineering, Vol 16 (4), pp 47-56.

Escriba, D M et al (2009), Chi-phase precipitation in a duplex stainless steel,Materials Characterization, Vol.60(11), pp.1214-1219.

Magnabosco, R (2009), Kinetics of sigma phase formation in a duplex stainless steel,Materials Research, Vol.12(3), pp.321-327.

Rosso M, (2013), About heat treatment and properties of Duplex Stainless Steels. J. Achiev. Mater. Manuf. Eng, Vol.59, pp.26-36.

Villalobos,Detal(2009),Microstructural changes in SAF2507 super duplex stainless steel produced by thermal cycle,Matéria (Rio de Janeiro), Vol.14(3), pp.1061-1069.

Wang,Y Q et al(2013),Effect of sigma phase precipitation on the mechanical and wear properties of Z3CN20. 09M cast duplex stainless steel. Nuclear Engineering and Design, Vol.259, pp.1-7.

9th International Engineering Symposium - IES 2020
March 3-5, 2020, Kumamoto University, Japan

Investigations on the Effect of combined Augmentation Technique using Circular Fins and Graphene Oxide Nanofluid in a Helical Coil in Shell Heat Exchanger

Ramakrishna N. Hegde[1], Niranjana Rai[2] and **Jagadeesh B[3]**

1 *Head of the Department of Automobile Engineering, Srinivas Institute of Technology, Mangaluru, Karnataka, India. email: rkhegderk@gmail.com*
2 *Assistant Professor, Department of Mechanical Engineering, Canara Engineering College, Mangaluru, Karnataka, India, email: niran4u@gmail.com*
3 *Assistant Professor, Department of Aeronautical Engineering, Srinivas Institute of Technology, Mangaluru, Karnataka, India.email: jagadishramb@gmail.com*

ABSTRACT: In this experimental study, synergistic effect of circular fins and Graphene Oxide (GO) nanofluid on the performance of a helically coiled Coil in Shell Heat Exchanger with fins (FCSHE) and without fins (CSHE) is investigated. The fins are attached in 2 orientations (45^0 and 90^0) to the surface of the coil and study were carried out by changing the cold fluid flow rate from laminar to turbulent regime ($500 \leq Re \leq 5500$) in 3 volume concentrations (0.05% - 0.15%) of GO nanofluid and for Hot Air Velocities (HAV=1m/s to 5m/s). The investigation reveals that heat transfer enhancement in FCSHE- 45^0 orientation with 0.15% GO/ water nanofluid concentration is about 26.38% higher compared to CSHE for the same flow condition and 37.23% higher when it uses distilled water in turbulent regime for HAV 3m/s. The thermal hydraulic performance attained a maximum value of 2.24 at Re 5500 for FCSHE- 45^0 which is 50.86% more than CSHE. FCSHE- 45^0 provides improved surface area of about 16 to 23%, due to the addition of circular fin arrangement.

Keywords*: Augmentation techniques, Circular fins, Heat Exchangerl, Nanofluid*

INTRODUCTION

The heat transfer augmentation of heat is significant in size reduction of the heat exchangers and is the topic of interest by the researchers worldwide. Use of Coil in Shell Heat Exchanger (CSHE) instead of straight pipes, gives the leverage of elevated heat transfer rate with an improved pressure drop. Helical coiled heat exchanger is incredibly compact as compared to straight pipes due to centrifugal action caused in the curved coil as fluid flows through it, which results in a secondary flow and increased turbulence. Use of nanofluid' in conjunction with this could trigger a cascading effect on heat transfer enhancement. Many literature available shed light on this, to name a few, Lin and Ebadian [1997] who studied the Nusselt number (Nu) in the completely developed thermal section of helical pipes, Jayakumar et al. [2010] who developed a correlation for the coil side Nu number for turbulent flow based on their experimental investigation, Pawar et al. [2013] who conducted experimented by varying curvature ratio (0.055-0.0757) and concentration of 10 %-20% 20 % glycerol/water mixture under both laminar and turbulent regime. Further to quote, Zeinab Hajjar et al. [2014 9] studied thermal conductivity of GO nanofluid and their result points out that the GO nanofluids have substantially superior thermal conductivities than the base fluid. The enhancement in thermal conductivity depends firmly on the concentration of GO and rises with increase in addition of graphene particles. Another literature from Jamshidi et al. [2013]

highlights the experiments on a helical coil tube in shell heat exchanger by considering flow characteristics and geometrical parameters such as coil diameter and pitch of the coil in pure water. The working fluid in all the experiments was pure water and in the laminar flow regime. They reported that the heat transfer rate improved with the higher coil diameter, coil pitch and mass flow rate in the shell and tube. Other literatures also focus on such studies [Akavan et al (2012), Fule et al (2017), Khosravi et al (2018), Roumsak et al (2015), Abhinav Gupta et al (2014)] which are not discussed here due to space limitations.

From the literature survey it is evident that the experimental investigations on CSHE using fins with various orientations and different nanofluids, a combined heat transfer augmentation technique, especially with GO nanofluid has further scope for research. a combined heat transfer augmentation technique Accordingly, a finned configuration with orientations is the focus of the present study.

EXPERIMENTAL DETAILS AND PROCEDURE

The experimental setup shown in figure 1(a), consists of two loops namely, shell region loop and helical coiled region loop handling respectively, hot air and GO nanofluid, with a counter flow arrangement. The major components of experimental setup include a test section, an air duct heating chamber (0-1500W, 3 numbers), a power meter (0 - 4.5kW), a rotameter (0 - 4 lpm) for cold fluid flow measurement, an anemometer (0- 10 m/s) for hot air velocity measurement, a centrifugal blower (1.5kW), a centrifugal pump for water circulating, K-type thermocouples (±99.990C), asbestos insulation rope, a condenser for cooling the nanofluid and a reservoir tank.

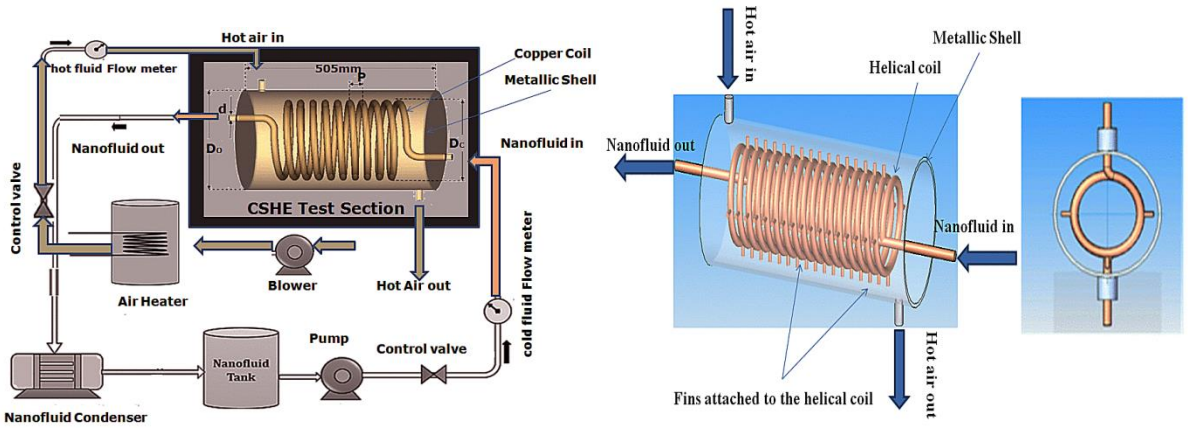

(a) **(b)**

Fig.1 (a) Schematic layout of Coil in Shell Heat Exchanger test rig (b) 3-D model of the test section

Figure 1(b) shows the test section made of a copper tube of 0.010 m inner diameter and 0.013 m outer diameter wound in helical shape with curvature ratio(δ) 0.142 and pitch 0.014 m, which is enclosed by shell of 0.116 m inner diameter, made up of stainless steel. The coil is 8.5 m long and has 36 turns.

PREPARATION OF NANOFLUID RUNNING TEXT

The preparation of the Graphene Oxide and its characterization is as per the same standard procedure followed in the previous work of the author [Hegde et al 2012], however with a Polyvinylpyrrolidone (PVP) surfactant, for better miscibility. Figure 2(a) shows the SEM image of GO nanoparticles, 45 nm size as tested using a Particle Size Analyzer. Owing to the existence of covalently bound oxygen and due to the sp^3 hybridized carbon atoms being displaced above and below the original Graphene plane, GO be likely to gather together to shape multilayer agglomerates[Stankovich et al, 2007].

For the present investigation, three volume concentrations of GO nanofluid, viz., 0.05%, 0.1% and 0.15% were prepared as shown in Figure 2(b).

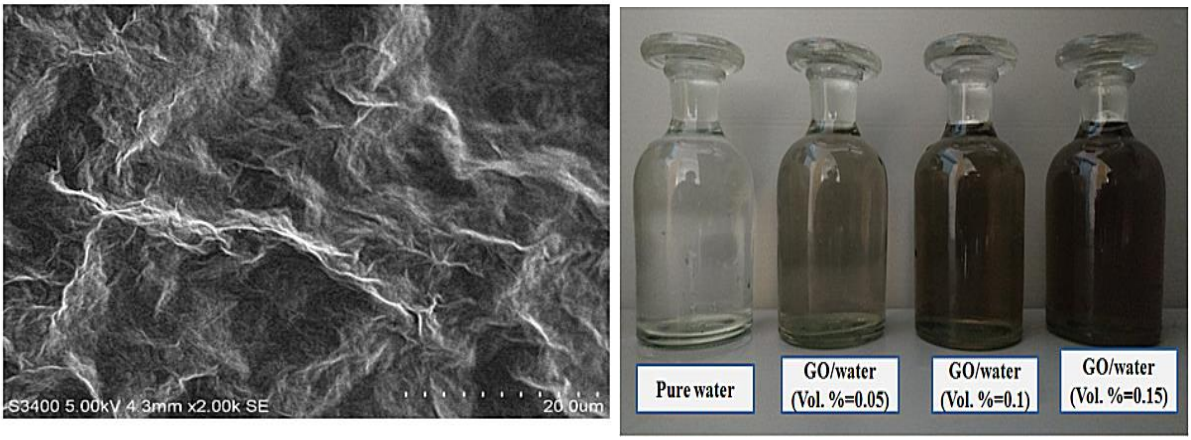

(a) **(b)**

Figure. 2 (a) SEM image of dispersed GO/water nanofluid (b) GO-Water Nanofluid in different volume concentrations

EXPERIMENTAL UNCERTAINTY AND PROCEDURE

The maximum uncertainties of derived quantities are computed and obtained in the range 0.48 to1.03% for Reynolds number, 0.9 to 2.18% for the heat gain, and 0.18 to 0.87% for heat transfer coefficient, 1.53 to 2.37% for Nusselt number,0.89 to 1.63% for friction factor, and 0.94 to 1.78% for thermal hydraulic performance respectively. The overall experimental uncertainty is 1.68% as explained by Klein and McClintock, (2013). Experimental test run comprised the following procedure with the already explained conditions.

- Conducting experiments using distilled water in CSHE and FCSHE
- Conducting experiments using various volume concentrations (0.05%, 0.10% and 0.15%) of GO nanofluid in CSHE and FCSHE (both 90^0 and 45^0 orientation).

DATA REDUCTION

The following relations available in the open literature are used to find the Logarithmic Mean Temperature difference (LMTD), heat transfer coefficient, and Nusselt number, friction factor' of the heat exchanger.

- The heat transfer (Q) for hot air and GO/water nanofluid (Heat gained)

$$Q = m_h C_{ph}\left(T_{hi} - T_{ho}\right) = m_c C_{pc}\left(T_{co} - T_{ci}\right) \quad (1)$$

- The surface temperature of the coil (T_S),

$$T_s = \frac{T_1 + T_2 + ... + T_{10}}{10} \quad (2)$$

- Bulk temperature of Cold fluid (T_{Bc}),

$$T_{Bc} = \frac{T_{ci} + T_{co}}{2} \quad (3)$$

- LMTD for the counter flow array is,

$$LMTD = \frac{\left(T_{hi} - T_{co}\right) - \left(T_{ho} - T_{ci}\right)}{\ln\left[\frac{T_{hi} - T_{co}}{T_{ho} - T_{ci}}\right]} \quad (4)$$

- Heat transfer coefficient (h),

$$h = \frac{Q}{A(T_S - T_{Bc})} \quad (5)$$

- Friction factor,

$$f_c = 0.046\,\mathrm{Re}^{-0.2}\left[De\right]^{\frac{1}{20}} \quad (6)$$

Also key dimensionless parameters of nanofluid flow through coil in shell, as well as 'Reynolds number (Re), Prandtl number (Pr) and Nusselt Number', for GO/Water nanofluid , are found using following relations.

- Reynolds Number,

$$\mathrm{Re} = \frac{\rho V d_i}{\mu} \quad (7)$$

- Prandtl Number,

$$\mathrm{Pr} = \frac{\mu C_p}{k} \quad (8)$$

- Nusselt Number,

$$Nu = \frac{h d_i}{k} \quad (9)$$

RESULTS AND DISCUSSION:

Experiments were conducted to evaluate the performance of counter flow coiled heat exchanger without fins (CSHE) and with fins (FCSHE: 90^0 and 45^0 orientations) in three volume concentrations (0.05%, 0.01% and 0.15%) of GO/water nanofluid. The performance of FCSHE is compared with CSHE based on the variation of Nusselt number, heat transfer coefficient, outlet temperatures of nanofluid and thermal hydraulic performance. It is seen that the maximum heat transfer improvement is achieved at turbulent region Re>4000 for the configurations and nanofluids concentrations.

EFFECT OF FINS AND GO NANOFLUID ON NUSSELT NUMBER

Figure 3 shows the variation of **Nusselt v/s Reynolds Number** in CSHE and FCSHE in 0.1% and 0.15% GO nanofluid concentrations at HAV = 3 m/s. It is observed that FCSHE - 90^0orientation with 0.1% GO nanofluid combination has 16.42% superior performance when compared with CSHE, with pure distilled water as cooling fluid when Re= 5500 (Figure 3a). Further, for HAV=5m/s in FCSHE - 90^0orientation with 0.1% GO nanofluid combination yields 20.67% superior performance when compared with CSHE when water is used as working fluid at Re=5500. When the nanofluid concentration was increased to 0.15% by volume, (Figure 3b), heat transfer enhancement in FCSHE - 90^0 is in 23.78% and 24.21% vis-à-vis CSHE/ pure distilled water combination respectively, for HAV= 3m/s and for HAV= 5m/s. It can be further noticed that at HAV= 3m/s the heat transfer enhancement in FCHE 45^0 orientation/ 0.15% GO nanofluid combination is about 26.38% when compared with CSHE plain/ distilled water and the maximum of 37.23% is reached at Re =5500. This could be attributed mainly due to the combined effect of nanofluid and the increased number of fins, resulting in more surface area exposed to hot air.

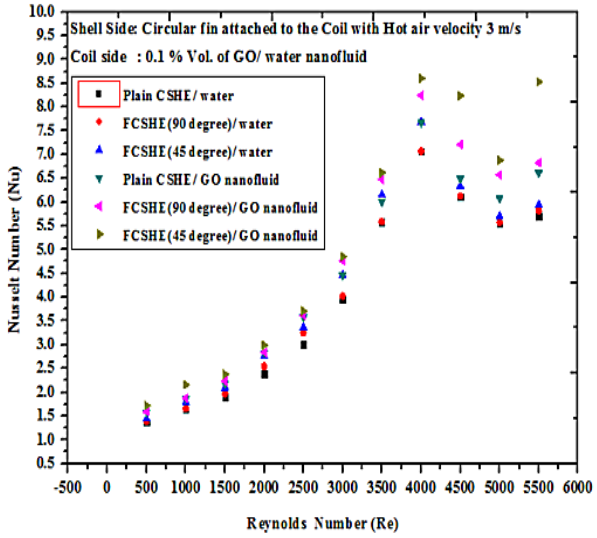

(a) 0.1% by volume of GO nanofluid

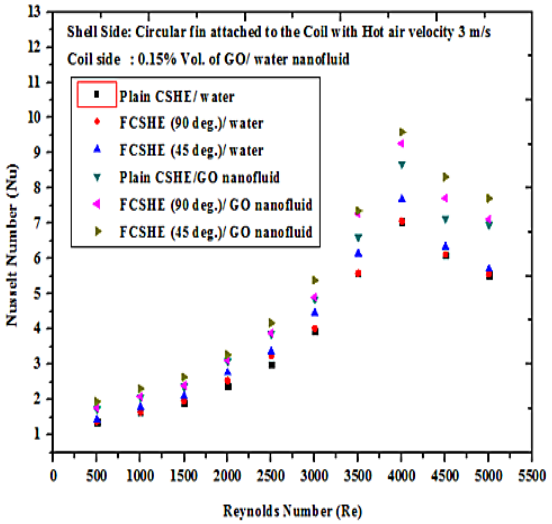

(b) 0.15% by volume of GO nanofluid

Figure.3 Nusselt v/s Reynolds Number for CSHE and FCSHE at HAV 3m/s

EFFECT OF FINS AND GO NANOFLUID ON HEAT TRANSFER COEFFICIENT

Figure 4(a) compares heat transfer coefficient, h_i v/s Re for in three volume concentrations of GO nanofluids (0.05%-0.15%) using a FCSHE-90^0 and 45^0 orientations and plain CSHE with distilled water, when HAV= 3m/s. For FCSHE 90^0 orientation /0.15% GO combination, heat transfer coefficient is respectively, 41.22% at HAV= 3m/s and 42.31% at HAV= 5m/s (graph not shown) higher than the plain CSHE /distilled water combination at Re= 4000. The maximum heat transfer coefficient obtained for FCSHE 45^0 orientation / 0.15% GO combination is 42.57% at HAV = 3m/s and 44 .65% at HAV= 5m/s, more than that of CSHE. In the turbulent regime the highest gain in heat transfer obtained for FCSHE 45^0 orientation /0.15% GO combination is 45.25% at HAV= 3m/s and 46.17% at HAV= 5m/s (graph not shown) superior than that of CSHE at R_e=5500 . The above results indicate slight improvement in heat transfer at higher HAV (=5m/s) when compared to lower HAV (=3m/s) for both the combinations. However, the FCSHE 45^0 orientation /0.15% GO combination gives better result for HAV=3m/s with minimum pressure drop in the heat recovery process.

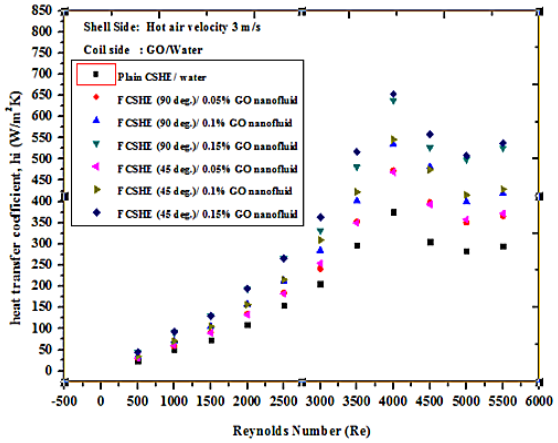

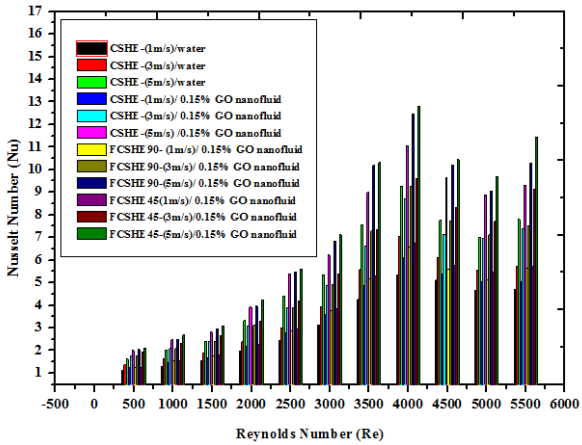

Figure.4 (a) Heat transfer coefficient v/s Re at HAV 3m/s and (b) Nu v/s Re at different HAV

Figure 4(b) shows Nu v/s Re at different HAV (1m/s-5m/s) with the FCSHE- 45^o orientation / 0.15% GO combination. As evident, when the hot air velocity is 3m/s, the

Nu is 29.62% (Re=4000) and 37.56% (Re= 5500) more than that at the lower velocity (1m/s), whereas for HAV 5m/s it shows only 31.78% rise at Re= 5500 (refer Figure 4 b) than that of lower velocity (1m/s). It is evident that the performance of FCSHE - 45^0 is reduced 5.78% at higher hot air velocity 5m/s when compared with HAV= 3m/s. This is due to the shorter availability of residence time for the hot air at higher velocity to exchange heat with the cold fluid.

THERMAL HYDRAULIC PERFORMANCE:

To verify the thermodynamic gain like effectiveness of FCSHE over CSHE it is necessary to analyze the above experimental results in terms of performance assessment criterion [Kannadasan et al (2012)] thermal hydraulic performance (t_{hp}) which can be expressed as

$$t_{h_p} = \left[\left(Nu_p / Nu_w\right)/\left(f_p / f_w\right)\right] \times (\delta)^{0.003} \qquad (10)$$

The comparison of t_{hp} of the CSHE and FCSHE (both orientations) and at different flow conditions (500 ≤ Re ≤ 5500) of the cold fluid and with 0.15% GO nanofluid is shown in Figure 5. The FCSHE-45^0 orientations - GO nanofluid combination shows better performance when compared to the other combination of FCSHE-90^0 orientations - GO nanofluid and CSHE with nanofluids. The maximum value of t_{hp} was 2.24, in the turbulent regime at Re=5500 in FCSHE-45^0 - combination at HAV= 5m/s, which is 42.78% higher than FCSHE-45^0orientation/0.15% GO nanofluid combination for HAV= 3m/s and 50.86% higher than the plain CSHE- 0.15% GO nanofluid combination at HAV=5m/s. Compared to FCSHE -90^0 orientation-0.15% GO nanofluid combination, the 45^0 orientation was 46.6% better in performance at Re= 5500 for the same flow conditions (HAV= 5m/s). The thermal hydraulic performance increased with increased Reynolds number, which was greater than unity especially in turbulent flow condition, in both the configurations of FCSHE, with increased volume concentrations of nanofluid. However, it is evident that FCSHE - 45^0orientation gives superior performance when used with nanofluid at higher air velocity. The cascading effect of curvature of the coil, circular fins attached to the coil with proper orientation, and the nanofluid as an effective heat transfer agent, could be attributed to the superior performance of the FCSHE.

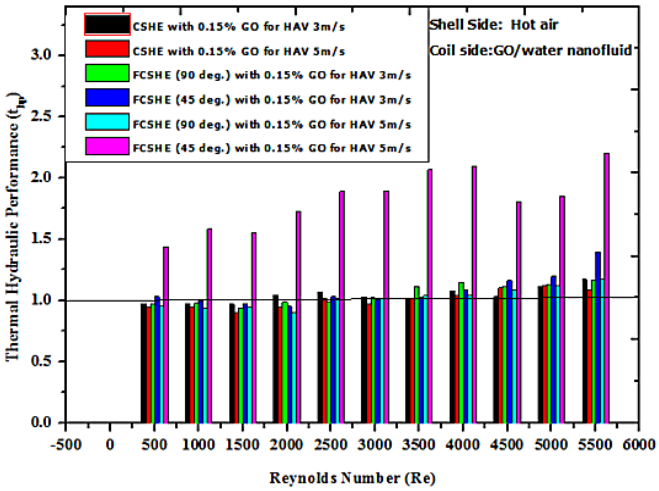

Figure.5 Thermal hydraulic performance of CSHE and FCSHE

CONCLUSIONS

In the present study, the performance of a horizontal counter flow helical coil in shell heat exchanger with (FCSHE) and without circular fins (CSHE) was investigated experimentally, using different volume concentrations (0.05% to 0.15%) of GO/water nanofluid under laminar and turbulent flow conditions (500 ≤ Re ≤ 5500). Based on the experimental findings, the following conclusions are drawn.

- Conjoint effect of nanofluid and finned configuration can enhance the heat transfer. Higher concentration of nanofluid and optimum (HAV=3m/s) air flow rate further augment the rate of heat transfer.
- Heat transfer enhancement in FCHE 45^0 orientation/ 0.15% GO nanofluid combination is 26.38% higher when compared with CSHE plain/ distilled water and the maximum of 37.23% is achieved at Re =5500 for same flow condition(HAV=3m/s).
- The thermo- hydraulic performance in the turbulent regime (Re>4000) for FCSHE-45^0 orientations - 0.15% GO nanofluid combination, is 50.13% greater than Plain CSHE- 0.05% GO nanofluid combination (HAV=5m/s).

ACKNOWLEDGEMENTS

The authors acknowledge VGST, Karnataka, India for the funding granted under KFIST-L2 scheme bearing GRD No 476.

REFERENCES

Abhinav Gupta, Ravi Kumar, Akhilesh Gupta, (2014), Condensation of R-134a inside a helically coiled tube-in-shell heat Exchanger, Experimental Thermal and Fluid Science, Vol. 54, pp. 279–289.

Akhavan-Behabadi M A, Fakoor Pakdaman M, Ghazvini M, (2012), Experimental investigation on the convective heat transfer of nanofluid flow inside vertical helically coiled tubes under uniform wall temperature condition, International Communications in Heat and Mass Transfer, Vol. 39, pp.556–564.

Fule P, Bhanvase B, Sonawane S, (2017), Experimental investigation of heat transfer enhancement in helical coil heat exchangers using water based CuO nanofluid, Adv.Powder Technol. ,Vol. 28, pp.2288–2294.

Jayakumar J, Mahajani S, Mandal J, Iyer K N, Vijayan P, (2010), CFD analysis of single phase flows inside helically coiled tubes", Comput. Chem. Eng., Vol. 34, No. 4, pp.430–446.

Jamshidi N, Farhadi M, Ganji D D, Sedighi K,(2013), Experimental analysis of heat transfer enhancement in shell and helical tube heat exchangers, Appl Therm Eng, Vol.51, pp. 644–52.

Kannadasan N, Ramanathan K, Suresh S, (2012),Comparison of heat transfer and pressure drop in horizontal and vertical helically coiled heat exchanger with CuO/water based nano fluids, Experimental Thermal and Fluid Science, Vol., 42, pp.64–70.

Khosravi-Bizhaem H, Abbassi A, (2018), Effects of curvature ratio on forced convection and entropy generation of nanofluid in helical coil using two-phase approach, Adv.Powder Technol, Vol. 29, pp. 890–903.

Klein S J, McClintock, (2013), The description of uncertainties in a single sample experiments, Mech. Eng. Vol.75, pp. 3–8.

Lin, C and Ebadian, M (1997), Developing turbulent convective heat transfer in helical pipes, Int. J. Heat Mass Transf., Vol. 40, No. 16, pp.3861–3873.

Pawar S, Sunnapwar V K, (2013), Experimental studies on heat transfer to Newtonian and non-Newtonian fluids in helical coils with laminar and turbulent flow, Exp Therm Fluid Sci., Vol. 44, pp.792–804.

Ramakrishna N Hegde, Shrikantha S Rao, R. P. Reddy, (2012), Investigations On Heat Transfer Enhancement In Pool Boiling With Water-CuO nanofluids, Journal of Thermal Science, Springer-Science Press, Vol. 21, No. 2, pp.179 -183.

Roumsak Boonsri and Somchai Wongwises, (2015), Mathematical Model for Predicting the Heat Transfer Characteristics of a Helical-Coiled, Crimped, Spiral, Finned-Tube Heat Exchanger, Heat Transfer Engineering, Vol.36, No.18, pp.1495–1503.

Stankovich S, Dikin D A, Piner R D, Kohlhaas K A, Kleinhammes A, Jia Y, Wu Y, Nguyen S T, Ruoff R S, (2007), Synthesis of graphene-based nanosheets via chemical reduction of exfoliated graphite oxide, Carbon, Vol.45, pp.1558–1565.

Zeinab Hajjar, Ali morad Rashidi, Ahmad Ghozatloo,(2014),Enhanced thermal conductivities of graphene oxide nanofluids, International Communications in Heat and Mass Transfer, Vol.57, pp.128–131.

NOMENCLATURE

A_s : Effective Surface area, m^2
C_p : Specific heat of water, kj/kg-K
D_c : Diameter of Helical coil, m
D_e : Dean Number
d_i : Inner diameter of coil tube, m
f_c : Friction factor
h_i : Heat transfer coefficients, W/m^2K
I : Current supplied, Ampere
k : Thermal conductivity, W/mK
L : Tube length, m
m : Mass flow rate, kg/s
N_u : Nusselt Number
p : Pitch of the coil, m
q : Heat flux, W/ m2
Q : Rate of Heat Transfer, kW
R_e : Reynolds Number
T : Temperature, K
V : Voltage, volts

SUBSCRIPTS

c : Coil
c_i : Cold fluid inlet
co : Cold fluid outlet
hi : Hot fluid inlet
ho : Hot fluid outlet
f : Base fluid
nf : Nanofluid
p : Particle
s : Surface
w : Water

GREEK/ROMAN/LATIN

ρ : Density(kg/m^3)
μ : Absolute viscosity(Ns/m^2)
φ:Volume Concentrations of nanofluids(%)
δ : Curvature ratio

ABBREVIATIONS

HAV : Hot Air Velocity
FCSHE: Finned Coil in Shell Heat Exchanger
CSHE : Coil in Shell Heat Exchanger
LMTD : Logarithmic Mean Temp. Difference

Experimental and Theoretical Study of Thermal Conductivity of Glass Fibre Filled with Silicon Hybrid Composite Materials

Aditya Rathore[1] and **Gurushanth B Vaggar**[2]

[1]*Undergraduate Student, Department of Mechanical Engineering, Alva's Institute of Engineering and Technology Karnataka, Moodbidri, Mangalore–574225, India. Email: adityarathore2017@gmail.com*
[2]*Associate Professor, Department of Mechanical Engineering, Alva's Institute of Engineering and Technology Karnataka, Moodbidri, Mangalore – 574225, India. Email: gvgr.aiet@gmail.com*

ABSTRACT: The silicon inserted glass fibre reinforced polymer composites have been prepared by using hand- lay- up technique. The thermal conductivity (K) of silicon inserted glass fibre reinforced polyester composites at different volume fractions of glass fibre and silicon is determined experimentally by using Lee's apparatus. The experimental results shows that the thermal conductivity of the composite increases with increase in silicon percentage. Experimental results are compared with rule of mixture model, Hashin formula and Maxwell model to describe the variation of the thermal conductivity versus the volume fraction of the silicon. All three models exhibited results close to each other at low fibre content. It has been found that the errors associated with rule of mixtures, parallel model and Maxwell's correlations with respect to experimental ones lie in the range of 50 to 70%, 45% to 68% and 33 to 65% respectively.

Keywords*: Error Analysis, Lees Apparatus, Glass fibre-Polymer Hybrid composites, Thermal Conductivity (K).*

INTRODUCTION

Recently, thermoplastic and thermoset polymers are combined with fillers to produce the composites, which possess better strength and good resistance to fracture. The reason for focus on glass fiber reinforced filler polymer matrix is because of its low cost, eco-friendly, low energy consumption, nonabrasive nature, and good insulator of heat and sound. Major industries such as automotive, construction and packaging have shown enormous interest in the development of new hybrid-composite materials. Unsaturated polyesters are extremely versatile in properties and applications. These are popular thermosets used as the polymer matrix in composites.

The advantages of composites include high strength to weight ratio, non-corrosiveness, less maintenance, high electrical resistance, wear resistance, electromagnetic transparency, appeasing appearance etc. Composites can be manufactured in different ways depending upon matrix, reinforcement and application. Different manufacturing methods include Hand-layup, Compression moulding, Resin Transfer Moulding (RTM), Pultrusion, Autoclave and Filament moulding etc. [1].

Effective thermal conductivity is an important characteristic of heat transfer properties of materials. The temperature field in composite materials cannot be determined unless the thermal conductivities of the media are known. Numerous theoretical and experimental approaches have been developed to determine the precise value of this parameter. Maxwell [2] studied the effective thermal conductivity of heterogeneous materials. By solving Laplace's equation, the effective thermal

conductivity of a random suspension was determined for sphere within a continuous medium. Agrawal et al. [3] studied the thermal conductivity and thermal diffusivity of oil-palm-fibre-reinforced untreated and differently treated composites using transient plane source technique at room temperature. All the silane and alkali treatments of the fibres increased the thermal conductivity and thermal diffusivity of the composites in comparison with the acetylated composite. Saxena et al. [4] studied the variation of thermal conductivity and thermal diffusivity of banana fibre reinforced polyester composite caused by addition of glass fibre. They observed that the thermal conductivity of composites increased when compared to neat matrix. However, the thermal conductivity of the composites with increased percentage of glass fibre decreases in comparison to composite of pure banana, Fu and Mai [5] studied the effect of fibre length and fibre orientation angle on the thermal conductivity of short carbon fibre reinforced composite materials. The thermal conductivity of the composite increased with fibre length but decreased with fibre orientation angle with respect to specified measured direction. Mangal et al. [6] studied the effect of volume fraction of pine apple leaf fibre on thermal properties of the composite using transient plane source technique. Increasing the fibre content in the matrix decreases the thermal conductivity and thermal diffusivity of the pine apple leaf fibre reinforced composite which means that it could not provide the conductive path to the heat energy in the composite material.

In the present work a study of thermal properties are carried out to the prepared specimens of silicon inserted hybrid composite materials (on silicon inserted glass – fiber chop strand). The specimens were prepared by hand layup followed by compression molding machine by non-heating molding technique, thermal conductivity (*K*), found experimentally and theoretically. Specimens and experimental setups are prepared as per the ASTM standards [7]. Thermal properties of any materials decides withstanding and sustainability of that material under variable temperature conditions it may be high temperature or low temperature.

1) Thermal Conductivity Models: Many theoretical and empirical models have been proposed to predict the effective thermal conductivity of two phase mixtures. For a two component composite the simplest alternative would be with the materials arranged in either parallel or series with respect to heat flow, which gives the upper and lower bounds of effective thermal conductivity

- **Series Model (Rule of Mixture):**

$$\frac{1}{K_h} = \frac{(1-\text{ø})}{K_m} + \frac{\text{ø}}{K_g} - - - -(1)$$

Where h- composite, m- matrix, g-glass fiber, Φ- volume fraction.

- **Hashin formula:**

$$K_h = K_m \left\{ \frac{K_m V_m + K_f(1+V_f)}{K_m(1+V_f) + K_f V_m} \right\} - -(2)$$

Where, V_m = Volume fraction of matrix epoxy resin, V_g = Volume fraction of E-glass Fiber, V_f = Volume fraction of silicon carbide filler

- **Maxwell equation:**

$$\frac{K_h}{K_m} = 1 + \left[\frac{3(K_f - K_m)}{(K_f + 2K_m)} \right] \text{ø} - - - (3)$$

2) Experimental Set up:

The thermal conductivity test is carried out with Lee's disc apparatus shown in Fig- 1. The brass disc (B) is hung from the stand with the help of three strings. On the brass disc (B), sample disc(S) is placed. Metallic disc (M) is placed on the top of the sample disc. On the metallic disc (M) a heating chamber (H) with facility of passage of steam in and out is created. Two holes are made in the brass disc (B) and metallic disc (M) for the insertion of thermometers to measure the temperature.

Experiment procedure:

- Mass of the brass disc (B) is measured using a balance. Diameter of the specimen or sample is measured using vernier caliper. Thickness of the specimen or sample is measured using a screw gauge.
- The heater (H) is started by sending steam through the heating chamber. The temperatures T1 and T2 are recorded at a

regular interval of 5 minutes till they reached the steady state.

- Then, the supply of steam is cut off and upper metallic disc (M) and specimen or sample disc (S) are removed. Steam is again passed in so that the brass disc is heated to a temperature 100 C above the steady state temperature T2. After that the heating chamber is removed and allowed the brass disc (B) to cool. Temperature is noted in every half a minute until the temperature falls about 100 C from steady state temperature T2.
- Graph is drawn with the time of cooling as abscissa and the temperature of brass disc (B) as ordinate. A tangent is drawn at the steady state temperature T2. The slope of this tangent gives the rate of cooling $\frac{dT}{dt}$ at steady state temperature T2.

METHOD TO PREPARE HYBRID POLYMER COMPOSITES

Machine moulding is used to prepare hybrid polymer composites by hand layup method. Mould box is prepared as per the size of the HPC with the proper mixture of resin hardener and filler particles pasted on glass fiber layups then pressure applied on mould by using compression moulding machine allowed cure for 24 hours under normal atmospheric conditions. This method of preparing hybrid polymer composites is the simplest and economical than other methods. Specimens dimensions as shown in figure 2.

RESULTS AND DISCUSSION

The effective thermal conductivity values obtained from the experimental study for the silicon filled hybrid polymer composites are compared with Rule of mixture thermal conductivity model, Hashin thermal conductivity model and Maxwell thermal conductivity model (Fig.3). It is noticed that the experimental results and all three models are close to each other at low fibre content. It has been found that the thermal conductivity of experimental study and all other three models are increased with increase of silicon contents. On comparison, it has been found that the errors associated with Rule of mixture model, Hashin formula and Maxwell correlations with respect to experimental ones lie in the range of 50 to 70%, 45 to 68% and 33 to 65% respectively. The values of thermal conductivities and percentage of errors associated with each method for individual composite are given in Table-1 and Table-2 respectively.

CONCLUSIONS

The following conclusions are inferred from this study.

- Thermal conductivity of hybrid polymer composite materials increases as the percentage of SiC filler material increases.
- Thermal conductivity show significant increase after 15% SiC filler fraction.
- The experimental results were compared with the theoretical thermal conductivity models, in that Maxwell's thermal conductivity model results found good correlation with experimental one.
- With the above results it is concluded that hybrid polymer composite materials can withstand high temperatures up to 300^0C. Silicon can be used as filler material in GFER composites successfully.

ACKNOWLEDGEMENTS

The Authors are very much grateful to Dr. Basava T, Dept. of Mechanical Engineering, SDMIT, Ujire, Karnataka, India. Dr. Satyanarayan, Dept. of Mechanical Engineering, AIET, Moodubidire, Karnataka, India for their valuable suggestions, guidance and support.

[1] Brian Y. Lattimer, Jason Ouellette. "Properties of composite materials for thermal analysis involving fires" Elsevier Composites, part A37 (2006) 1068-1081.

[2] Maxwell J.C., "A Treaties on Electricity and Magnetism," 3rd Ed. New York: Dover, 1954.

[3] Agrawal, R., Saxeena, N.S., Sreekala, M.S., and Thomas, S., "Effect of Treatment on the Thermal Conductivity and Thermal Diffusivity of Oil Palm Fibre Reinforced Phenol Formaldehyde Composites," Jou. Polym. Sci. B. Vol. 38, 2000, pp. 916-921.

[4] Saxena, N. S., Agarwal, R., Sharma, K. B., Thomas, S. and Pathan, L. A., "Thermal Conduction and Diffusion through Glass- Banana Fibre Polyester Composites," Ind. J. Pure Appl. Phys., Vol.41 (6), 2003, pp. 448-452.

[5] Fu, S. Y. and Mai, Y.W., "Thermal Conductivity of Misaligned Short Fibre Reinforced Polymer Composites," J. Appl. Polymer Sci., Vol. (88), 2003, pp. 1497-1505.

[6] Mangal, R., Saxena, N. S., Sreekala, M., S., Thomas and Singh, K., "Thermal Properties of

Pine Apple Leaf Fibre Reinforced Composites," Aterial Sci, Eng., Vol. 339 (1), 2003, pp. 281-285.
[7] K. Devendra and T. Rangaswamy. "Thermal Conductivity and Thermal Expansion Coefficient of GFRP Composite Laminates with Fillers". ISSN: 2320-2491 (2013).

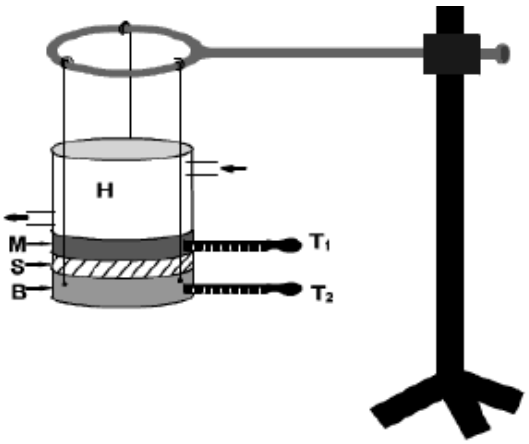

Fig. 1 Thermal conductivity experimental setup.

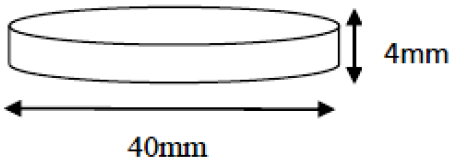

Fig. 2 Dimensions of specimen.

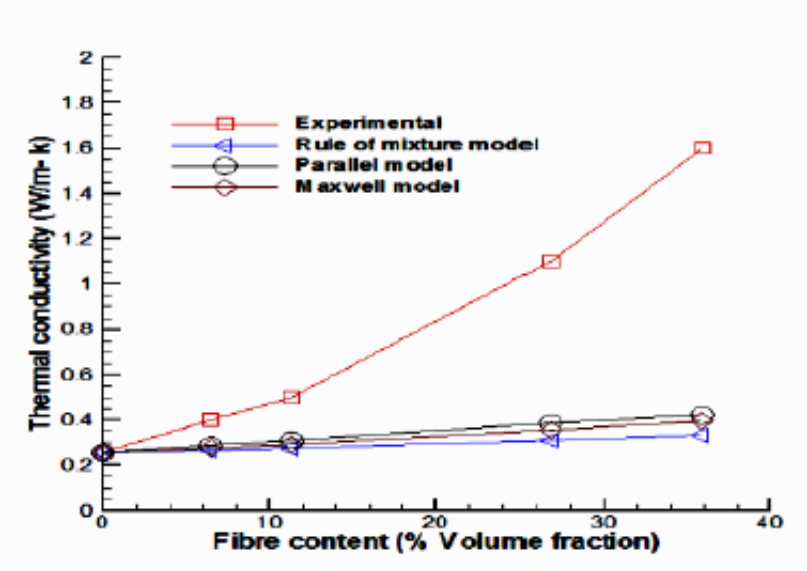

Fig. 3 Thermal conductivity values for different models.

9th International Engineering Symposium - IES 2020
March 3-5, 2020, Kumamoto University, Japan

Effect of injection pressure on Performance and Emission Characteristics of CI Engine Fuelled With blends of Honge hybridbiodiesel With Diesel

K.V.Suresha[1,2],Rohan Prabhu[3], Peter Fernandes[4],Raju K[5]

1 *Research scholar, Department of Mechanical Engineering,St. Joseph Engineering college Mangalore, 575028, India.email:*kvs_a@yahoo.com
2 *Professor, Department of Mechanical Engineering,Alva's Institute of Engineering and Technology, Moodabidri, 574225 India.email:*kvs_a@yahoo.com
3 *UG Student, Department of Mechanical Engineering, Alva's Institute of Engineering and technology Moodabidri574225, India.email:rohanprabhu2017@gmail.com*
4 *Professer, Département of Mechanical Engineering, Alva's Institute of Engineering and Technology, Moodabidri, 574225, India.email:principalaiet08@gmail.com*
5 *Professer, Department of Mechanical Engineering, St. Joseph Engineering college Mangalore, 575028, India.email:rajuksjec@gmail.com*

ABSTRACT:
In this experimental study the performance and emissions of a diesel engine using Honge and Rice bran methylester (RBO) blend with diesel.The bio-fuel blends B10 (5% honge+5%RBO+90% diesel),B15, B20 and B25 (20% honge+5% RBO+75% diesel) were prepared and tested at various load like 0%,25%, 50%, 75% and full load conditions and compared with baseline diesel at varied injection pressures such as 180 bar,200bar and 220 bar at 16.5 compression ratio. The test results showed that, the 20H+5R+75D blends at 220 bar injection pressure exhibited best performance with low emission than at low injection pressures other than No_x. Results were also showed that performance and emissions of Honge and RBO bio diesel blends were near to diesel

***Keywords**: Injection Pressure, biodiesel, blends, Honge oil, Emission,Rice bran oil*

INTRODUCTION

The internal combustion engine plays a major role in the power generation sector, power utilised in irrigation, transportation, marine sector, electricity production, transportation, defence, etc. is mainly produced from internal combustion (IC) engines. At present most IC engines are operated by fossil fuels. It is a known fact that the reserves of fossil fuels are depleting at a fast rate, and also the burning of fossil fuels leads to environmental problems such as smog, acid rain, depletion of the ozone layer, global warming reported by Bora et al (2014).Biodiesel is the name of a clean burning alternative fuel produced from domestic,renewable resources such as soybeans,Sunflowers,Honge,waste cooking oil or animal fats.Bio diesel is made through chemical process called Transesterificatio in which glycerine is separated from fat or vegetable oil.The depletion of world oil reserves leads to the development of bio fuels since these fuels are promising alternatives to substitute fossil fuels according to Lin et al.(2011) and Dharma.et.al (2016).Nowadays, there is great interest in mixing biodiesels produced from different feedstock in order to exploit the benefits of each type of biodiesel.A number of researchers have adopted approach an implemented these fuels in diesel engines as per KentHoekmanet.al(2012).The biodiesel is produced by trans-esterification of oil or fats in medium such as methanol or ethanol with NaOH or KOH as catalyst.

Methanol is used frequently because of less cost compared to other alcohols as reported by Meher et al. (2006).Karanja biodiesel was blended with diesel up to 30% and tested in a constant-speed diesel engine. The B20 blend (i.e. 20% biodiesel and 80% pure diesel) gave high thermal efficiency with low smoke emission compared to the other blends used in thatstudy by mohitekumar (2016) Saravanan et al.(2010) conducted an experiment to investigate the combustion characteristics of a CI engine using crude rice bran oil methyl ester (B20). The authors reported lower smoke and higher NOx for the biodiesel compared.Kapilan et al.(2006) studied the effect of fuel IP on the performance and emissions of a four-stroke single-cylinder DI diesel engine filled with karanja methyl ester blends (B20) as fuel. At 200 bar IP, B20 presented improved performance and reduced emissions than for other IPs. In addition, there was less CO, HC, NOx and smoke emissions as compared to diesel, and the B20 blend at 200 bar showed BTE similar to diesel.As per Bora et al. (2012) investigated the characteristics of biodiesel produced bymixing three types of feedstock (polonga, koroch, and Jatropacurcas) and found that there is a significant enhancement in the physicochemical properties of the biodiesel obtained from mixed feed stocks compared to those for individual biodiesels. In this study two biodiesel namely honge and Rice bran oil methyl ester were mixed in different proportion with diesel and investigate the performance and emission characteristics of single cylinder 4 stroke diesel engine at 3 different injection pressures.

2. Materials and Methodology

2.1Materials

Honge oil is also called Karanja oil. Its botanical name is Pongamiapinnata L, belongs to family of Leguminaceae or papilionaceae. It can grow on most soil types ranging from stony to sandy to clayey. Karanja is a medium sized fast growing evergreen tree, which reaches 40 feet in height andThe seeds are usually elliptical,2 cm long and 1.8 cm broad, wrinkled with reddish browncolor. The time needed by the tree to mature ranges from 4 to 7 years and depending on the size of the tree the yield of kernels per tree is between 8 to 24 kg and the yield ofpotential per hectare is 900 to 9000 kg/hectare reported by Yaliwal.V S et.al (2010).Extraction requires passing the seeds through a screw crusher, generally called expellers. The oil is then filtered to make it clean enough for processing stated by C.V. Mahesh (2012)It is found that the maximum yields were obtained by the Solvent extraction method Hongeoil was collected locally.

2.2 Transesterification of Honge and Rice bran oil

According to Srivastava andPrasad R (2004)there are four different ways through which non-edible oils can be converted into methyl esters are transesterification,blending,emulsion and pyrolysis out of which transesterification is used commonly reprted by Dharmadhikariet.al(2012) stated that Free fatty acid (FFA) content should be known for the raw oil FFA will be determined by simple chemical titration.

One litre of Hongeoil is heated in open beaker to a temperature for 100^{o}C to remove water particles present in oil followed by filtration of oil. The oil is processed under alkali based catalyzed transesterification method since FFA valuewas found to be 2.76%.The oil is mixed with300ml of methanol and 6 grams of sodium hydroxide pallets in round bottom flask stirred on a hot plate magnetic stirrer for 90 minutes at 60^{o}C and then it is allowed to settle down for about 6 to 8hrs to obtain biodiesel and glycerol. The biodiesel obtained in the process is further washed with water to remove acid content and heated above 100^{o}C to remove the moisture. Hence pure honge biodiesel is obtained.Since the FFA Value of Rice bran methyl ester (RBO) was found to be 0.846% single stage is used and above procedure is follows as shown in Fig.1.

2.3 Physico-Chemical properties of fuel samples

Haiter LeninK et.al (2012) and Senthil Kumaret.al(2012) stated that some of the properties like flash point, viscosity, density, specific gravity and calorific value are needed for using the bio-diesel as

vehicular fuel. The flash and fire points were determined by ASTM Standard.In this study 2 blends in the proportion of 10H+5R+85D (10%Honge biodiesel +5% ricebranbiodiesel+85%diesel) and 20R+5H+75D (20%Honge biodiesel +5%Rice bran biodiesel+90%diesel)were used. Table 1 gives the properties of above cited biodiesels

2.4 Details of Diesel Engine Test Rig

The engine tests were conducted on a computerized single cylinder four-stroke, water-cooled diesel engine test rig (Fig.2). It was directly coupled to an eddy current dynamometerThe load on the engine can be varied by Eddy Current dynamometer. The specifications of the engine are shown in Table 2. The exhaust gases are analyzed by using gas analyzer.Initially the experiments were performed fordiesel at 3 injection pressure like 180bar, 200bar and 220bar and then 10H+5R+85D and 20H+5R+75D blends at different injection pressure as mention earlier.The enginE performance like brakepower,brake specific fueL consumption,brake thermal efficiency, and emission likeHC,CO and Nox were obtained and then compared the performance of blends with those of D100 at 220bar.Based on the experimental methodology the following results were obtained

3 RESULTS AND DISCUSSION

3.1Performance characteristics

Brake Specific Fuel Consumption (BSFC): The variation of BSFC against load is shown in figure 3. From the results it has been observed that the blend of 20H+5R+75D gives the minimum BSFC of 0.26 kg/kW-hr at 220 bar injection pressure and minimum BSFC of 0.26 kg/kW-hr for 10H+5R+85D blend which found to be more than diesel i.e. 0.25 kg/kW hr at full load at same 220 bar injection.BSFC values of biodiesel will be always greater than diesel due to Calorific value which is less than diesel.BSFC decreases with respect to load and shows close results to diesel. This may be due toimproved combustion, low viscosity and high volatility of the test fuels as compared todiesel at full load but more in low injection pressure at all loads.

Brake Thermal Efficiency (BTE)

Figure 4.shows that the variation of brake thermal efficiency against load.As the load increases the brake thermal efficiency also increases for the fuel samples at different injection pressures used in the test.It was observed that the 20H+5R+75D blend at 220bar gave the maximum brake thermal efficiency of 33.34% at full load which was Brake Thermal Efficiency of diesel i.e. 34.36 %.This may be higher heat content, low viscocity,lower density and higher volatility.It was observed that the blend at 180 bar injection pressures gave low BTE. Since the viscosity and density of that blend nearer to that of diesel and better spray at 220 bar injection pressure ensures finer breakup of fuel droplets which helps in better combustion process and also providing more surface area and better mixing with air.

3.2 Emission characteristics

Hydrocarbon (HC) emission

The variation of Hydrocarbon emission against load is shown in Figur 5. It was observed that the emission of HC increases with increase in load.It has been observed that 20H+5R+75D blend gave low HC emission at 220 bar injection pressure similar to that of diesel. The unburnt hydrocarbons emissions are higher at low injection pressures (180bar) and lowest emission at 220 bar injection pressure in all blends at all loads because low atomization and large droplets are formed leading to more unvapourised hydrocarbons in the exhaust.This improper mixing is caused due less surface contact with air and leads to improper combustion and hence more amount of HC is emitted from the engine..

Carbon monoxide emission

The variation of Carbon monoxide against load is shown in Figure 6.It was observed that 20H+5R+75D blend gave low CO emission 0.046 % at 220 bar injection pressure compared to diesel CO emission is 0.044%.The CO emissions are minimum at 220bar and higher at low injection pressures (180bar)because low atomization. Low CO emission observed the blends of Honge and Rice bran oil methyl esters at 220bar compared diesel likely due to oxygen content inherently present in the biodiesel which helps in the more complete oxidation of fuel

Oxides of Nitrogen (NO_X)

The Figure 7.depicts the variation of oxides of nitrogen against load. It has been observed that 20H+5R+75D blend gave best NOx value (777ppm) compared to diesel (764ppm) at 180 bar and more (835ppm)at 220 bar injection pressure. The emission of NO_X is a phenomenon depends mainly on the combustion temperatureIt has been observed that The Noxemissions are more at 220 bar injection pressure compared low injection pressures. However blends at higher Nox are observed at higher injection pressure due to high cylinder pressure and temperature at higher loads**.** High temperature and availability of oxygen are the two primary reasonsfor high NO_Xformation as nitrogen and oxygen respond at higher temperature.

4.CONCLUSIONS

Based on the above results and discussion the following conclusion is drawn.

* The performance characteristics like brake specific consumption (BSFC), and brake thermal efficiency (BTE) for the hybrid blend 20H+5R+75D at 220 bar injection pressure is better than the low injection pressure (180 bar)
* The HC and CO emission of the hybrid blend 20H+5R+75D at 220 bar gives good result compared low injection pressure except Nox.
* By considering the above characteristics, this blend 20H+5R+75D may be used as a vehicular fuel for single cylinder four stroke diesel engines without any modifications

5.REFERENCES

[1] Bora BJ et al(2014) Effect of compression ratio on performance,combustion and émission characteristics of a dual fuel diesel enginerun on rawbiogas. Energy Convers Management;87:1000–1009.

[2) Lin, L.et,al (2011) "Opportunities andchallenges for biodiesel fuel". Appl Energy 88, 1020-1031

[3] Dharma, S.et.al(2016a) "Optimization of biodiesel production process for mixed Jatrophacurcas–Ceiba pentandra biodiesel using response surface methodology. Energ Convers Manage 115, 178-190.

[4]KentHoekman.Set.al (2012)" Review of biodiesl, composition,properties,andspecifications".Renewablea nd SustainableEnergyReviews16, pp 143– 169.

[5] Meher, L C et al. (2006), Technical aspects of biodiesel production by transesterification – a review, Renewable and Sustainable Energy Reviews, Vol. 10, No. 3, pp. 248-68.

[6] Mohite S et.al(2016)"Experimental studies on use of Karanja biodiesel as blend in a compression ignition engine". Int J Renew Energy Res.;6(2):355–360.

[7]SaravananS.al(2010)."Combustion characteristics of a stationary diesel engine fuelled with a blend of crude rice bran oil methyl ester and diesel. Energy. 2010;35:94–100.

[8] Kapilan N et.al(2006)."Effect of Injection Pressure on the Performance and Emission of Diesel Engine using Blend of Methyl Esters of Karanja Oil and Diesel as Fuel". SAE Technical Paper, 2006-32-0025

[9].Bora, D.K.et.al(2012)."Performance of diesel engine using biodieselobtained from mixed feedstocks". Renew SustEnergRev,16, 5479-5484

[10]YaliwalV.S.et.al(2010)."Production and Utilization of Renewable Liquid Fuel in a Single Cylinder Four Stroke Direct Injection Compression Ignition Engine, International Journal of EngineeringScience and Technology, Vol. 2(10) pp. 5938-5948

[11]Mahesh.V.S& E.T. Puttaiah, Studies on Performance and Emission characteristics of non-edible oil (honge oil) as alternate fuel in CI engine, *International Journal of Engineering Research and Applications,* Vol. 2, Issue 3 (2012) pp. 2288-2293

[12]Srivastava A and Prasad R (2004) "Triglycérides based biodiesel fuels,Renewable and sustainable energy reviews,4,111-133

[13]Dharmadhikari.H.Met.al(2012)"Performanceande missions of CI engine using blend sof biodiesel and diesel at different injection pressures .International Journal of Applied Research in Mechanical Engineering (IJARME) ISSN: 2231 –5950, Vol-2,Iss-2,

[14] HaiterLenin.A and K. Thyagarajan(2012), 'Performance evaluation of dieselengine fuelled with methyl ester of pongamia oil', International Journal of Energy and Environment, Vol. 3, pp. 939-948

[15]SenthilKumar.R, and R.Manimaran,(2013) 'Performance and emission characteristics on 4-stroke single cylinder C I engine using cotton seed bio fuels' Asian Journal of Engineering Research, 2013, Vol. 1,Issue II, pp. 1 – 3.

Table 1.Properties of biodiesel

Properties	Higher Calorific value (kJ/kg)	Density (kg/m^3)	Kinematic Viscosity@ 40°C (cSt)	Flash Point (°C)
ASTM Standard	D 240	D 4052	D 445	D 93
Diesel	42850	823	2.63	42
Honge methyl ester H100	34915	834	5.43	203
Rice bran methyl ester R100	40795	873	4.41	178
5H+10R+85 Diesel	42256	771	2.55	49
5H+20R+75 Diesel	42070	764	3.63	50

Table 2.Engine specification

S. No.	Parameters	Specification
1	Engine	4 Stroke, Single Cylinder, Constant Speed, Water Cooled Diesel Engine
2	Make	Kirloskar
3	BHP	3.73 kW @ 1500 RPM
4	Stroke Length	110 mm
5	Compression Ratio	16.5:1
6	Displacement Volume	553cc
7	Starting	Crank Start
8	Lubrication	Forced

Figure 1.Transesterification process

Figure 2.Engine setup

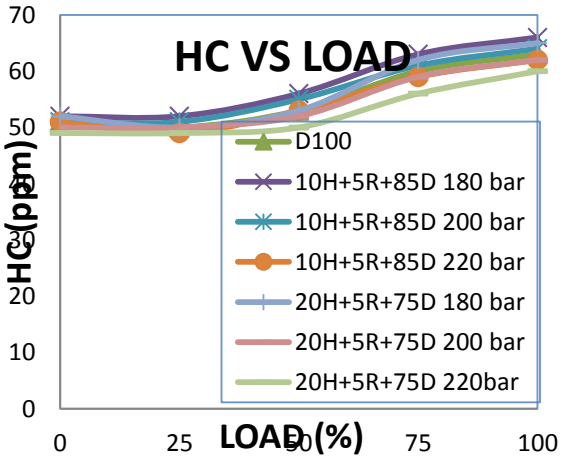

Figure5.variation of HC against load

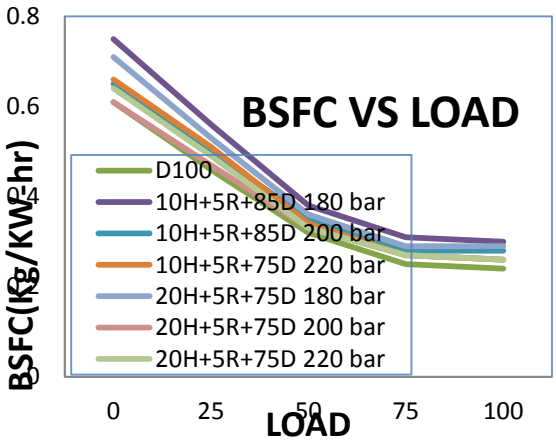

Figure 3.variation of BSFC aaginst load

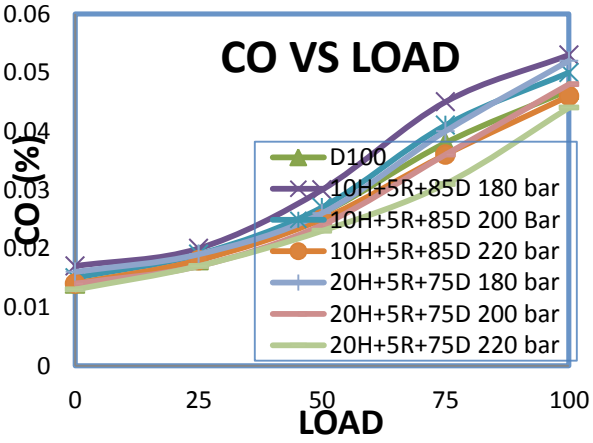

Figure 6. variation of CO against load

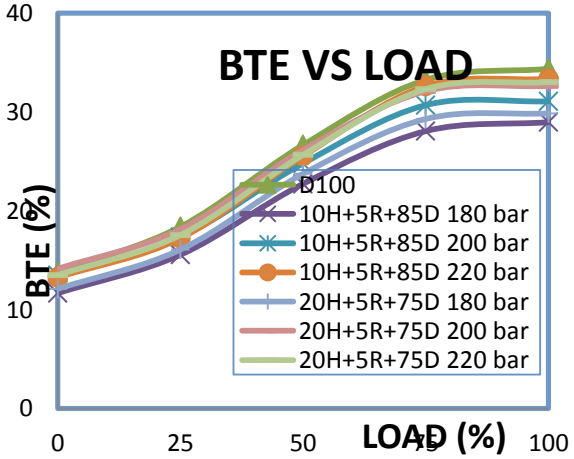

Figure 4.variation of BTE aaginst load

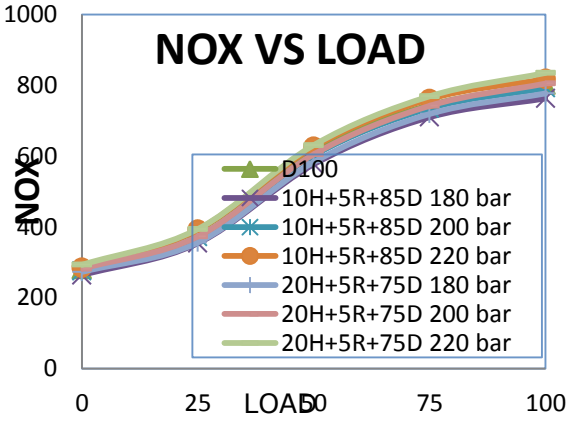

Figure 7.variation of NOx aaginst load

Machining of Non-conductive material using ECDM process

Inamdar Pavan[1], Sadashiv Bellubbi [1], Sathisha N[2]

[1] Dept. of Mechanical Engineering, Alva's Institute Of Engineering & Technology, Moodbidri- 574225, Mangaluru, Karnataka, India

[2] Dept. of Mechanical Engineering, Yenepoya Institute of Technology, Moodbidri- 574225, Mangaluru, Karnataka, India

Abstract

The machining of brittle and hard materials to the required profile and accuracy is a challenging task to the manufacturers. Such materials are difficult to machine by traditional machining methods. This has led to the development of non-traditional machining methods with use of some form of energy (Mechanical, Thermal, chemical) for machining. Electro Discharge Machining (EDM) and Electro Chemical Machining (ECM) are two such processes used for machining electrically conducting materials but they cannot be used to machine non-conducting materials. Electro Chemical Discharge Machining (ECDM) is a hybrid machining technology that combines the features of ECM and EDM. It is an emerging non-traditional machining process that involves high-temperature melting and chemical etching under the high electrical energy discharged on the electrode tip during electrolysis. In this work an experimental setup of ECDM was developed with various features to machine nonconductive materials. The effect of the process parameters like electrolyte concentration, applied voltage, inter electrode gap were selected on the machining characteristics of borosilicate glass on Material Removal Rate (MRR). It was observed as applied voltage and electrolyte concentration increases MRR also increases, but as inter electrode gap increases MRR decreases. Also significance of input parameters were analyzed by analysis of variance.

Keywords: ECDM, Borosilicate glass, NaOH, MRR

1. Introduction

The non-conventional machining processes, utilize several forms of energies like mechanical, chemical, thermal etc., to carryout machining. Some of the mechanical machining processes are Ultra Sound Machining (USM), Water Jet Machining (WJM), Abrasive Jet Machining (AJM) and Abrasive Water Jet Machining (AWJM) etc., chemical machining processes are Electro Chemical Machining (ECM), Electro Chemical Grinding

(ECG) etc., and thermal machining processes are Electro Discharge Machining (EDM), Ion Beam Machining (IBM), Plasma Arc Machining (PAM), Laser Beam Machining (LBM) etc. Out of all these non-conventional machining processes, electrochemical discharge machining (ECDM) is a hybrid machining process which combines the features of electro chemical machining (ECM) and electro discharge machining (EDM). The electrical discharges assure a chain of micro explosions in the workpiece surface layer; thus, micro quantities of workpiece material are removed[1] as it involves high-temperature melting and accelerated chemical etching under the electrical energy discharged on the electrode tip during electrolysis, the ECDM process is capable of machining very hard and non-conducting materials such as borosilicate glass, quartz, ceramics etc., efficiently and economically[2]. Much of the work in ECDM had been concentrated on glass which has useful properties such as its chemical resistance or biocompatibility. The non-conductive materials like Glass and Ceramics play a major role in automobiles, aeronautics & other industrial applications due to their enhanced mechanical properties[1]. The importance of glass is also growing in the field of Micro Electro Mechanical Systems (MEMS). Some promising applications of glass in the MEMS field are micro accelerometers, micro reactors and medical devices such as flow sensors or drug delivery devices. All these applications provoke to the need of effective and economical machining of glass. To meet this need and industrial requirement of machining of brittle non-conducting materials, studies are needed to improve the quality characteristics of ECDM process[1].

Various researchers have studied on different parametric optimization of electrochemical discharge machining process. Yang et al.[3] investigated the effect of surface roughness of different tool materials on gas film formation and then the machining characteristics. Harugade et al.[4] discussed the effect of different electrolyte solution on MRR in ECDM. The obtained results evidence that applied voltage was found to be most influencing parameter for MRR and KOH shows the better removal rate than other proposed electrolyte solutions used in an experiment. Jui et al.[5] researched and explored the feasibility of machining high aspect ratio micro holes in glass. Athereya et al.[6] presented the optimization procedure used in Taguchi method. Krishankant et. al.[7] discussed the application of Taguchi method for optimizing turning process by the effects of machining. Somashekhar et al.[8] developed an ECDM setup for machining several profile cuttings on non-conducting materials like glass and composites. In their added work, they observed that side sparks affect the diameter of machined hole on several glass pieces. Han et al.[9] machined micro channels on glass material at 35 V and 20 wt% NaOH solution using tungsten carbide as work tool. The insulated tool-tungsten carbide was covered with a ceramic tube. They observed that, the electrode without coating generated unstable spark pulses and non-uniform- width and linearity of

the machined channels, because of the fluctuations in the gas film thickness. Bhattacharyya et al.[1] conducted the experiments using different electrolyte concentrations and voltage combinations. It is observed that the tapered side wall and flat front tool tip shape is observed to be the most effective for producing circular holes. Wuthrich and Fascio[10] conducted experiments with electrodes of dissimilar sizes in which anode size was much bigger than the cathode. Wuthrich et al. [11] have reported that current-voltage characteristics of electrochemical cell are depended on the bubble generation during machining process. They created a mathematical model for the evolution of bubbles evolved at the working electrodes. Doloi et al.[12] was used Taguchi method of optimization for the design optimization of the machining parameters of ECDM process for drilling hole in non-conducting zirconium oxide ceramic components. The applied voltage, electrolyte concentration and inter electrode gap are the three affecting parameters which significantly affect the MRR as well as ROC of ECDM process.

In this work, drilling of borosilicate glass is carried out by using ECDM with the use of stainless steel as tool and sodium hydroxide (NaOH) as electrolyte. Experiments were conducted as per L_9 orthogonal array by selecting different parameters like electrolyte concentration, applied voltage and inter electrode gap with various levels, material removal rate was calculated for all the experiments and percentage contribution of input parameters were measured through analysis of variance (ANOVA).

2. **Experimentation**

Developments in ECDM process contains micro machining of glass, steel, ceramics, composites and super-alloys with improved output characteristics [13]. For this, important components of ECDM machining setup are tool electrode, auxiliary electrode, workpiece, DC source and electrolyte. The performance of ECDM in terms of rate of machining and material removal rate is affected by many factors. With concern to material removal mechanism of an ECDM process, it is necessary to control the gap width, applied voltage, electrolyte concentration, temperature of the electrolyte, type of auxiliary electrode, inter electrode gap and pulse parameters of the regulated power supply at an optimum level to obtain higher performance in terms of machining accuracy, surface finish and metal removal rate.

2.1 Material selection

In this present work, borosilicate glass of dimensions 76×26×1.25mm was used as workpiece which was manufactured by Pyrex glass and it was having composition of silica (70-80%) and boric oxide (7-13%) with smaller amount of alkalis (sodium and potassium oxides) and aluminum oxide, also it had properties of excellent chemical

durability and thermal shock resistance which made it suitable for machining through ECDM and stainless steel material of diameter 0.53mm as tool, sodium hydroxide (NaOH) as electrolyte and GI sheet of dimensions 150 × 80 mm was used as auxiliary electrode.

2.2 Experimental setup

ECDM cell was fabricated using a chemical resistant acrylic flask of 200 mm diameter and 70 mm height. The arrangement of tool, auxiliary electrode, workpiece and work holding fixture are as shown in Figure 1. The tool electrode as cathode and auxiliary electrode was connected as anode which is chemically resistant to the electrolyte; anodic dissolution of auxiliary electrode material is limited by the very large surface area than tool electrode and NaOH aqueous solution was used as electrolyte which provides electrical conductivity required for the formation of gas film around tool and assist the machining by etching process, electrolyte level maintained 2mm above the workpiece material. The tool was dipped in the electrolyte and is maintained at a fixed distance which was sufficient enough to produce the spark. The gap between the cathode tool tip and the workpiece was maintained less than 1mm.

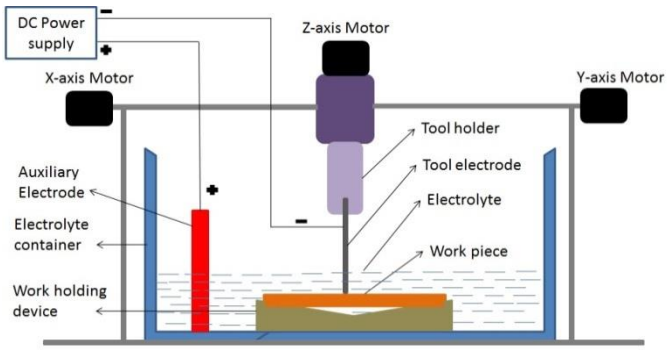

Fig 1: Schematic diagram of ECDM process

In this study, experimentation was conducted by selecting various parameters like electrolyte concentration, applied voltage and inter electrode gap with different levels to machine a borosilicate glass, different levels of input parameters are shown in Table 1.

Table 1: Input factors with their levels

Factor	Process parameter	Levels		
		1	2	3
A	Applied Voltage (V)	30	40	50
B	Electrolyte concentration (%)	15	20	25
C	Inter electrode gap (mm)	35	45	55

Based on the levels of the input parameters selected, the experimental planning was done using L_9 orthogonal array. Experiments were conducted by varying each of the process parameters according to the experimental plan and response material removal rate is tabulated in Table 2.

3. Results and discussion

Experiments were conducted to study the effect of process parameters on the MRR according to the design matrix given in Table 2. The obtained results were analyzed through Minitab software for mean variance study to evaluate the influence of control factors on drilled portion. The larger is the better condition was adopted to determine the mean response.

Table 2: Design matrix and experimental results

Trial No.	A	B	C	MRR (gm/min)
1	30	15	55	0.0341
2	30	20	45	0.0452
3	30	25	35	0.0901
4	40	15	55	0.0932
5	40	20	45	0.1737
6	40	25	35	0.1958
7	50	15	55	0.1218
8	50	20	45	0.1810
9	50	25	35	0.2533

3.1 Effect of process parameters

From the figure 2 it was observed that the MRR increases with increased applied voltage and electrolyte concentration, MRR decreases as inter electrode gap increases. It shows MRR is directly proportional to voltage and electrolyte concentration, inversely proportional to inter electrode gap. This effect on MRR noticed that, by increasing voltage the intensity of spark increases and it causes high material removal rate. The MRR increases with increase in electrolyte concentration and voltage as the more electrochemical reactions occur between the cathode and the anode which generates greater number of sparks. This results in more gas bubbles at the sparking zone. Sathisha N et al. [14] also stated in their conclusion that electrolyte concentration is the most significant factor for the ECDM for the maximization of MRR. Jawalkar et al.[4] have concluded from the experimental result that applied voltage was the most influencing parameter in both material removal rate and tool wear rate studies.

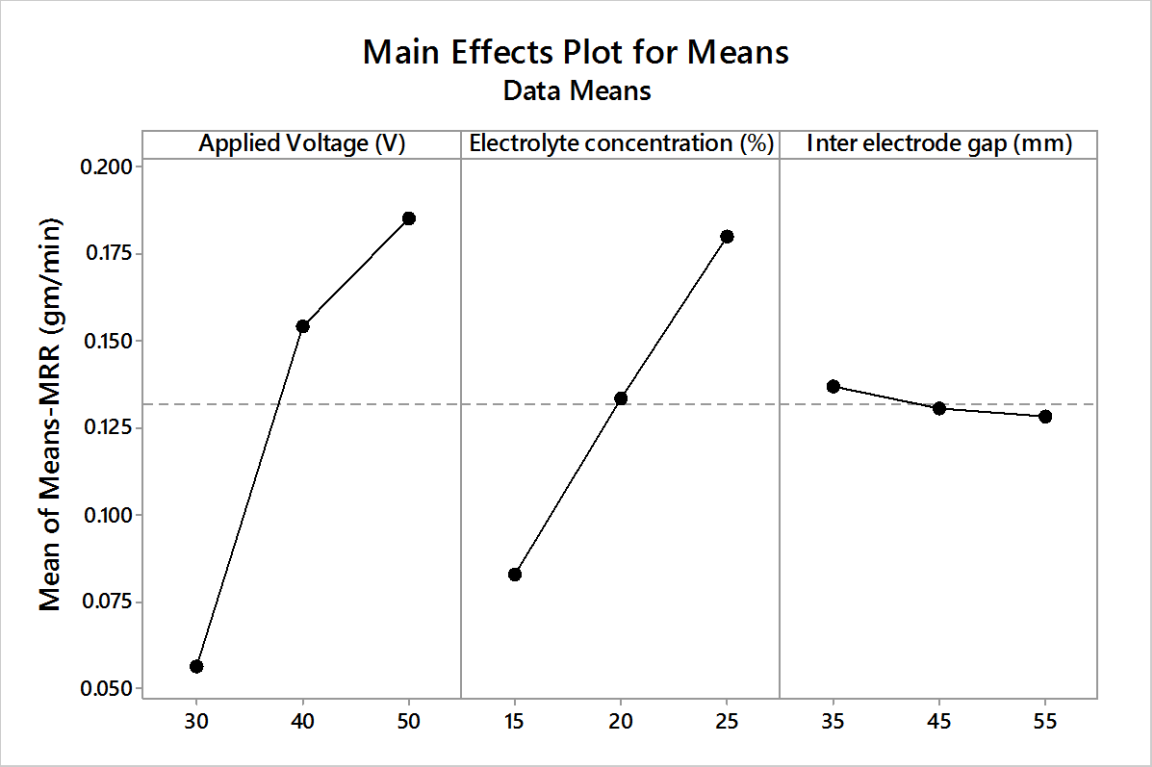

Fig 2: Effect of process parameters on Material Removal Rate

Further, Analysis of Variance was adopted to know the percentage contribution of machining parameters and to identify the factors effect on response variable based on a 95% confidence level; Table 3 shows the ANOVA table for Material Removal Rate. From, Table 3 it was found that the applied voltage (65.52%) has higher contribution for getting higher MRR in borosilicate glass followed by Electrolyte concentration (26.23%) and Inter electrode gap (3.93%).

Table 3 Analysis of Variance

Source	DF	Adj SS	Adj MS	% contribution
Applied Voltage (V)	2	0.02714	0.013571	62.53
Electrolyte concentration (%)	2	0.01403	0.007017	32.33
Inter electrode gap (mm)	2	0.000116	0.000058	0.27
Error	2	0.002115	0.001058	4.87
Total	8	0.043408	--	100

4. **Conclusion**

In this work the effect of applied voltage, Electrolyte concentration and inter electrode gap on MRR for borosilicate glass have studied by using Taguchi's orthogonal array experimental. The following important conclusions were drawn from this study.

1. The increase in applied voltage, Electrolyte concentration leads to an increase in the material removal rate. But MRR decreased as inter electrode gap increases.
2. The applied voltage shows the most significant effect on Material removal rate followed by Electrolyte concentration and inter electrode gap.
3. The optimal machining parameters to maximize material removal rate based on Taguchi analysis for ECDM of borosilicate glass include 50V voltage, 25% Electrolyte concentration, 35 inter electrode gap.i.e [A3-B3-C1].

5. **REFERENCES**

[1] Bhattacharyya, B., Doloi, B.N., Sorkhel, S.K. Experimental investigations into ECDM of non-conductive ceramic materials. Journal of Materials Processing Technology 1999; 95: 145-154.

[2] Cotea, L. Sl tineanu, O. Dodun, Ciofu C "Electrochemical discharge machining of small diameter holes" International Journal of Material Forming. (2008) 1: pp1327 – 1330

[3] Cheng-Kuang Yang, Chih-Ping Cheng, Chao-Chuang Mai, A. Cheng Wang, Jung-Chou Hung, Biing-Hwa Yan, (2010) Effect of surface roughness of tool electrode materials in ECDM performance, International Journal of Machine Tools & Manufacture (50), 1088–1096.

[4] M. L. Harugade, M.V. Kavade, N.V. Hargude, An Experimental Investigation Of Effect Of Electrolyte Solution On Material Removal Rate In ECDM, International Journal of Engineering Research & technology (IJERT), 2(1), 1-8.

[5] Sumit K. Jui, Abishek B, Kamaraj, Murali M. Sundaram, (2013) High aspect ratio micromachining of glass by electrochemical discharge machining (ECDM), Journal of Manufacturing Processes (15), 460–466.

[6] Srinivas Athreya and Y.D. Venkatesh, (2012) Application Of Taguchi Method For Optimization Of Process Parameters In Improving The Surface Roughness Of Lathe Facing Operation, International Refereed Journal of Engineering and Science (IRJES), 1(3), 13-15.

[7] Krishankant, Jatin Taneja, Mohit Bector, Rajesh Kumar, (2012) Application of Taguchi Method for Optimizing Turning Process by the effects of Machining Parameters, International Journal of Engineering and Advanced Technology (IJEAT) , 2 (1), 263-274.

[8] Somashekhar S H, K Sadashivappa,Y Vrushabhendrappa and M Singaperumal, A modern machining method for cutting micro-profiles on non-conducting materials. Proceedings of the OPTO'2000, Special Session on Innovative Products, Erfurt, Germany 2000; S8: May 9-11.

[9] Min-Seop Han, Byung-Kwon Min and Sang Jo Lee. Modeling of gas film formation in electrochemical discharge machining process using a side-insulated electrode. J Micromech. Microeng 2008; 18: 045019-045027.

[10]Wuthrich, R., Fascio, V. Machining of non-conducting materials using electrochemical discharge phenomenon-an overview. International Journal of Machine Tools and Manufacture 2005; 45: 1095-1108.

[11] Wuthrich, R., Fujisaki,, Couthy, P., Hof, L.A.,Bleuler, H. SACE in micro-factory. J. of Micromechanics and Micro Engg. 2005; 15: 276-280.

[12] B. Doloi, B. Bhattacharyya and S. K. Sorkhel "Electrochemical Discharge Machining of Non- Conducting Ceramics" Defence Science Journal, Vol49, No 4, August 1999, pp. 331-338

[13] Singh, Manpreet, and Sarbjit Singh. "Machining of difficult to cut materials by electrochemical discharge machining (ECDM) process: a state of art approach." Advanced Manufacturing and Materials Science. Springer, Cham, 2018, 139-149.

[14] Sathisha, N., Somashekhar S. Hiremath, and J. Shivakumar. "Prediction of material removal rate using regression analysis and artificial neural network of ECDM process." *International Journal of Recent Advances in Mechanical Engineering* 3.2 (2014): 69-81.

[15] C.S. Jawalkar, Apurbba Kumar Sharma, Pradeep Kumar, (2012) Micromachining with ECDM: Research Potentials and Experimental Investigations, World Academy of Science, Engineering and Technology (61), 90-95.

Experimental investigations of machining force, MRR and power in turning of AISI 304 Stainless steel

Kishor H H[1], Sadashiv Bellubbi[1]

[1]Department of Mechanical Engineering, Alva's Institute of Engineering and Technology, Moodbidri-Karnataka-INDIA

ABSTRACT

A machining process involves many process parameters which directly or indirectly influence the surface quality of the product. A precise knowledge of these optimum parameters facilitate reduce the machining costs and improve product quality. Current investigation aims to investigate the effect of process parameters; cutting speed, feed and depth of cut in turning of SS-304 which is widely used in automobile industries, each varying in three levels. The response characteristics considered for study were machining force, material removal rate and power. Experiments were planned according to Taguchi full factorial design using L_{27} orthogonal array. The machining was carried out using cemented carbide cutting tool and various forces acting on the cutting tool were measured using lathe tool dynamometer. Results indicated that cutting speed and tool feed rate have a significant effect than that of depth of cut on the quality characteristics.

Keywords: Cutting forces, Machining force, MRR, Specific cutting force

INTRODUCTION

Austenitic stainless steel is one of the most important engineering materials with wide variety of applications. Superior resistance to corrosion and compatibility in high temperature and high vacuum has particularly made it an attractive choice. Grade 316 is the standard molybdenum-bearing grade. Molybdenum gives 316 better corrosion resistance properties than crevice corrosion in chloride environment. It has excellent forming and welding characteristics.

As P 30 grade of cemented carbide would provide excellent balance of hardness, wear resistance and toughness, the same grade has been chosen for machining of stainless steel as cutting tool. Also effect of cutting speed, feed, and depth of cut on various characteristics during machining of austenitic stainless steel was studied. According to Ciftci (2005)[1] AISI 316 resulted in higher forces at all cutting speeds employed than AISI 304. Zhuang et al. (2010)[2] studied on two steels, free cutting austenitic stainless steel and austenite stainless steel 1Crl8Ni9Ti at various cutting speeds; they find that the cutting forces generally decreased with the increase of cutting speed in the range 10 – 80 m/min. They reached 418 N and 336 N at 10 m/min cutting speed for steel A and B respectively and at cutting speed of 80 m/min principal forces were 343 N and 275 N for steel A and B respectively. Benardos et al. [3] adopted an abdicative network to construct a prediction model for surface roughness and cutting force. Regression analysis was also adopted as second prediction model for surface roughness and cutting force. Comparison was made on the results of both models indicating that adductive network was found more accurate than that by regression analysis. Sing and Kumar (2006) [4] studied on optimization of feed force through setting of optimal value of process parameters namely speed, feed and depth of cut in turning of EN24 steel with TiC coated tungsten carbide inserts. The authors used Taguchi's parameter design approach and concluded that the effect of depth of cut and feed in variation of feed force were

affected more as compare to speed. Kumar et al. (2013)[5] proposed the methodology for prediction of machining forces using multi-layered perceptron trained by genetic algorithm (GA). Mahmoud and Abdelkarim (2006)[6] studied on turning operation using High-Speed Steel (HSS) cutting tool with 45° approach angle. Sardinas et al. (2006)[7] presented a multi-objective optimization technique, based on genetic algorithms, to optimize the cutting parameters in turning processes. Gusri et al. (2008) [8] applied Taguchi optimization methodology to optimize cutting parameters in turning Ti-6Al-4V ELI with coated and uncoated cemented carbide tools. Thamma (2008) [9] constructed the regression model to find out the optimal combination of process parameters in turning operation for Aluminium 6061 work pieces. M. Nalbalt et al (2006)[10] use L9 orthogonal array to study the performance characteristics in turning operations of AISI 1030 steel bars using TiN coated tools. Three cutting parameters namely, insert radius, feed rate, and depth of cut, are optimized with considerations of surface roughness. E.D Kirby et al (2005)[11] use the application of the Taguchi parameter design method to optimizing the surface finish in a turning operation. In the present work, the effect of cutting parameters; cutting speed (V), feed (f) and depth of cut (d) on the quality characteristics such as machining force (Fm), material removal rate (MRR) and power were investigated. Various forces induced during machining were measured through lathe tool dynamometer.

EXPERIMENTATION

Classical experimental design methods are too complex and are laborious, expensive and time consuming as large number of experiments are required to be conducted. To overcome this problem, Taguchi method is used which is based on special design of orthogonal arrays resulting in fewer numbers of experiments. The experiments were carried out with three independent factors such as cutting speed (V), feed rate (f) and depth of cut (d), each with three different levels. In this work standard L_{27} orthogonal array is used. The various factors and their levels are shown in Table 1.

Experiments were conducted on Kirloskar (Model: Enterprise 355) lathe equipped with lathe tool dynamometer as depicted in Figure.1. Figure 2 shows the raw material and machined specimens of SS 316. Obtained cutting force (F_c), thrust force (F_t) and radial force (F_r) are tabulated in Table 2.

***Table 1:** Factors and Levels.*

Factors	Level 1	Level 2	Level 3
Cutting Speed, V (m/min)	34	51	68
Feed, f (mm/rev)	0.05	0.125	0.16
Depth of cut, d (mm)	0.5	1.0	1.5

***Table 2.** Experimental layout plan of full factorial L_{27} Taguchi orthogonal array.*

Expt. No.	V (m/min)	f (mm/rev)	d (mm)	F_c (N)	F_t (N)	F_r (N)
1	34	0.05	0.5	313.92	245.25	98.10

2	34	0.125	0.5	362.97	127.53	49.05
3	34	0.16	0.5	402.21	117.72	49.05
4	51	0.05	0.5	245.25	156.96	137.34
5	51	0.125	0.5	343.35	98.10	88.29
6	51	0.16	0.5	421.83	88.29	58.86
7	68	0.05	0.5	264.87	156.96	9.81
8	68	0.125	0.5	382.59	107.91	39.24
9	68	0.16	0.5	421.83	98.10	29.43
10	34	0.05	1.0	402.21	137.34	98.10
11	34	0.125	1.0	667.08	98.10	29.43
12	34	0.16	1.0	716.13	58.86	39.24
13	51	0.05	1.0	372.78	78.48	68.67
14	51	0.125	1.0	706.32	78.48	68.67
15	51	0.16	1.0	765.18	117.72	49.05
16	68	0.05	1.0	382.59	117.72	78.48
17	68	0.125	1.0	686.70	107.91	78.48
18	68	0.16	1.0	745.56	117.72	117.72
19	34	0.05	1.5	490.50	215.82	117.72
20	34	0.125	1.5	951.57	245.25	235.44
21	34	0.16	1.5	1059.48	235.44	196.20
22	51	0.05	1.5	568.98	304.11	127.53
23	51	0.125	1.5	1108.53	372.78	362.97
24	51	0.16	1.5	1216.44	372.78	372.78
25	68	0.05	1.5	519.93	255.06	68.67
26	68	0.125	1.5	1049.67	274.68	245.25
27	68	0.16	1.5	1118.34	333.54	294.30

Machining force, material removal rate and power were calculated using equations Eq.1, Eq.2 and Eq.3 respectively and sample calculations to determine Fm, MRR and power are shown below.

Machining force, $F_m = \sqrt{(F_c^2 + F_t^2 + F_r^2)}$ N ——— Eq.1

Material removal rate, $MRR = V \times f \times d \times 100$ mm^3/min ——— Eq.2

Power, $P = V \times F_c \times 60$ W ——— Eq.3

Sample calculation is shown for the Expt. No.1as below

$F_m = \sqrt{(313.92+245.25+98.10)} = 410.26$ N

$MRR = 34 \times 0.05 \times 0.5 \times 1000 = 850\ mm^3/min$

$P = 34 \times 313.92 \times 60 = 177.89$ W

RESULT AND DISCUSSION:Response characteristics Fm, MRR and Power were computed as discussed in section 2 and are tabulated in Table 2.

Influence of Machining Parameters on Response Characteristics The influence of cutting parameters on response characteristics were discussed below. Graphs are plotted for response characteristics; Machining force, material removal rate and power against by considering two cutting parameters and keeping other parameter as constant.

Gragh 1: Effect of cutting speed vs feed on Fm

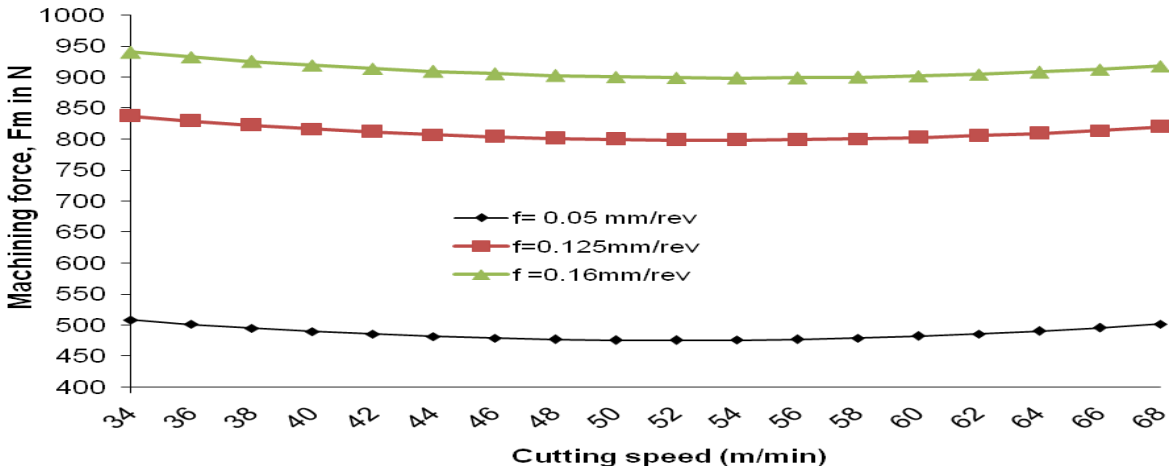

Figure 1

Figure 1(a) depicts interaction effect of cutting speed and feed on machining force where as depth of cut kept constant, as cutting speed goes on increases Fm increases upto certain point and later decreases for all values of feed rates f= 0.05, 0.125 and 0.16 mm/rev.

Graph 2 : Effect of feed vs depth of cut on Fm

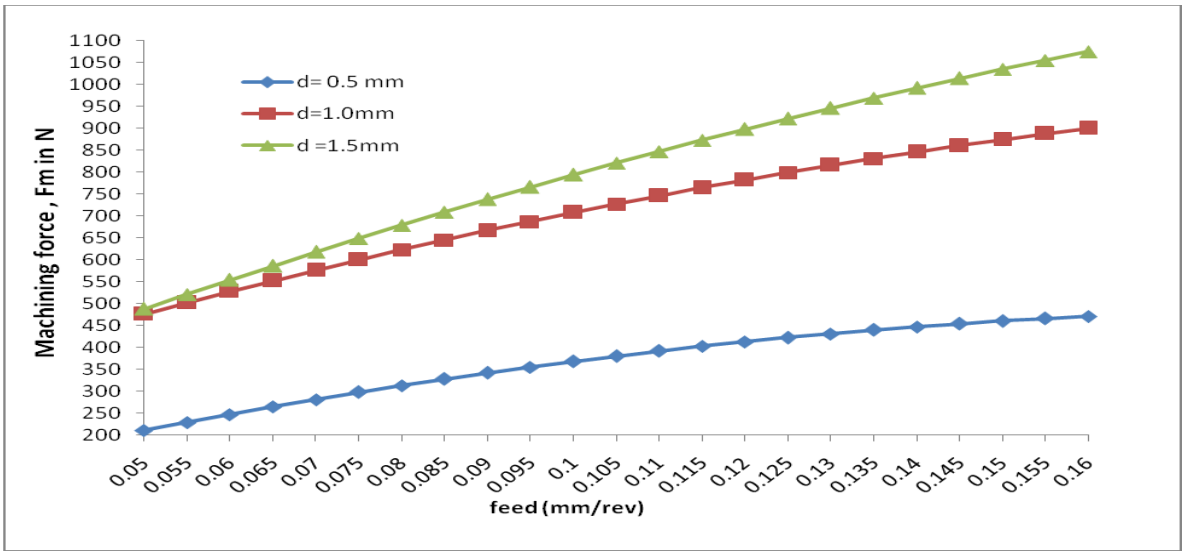

Figure 2

Interpretation: Above graph depicts the interaction effect of depth of cut and feed rate on machining force. Machining force increases as feed rate and depth of cut increases. Machining force is more at higher depth of cut i.e d=1.5 mm

Graph 3: Effect of cutting speed vs depth of cut on Fm

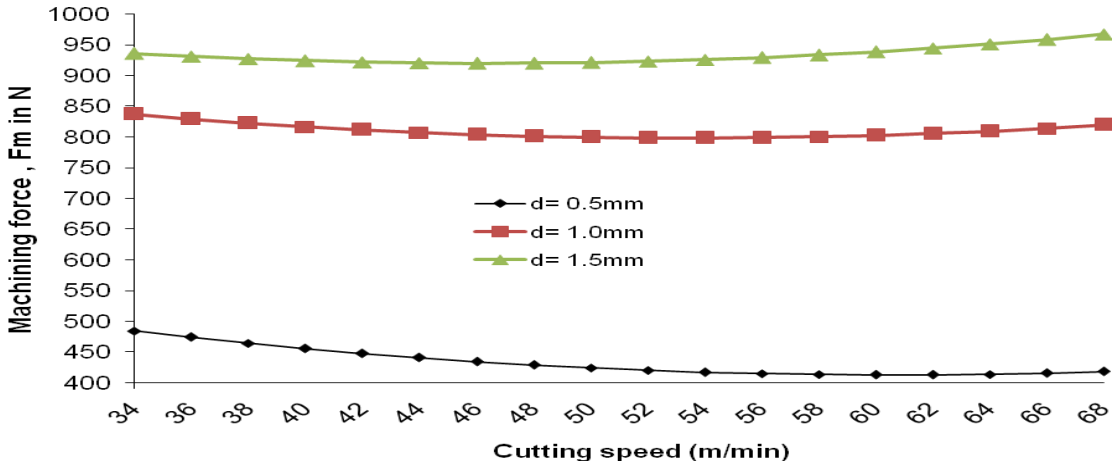

Figure 3

Interpretation: Above graph depicts the interaction between depth of cut and cutting speed on machining force, machining force decreases & reaches certain point and again increases as cutting speed increases for d=1.0 mm & 1.5 mm. But for d=0.5 mm machining force decreased as cutting speed increases.

Graph 4: Effect of cutting speed vs feed on MRR

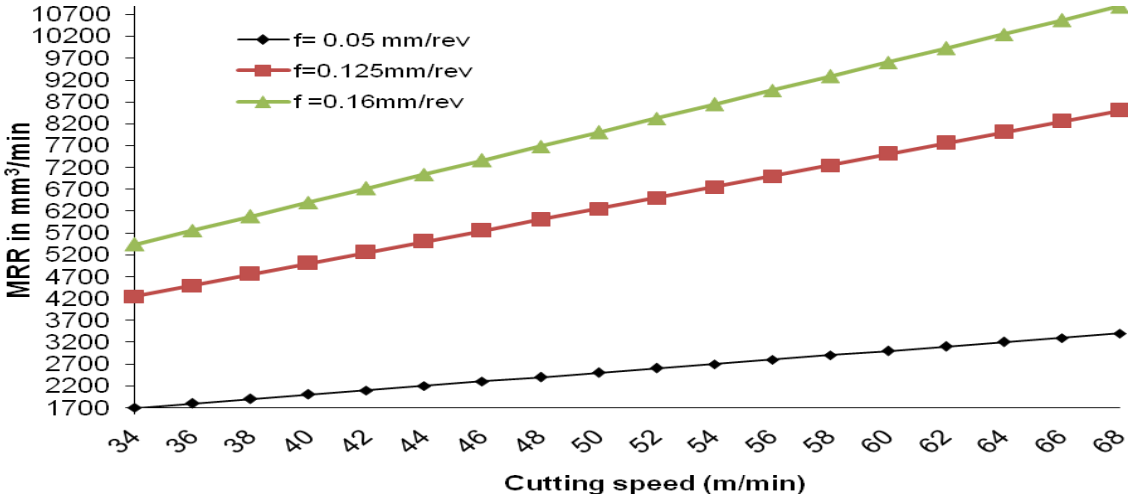

Figure 4

Interpretation: Above graph depicts interaction between feed rate and cutting speed on material removal rate, Material removal rate increases as cutting speed and feed rate increases.

Graph 5: Effect of feed vs depth of cut on MRR

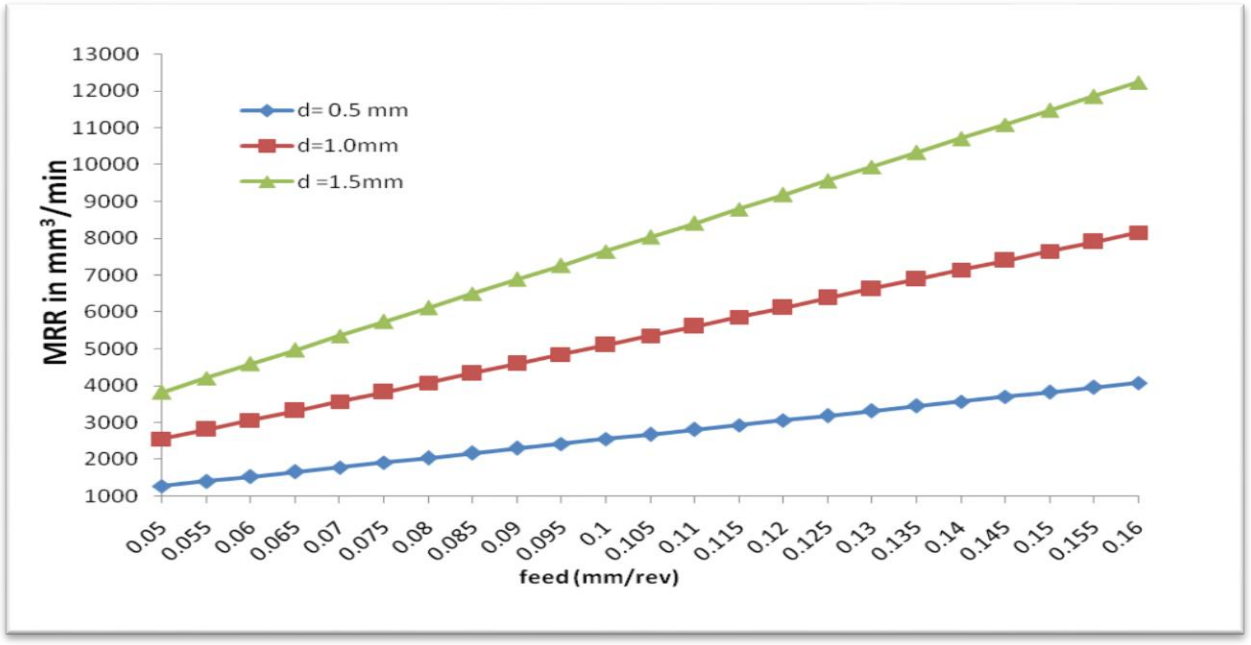

Figure 5

Interpretation: Above graph depicts interaction between depth of cut and feed rate on material removal rate, Material removal rate increases as feed rate and depth of cut increases. Material removal rate is higher at higher the value of depth of cut.

Graph 6: Effect of cutting speed vs depth of cut on MRR

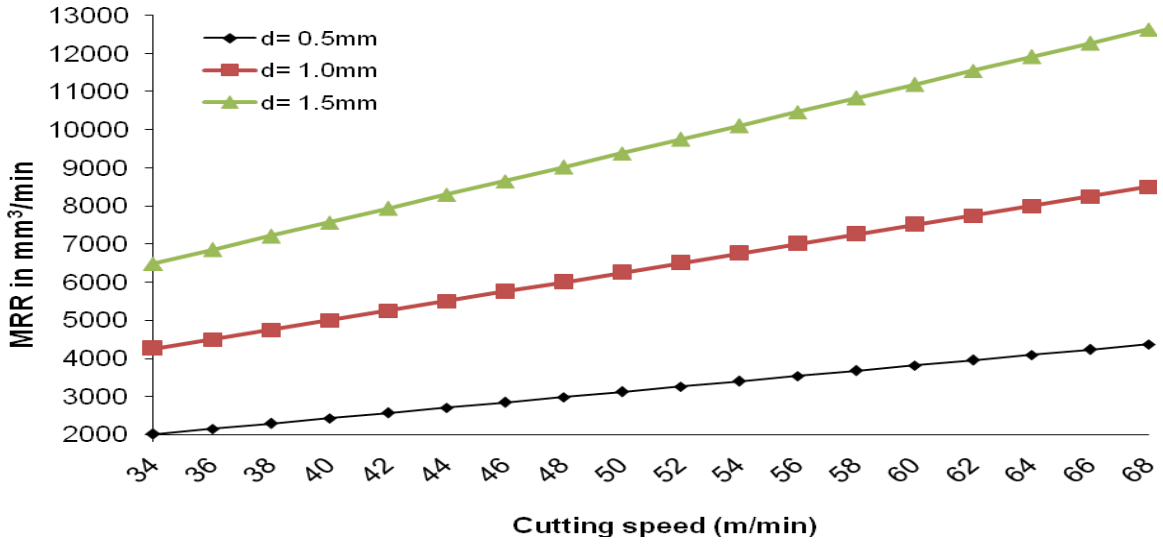

Figure 6

Interpretation: Above graph depicts the interaction between depth of cut and cutting speed on material removal rate, Material removal rate increases as depth of cut and cutting speed increases. Material removal rate is higher at higher the value of depth of cut.

Graph 7: Effect of cutting speed Vs feed on SCF

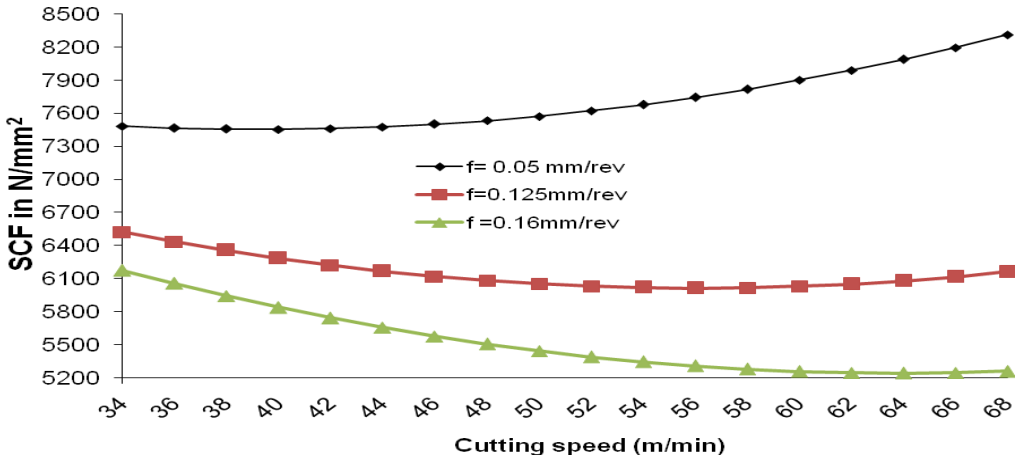

Figure 7

Interpretation: Above graph depicts interaction effect of feed rate and cutting speed on SCF,
SCF is constant up to certain point and increases as cutting speed increases for feed value of f=0.05mm/rev.
SCF decreases up to certain point and later it increases as cutting speed increases For feed value of f=0.125 mm/rev
SCF decreases as cutting speed increases for feed value f= 0.16 mm/rev

Graph 8: Effect of feed vs depth of cut on SCF

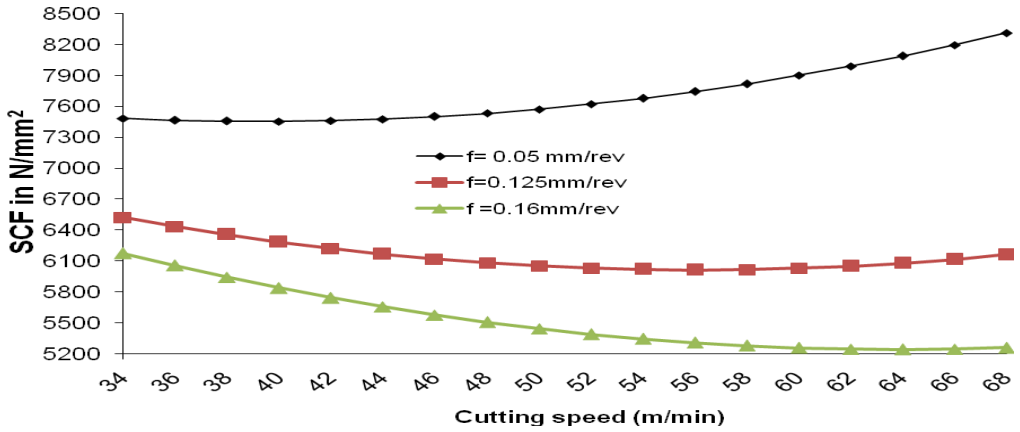

Figure 8

Interference: Above graph depicts interaction between depth of cut and feed rate on specific cutting force,SCF decreases as feed rate increases for all values of depth of cut, SCF is least at higher value of depth of cut.

Graph 9: Effect of cutting speed vs depth of cut on SCF

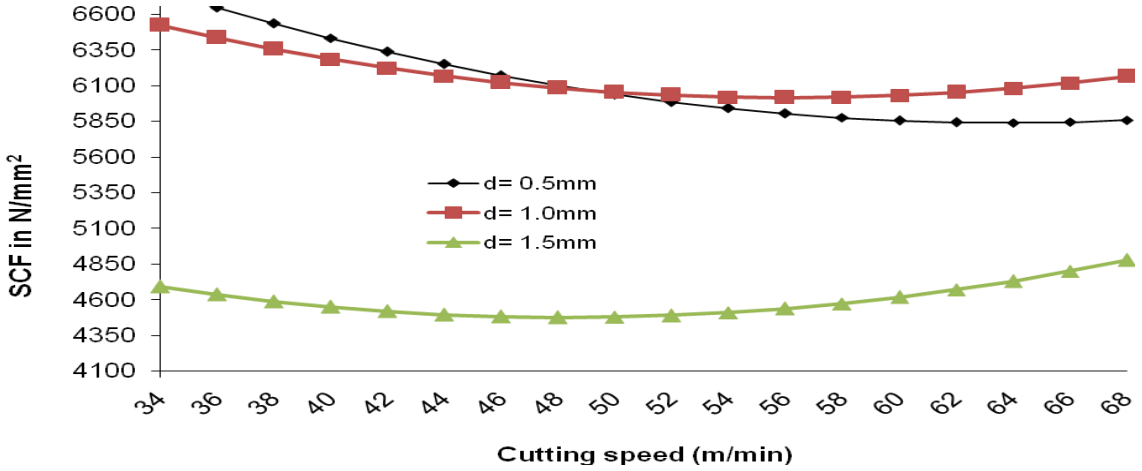

Figure 9

Interpretation: Above graph depicts interaction effect of depth of cut and cutting speed on SCF, The SCF decreases up to certain point & again increases as cutting cutting speed increases for values d= 1.0 mm and 1.5 mm But SCF continuously decreases for the value d=0.5 mm

CONCLUSION

This study reveals that during machining of AISI 304 Stainless steel on conventional lathe machine, selecting three process parameters such as cutting speed, feed rate and depth of cut with three different levels by using design of experiments with regression modeling. Plotting graphs interaction between cutting speed Vs feed rate, feed rate Vs depth of cut and cutting speed Vs depth of cut on Machining force, Material removal rate and Specific cutting force individually.

Machining force is affected by all the process parameters viz cutting speed, feed rate and depth of cut. MRR is affected by all the process parameters viz. cutting speed, depth of cut and feed rate. The MRR is increased by increasing any of the process parameters. The effect of variation in cutting speed and feed rate is more as compared to depth of cut. Specific cutting force is affected by all process parameters.

This study is carried out for bracketing the optimum range of three input parameters for carrying out further research.

REFERENCE

1. Cutting tool specifications from brazed cutting tools , SANDVIK coromant manual

2. P. Munoz-Escalona, Z. Cassier, Influence of the critical cutting speed on the surface finish of turned steel, Wear 218 (1998)

3. A.K. Ghani, I.A. Choudhury, Study of tool life, surface roughness and vibration in machining nodular cast iron with ceramic tool, Journal of Materials Processing Technology 127 (2002)

4. Dr. V. N. Gaitonde & J. Paulo Davim, S.R. Karnik**,** Investigations into the effect of cutting conditions on surface roughness in turning of free machining steel by ANN models, journal of materials processing technology 2 0 5 (2 0 0 8)

9th International Engineering Symposium - IES 2020
March 3-5, 2020, Kumamoto University, Japan

GALVANIC CORROSION BEHAVIOUR OF COUPLED ZE41MG – AL7075 AL ALLOY IN 3.5 WT% NACL

Prithivirajan S[1]*, Mayur Bapu Nyahale [2], Narendranath S[3], Vijay Desai[4]

1 *Research Scholar*, Department of Mechanical Engineering, National Institute of Technology Karnataka, Surathkal, Mangalore 575025, India. email:sekarprithiviraj@gmail.com*
2 *Postgraduate Student, Department of Mechanical Engineering, National Institute of Technology Karnataka, Surathkal, Mangalore 575025, India. email: mayurnyahale@gmail.com*
3 *Professor, Department of Mechanical Engineering, National Institute of Technology Karnataka, Surathkal, Mangalore 575025, India. email: narenbayalu@gmail.com*
4 *Professor, Department of Mechanical Engineering, National Institute of Technology Karnataka, Surathkal, Mangalore 575025, India. email: vijayhdesai64@gmail.com*

ABSTRACT: In this paper, the corrosion behaviour of ZE41 Mg alloy and Al7075 aluminium is studied in 3.5Wt% NaCl by standard corrosion measurements. In contrast, the galvanic corrosion behaviour of ZE41 Mg–Al7075 Al alloy couple is analysed using Zero Resistance Ammeter (ZRA) circuit. The nature of surface film and corrosion rate of individual alloy and galvanic couple is obtained from electrochemical impedance spectroscopy and potentiodynamic polarization. Al7075 alloy exhibited lesser corrosion rate than that of ZE41 Mg alloy. It is also observed that the corrosion rate of ZE41Mg – Al7075 Al alloy couple is higher than ZE41Mg alloy due to macro-galvanic corrosion and the availability of additional surface for hydrogen evolution.

***Keywords**: Galvanic corrosion, Magnesium, Electrochemical impedance spectroscopy*

INTRODUCTION

Magnesium being the lightest of all structural engineering materials is a boon to the automobile industry. Unfortunately, the higher corrosion rate of Magnesium remains a hindrance to expanding its application. With the advancement in research and development researchers focus on all possible ways to enhance the corrosion resistance of magnesium and its alloys. The core idea involved in improving the corrosion resistance is to reduce the micro-galvanic corrosion between magnesium and secondary phase particles. Most of the researchers concentrate on micro-galvanic corrosion while few researchers studied the macro galvanic corrosion or galvanic corrosion G.Song and A.Atrens(2003).Galvanic corrosion is inevitable in nature because in a more practical environment magnesium always come in contact with steel or Aluminium. This interaction of magnesium with other metals further increases the corrosion rate of magnesium. Thus studying galvanic corrosion of magnesium and selecting the galvanic couple is more important. G.Song et.al (2004) studied the corrosion behaviour of AZ91D

Mg alloy coupled with Zinc, Al380 and steel 4150. They concluded that aluminium offers the best resistance to galvanic corrosion during salt spray condition. K.B. Deshpande (2010) reported the corrosion behaviour of AE44 Mg coupled with mild steel and AA6063 by Scanning Vibrating Electrode Technique and immersion method. He concluded that the corrosion rate of AE44 Mg- Mild steel couple is greater than AE44 Mg- AA6063 couple. However from the literature it is observed that the galvanic corrosion behaviour of rare earth containing ZE41 Mg is not yet studied. Hence the objective of present study is to get insights into macro-galvanic corrosion experienced by ZE41 Mg-Al7075 couple in 3.5 Wt% NaCl.

EXPERIMENTAL DETAILS

Rare earth containing ZE41 Mg and Al7075 alloy samples of 16mm diameter and 3mm thickness were cut from cast ingots using metallurgical sample saw. The rear end of samples were soldered using copper wire and the connectivity was checked by using Multimeter. These samples were then abraded with #400, #1000, #1500, #2000 grade SiC papers followed by 0.5 µm diamond paste to obtain a mirror like surface. The corrosion behaviour of ZE41 Mg, Al7075 alloy and ZE41 Mg - Al7075 galvanic couple was studied in 3.5 Wt% NaCl.

RESULTS AND DISCUSSION

The thermodynamic nature of corrosion is generally obtained from open circuit potential. The open circuit potential of Al7075 alloy, ZE41 Mg and coupled ZE41 Mg–Al7075 alloy is represented in the Fig.1.The OCP value at the end of 2000 seconds time duration is found to be -789 mV and -1621mV for Al7075 alloy and ZE41 Mg respectively. It is also interesting to observe that the OCP value of ZE41 Mg–Al7075 galvanic couple (G) is -1548 mV which is relatively higher than that of ZE41 Mg alloy. The OCP values of Al7075 and ZE41 Mg are in line with the galvanic series and research findings A.Atrens et.al (2008). Noble potential in OCP curve signifies better corrosion resistance. Hence, the corrosion resistance of materials considered in this study is ranked in order as follows Al7075 alloy> coupled ZE41 Mg–Al7075> ZE41 Mg.

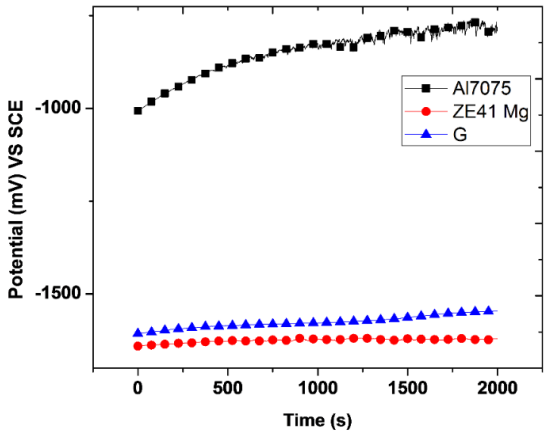

Fig.1 Open Circuit potential of Al7075, ZE41 Mg and coupled ZE41 Mg-Al7075

But this order of corrosion resistance cannot be concluded from OCP curves because it does not give any information about corrosion rate. In general Nyquist plot gives detailed information about the formation of surface film and its nature. Nyquist plot of Al7075 alloy, ZE41 Mg and coupled ZE41 Mg–Al7075 alloy tested in 3.5Wt% NaCl is represented in the Fig. 2(a). It is apparent that the diameter of Al7075 alloy is significantly higher in the range of 35000 ohm.cm^2. Fig.2 (b) depicts the expanded view of Fig .2(a). It is observed that the diameter of semi-circle reaches maximum at imaginary impedance value of 376 ohm.cm^2 and 39 ohm.cm^2 for ZE41 Mg and couple ZE41 Mg - Al7075 alloy.

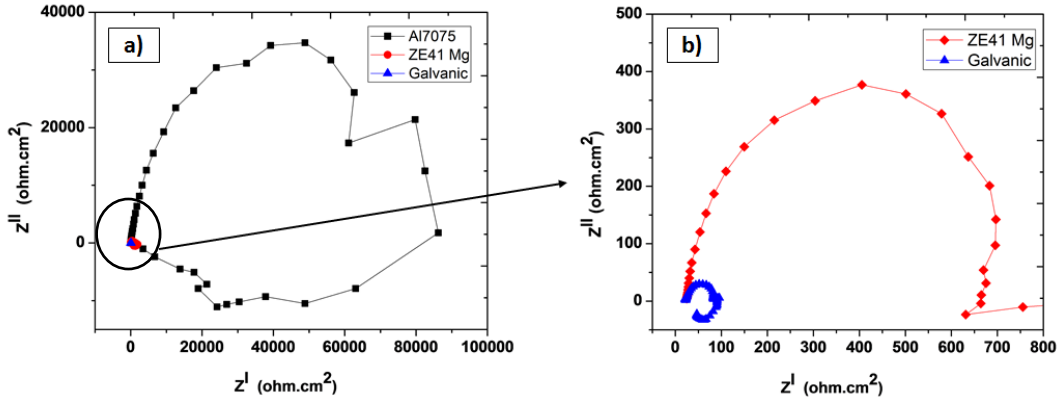

Fig.2 (a) Nyquist plot of Al7075, ZE41 Mg and coupled ZE41 Mg-Al7075 (b) Expanded view of Figure (a).

Fig.3 depicts the Potentiodynamic polarisation plot of Al7075 alloy, ZE41 Mg and coupled ZE41 Mg – Al7075 alloy tested in 3.5Wt% NaCl. The Potentiodynamic polarization curve of Al7075 alloy is at the most noble potential of -800mV. It is interesting to observe that the potential of both ZE41 Mg and coupled ZE41 Mg–Al7075 alloy is -1500mV approximately. The significant difference between them is the position of cathodic slope. This is due to the fact that when ZE41 Mg is tested in 3.5Wt% NaCl, micro galvanic corrosion occurs due to potential difference between magnesium acting as anode and Mg_7Zn_3RE acting as cathode as represented in figure 4(a). The anodic partial reaction at bulk magnesium occurs by the dissolution of magnesium and release of an electron as mentioned in equation (2). This electron is taken up at Mg_7Zn_3RE cathodes resulting in hydrogen evolution as shown in equation (1). In addition to electrochemical mode of corrosion, dissolution of magnesium occurs by chemical reaction which is referred as anodic hydrogen evolution mentioned in equation (3).

$$2H^+ + 2e = H_2 \text{ (cathodic partial reaction)} \quad (1)$$

$$2Mg = 2Mg^+ + e \text{ (anodic partial reaction)} \quad (2)$$

$$2\,Mg^+ + 2\,H_2O = 2Mg^{2+} + 2OH^- + H_2 \text{ (chemical reaction)} \quad (3)$$

$$2\,Mg + 2H^+ + 2\,H_2O = 2Mg^{2+} + 2OH^- + 2H_2 \text{ (overall reaction)} \quad (4)$$

$$Mg^{2+} + 2OH^{-} = Mg(OH)_2 \text{ (product formation)} \quad (5)$$

This is the main reason for deviation from Tafel behaviour which is apparent from Figure.3.The overall reaction represented in the equation (4) includes corrosion of magnesium by electrochemical and chemical mode G.song and A.Atrens(2003). In contrast when tested as couple i.e ZE41 Mg–Al7075 alloy the magnesium in ZE41 Mg possessing lower or active potential becomes anode while Al7075 alloy having a relatively higher potential becomes cathode. Higher the area of cathode higher is the hydrogen evolution at cathode. Eventually, higher hydrogen evolution will result in higher anodic dissolution. This is the reason for shift in the cathodic slope towards a region of higher corrosion current density when Al7075 alloy is galvanically coupled to ZE41 Mg alloy.

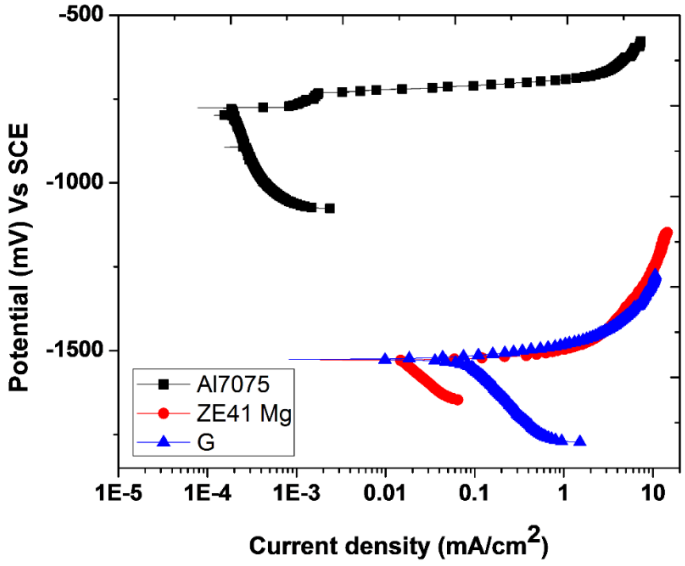

Fig.3 Potentiodynamic polarization curve of Al7075, ZE41 Mg and coupled ZE41 Mg-Al7075

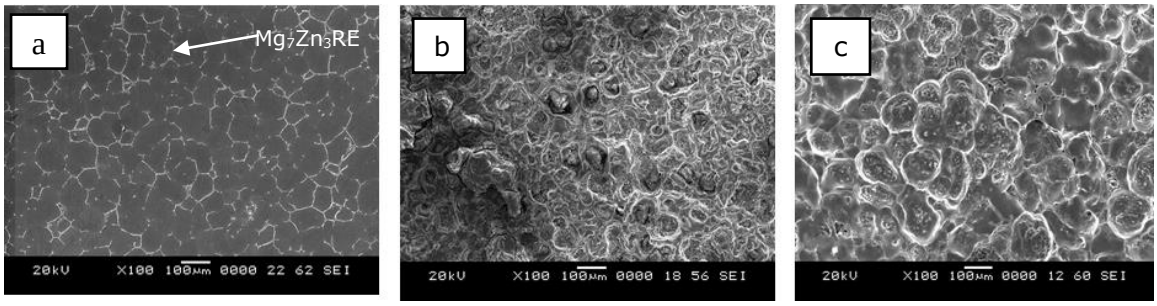

Fig.4 SEM images of (a) ZE41 Mg (b) corroded ZE41 Mg (c) corroded galvanic ZE41 Mg

The corrosion rate is calculated from the equation (6) mentioned below.

$$\text{Corrosion Rate [CR] (mm/year)} = 22.85\ i_{corr}\ (mA/Cm^2) \ldots\ldots\ldots \quad (6).$$

The corrosion rate of ZE41 Mg and coupled ZE41 Mg – Al7075 is calculated to be 0.83 mm/yr and 6.21 mm/yr and is in accordance with corroded SEM images depicted in figure.4(b) and (c) respectively. Also during galvanic corrosion, ZE41 Mg corrosion leads to product $Mg(OH)_2$ formation shown in equation (5). Similarly, Al7075 alloy corrosion results in $Al_2(OH)_6$ precipitate formation which offers passivation M.C.Zhao et.al(2008). But, the corrosion rate of ZE41 Mg- Al7075 couple is approximately five times that of ZE41 Mg. So, it can be concluded that the destructive nature of chloride ions in 3.5Wt% NaCl is predominated by passivation effect offered by corrosion products from Al7075 alloy.

CONCLUSIONS

The galvanic corrosion of ZE41 Mg-Al7075 couple is studied using zero resistance ammeter and compared with ZE41 Mg. The following conclusions were drawn

- The corrosion rate of Al7075 alloy, ZE41 Mg and coupled ZE41 Mg – Al7075 is calculated to be 0.02 mm/yr, 0.83 mm/yr and 6.21 mm/yr.
- The trend of corrosion behavior obtained from electrochemical impedance spectroscopy is in complete agreement with potentiodynamic polarization studies.
- The destructive nature of chloride ions dominated passivation effect offered by $Al_2(OH)_6$ precipitate formation during galvanic corrosion of ZE41 Mg – Al7075 due to the availability of additional surface for hydrogen evolution.

ACKNOWLEDGEMENTS

We are grateful to Defence Research and Development Organisation – Naval Research Board, Government of India for their extended support. Project Grant number NRB/4003/PG/366.

REFERENCES

Atrens, A., Song, G.L., Liu, M., Shi, Z., Cao, F. and Dargusch, M.S., 2015. Review of recent developments in the field of magnesium corrosion. *Advanced Engineering Materials*, *17*(4), pp.400-453.

Deshpande, K.B., 2010. Experimental investigation of galvanic corrosion: Comparison between SVET and immersion techniques. *Corrosion Science*, *52*(9), pp.2819-2826.

Song, Guangling, and Andrej Atrens. "Understanding magnesium corrosion—a framework for improved alloy performance." *Advanced engineering materials* 5, no. 12 (2003): 837-858.

Song, Guangling, Birgir Johannesson, Sarath Hapugoda, and David StJohn. "Galvanic corrosion of magnesium alloy AZ91D in contact with an aluminium alloy, steel and zinc." *Corrosion Science* 46, no. 4 (2004): 955-977.

Song, G. and Atrens, A., 2003. Understanding magnesium corrosion—a framework for improved alloy performance. *Advanced engineering materials*, *5*(12), pp.837-858.

Zhao, M.C., Liu, M., Song, G.L. and Atrens, A., 2008. Influence of pH and chloride ion concentration on the corrosion of Mg alloy ZE41. *Corrosion Science*, *50*(11), pp.3168-3178.

PHYSICS, ELECTRICAL, ELECTRONICS, COMPUTER SCIENCE & RELATED FIELDS

9th International Engineering Symposium - IES 2020
March 3-5, 2020, Kumamoto University, Japan

Application of MQTT Algorithm with IOT for water quality monitoring

Deepa V.P [1], Ranjitha.S [2] and **Poornima C.H [3]**

1 *Assistant Professor, Department of Electronics and communication, Government Engineering college, Doddamannina Gudd, Ramanagaram 562159, India. email:deeps.venkat@gmail.com*
2 *Undergraduate Student, Department of Electronics and communication, Government Engineering college, Doddamannina Gudd, Ramanagaram 562159, India. email: ranjithas26198@gmail.com*
3 *Undergraduate Student, Department of Electronics and communication, Government Engineering college, Doddamannina Gudd, Ramanagaram 562159, India. email: poornimach4@gmail.com*

ABSTRACT: In recent days the quality of the water is getting degraded at a very fast rate and has become a common problem. The procedure that is been followed to test water is by collecting the water samples by different locations and testing it in laboratory using rigorous skills. These approaches are time consuming, costly and no longer considered to be efficient, the results are not precise. Considering these issues, a low cost water quality monitoring system is developed and designed that can monitor water quality in real time using IOT and WSN. In our system the parameters are measured by different sensors like pH, temperature and turbidity for communicating data on to a platform via microcontroller system. This can be achieved by MQTT (Message Queuing Telemetry Transport) which allows publishing and subscribing of data between the sensor and end device. MQTT algorithm will be implemented to make the system feasible, Modular and cost effective.

Keywords*: Internet of things (IOT), ARM7, WSN, PH, Turbidity, temperature, GPRS, MQTT and End device etc.*

I. INTRODUCTION

The challenges of climate change, population, growth, demographic change, urbanization and resource depletion are the greatest threats the world is going to face over the coming decades. Drinking water is one of the most essential natural resource that has been gifted to the mankind. The online water quality monitoring system which is been used in many countries is said to have significant issues related to environment pollution. The environmental authorities have to ensure that industrial and domestic pollutants are kept below the threshold values [Goib Wiranto et.al (2015)]. The World health organization (WHO) has estimated that in India around 77 million people are suffering due unsafe water. It is also estimated that 21%of diseases are related to unsafe water in India [Jayti Bhatt, Jignesh Patoliya (2016)]. Therefore this raises an alarm to have a check on various water quality parameters such as dissolved oxygen (DO), conductivity, PH, turbidity and temperature in real time. The water quality parameter PH determines whether the water is acidic or basic. Pure water has a PH of 7 value. A value less than 7 indicate acidity and more than 7 indicate alkalinity. The normal range PH is 6 to 8.5. If PH is not maintained it causes irritation to eyes, skin and mucous membranes. The turbidity indicates the quality of water being cloudy, opaque or thick with suspended matter and the transparency of water. It is considered as a good

measure of the quality of water. Temperature indicates how cold or hot water is. The central pollution control board monitors the water quality on either monthly or yearly basis [Brinda das, P.C Jain (2017)]. With the introduction of IOT in the modern world many problems have been solved like data collection, data analysis, communication and works are still going on. The technologies and protocols are combined to get the desired output. Systems are designed for continuous monitoring of water quality data where the officials can access the data on smart phone /PC through internet. The remote sensor network can be used for stationary or mobile sensor network. The remote sensor network is used for many purposes such as environment monitoring, research in agriculture, border security, traffic management, forestry management, fishing surveillance, telemedicine of remote health care and disaster prevention. Though the WSN originally were used in military and heavy industries, today WSN applications are used for different purposes from light industries to heavy industry machines. The WSN system allows the user's to control and monitor the connected devises from the base station through different wireless communication standard such as Wi-Fi, GPRS, ZigBee, Bluetooth, RFID and cellular technologies as stated by choZin Myint et.al (2017)]. The advantage of WSN are remote monitoring, low power consumption, fast network establishment, redundant data acquisition and high monitoring precision. IOT was developed in parallel to WSN. This became the physical network which connects all things in order to exchange data and information with devices such as sensors actuators and computers in line with relevant protocols. The combination of low power and inexpensive sensor into IOT is a major evolution of WSN. In the present study we are monitoring the water quality parameters from industrial waste, sewage water and treated water which is let to lakes and rivers using WSN and compared with the threshold Values of normal water. MQTT algorithm will be implemented in order to make the system feasible, modular, scalar and cost efficient. This also allows simultaneous flow of data between sensors and servers.

METHODOLOGY

In the present study an attempt is made to check the water quality using pH, temperature and turbidity sensors. WSN technology is used. Following sections gives details about the devices used to carry out the experiments. Section I gives information about Message Queue Telemetry Transport (MQTT) protocol and Internet of Things (IOT). Section II reveals about hardware components used in the system. Section III about the system design and Implementation.

I. MQTT protocol

Message Queue Telemetry Transport (MQTT) is an open OASIS and ISO standard lightweight, publish-subscribe network protocol. The protocol runs over TCP/IP. MQTT is described as a machine-to-machine (M2M)/"Internet of Things" connectivity protocol. It was built as an extremely lightweight publish/subscribe messaging transport.

Features of MQTT

- It's a light weight protocol. It is straightforward to implement software and quick in data transmission.
- It's build on messaging technique.
- Each control packet has a certain purpose and every bit is meticulously drafted to reduce the message size.
- As the message size is less, network usage is also reduced.
- As low network usage intern decreases power usage and saves the device battery.
- It is real time, so it works ideal for Iot applications.

Figure 1 shows the working principal of MQTT. MQTT algorithm has a broker and client. The server is called a broker and the clients are simply the connected devices.
When a client wants to send data to the broker, it is done with a "publish" operation. When a client wants to receive data from the broker, it is done with a "subscribe" operation.

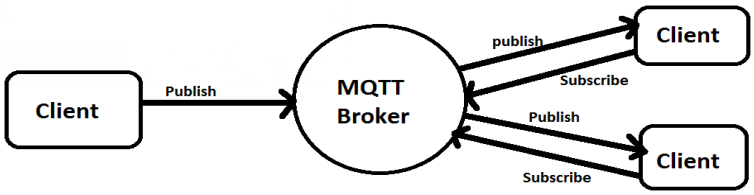

Figure1: Working Principal of MQTT

The clients initiate all interactions with the broker. A MQTT client can make use of both publish and subscribe. The communication between clients and broker is done on topics to identify a resource in a publish subscribe system. The Quality of Service (QoS) level is an agreement between the sender of a message and the receiver of a message that defines the guarantee of delivery for a specific message. There are 3 QoS levels in MQTT:

- At most once - the message is sent only once to the client and broker and no Acknowledgements.
- At least once - the message is re-tried until acknowledgement is received
- Exactly once - a 4 way hand shake is used for the delivery of the message.

Building Blocks of IoT

The basic building block of IoT system are sensors, processors, gateway, and applications. Each of these nodes has to have their own characteristics in order to form a useful IoT system. Sensors form the fore front of the IoT devices. These are called "Things" of the system. The main purpose is to collect data from its surrounding (sensors) or give out data to its surrounding. Processors are the brain of the IoT system. Their main function is to process the data captured by the sensors and process them so as to extract the valuable data from raw data collected. Gateways are responsible for routing the processed data and send it to proper locations for its proper utilization. To communicate in an IoT system, network connectivity become very crucial. For proper utilization of the data collected applications are very vital. These cloud based applications which are accountable for contributing effective meaning to the data collected.

II. Hardware components

A. Microcontroller

By referring to figure 2, the LPC2148 microcontroller unit (MCU) are based on a 32-bit ARM7CPU with real-time emulation and embedded trace support that combines the microcontroller
With embedded high-speed flash memory ranging from 32 kB to 512 kB. A 128-bit wide memory interface and unique accelerator architecture enable 32-bit code execution at the maximum clock rate. For critical code size applications, the alternative 16-bit. A blend of serial communications interfaces ranging from a USB 2.0 Full Speed device, multiple UARTS, SPI, SSP to I2Cs and on-chip SRAM of 8 kB up to 40 kB, make these

devices very well suited for communication gateways and protocol converters, soft modems, voice recognition and low-end imaging, providing both large buffer size and high processing power. Various 10-bit ADC, 10-bitDAC, PWM channels and 45 fast GPIO lines with up to nine edge or level sensitive external interrupt pins make these microcontrollers particularly suitable for industrial control and medical systems.

Figure 2: LPC2148 Microcontroller

Features:
• 32-bit ARM7 microcontroller in a tiny LQFP64 package.
• 8 to 40 kB of on-chip static R AM and 32 to 512 kB of on-chip flash program memory.
• In-System/In-Application Programming (ISP/IAP) via on-chip boot-loader software. Full chip erase in 400 ms and programming of 256 bytes in 1 ms.
• USB 2.0 Full Speed Compliant Device Controller with 2 kB of endpoint RAM. In addition, theLPC2146/8 provides 8 kB of on-chip RAM accessible to USB by DMA.
• One or two 10-bit A/D converters provide a total of 14 analog inputs, with conversion times as low as 2.44 µs per channel.
• Single 10-bit D/A converter provides variable analog output.

B. pH Sensor

pH sensor shown in figure **3** is used to measure the acidity and alkalinity of water soluble substances (pH stands for potential of Hydrogen). A pH value is a number from 1 to 14, with 7 as the neutral point. Values below 7 indicate acidity 1 being the most acidic.

Figure 3: pH sensor

C. Turbidity Sensor

The turbidity sensor shown in figure 4 detects water quality by measuring the levels of turbidity. It uses light to detect suspended particles in water by measuring the light transmittance and scattering rate, which changes with the amount of total suspended solids (TSS) in water. As the TSS increases, the liquid turbidity level increases.

Figure 4: Turbidity sensor

D. Temperature Sensor

The temperature sensor is based on chip consisting of a waterproof probe and long wire shape, which is perfect for immersive temperature detection or detecting something far away. The DS18S20 provides 9 to 12 bit (configurable) temperature reading over a 1-Wire interface, so that only one wire (and ground) needs to be connected from a central microprocessor. In addition, the DS18S20 can derive power directly from the data line ("parasite power"), eliminating the need for an external power supply. Figure 5 shows temperature sensor.

Figure 5: Temperature sensor

III. System Design and implementation

The sensors that are used for measuring water quality parameters such as pH, temperature, and turbidity are connected to microcontroller Unit for processing the data, serial communication unit acts as a phase between MCU and GPRS module, GPRS module transmit the data to server and later the data is used for further analysis. Figure 6 shows the block diagram of water quality monitoring system.

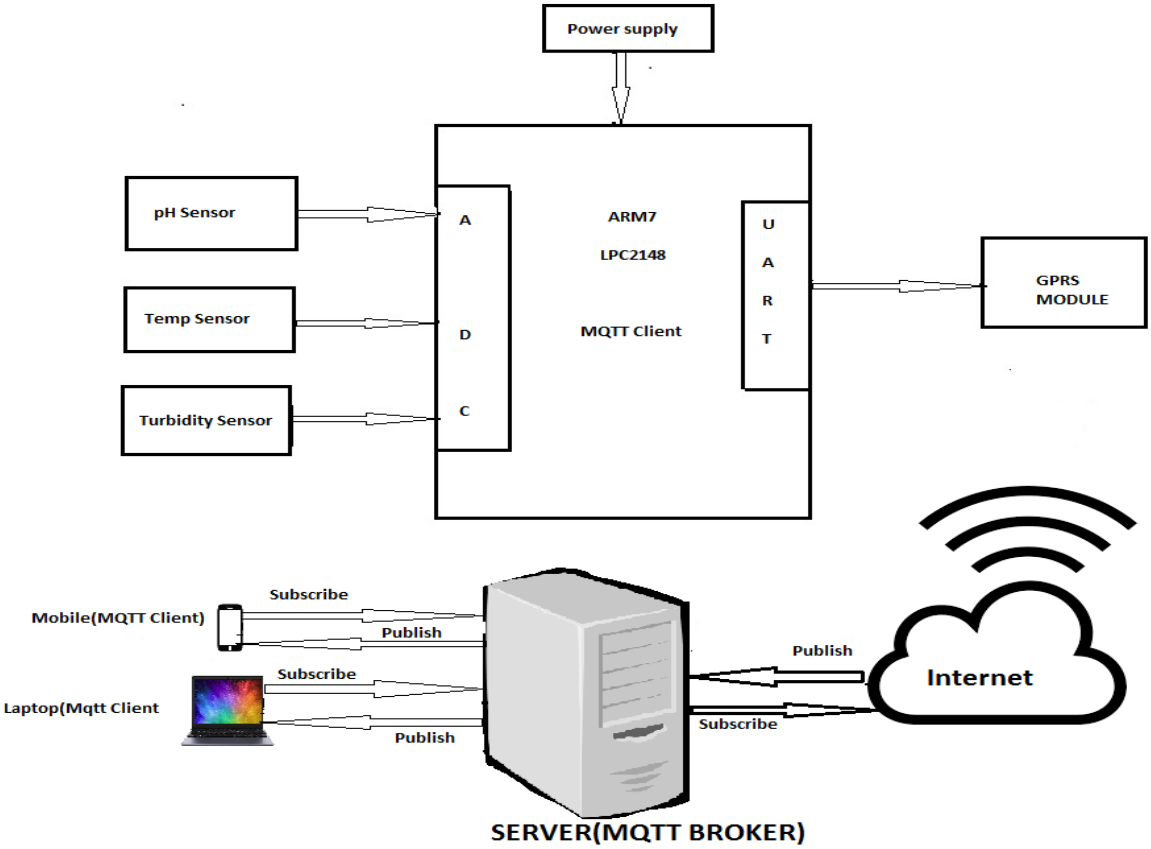

Fig 6: Block diagram of water quality monitoring system

Experimental Investigation

The experiment is conducted in two phases and figure 7 shows the flow chart of the monitoring system

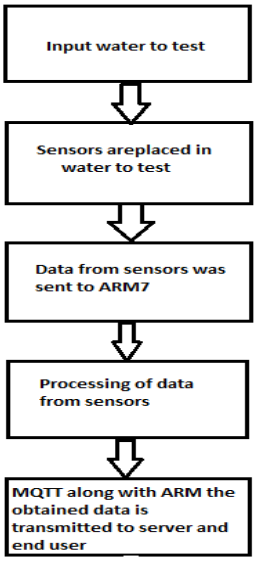

Fig 7: Flow chart of water quality monitoring system using IoT.

First phase, is to find out the water parameters used for determining the condition of water quality. Here we are using pH, turbidity and temperature, secondly we have used water samples from industry waste water and treated water for the data analysis. To transfer the data obtained from the sensors, a setup is created which consists of an ARM processor, GPRS module along with the sensors. All the device is interconnected to each other. The GPRS module creates the connection between the sender and receiver. In the next phase the server acts as a MQTT broker which collects the data from the sensors to the server. The server is running Mosquitto which is an open source message broker running MQTT protocol. The whole process takes place in real time taking it simultaneous and fast. The data is saved in a database for further analysis. Figure 8 shows the implementation of water quality monitoring system.

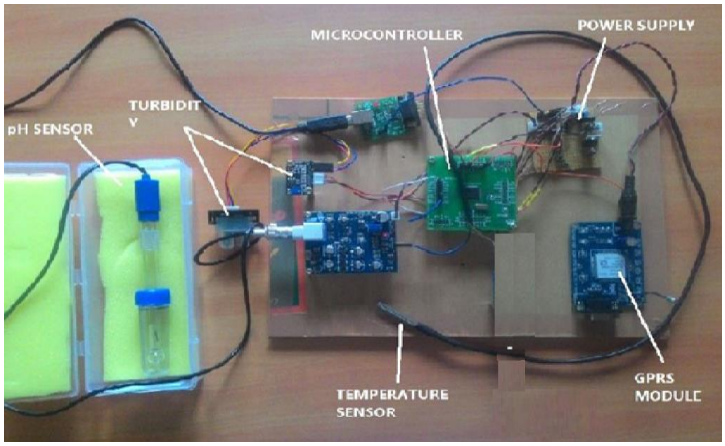

Fig 8: Implementation of water quality monitoring system using IoT

Results and Discussions

In the present study three types of water samples were collected viz.

1. Industry waste water sample 2. Treated water sample1 3. Treated water sample2.

All the three samples were tested for its quality using pH, temperature and turbidity sensors. Table 1 shows the results of the same. The data collected was saved in the database and can be used for further analysis.

Table 1: Various types of water were tested and their corresponding values

Sl No.	Type of water	pH value	Temperature	Turbidity
Sample 1	Industry waste water sample	8.92	29.3	31.4
Sample 2	Treated water1	7.66	25.3	21.2
Sample 3	Treated water2	7.23	25.8	5.4
Sample 4	Potable water	7.1	25	5

Table 1 clearly shows the comparison between all four samples. The permissible value for ph ranges from 5.5 to 9.00, the threshold value for turbidity should not be more than 10 and the temperature shall not exceed 5 degree Celsius above the receiving water. In the above table we can see that the turbidity value of the sample 1 and 2 are more than the permissible level, in which case a message is sent to the end user immediately for the implication of further action.

Conclusion

In this paper we have proposed the application of MQTT protocol for real time water quality monitoring system. Here the transmission/reception of data between server and client (end User) is done using MQTT protocol. The advantages of using MQTT protocol when compared to other technologies like GSM network or other technology are

- MQTT messages are delivered asynchronously through publish and subscribe architecture which reduces buzz and delay in transmission.
- Each control packet has a specific purpose and every bit in the packet is carefully crafted to reduce the data transmitted over the network.
- Since the data transmitted over the network is less further reduces the power usage and increase in the life of battery.
- A large amount of data is sent continuously without any hurdle making the system more efficient mode for communication.

REFERENCES

[1]Brida Das,P.C Jain(2017)',Real-Time Water Qualitymonitoring system using Internet of things,International conference on computer ,Communications and Electronics Manipal University Jaipur,Malaviya National Institute of Technology Jaipur and IRISWORLD

[2]Cho Zin Myint, Lenin Gopal, and Yan Lin Aung (2017), Reconfigurable Smart Water Quality Monitoring System in IOT Environment.IEEE ICIS, Wuhan, China

[3]GoibWiranto, Grace A Mambu, Hiskia, I DewaPutuHermida, SlametWidodo,"Design of Online Data Mesurement and Automatic Sampling System for Continous Water Quality Monitoring " Proceedings of 2015 IEEE International Conference on Mechatronics and Automation, Aug 2-5, Beijing, China, Aug., 2015, pp-2331-2335

[4] Jayti Bhatt,Jignesh Patoliya(2016),IOT based water quality monitoring system,International Journal of Industrial Electronics and Electrical Engineering ,ISSN:2347-6982,Vol 4,Issue-4

[5] JyothirmayaIjaradar, Subhasish Chatterjee, (2018) International Research Journal of Engineering and Technology Vol 5, Issue 3

[6] Nikkam, S. M. G., & Pawar, V. R. (2016). Water parameter analysis for industrial application using IoT. 2016 2nd International Conference on Applied and Theoretical Computing and Communication Technology (iCATccT).

[7]N.Thirupathi Rao,Debnath Bhattacharyya,V,Madhusudhan Rao,Tai-hoon Kim(2019),International Journal of Innovative Technology and Exploring Engineering Vol 8, Issue 5

[8] Pradeep Kumar, Somasundaram and Dharon Joseph(2013), Monitoring Water Quality using RF Module,International Journal of Application or Innovation in Engineering and Management Vol 2,Issue 7.

[9] Shruti Sridharan(2014), Water Quality Monitoring System Using Wireless Sensor Network, International Journal of Advanced Research in Electronics and Communication Engineering (IJARECE) Volume 3, Issue 4.

[10] Saravanan, M., Das, A., & Iyer, V. (2017). *Smart water grid management using LPWAN IoT technology. 2017 Global Internet of Things Summit (GIoTS).*

[11] Wiranto, G., Mambu, G. A., Hiskia, Hermida, I. D. P., & Widodo, S. (2015). *Design of online data measurement and automatic sampling system for continuous water quality monitoring. IEEE International Conference on Mechatronics and Automation (ICMA)*

9th International Engineering Symposium - IES 2020
March 3-5, 2020, Kumamoto University, Japan

Design of Low Power and High Speed VLSI Domino Logic Circuit

Praveen J[1], Bhuvanesh M[2]

1 *Dean (Academics) and Professor, Department of Electronics and Communication Engineering, Alva's Institute of Engineering and Technology, Moodbidri 574-225, India*
email: praveenj_vishruth@yahoo.com
2 *Undergraduate Student, Department of Electronics and Communication Engineering, Alva's Institute of Engineering and technology, Moodbidri 574-225, India email:bhuvaneshm2016@gmail.com*

ABSTRACT: The power dissipation of the circuit is reduced in normal mode of operation compared to test mode for any low power VLSI designs. This intern reduces the battery life of the device. Therefore, reducing power dissipation during normal operation has become a critical objective in today's any VLSI circuit designs. In the present study, various design approaches had been investigated for realizing domino CMOS. Both conventional and proposed circuits are used to for the study. Initially power, delay and power delay product is calculated for conventional domino Standard Footless Domino Logic for OR gate, Diode Footed Domino Logic for OR gate, Current Comparison Domino Logic for OR gate. Further, the conventional domino logic design was modified as proposed circuit 1 for domino logic OR gate and proposed circuit 2 for domino logic OR gate. The proposed circuit was designed for the 90nm technology with 1.8 supply voltage and 100 MHz frequency using cadence virtuoso flat form. Results indicated that proposed circuit exhibited, better power dissipation, delay and power delay product compared to conventional designs.

Keywords*: Domino logic, Low power dissipation, CMOS*

I. INTRODUCTION

The growth of the low-power VLSI designs over the past 50 years has significant change in our life style. Integrated circuits are everywhere from computers to automobiles, from cell phones to home appliances. The growth of the low-power circuits is predicted to continue at a faster pace. Since the first integrated circuit was invented in the labs of Texas instruments in 1958 [1]. With the dramatic increase in chip complexity of Ultra Large Scale Integration (ULSI), number of transistors and power consumption are growing rapidly. The objective of designing digital VLSI circuits is to minimize silicon area per logic circuit as to have a large number of gates per chip. Area reduction occurs in three different ways such as 1 Advances in processing technology that enables a reduction of the minimum device size, 2 Circuit design techniques and 3 Careful chip layout. Power consumption and signal delay are crucial elements in designing of high-performance low voltage VLSI circuits.

The reduction of power dissipation and the improvement of the speed require optimization at all levels in the design procedure. In Nano scaling, enormous power is consumed as static power dissipation. The domino circuits are used in various circuits, especially-memory [2-4], multiplexor, comparator [5] and arithmetic circuit [7-8] and also used in full adders that are the most important part of a CPU. Additionally, domino circuits are important components in other applications such as Digital Signal Processing (DSP) architectures and microprocessors [8], which rely on the efficient implementation of generic arithmetic logic and floating point units to execute dedicated algorithms.

Various design approaches had been investigated for realizing domino CMOS topologies in the literature [9].

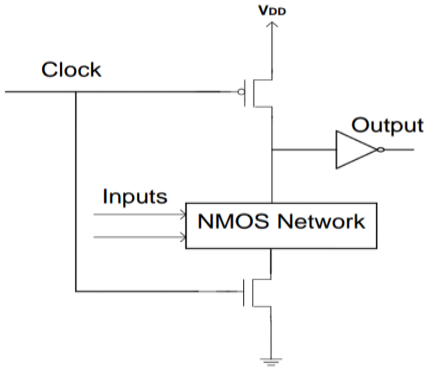

Fig. 1. A Domino CMOS circuit

Fig. 1. Shows non inverting domino cell and it contains dynamic logic along with additional inverter. During the precharged phase, only the output capacitor gets charged. But the output is valid only during the evaluated phase when the clock transition occurs between high to low. The gates like AND, OR and inverter are used to achieve non inverting output implementation at domino logic level [6]. But gets like NAND, NOR and Inverters cannot be used. In most of the design inverting functions are unavoidable, this would appear at first thought to preclude the general applicability of domino logic. Furthermore, only low to high input transitions is valid as the evaluation node is recharged in domino logic cells but this is generally not acceptable.

In the present study**,** attempts are made to design a domino CMOS circuit in 180nm technology by characterizing the all the transistor in saturation region by keeping 1.8V supply voltage with 100 MHz frequency. Further power, area and delay for the design were calculated. An effort was made to bring some changes in the structural and logical implementation to reduce power, area and delay even further. In the study also, a new technique to implement the same Domino CMOS circuit even reduced power, area and delay was investigated and the proposed technique was compared with existing conventional technique in terms of power, area and delay. Based on the same, attempts are made to implement the proposed Domino CMOS circuit in one of the application circuits.

II. DESIGN AND IMPLIMENTATION OF DOMINO LOGIC CIRCUIT OF OR GATE

In the study, the following three types of conventional Domino CMOS for OR Gate were designed. They are

- Standard Footless Domino Logic
- Diode Footed Domino Logic
- Current Comparison Domino Logic

Footless domino logic OR gate is a standard domino logic circuit shown in Fig. 2. In conventional Footless domino logic, a keeper transistor is utilized as a feedback for retaining the state of the dynamic node and to reduce charge sharing problem, but the resulting contention between the keeper transistor and pull down networks reduces the power and speed characteristics of the circuit [10-11].

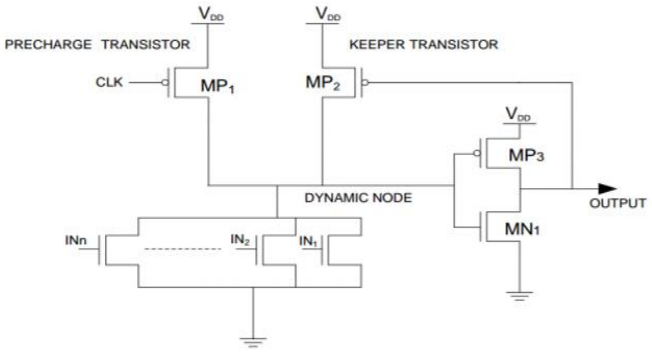

Fig. 2. Standard Footless Domino Logic for OR gate

Diode footed domino OR gate is shown in Fig.3 [12]. Customization to the standard domino circuit has been done by adding an NMOS transistor in a diode configuration in series with the evaluation network as shown in Fig. 3. The diode footer (M1) results in the sub threshold leakage reduction due to the stacking effect [13-14]. But there is performance degradation due to the diode footer that's why mirror transistor (M2) is employed to increase the performance characteristic.

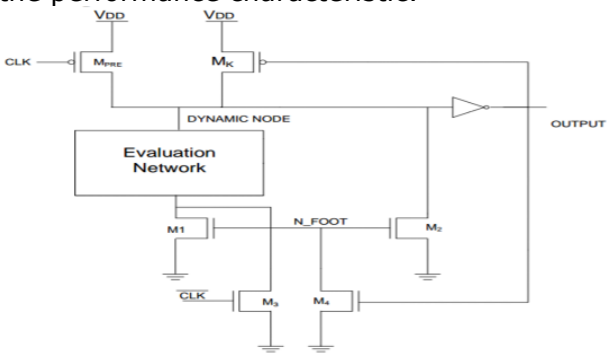

Fig. 3. Diode Footed Domino for OR gate

Fig. 4. Shows 2-input current Comparison Domino OR gate. This technique uses the difference and the comparison between the switching current of the ON transistors and the leakage current of the OFF Transistors of the pull down network to control the PMOS keeper transistor, yielding reduction of the contention between keeper transistor and the pull down network from which previously proposed techniques have suffered. Moreover using the stacking effect, leakage current is reduced and the performance of the current mirror is improved.

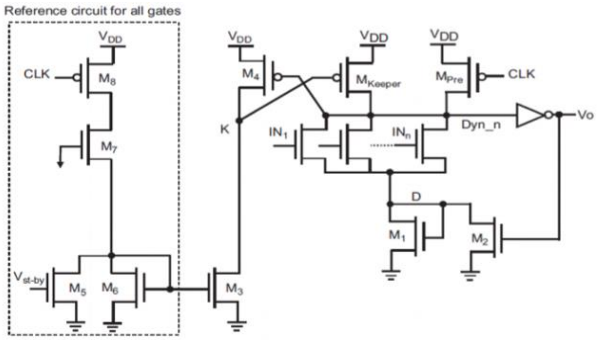

Fig. 4. Current Comparison Domino for OR gate

Initially three different types of conventional OR gate is designed. Then the following two types of proposed domino CMOS circuits for OR gate are designed using CMOS logic design style. They are:

Proposed circuit 1 (Fig 5): It is obtained just by excluding clock input PMOS. Clock input is excluded the PMOS transistor and a weak PMOS is being used instead of clock driver. The weak device charging rate is very slow, so when there is no input applied for a long time this transistor makes dynamic node to charge up to supply voltage level. So there will be no contention problem with this circuit. So any separate path is not needed to discharge at the beginning of the evaluation phase. The delayed version of the clock can be excluded. The modified domino circuit for full static operation is shown in Fig. 5.

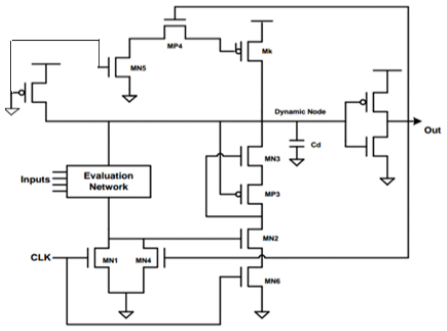

Fig. 5. Proposed Circuit 1 for Domino Logic OR gate

Proposed circuit 2 (Fig 6): It consists of an extra enable signal, which should be enabled always to get static output even in precharge phase. The circuit operation is as follows: when the clock is low (normally said as recharge phase), the transistor MN1 is in OFF condition. According to the input logics dynamic node may charge to VDD or discharged to GND. If inputs make dynamic node to discharge to footer voltage, then this potential makes use of level restorer to discharge and also can provide the exact outputs irrespective of the clock. An external enable signal here, so the GND level is brought up to the keeper circuit if no inputs makes to discharge the dynamic node and more than one transitions are allowed in every case.

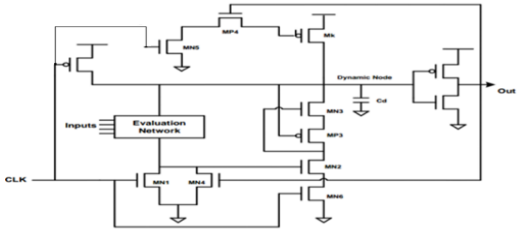

Fig. 6. Proposed Circuit 2 for Domino Logic OR gate

III. DESIGN IMPLIMENTATION

The designed conventional domino Standard Footless Domino Logic for OR gate, Diode Footed Domino Logic for OR gate, Current Comparison Domino Logic for OR gate and proposed circuit 1 for domino logic OR gate and proposed circuit 2 for domino logic OR gate is implemented for one of the application circuit called SR latch. The circuit diagram of Gated SR latch constructed from NOR gates is shown in Fig. 7.

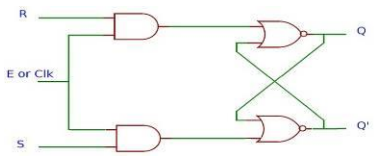

Fig. 7. Circuit Diagram of SR Latch

IV. SIMULATION RESULTS

Fig. 8 shows the circuit design of Standard Footless Domino Logic for OR gate using cadence platform for 90 nm technology with supply voltage of 1.8v and 100 MHz frequency.

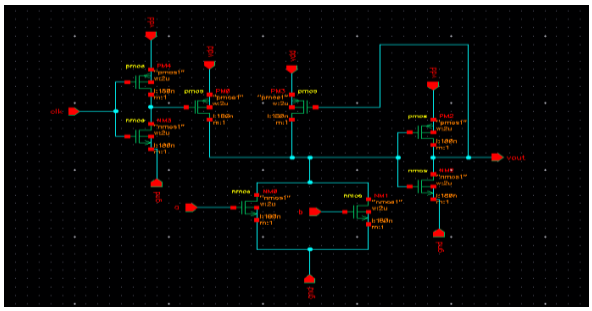

Fig. 8. Circuit Design of Standard Footless Domino Logic OR gate

Fig. 9 shows, simulation result of Standard Footless Domino Logic for OR gate and output waveforms is compared to standard truth table of the OR gate.

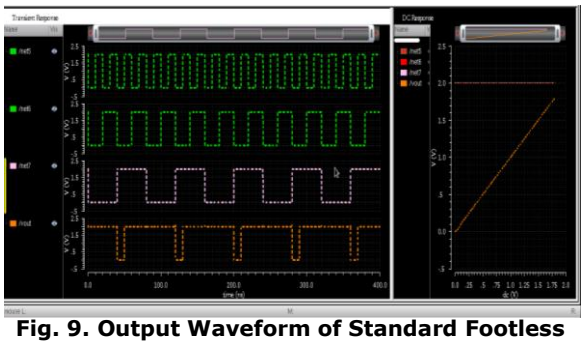

Fig. 9. Output Waveform of Standard Footless Domino Logic

Fig. 10 shows the circuit design of Diode Footed Domino Logic for OR gate using cadence platform for 90 nm technology with supply voltage of 1.8v and 100 MHz frequency.

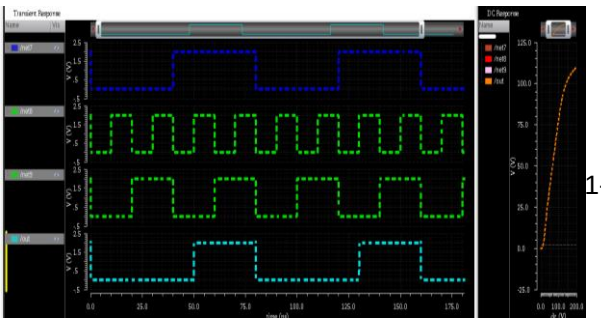

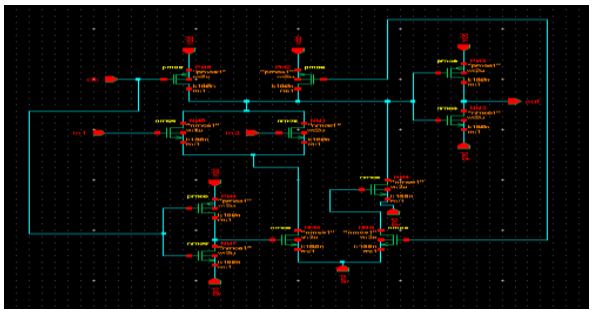

Fig. 10. Circuit Design of Diode Footed Domino Logic OR gate

Fig. 11 shows, simulation result of Diode Footed Domino Logic for OR gate and output waveforms are compared with standard truth table of OR gate.

Fig. 11. Output Waveform of Diode Footed Domino Logic OR gate

Fig. 12 shows the circuit design of Current Comparison Domino logic for OR gate using cadence platform for 90 nm technology with supply voltage of 1.8v and 100 MHz frequency

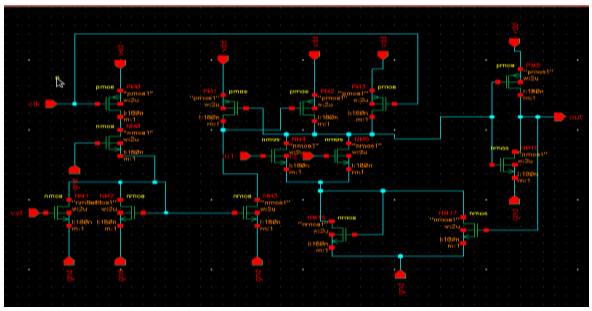

Fig. 12. Circuit Design of Current Comparison Domino logic for OR gate

Fig. 13 shows simulation result of Comparison Domino logic for OR gate and

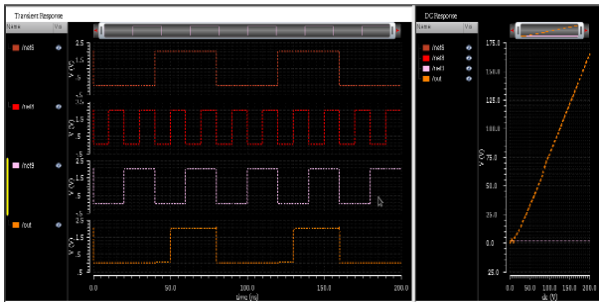

output waveform is compared to standard truth table of OR gate.

Fig. 13. Output Waveform of Current Comparison Domino logic for OR gate

Fig. 14 shows the circuit design of proposed circuit 1 domino logic for OR gate using cadence platform for 90 nm technology with supply voltage of 1.8v and 100 MHz frequency.

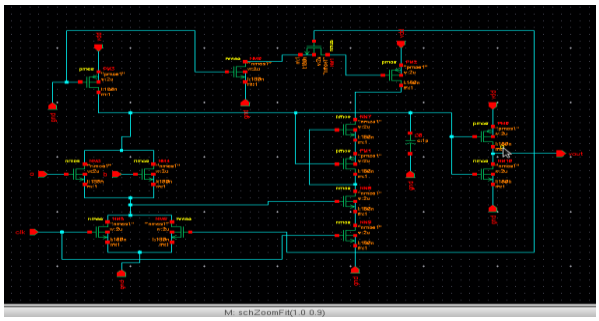

Fig. 14. Circuit Design of Proposed circuit 1 domino logic for OR gate

Fig. 15 shows, simulation result of proposed circuit 1 domino logic for OR gate and output waveforms is compared to standard truth table of OR gate.

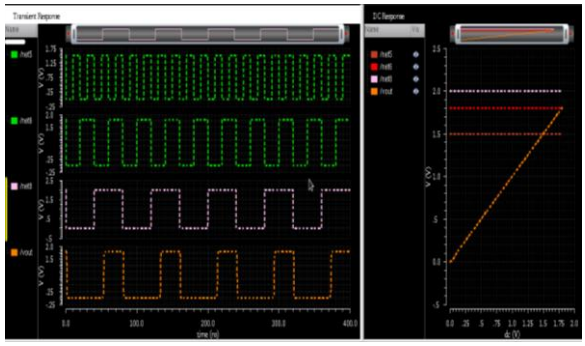

Fig. 15. Output Waveform of Proposed Circuit 1 domino logic for OR gate

Fig. 16 shows the circuit design of proposed circuit 2 domino logic for OR gate using cadence platform for 90 nm technology with supply voltage of 1.8v and 100 MHz frequency.

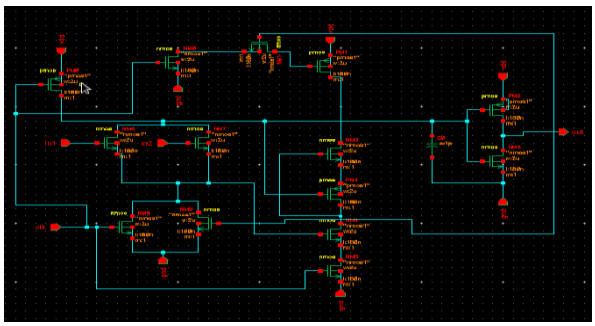

Fig. 16. Circuit Design of Proposed circuit 2 domino logic for OR gate

Fig. 17 shows simulation result of proposed circuit 2 domino logic for OR gate and output waveforms is compared to standard truth table of OR gate.

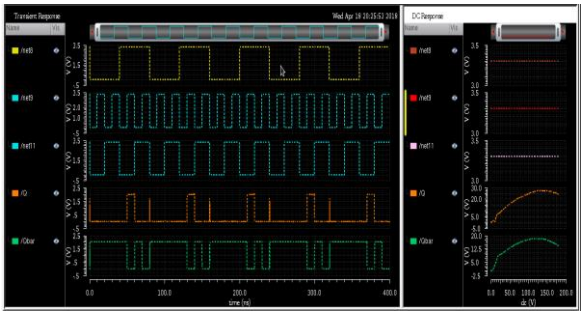

Fig. 17. Output Waveform of Proposed Circuit 2 domino logic for OR gate

Fig. 18 shows the circuit design of SR Latch using proposed circuit 1 domino Logic for OR gate using cadence platform for 90 nm technology with supply voltage of 1.8v and 100 MHz frequency.

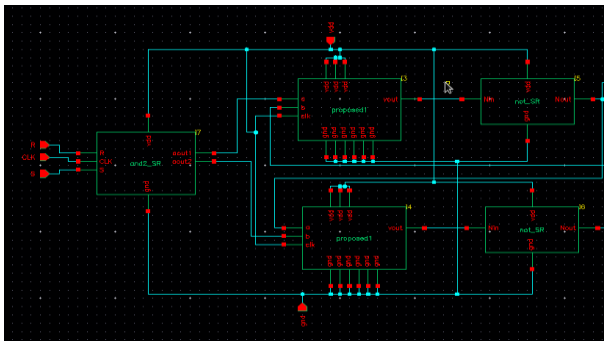

Fig. 18. Circuit Design of SR Latch using proposed circuit 1 domino logic for OR gate

Fig. 19 shows simulation result of proposed circuit 1 domino Logic for OR gate and output waveform is compared to standard truth table of OR gate.

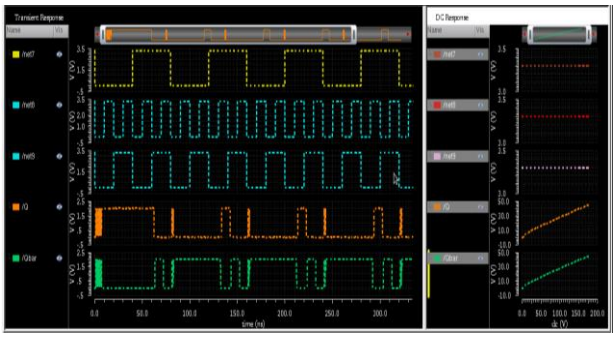

Fig. 19. Output Waveform of SR Latch using Proposed Circuit 1domino logic for OR gate

Fig. 20 shows the circuit design of SR Latch uses proposed circuit 2 domino Logic for OR gate using cadence platform for 90 nm technology with supply voltage of 1.8v and 100 MHz frequency.

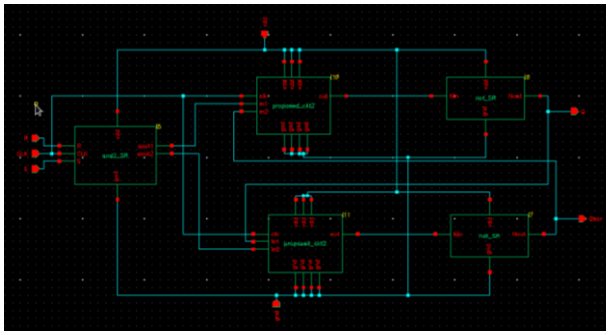

Fig. 20. Circuit Design of SR Latch using proposed circuit 2 domino logic for OR gate

Fig. 21 shows simulation result of proposed circuit 2 domino Logic for OR gate and output waveform is compared to standard truth table of OR gate.

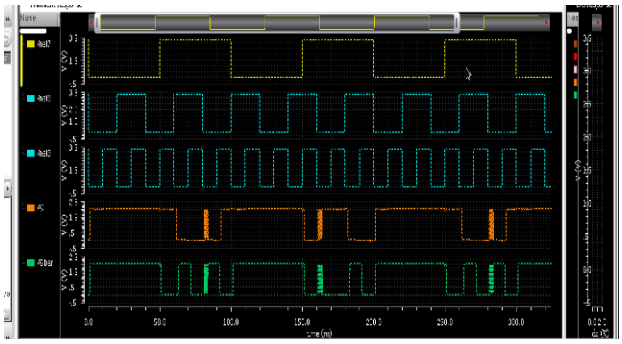

Fig. 21. Output Waveform of SR Latch using Proposed Circuit 2domino logic for OR gate

V. EXPERIMENTAL RESULTS

Table 1 shows the comparison with experimental result of Power, Delay and Power Delay Product for all the three designed conventional domino logic for OR gate and proposed circuit 1 domino logic for OR gate and proposed circuit 2 domino logic for OR gate. From the Table 1, it is clear that Power, Delay and Power Delay Product of the proposed circuit 2 domino logic for OR gate is reduced compared to all the three conventional circuits.

Table1: Comparison Table for Power, Delay and PDP

Domino Logic Circuits	Power (µW)	Delay (nS)	PDP (fJ)	Area
Standard Footless Domino Logic (SFDL)	428.8	50.06	21.46	8
Diode Footed Domino Logic (DFDL)	338.5	9.957	3.369	11
Current Comparison Domino Logic (CCDL)	347.6	50.07	17.4	14
Proposed Circuit 1 (PC 1)	338.6	8.604	2.913	14
Proposed Circuit 2 (PC 2)	58.37	8.324	0.485	14

Table 2 shows the comparison with experimental result of Power, Delay and Power Delay Product of all the three implemented SR latch using conventional domino logic for OR gate and implemented SR latch using proposed circuit 1 domino logic for OR gate and implemented SR latch proposed circuit 2 domino logic for OR gate.
It is clear that Power, Delay and Power Delay Product of the implemented SR latch for proposed circuit 2 domino logic for OR gate is reduced compared to all the three implemented SR latch for conventional circuits.

Table 2: Power, Delay and PDP Comparison Table of Implemented Circuits

Implemented Circuits	Power (µW)	Delay (nS)	PDP(fJ)	Area
Imp1 using Standard Footless Domino Logic	1807	19.99	36.12	32
Imp2 using Diode Footed Domino Logic	1569	9.994	15.68	38
Imp3 using Proposed Circuit 1	1497	8.412	12.59	44
Imp 4 using Proposed Circuit 2	975.9	1.107	1.08	44

VI. CONCLUSION AND SCOPE FOR FUTURE DIRECTIONS

Based on the results and discussion the following conclusions are drawn, The conventional domino logic design is modified as proposed circuit 1 for domino logic OR gate and proposed circuit 2 for domino logic OR gate, which results in better power dissipation, delay and power delay product compared to conventional designs. The OR gates of conventional domino logic and proposed domino logic is applied to standard SR latch for which power, delay and power delay products are calculated. The obtained results show that the proposed circuit 2 domino logic for OR gate results in reduction of power dissipation, delay and delay product compare to conventional domino logic for OR gate.

REFERENCES

[1] Domino logic design for high performance and leakage tolerant applications Farshad and Moradi tua von cao "ELSEVIER 2011" Vlsi journal.
[2] Tam S., Rusu S., Nagarji Desai U., Kim R., Zhang J., Young I, "Clock Generation and Distribution for the First IA-64 Microprocessor", IEEE J. Solid-state Circuits, Vol-11, No. 35, pp. 1545–1552. 2000.
[3] R. K. Krishnamurthy, A. Alvandpour, G. Balamurugan, N. R. Shanbhag, K. Soumyanath and S. Y. Borkar , "A 130-nm 6-GHz 256 × 32 Bit Leakage-Tolerant Register File," IEEE Journal of Solid-State Circuits, vol. 37, No. 5, pp. 624-632, 2002.
[4] M. W. Allam, M. H. Anis, M. I. Elmasry," High Speed Dynamic Logic Style for Scaled-Down CMOS and MTCMOS Technologies," Proceedings of The International Symposium on Low Power Electronics and Design, pp. 155-160, 2000.
[5] A. Alvandpour, R.K. Krishnamurthy, K. Soumyanath, S.Y. Borkar, "A Sub-130- nm Conditional Keeper Technique," IEEE Journal of Solid-State Circuits, pp. 633–638. 2002
[6] R. H. Krambeck, C.M. Lee, and H.-F. S. Law, "High-Speed Compact Circuits with CMOS," IEEE Journal of Solid-State Circuits, vol. 17, no. 3, pp.614–619, 1982.
[7] H. Veendrick, "Short Circuit Dissipation of Static CMOS Circuitry and Its Impact on the Design of Buffer Circuits," IEEE Journal of Solid-State Circuits, vol. 19, no. 4, pp. 468– 473, 1984.
[8] T. Sakurai and A. R. Newton, "Delay Analysis of Series-Connected MOSFET Circuits," IEEE Journal of Solid-State Circuits, vol. 26, no. 2, pp. 122–131, 1991.
[9] N. Hedenstierna and K. Jeppson, "CMOS Circuit Speed and Buffer Optimization," IEEE Transactions on Computer-Aided Design of Integrated Circuits and Systems, vol. 6, pp. 270–281, 1987.
[10] J. Wang, N. Gong, L. Hou, X. Peng, R. Sridhar, and W. Wu, "Leakage current, active power, and delay analysis of dynamic dual Vt CMOS circuits under P-V-T fluctuations", Microelectronics Reliability,vol.51, pp.1498-1502, 2011.
[11] A. K. Pandey, V.Mishra, R. A. Mishra, R. K. Nagaria and V. K. Rao, "Conditional precharge dynamic buffer circuits", International Journal of Computer Applications, vol.60, no.6, pp.45- 52, 2012.
[12] A. Alvandpour, P. Larsson-Edefors, and C. Svensson, "A Leakage-Tolerant Multi-Pha Keeper for Wide Domino Circuits," in Proceedings of the 1999 IEEE International Conference on Electronics, Circuits and Systems, 1999.
[13] S. Wairya. R. K. Nagaria and S. Tiwari, "New design methodologies for high speed mixed-mode CMOS full adders circuits", International Journal of VLSI design and Communication Systems(VLSICS), AIRCC Publication, Vol.2, no 2, pp.78-98, 2011.

9th International Engineering Symposium - IES 2020
March 3-5, 2020, Kumamoto University, Japan

Face Recognition using Artificial Intelligence

Tahir Naquash H B [1], Apoorva U[2], Harish Kunder [3]

1 *Assistant Professor, Department of Computer Science & Engineering, Alva's Institute of Engineering and technology, Moodbidri 574 225, India*
email:tahirnaquash@gmail.com
2 *Undergraduate Student, Department of Computer Science & Engineering, Alva's Institute of Engineering and technology, Moodbidri 574 225, India*
email:uapoorva0818@gmail.com
3 *Associate Professor, Department of Computer Science & Engineering, Alva's Institute of Engineering and technology, Moodbidri 574 225, India*
email:harishkunder@aiet.org.in

ABSTRACT: Face recognition is one of the most popular applications of image analysis. In present scenario, face recognition plays a major role in security, personal information accesses, improved human machine interaction and personalized advertising. Hence a recognition system that is inexpensive to use at any location, performs quicker matching, handles large database and do recognition in a varying environment is the need of the hour. It is a true challenge to build an automated system which parallels human ability to recognize faces. Since the faces are highly dynamic and pose more issues and challenges to solve, pattern recognition and artificial intelligence are used to propose solutions to reduce such difficulties so as to improve the robustness and recognition accuracy.

Keywords*: Face Recognition, Artificial Intelligence*

Introduction

Face Recognition is one of the areas from Computer Vision that has drawn more interest for long. The practical applications for it are many, ranging from biometrical security, to automatically tagging your friends pictures, and many more. Because of the possibilities, many companies and research center have been working on it. The uses for an automatic face recognition system are many. Typical ones are biometric identification usually combined with other verification methods, automatic border control, or crowd surveillance. One of its main advantages is its non intrusivity. Most identification methods require some action from people, either putting the fingerprint in a machine, introducing a password, etc. On the contrary, face recognition can work by simply having a camera .Deep learning is a subfield of machine learning concerned with algorithms inspired by the structure and function of the brain called artificial neural networks. Deep learning applies multiple processing layers to learn representations of data with multiple levels of feature extraction. This emerging technique has reshaped the research landscape of face recognition. One of the key aspects in most machine learning methods is the way data is represented, that is, which features to use. If the features used are badly chosen, the method will fail regardless of its quality. Even more, this selection affects the knowledge with which the method can work, if you have trained your market analysis algorithm with numerical values, it will not be able to make any sense from a written report, no matter its quality. Therefore, it is no surprise that there has been an historical interest on finding the appropriate features. This becomes especially relevant in the case of Computer Vision problems. The reason is that, when

faced with an image, there are usually way too many features, a simple 640 × 480 RGB image has almost 1 million pixels, and most of them are irrelevant. Because of this, it is important to find some way of condensing this information in a more compact way.

Related works

The system uses Deep Learning, which uses a massive instances dataset for training. They must be credited with being able to make use of that much data in such a successful way. Given the quality of the results, the robustness of the method and the fact that they provide a description on how they implemented it makes it suitable for our work. The Histogram of oriented gradients is inferred by the work of Navneet Dalal and Bill Triggs et al (2005). The face land landmark algorithm is used for marking landmarks on faces, it can be done by other approaches by Vahid Kzemi and Josephine Sullivan, 2014. The learning task for neural networks consists in finding the right weights, although there are many other architectures to do this. There are also other ways of learning the weights, such as genetic algorithms [Montana and Davis, 1989] or simulated annealing [Aarts and Korst, 1989; Yamazaki, Souto, and Ludermir, 2002]. The face recognition method developed, called DeepFace [Taigman et al., 2014] is also very useful by considering its factors such as feasibility or implementing them or quality of description.

PROPOSED WORK

The proposed system makes use of the deep learning for performing face recognition among a set of stored faces. The system is composed of two main parts: the extraction of features and using these features to identify a person.

Face Detection using Histogram of oriented Gradients.

Histogram of oriented gradients proposed by Navneet Dalal and Bill Triggs et al (2005) is also used as feature descriptor where the important feature of the images are outlined. In our experiment, we are converting the image into a black and white image and then mark the darker pixels where we get the outline of the face and when compared with the HOG features of the other training data detects the face in the image.

Repositioning the faces in the images

The images usually donot appear in the way we desire. There are chances in which the face appears to be sideways, so we face difficulty in identifying the images. Therefore we have to reposition the image in such a way so that the eyes lips and other feature identified appears at the same position. Therefore the algorithm called face landmark estimation, where the algorithm is trained to identify the specific points on the face such as the outside edge of each eye, inner edge of each eyebrow, the outline of the lips and nose. Once these points have been recognised, the image is rotated and scaled to center the eyes, mouth and other features. This can also be done by other approaches proposed by Vahid Kzemi and Josephine Sullivan, 2014.

Feature Extraction using Convolutional Neural Network

The Deep Convolutional Neural Network is trained to recognise the faces in the images by a process called embedding where the measurements of the faces are produced when the images are fed to the network. All the images fed give the same number of measurements for them and depending on the difference in the measurements, we can tell that the image belongs to different people.

Face recognition using Support Vector Machine Classifier

The classifier is trained to take the measurements from the new test image and compare is with the closest match by running the classifier .The matched measurements with then produce the name of the person as a result.

Result Analysis

The dataset is trained to recognise the person in the image. The input given is a picture consisting of a single person, which is then trained to recognise the person in any image that is fed. It's predicted to be 99.38% when compared with the existing systems with the result being the square box around the face recognized with their names displayed.

CONCLUSION

The following conclusions are deduced:

- The proposed method is found to be better than the other existing systems.
- It's predicted to be 99.38% accurate with other real time applications.
- It can be extended to recognize faces in the live video.
- It can be improvised with other deep learning algorithms and classifiers.

REFERENCES

[1] Navneet Dalal and Bill Triggs et al.(2005),Histograms of Oriented Gradients for Human Detection, INRIA Rhone-Alps.
[2] Vahid Kazemi and Josephine Sullivan et al.(2014),One Millisecond Face Alignment with ana Ensemble of Regression Trees, Royal Institute of Technology.
[3] L.Ding and A.M.Martinez. Precise detailed detection of faces and facial features.In CVPR,2008.
[4] V.Kazemi and J.Sullivan.Face alignment with part-based maodeling.In BMVC,2011.
[5] Florian Schroff,Dmitry Kalenichenko,James Philbin el al.(2015),FaceNet:A Unified Embedding For Face Recognition and Clustering,Google
[6] Taigman, Yaniv et al. (2014). "DeepFace: Closing the Gap to Human-Level Performance in Face Verification". In: Proceedings of the 2014 IEEE Conference on Computer Vision and Pattern Recognition.
[7]Hassner,Tal et al. (2015)."Effective Face Frontalization in Unconstrained Images". In: IEEE Conf. on Computer Vision and Pattern Recognition (CVPR).
[8] Huang, Gary B. et al. (2007). Labeled Faces in the Wild: A Database for Studying Face Recognition in Unconstrained Environments.
[9] Parkhi, Omkar M, Andrea Vedaldi, and Andrew Zisserman (2015). "Deep face recognition". In: British Machine Vision Conference.
[10] Santamaría, Mauricio Villegas and Roberto Paredes Palacios (2005),Comparison of illumination normalization methods for face recognition.
[11] Montana, David J. and Lawrence Davis (1989). "Training Feedforward Neural Networks Using Genetic Algorithms".
[12] Aarts, Emile and Jan Korst (1989). Simulated Annealing and Boltzmann Machines:A Stochastic Approach to Combinatorial Optimization and Neural Computing.

Fig 1. Result1: Shows the face recognised with the names being displayed in image1.

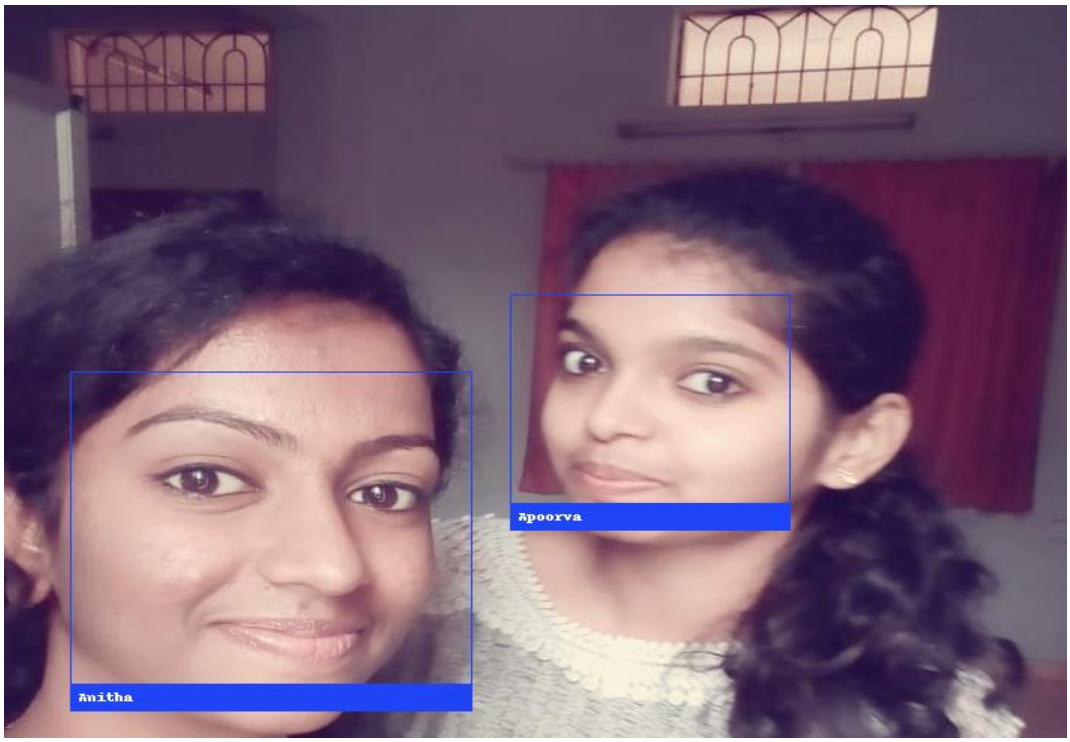

Fig 2. Result2: Shows the face recognised with the names being displayed in image2.

9th International Engineering Symposium - IES 2020
March 3-5, 2020, Kumamoto University, Japan

DETECTION OF BIAS IN MACHINE LEARNING MODELS USING FAIR ML

Tahir Naquash H B [1], Amogha U[2], Harish Kunder [3]

1 *Assistant Professor, Department of Computer Science & Engineering, Alva's Institute of Engineering and technology, Moodbidri 574 225, India*
email:tahirnaquash@gmail.com
2 *Undergraduate Student, Department of Computer Science & Engineering, Alva's Institute of Engineering and technology, Moodbidri 574 225, India*
email:uamogha98@gmail.com
3 *Associate Professor, Department of Computer Science & Engineering, Alva's Institute of Engineering and technology, Moodbidri 574 225, India*
email:harishkunder@aiet.org.in

ABSTRACT: In recent times, the identification of bias in machine learning models has become very critical. Bias in a machine learning model is about the model making predictions which tend to place certain privileged groups at a systematic advantage and certain unprivileged groups at a systematic disadvantage. The primary reason for unwanted bias in the training data is due to under-sampling or over-sampling of data. Identification and avoidance of bias is required in the field of finance, banking and insurance companies and other business to provide loans, for hiring and other social service benefits. Fair ML adopts the technique of finding relative significance/importance of the features used in the machine learning model to detect bias in the model.

Keywords*: Machine Learning, Bias, Fair ML*

Introduction

The growth of technology has also resulted in its increased requirement in various fields. Earlier, decisions to issue loans or insurance to its applicants, employment decisions and decisions regarding providing admissions to students were made manually. But, due to the increase in population over the years has made these tasks difficult to perform manually. The need to make such crucial and cumbersome decisions have led to the use of predictive models in these fields. The ability to decrease human effort and make correct decisions has made predictive models to be used in almost all industries. The predictive models not only provide efficiency but also provide productivity. Although predictive models provide greater advantage in terms of efficiency and productivity we may face problems in its decision making due to unintentional discrimination. If the inputs that are provided to the predictive model has biased patterns then its decision will also be biased. Therefore to determine the relative significance of the inputs of a model in determining outcomes, we need to focus on auditing predictive models.

Bias

Machine learning models cannot make decisions naturally but are trained by feeding them data sets. The amount of data and the type of data selected makes the model's prediction susceptible to bias.
There are different types of bias:

- Reporting bias: This occurs when frequency of outcome in dataset do not reflect to that of real world frequency.
- Automation bias: The results generated by automation systems are favoured over results generated by non-automated systems.
- Selection bias: This type of bias occurs if the data is not selected in a representative manner or if

proper randomization is not done during data collection.

- Implicit bias: This occurs when assumptions made are based on personal experience and need not be applied generally.

Related works

A new class of study has emerged to identify and correct bias throughout predictive modelling process. It can be broadly classified into three categories: data transformation, algorithmic manipulation and outcome manipulation methodologies proposed by Andrea Romei and Salvatore Ruggieri et al. (2014). Sorelle Friedler, Carlos Scheidegger, and Suresh Venkatasubramanian et al. (2014), present a data 'repair' method for transforming data into one that predictive models can hopefully learn fair models on. In order to reduce discrimination, algorithm manipulation methods aim to augment the underlying algorithm. Algorithm augmentation is usually done via a penalty that adds a cost of discrimination to the model's cost function as proposed in Rich Zemel, Yu Wu, Kevin Swersky, Toni Pitassi, and Cynthia Dwork et al. (2013). These algorithms add regularizers that determine the degree of bias acceptable. The analysis of Toshihiro Kamishima, Shotaro Akaho, and Jun Sakuma et al. (2011), is a major work in this field where bias is quantified by the introduction of a regularizer based on mutual information to the cost function of a logistic regression model. Since the Toshihiro Kamishima, Shotaro Akaho, and Jun Sakuma et al. (2011) work, more approaches that seek to change underlying cost functions with regularizers for statistical parity have emerged for other kinds of algorithms like decision trees and support vector machines. Techniques presented in this area, work for only one particular method like Logistic regression or Naïve-bayes, so the overall impact can be limited. Algorithm manipulation methods also assume that underlying predictive models are known, completely specified, and with well-behaved cost functions. Sometimes, ensemble models do not have well-defined cost functions, so the application of algorithm manipulation techniques to ensemble models can be difficult. In the third approach, other studies have presented works that manipulates the outcomes of predictive models towards achieving statistical parity across groups. Dino Pedreshi, Salvatore Ruggieri, and Franco Turini et al. (2008) alter the confidence of classification rules inferred. Toon Calders and Sicco Verwer et al. (2010) transform the output possibilities of a Naïve-bayes model. The thesis of Julius A. Adebayo et al. (2016) presents a FairML model that provides a graphical plot of attribute ranking among input variables using ranking methodologies such as IOPF, MRMR and LASSO.

PROPOSED WORK

The proposed FairML model uses the basic architecture provided by Julius A. Adebayo et al. (2016) but using different variable ranking methodologies such as random forest algorithm, support vector machine algorithm and logistic regression to provide a graphical model to show attribute ranking among input variables which shows model's dependence on its inputs which can be further utilized to predict model's fairness. The proposed model architecture is as shown in Figure 1.

Data processing

In Figure 1, although data processing is not specified it is the first step to be taken. The data processing plays a crucial role in detecting duplicate attributes and also missing data. The data processing model is basically used to validate and convert the matrix form of input-output data of the black-box predictive model being validated into a form suitable for ranking.

Variable Ranking module

The variable ranking module consists of three input ranking algorithms: Random forest algorithm, support vector machine and logistic regression model.

Random forest

Random forest provides an ensemble model by combining decision trees learned using large samples of input data. Gilles Louppe, Louis Wehenkel, Antonio Sutera, and Pierre Geurts et al. (2013) proposed

that Random forest is particularly useful for determining variable importance. One way is using depth of attributes in decision tree to measure their importance. The higher the attributes are present in the tree more likely they are to affect the major portion of data used to learn the tree model. Second methodology is mean decrease in accuracy variable importance estimation where the attribute values are randomly permuted and accuracy is estimated for the tree. This is performed for all the trees in the forest and performance change is averaged across all the trees. The change in the accuracy would be high if the attribute is highly significant.

Support Vector Machine

Support Vector Machine is another supervised machine learning algorithm used for both classification and regression analysis. The algorithm provides variable importance using any one of the three methods: filter, embedded and wrapper method. Firstly, filter method assess the relevance of the variables by only looking at its intrinsic properties and not taking into account information provided by classification algorithm. In most of the cases the variable relevance score is calculated and low scoring variables are removed and high scoring variables are retained. Secondly, embedded method have feature selection method such as regularization method which is also called as penalization method that introduces additional constraints into optimization of a predictive algorithm that bias the model toward lesser complexity or fewer coefficients. Thirdly, wrapper method where Guyon I, Weston J, Barnhill S, Vapnik V et al.(2002) proposed one of the most popular wrapper approaches for variable selection in SVM. The method is known as SVM-Recursive Feature Elimination (SVM-RFE).The final output of this algorithm is a ranked list with variables according to their relevance.

Logistic Regression

Logistic regression is a classification algorithm used to assign observations to discrete set of classes. The variable importance in logistic regression is assessed using recursive feature elimination method which is a method that recursively removes attributes and building a model from those attributes that remain. It uses model accuracy to identify which attributes contribute the most to predicting the target attribute. The attribute that are eliminated last are ranked higher than the attributes that are eliminated in earlier stages.

GRAPHICAL MODULE

The output generated by the ranking algorithms are used as input to the graphing module. It is further used to provide a graph which shows the attribute ranking with respect to each ranking methodology which is the final output of the proposed model which shows the variable importance provided by each of the algorithm based on the input-output dataset provided by predictive model and an aggregated graph showing dependences across all methodologies.

Experiment and Result Analysis

Figure 2 to Figure 4 shows the graph generated from Random forest, Support Vector Machine and Logistic regression model which shows the dependence of the ranking methodologies on that respective input attribute. Figure 5 is a graph that shows the aggregated dependence of all the ranking methodologies on the input variables showing dependence on attributes which can be used to predict the fairness of any model. Here we have taken the input dataset from propublica datasets. The dataset is pertaining to crime information in USA. The proposed system is used to check whether a prediction model for determining the crime to be committed by a person in future is biased. The proposed system is provided with the input dataset containing the input and output data provided by prediction model and graphs are obtained for each ranking methodology and lastly an aggregated graph is drawn from the three graphs obtained from each of the algorithm which shows the attribute dependence across all the methodologies as output. In Figure 2, the graph provided by Random forest shows the attribute “No of Priors” meaning number of crimes committed by a person

before is highest ranked among other attributes but other attributes such as "African American", "Female" are also given higher importance than other attributes and in both Figure 3 and Figure 4 these attributes (Female and African American) are again ranked higher than other attributes. The final graph (Figure 5) shows the combined attribute ranking which shows that the prediction is highly based on attribute "No of Priors" but also given more importance to race and gender. This shows that the model makes unfair prediction and is dependent on the race and gender of a person while doing predictions along with the number of crimes committed before. The proposed system helps the analyser to find that the predictive model provides biased predictions and to tune the model so that the future predictions are less biased.

CONCLUSION

The following conclusion can be drawn from the present study:

- The proposed system helps in understanding how variable importance varies across different methodologies.
- The proposed system helps to determine whether a predictive model is biased or not.
- The proposed system also provides the users an easy to understand method by providing output in graphical form.

REFERENCES

[1] Andrea Romei and Salvatore Ruggieri et al. (2014), A multidisciplinary survey on discrimination analysis. The Knowledge Engineering Review, 29(05):582-638,

[2] Dino Pedreshi, Salvatore Ruggieri, and Franco Turini et al. (2008), Discrimination-aware data mining. In Proceedings of the 14th ACM SIGKDD international conference on Knowledge discovery and data mining, pages 560-568. ACM.

[3] Faisal Kamiran and Toon Calders et al. (2009), Classifying without discriminating. In Computer, Control and Communication, 2009. IC4 2009. 2nd International Conference on, pages 1-6. IEEE.

[4] Gilles Louppe, Louis Wehenkel, Antonio Sutera, and Pierre Geurts et al. (2013), Understanding variable importances in forests of randomized trees. In Advances in Neural Information Processing Systems, pages 431-439.

[5] Guyon I, Weston J, Barnhill S, Vapnik V et al. (2002), Gene selection for cancer classification using support vector machines. Mach Learn. 2002; 46:389–422.

[6] Julius A. Adebayo et al. (2016), FairML: ToolBox for Diagnosing Bias in Predictive Modeling.

[7]Rich Zemel, Yu Wu, Kevin Swersky, Toni Pitassi, and Cynthia Dwork et al. (2013), Learning fair representations. In Proceedings of the 30th International Conference on Machine Learning (ICML-13), pages 325-333.

[8] Sorelle Friedler, Carlos Scheidegger, and Suresh Venkatasubramanian et al. (2014), Certifying and removing disparate impact. arXiv preprint arXiv:1412.3756.

[9] Toon Calders and Sicco Verwer et al. (2010), Three naive bayes approaches for discriminationfree classification. Data Mining and Knowledge Discovery, 21(2):277-292.

[10] Toshihiro Kamishima, Shotaro Akaho, and Jun Sakuma et al. (2011), Fairness-aware learning through regularization approach. In Data Mining Workshops (ICDMW), 2011 IEEE 11th International Conference on, pages 643-650. IEEE.

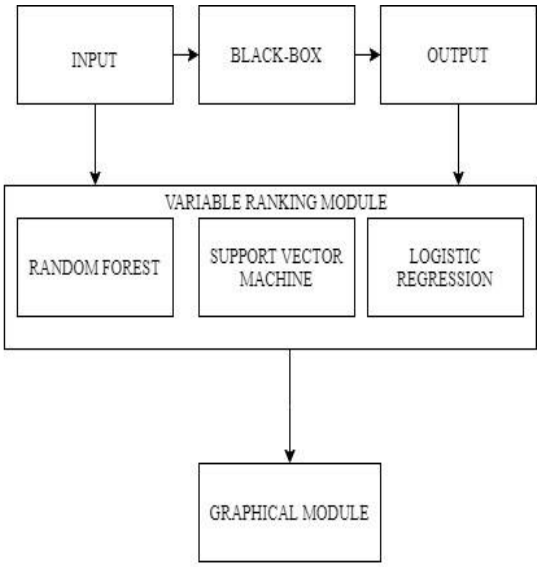

Fig1. The proposed FairML model

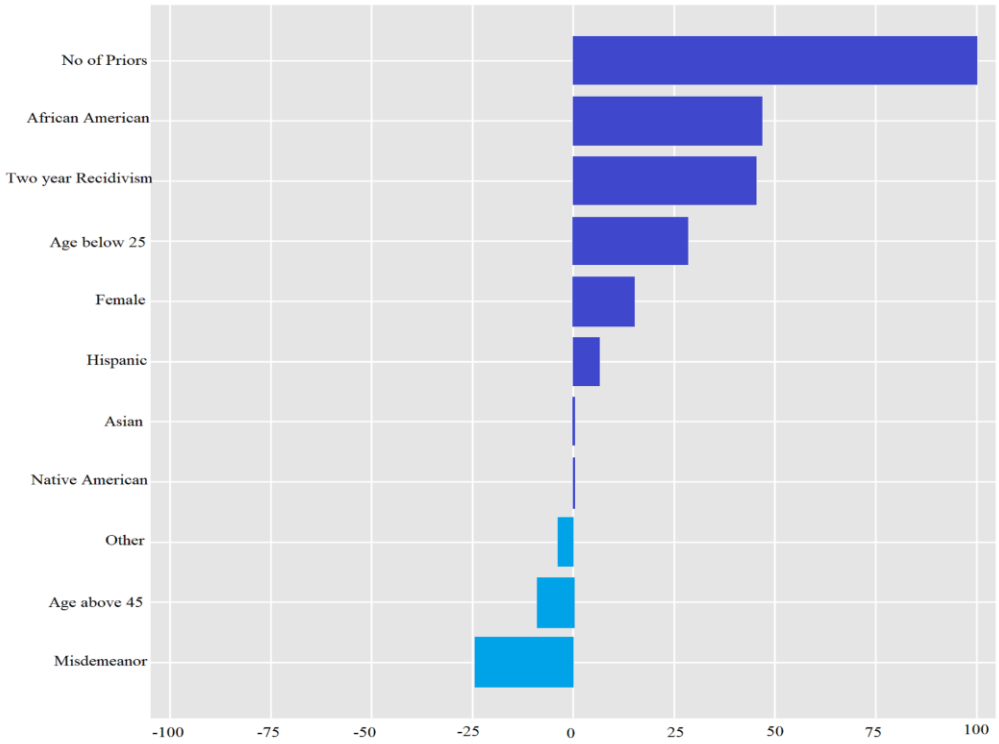

Fig 2.Attribute Ranking using Random Forest

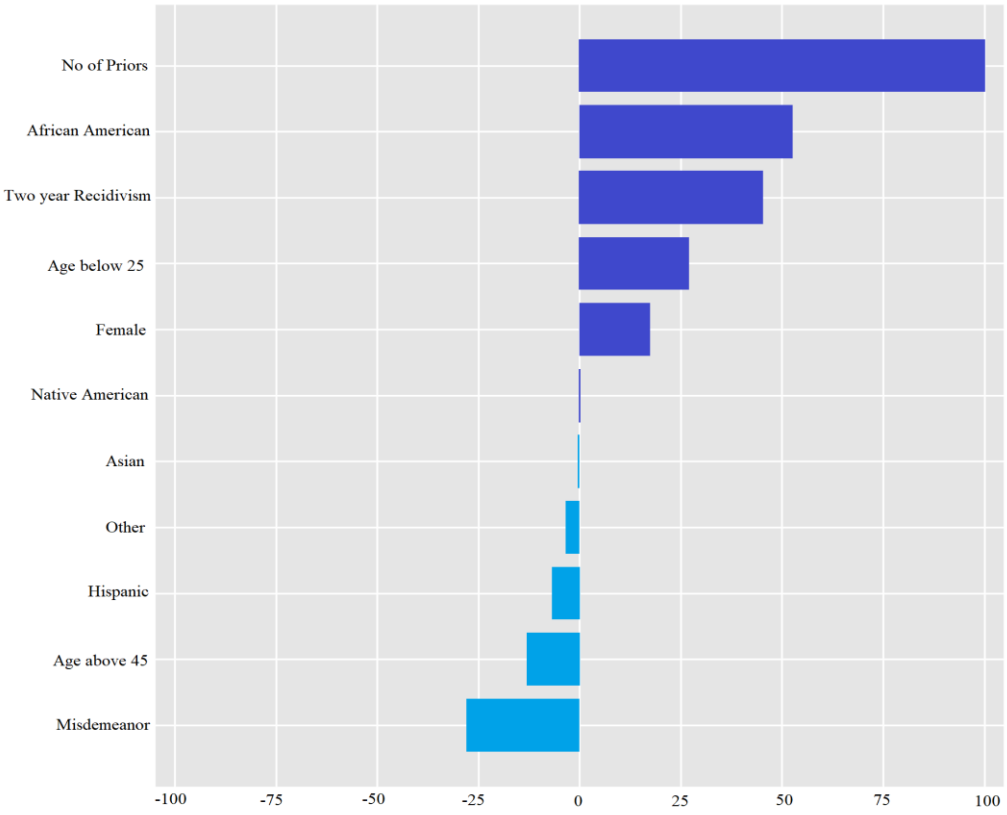

Fig 3.Attribute Ranking using Support Vector Machine

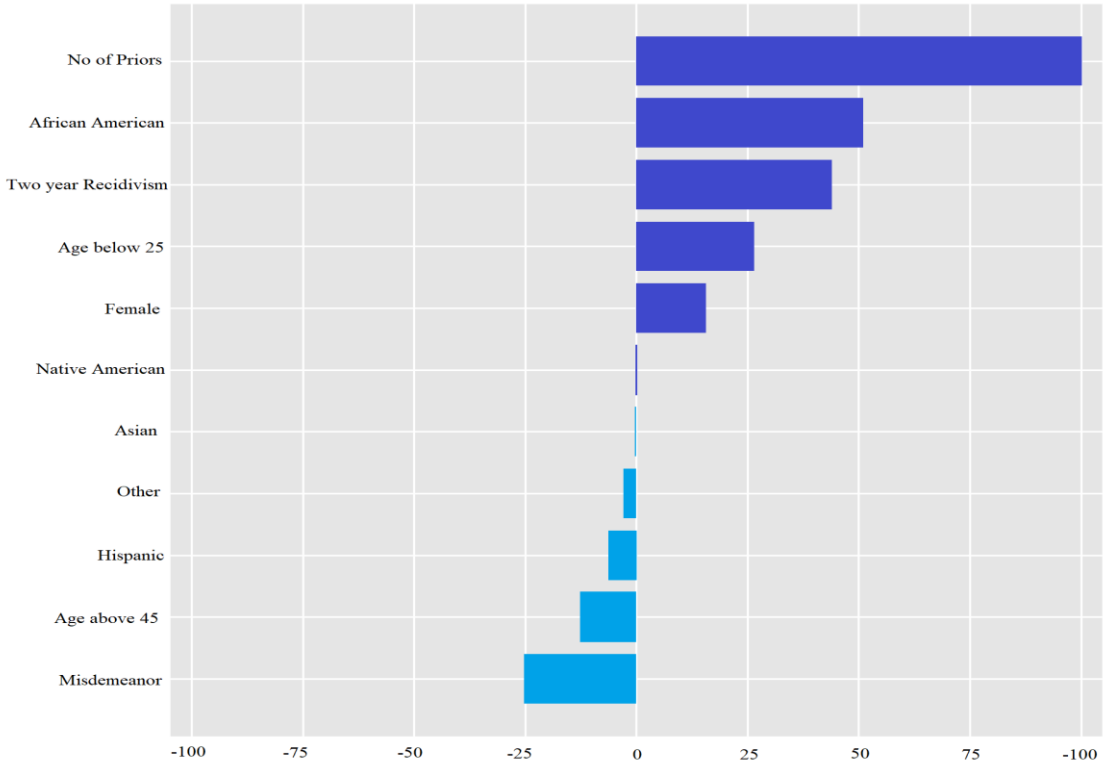

Fig 4. Attribute Ranking using Logistic Regression

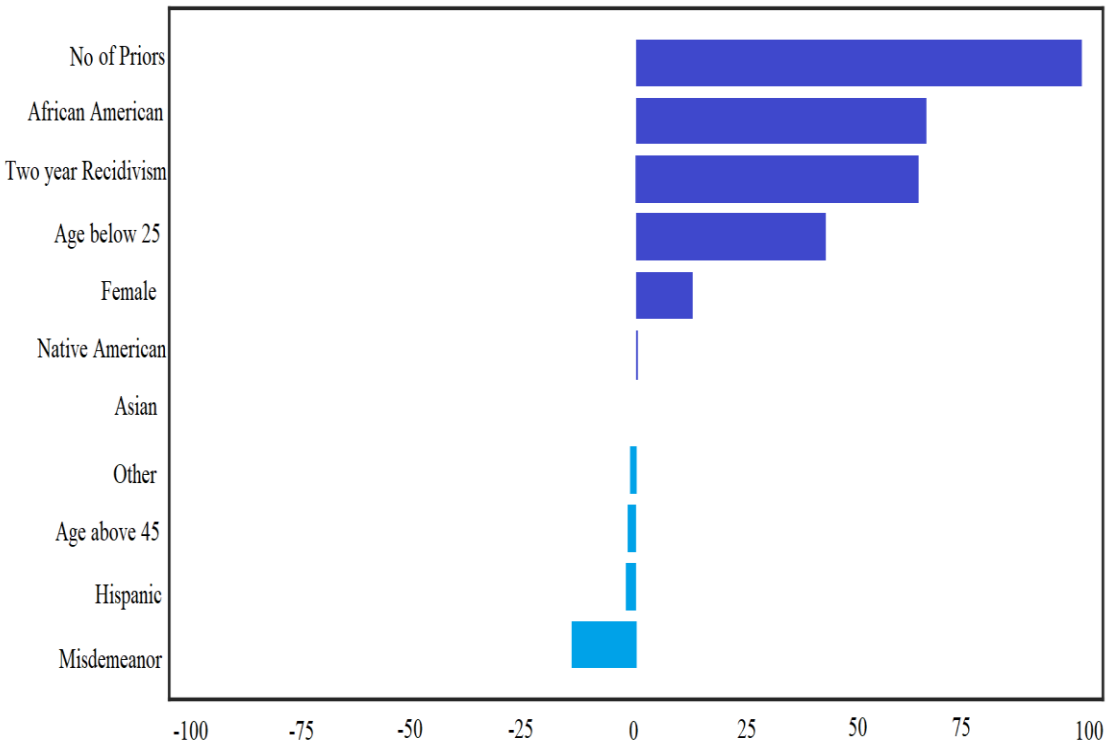

Fig 5. The graph showing attribute ranking across all methodologies

9th International Engineering Symposium - IES 2020
March 3-5, 2020, Kumamoto University, Japan

SECURED CUSTOMIZED MONITORING SYSTEM TO KEEP TRACK OF TRADED DATA & ENHANCING EFFICIENCY OF CLOUD APPLICATIONS

Harish Kunder[1], Anitha Lakshmi T N[2] and **Manjunath Kotari[3]**

1 *Senior assistant Professor, Department of Computer Science &Engineering, Alva's Institute of Engineering and Technology, Moodbidri 574 225, India.*
email: harishkunder@aiet.org.in
2 *Undergraduate Student, Department of Computer Science &Engineering, Alva's Institute of Engineering and Technology, Moodbidri 574 225, India.*
email:anithalakshmi1012@gmail.com
3 *Professor & Head, Department of Computer Science & Engineering, Alva's Institute of Engineering and Technology, Moodbidri 574 225, India.*
email:aietcse08@gmail.com

ABSTRACT: The facility of cloud computing presents significant benefit to the users. The cloud infrastructure environment helps the user of the system to store and retrieve massive amounts of information. However, monitoring may be required to manage the cloud resources among users securely. For an instance, the data owner creates a data file and places in cloud service provider. The secure customized monitoring mechanism may be required to keep track of these traded data file. In the field of Cloud Computation many open monitoring tools do exist but secured customized monitoring tools frameworks are not available from which owner of huge data can feel comfortable for confidentiality and data leakage.Implemented framework for security mechanism may be made application-specific rather than making it very general.Monitored parameters of secure customized monitoring tool can be used for fault predictions and avoidance in mission critical applications.

Keywords*: cloud computing, security, traded data*

INTRODUCTION

The facility of cloud computing presents significant benefit to the users. The cloud infrastructure environment helps the user of the system to store and retrieve massive amounts of information. This would enable the users of the distributed systems to avail the services provided on cloud environments. However, monitoring may be required to manage the cloud resources among users securely. The monitoring of cloud applications may enhance efficiency of the entire cloud applications. In this regard, the secure customized monitoring may help the cloud computing environments to get the accountability of cloud resources. For an instance, the data owner creates a data file and places in cloud service provider.

The secure customized monitoring mechanism may be required to keep track of these traded data file. The customized monitoring allows the users to independently audit dealing of their data files by cloud service provider. The secure customized monitoring framework for cloud provides the apparent, fine- grained data tracking for data owners. The security may be increased by encrypting the log file of monitored data file. This enables the data owner to offer additional security against unintentional data

leakage. In this way, the secure customized monitoring framework may help the data owner to maintain the accountability of created data.
To provide deliberate functionalities and services continuously with suitable level of quality; distributed systems need to be monitored constantly.
But the monitoring system may be overtaken by unauthorized user. In such cases, if monitoring process is restricted for the purpose of protection; it may lead to severe limitations on the capacity of the adaptive system. Achieving adaptation with minimal impact on security mechanism is a challenging task

- The framework of security mechanisms deals with the general monitoring mechanisms of various monitoring tools and its security issues in the context of adaptive distributed systems
- Secure customized monitoring tool can be further improved from the security perspective, so that it can be used in implementing applications on cloud.
- Implemented framework for security mechanism may be made application-specific rather than making it very general.
- Monitored parameters of secure customized monitoring tool can be used for fault predictions and avoidance in mission critical applications

Many web servers nowadays use TLS by default; our secure customized monitoring tool can be combined with Transport Layer Security (TLS) for website monitoring. So, finally the secure customized monitoring may be used in content distribution networks (CDNs) to protect the contents of the websites.

LITERATURE SURVEY

In Cloud computing, the main problems are related to data security, backups, network traffic, file system, and security of host as discussed by Neha Jain and Gurpreet Kaur (2014) and cryptography can resolve these issues to some extents. For secure communication between the host domain and the guest domain, or from hosts to management systems, encryption technologies, such as Secure HTTP (HTTPS), encrypted Virtual Private Networks (VPNs), Transport Layer Security (TLS), Secure Shell (SSH), and so on should be used. Ronald L. Krutz and Russell Dean Vines (2012) had mentioned that Encryption will help prevent such exploits as man-in-the-middle (MITM), spoofed attacks, and session hijacking. AL.Jeeva, Dr.V.Palanisamy And K.Kanagaram (2012) described 'Symmetric-key algorithms' as the algorithms which use the same key for both encryption and decryption. Hence the key is kept secret. Symmetric algorithms have the advantage of not consuming too much of computing power and it works with high speed in encryption. Symmetric-key algorithms are divided into two types: Block cipher and Stream cipher. In block cipher input is taken as a block of plaintext of fixed size depending on the type of a symmetric encryption algorithm, key of fixed size is applied on to block of plain text and then the output block of the same size as the block of plaintext is obtained. In Case of stream cipher one bit at a time is encrypted.
The Data Encryption Standard (DES) is a symmetric- key block cipher published as FIPS-46 in the Federal Register in January 1977 by the National Institute of Standards and Technology (NIST). At the encryption site, DES takes a 64-bit plaintext and creates a 64-bit cipher text, at the decryption site, it takes a 64-bit cipher text and creates a 64-bit plaintext, and same 56-bit cipher key is used for both encryption and decryption. The encryption process is made of two permutations (P-boxes), which we call initial and final permutation, and sixteen Feistel rounds. Each round uses a different 48-bit round key generated from the cipher key according to a predefined algorithm.
Advanced Encryption Standard is a symmetric- key block cipher published as FIPS-197 in the Federal Register in December 2001 by the National Institute of Standards and Technology (NIST). AES is a non-Feistel cipher. AES encrypts data with block size of 128-bits. It uses 10, 12, or fourteen rounds. Depending on the number of rounds, the

key size may be 128, 192, or 256 bits. AES operates on a 4×4 column major order matrix of bytes, known as the state.
A quite simple way of increasing, the key size of DES is to use Triple DES, to guard it against attacks without the need to design a completely new block cipher algorithm. DES itself can be adapted and reused in a more secure scheme. Many former DES users can use Triple DES (TDES) which was described and analyzed by one of DES's patentees. It involves applying DES three times with two (2TDES) or three (3TDES) different keys as shown in figure 2. TDES is quite slow but regarded as adequately secure.
G. Devi and M. Pramod Kumar (2012) have discussed about the Blowfish algorithm which is a symmetric block cipher algorithm. It uses the same secret key to both encryption and decryption of messages. The block size for Blowfish is 64 bits; messages that aren't a multiple of 64-bits in size have to be padded. It uses a variable –length key, from 32 bits to 448 bits. It is appropriate for applications where the key is not changed frequently. It is considerably faster than most encryption algorithms when executed in 32-bit microprocessors with huge data caches. Data encryption happens via a 16-round Feistel network.
Asymmetric-key algorithms are those algorithms that use different keys for encryption and decryption. The two keys are: Private Key and Public Key. The Public key is used by the sender for encryption and the private key is used for decryption of data by the receiver. In cloud computing asymmetric-key algorithms are used to generate keys for encryption. Maha TEBAA, Saïd EL HAJJI and Abdellatif EL GHAZI (2012) introduced Homomorphic Encryption Cloud in which consumer encrypts its data before sending to the Cloud provider, But, each time he has to work on that will have to decrypt that data. The consumer will require giving the private key to the server to decrypt the data before to perform the calculations required, which might influence the confidentiality of data stored in the Cloud. Homomorphic Encryption systems are needed to perform operations on encrypted data without decryption (without knowing the private key); only the consumer will have the secret key. When we decrypt the result of any operation, it is the same as if we had performed the calculation on the plaintext (or original data). The Homomorphic encryption is distinguishing, according to the operations that are performed on raw data. RSA cryptosystem realizes the properties of the multiplicative Homomorphic encryption . Ronald Rivest, Adi Shamir and Leonard Adleman have invented the RSA algorithm and named after its inventors. RSA uses modular exponential for encryption and decryption. RSA uses two exponents, a and b, where a is public and b is private.
In 1976, Whitfield Diffie and Martin Hellman introduced a key exchange protocol with the use of the discrete logarithm problem. In this protocol sender and receiver will set up a secret key to their symmetric key system, using an insecure channel.

RESEARCH GAP IDENTIFY

In the field of Cloud Computation many open monitoring tools do exist, but secured customized monitoring tools frameworks are not available from which owner of huge data can feel comfortable for confidentiality and data leakage.

Most of the authors discussed about Amazon cloud is a good solution, however it is restricted to only AWS products. So, need of customized monitoring tool in cloud application is required.

OBJECTIVES OF THE PROPOSED WORK WITH JUSTIFICATION

Monitoring system may be required to manage the cloud resources among users securely. The monitoring of cloud applications may enhance efficiency of the entire cloud environments. In this regard, the secure customized monitoring system requires the cloud computing environments to get the accountability of cloud resources. The clients

or users of the cloud may access the data file securely but, cloud service provider may sell these data to the other users of the cloud without maintaining any accountability. In this case, it is very difficult for data owner to get the accountability of traded data file. In such cases, the data owner needs to keep track of data file which was created and placed in cloud service provider earlier.

Objectives of the Proposed Research

- To develop Secured customized monitoring system by using end to end encryption technique
- To enhances the efficiency of the cloud transactions using Unicode for storage of data
- To keep track of the traded data by creating log files for each transaction.
- PCMONS and RMCM tools are available to monitor clouds but configuration of monitoring need to be done manually. The manual configuration leads to security breaches such as scalability & automaticity

METHODOLOGY

The following method is planned for customized cloud security and privacy which are:

1. Access control method which is an application of Role Based Access control (RBAC).
2. Policy integration method which is a dynamic policy control mechanism.
3. Identity management method which prevents the unauthorized secondary usage of data.
4. User control method which solves the problem of cloud users losing control of their data.
5. Implementation of end to End encryption by TLS protocol.
6. Implementation of log files for traded data to keep track of data.

In recent years network security has become an important issue. Encryption has come up as a solution, and plays an important role in information security system. Many techniques are needed to protect the shared data. The present work focus on cryptography to secure the data while transmitting in the network. Firstly the data which is to be transmitted from sender to receiver in the network must be encrypted using the encryption algorithm in cryptography. Secondly, by using decryption technique the receiver can view the original data.

Cloud computing has three main aspects: SaaS (software as a service), PaaS (platform as a service) and IaaS (infrastructure as a service). As shown in Figure 2, SaaS provider hosts and manages a given application in their data center and makes it available to multiple users over the Web. Oracles CRM on Demand, Salesforce.comare some of the well-known SaaS examples.

It is an evolution of traditional hosting that does not require any long term commitment and allows users to provision resources on demand. Amazon Web Services Elastic Compute Cloud (EC2) and Secure Storage Service (S3) are examples of IaaS services. Cloud computing faces a lot of different challenges. Security is one of the key challenges, and has become the key of popularization cloud computing and restrictive factor. In recent years, the cloud services appear many security accidents. For example, in March 2009, Google leaked a large number of documents. Microsoft Azure platform stopped working for about 22 hours. In April 2011, Amazon's EC2 service disruptions, influences the service of Quora, Reddit etc. When happened, these security problems caused a great loss, even devastating blow. Therefore, to make the enterprise and the organization accept cloud computing services, it is necessary to solve the security problems.

There are some potential threats to cloud computing and their remedies are discussed below

- Changes to business model

Mitigation: A reliable end-to-end encryption and appropriate trust management scheme can simplify such threat to some extent.

- Abusive use of cloud computing
  Mitigation: Initial registration should be through proper validation and through stronger authentication. In addition to this, the user's network traffic should be monitored.
- Insecure interfaces and API
  Mitigation: Can be avoided by using proper security model for cloud provider's interface and ensuring strong authentication and access control mechanism with encrypted transmission.
- Malicious insiders
  Mitigation: To avoid this risk more transparency is required in security and management process including compliance reporting and breach notification.
- Shared technology issues/multi-tenancy nature
  Mitigation: Implementation of SLA for patching, strong authentication, and access control to administrative tasks are some of the solutions.
- Data loss and leakage
  Mitigation: Security of API, data integrity, secure storage for used keys, data back up and retention policies.
- Service hijacking
  Mitigation: Security policies, strong authentication and activity monitoring
- Risk profiling
  Mitigation: Cloud provider should disclose partial infrastructure details, logs, and data. In addition to this, there should be a monitoring and alerting system.
- Identity theft
  Mitigation: Using strong authentication mechanisms.

There are some potential attacks on cloud computing and their remedies are discussed below

- Zombie attack
  Mitigation: Better authentication and authorization and IDS/IPS can provide protection against such attack.
- Service injection attack
  Mitigation: Service integrity checking module should be implemented. Strong isolation between VMs may disable the attacker from injecting malicious code in the neighbor's VM.
- Attacks on virtualization
  Mitigation: By monitoring through IDS (Instruction Detection System)/IPS (Intrusion Prevention System) and by implementing firewall.
- Man in the middle attack
  Mitigation: Proper SSL configuration and data communication tests between authorized parties.
- Metadata spoofing attack
  Mitigation: Information about services and applications should be kept in encrypted form. Strong authentication should be enforced for accessing such critical information.
- Back door channel attack
  Mitigation: Better isolation and authentication between VMs can provide protection against such attacks.

Security mechanism has been employed in order to protect the traded data.data need to encrypt the information in RSA algorithm or other equivalent algorithm while sending. In proposed research work, we have used RSA 1024-bit encryption procedure. When the intruder tries to access this information through existing monitoring tool, only an encrypted message is displayed on the screen of the intruder. The code snippet shown below explains about the generation of public key and private keys of RSA algorithm.

```
RSA_Algorithm()
{
// Declaration of bit length of RSA using bit_length = 1024
// Use of SecureRandom() function for getting random number
// Select any 2 large prime using function BigInteger(bit_length / 2, 100, random)
// Compute n by using n = p.multiply(q)
//Calculate z ; z=(p.subtract(BigInteger.ONE)).multiply(q.subtract(BigInteger.ONE));
// Generation of key pairs, private and public keys
en_key = new BigInteger("3");
while (msg.gcd(en_key).intValue() > 1)
{
en_key = en_key.add(new BigInteger("2"));
}
dec_key = en_key.modInverse(z);
}
```

The RSA algorithm has been used mainly for two purposes, namely; it is a factor-based algorithm and its computing power increases constantly. RSA-1024 is considered as safe enough for protecting most of the vital information in the web. However, unencrypted messages take comparatively less processing time. On the other hand these unencrypted messages are not confidential while transmission. During the experimental process, Public Key Infrastructure (PKI) has been adopted between the users with pairs of RSA 1024 bits asymmetric keys. To enable secure communication between the involved parties during the monitoring, each party must receive a list of the public keys of the other users that they will communicate with. In that case, each user receives the other user's public key for encryption process.
The PKI needs to perform in order to provide trust and security to electronic communication. The following functions are involved in working of PKI based key management.

- Generating public key and private pairs for creating and authenticating digital signatures.
- Providing authentication to control access to the private key.
- Creating and issuing certificates to authenticate users.
- Registering new users to authenticate them.
- Maintaining history of keys for future references.
- Revoking certificates that are not valid.
- Updating and recovering keys in case of key compromise.

Cryptosystems techniques are proven safe. In this regard, the only analysis can be made to outline how to decrypt a message without knowing the decryption key. Brute force methods are very simple, but lengthy to crack a message for attacker. However, attackers need not to crack entire encryption scheme to get portion of the message. In spite of several attempts, no one has been succeeded with 1024 bits of RSA algorithm. Such a resistance to attack makes RSA secure in practice. In RSA, it has been proved that, it is very difficult for factorizing large prime numbers. Suppose, if large prime numbers p and q are having 100 digit numbers, then resulting *n* would be approximately 200 digits. The factorization of above case would take far too long time for breaking the code. Similarly, methods for determination of *d* are also difficult. Factorization of algorithm is still an age-old mathematical problem, contributed by Fermat and Legendre.

An RSA algorithm is used instead of ECC (Eliptic Curve Cryptography) because of following reasons

- RSA uses a Public key operation (encryption/sig verification) and are still faster than for ECC with same strength. However public-key operations are rarely a bottleneck and which has about 8000 ECDSA (Eliptic Curve Digital Signature Standard) verifications per second vs 20000 RSA verifications per second.
- An additional interoperability issue is that elliptic-curve operations can be made over curves of distinct types. NIST has defined 15 standard curves. However, in practice, many implementations only support two of them, P-256 and P-384, because that's what is recommended by NSA(National Security Agency).
- RSA is that its mathematics is somewhat simpler than those involved for ECC.

```
// Encryption of given message
 public BigInteger encrypt(BigInteger msg)
{
   return msg.modPow(en_key, n);
 }

// Decryption of given message
   public BigInteger decrypt(BigInteger msg)
{
   return msg.modPow(dec_key, n);
 }
```

Fig.1 Pseudo code of RSA encryption and decryption

The RSA has been used widely in most of the application for following reasons

- RSA provides privilege of key revocation
- RSA provides distribution of new key during revocation of existing key
- RSA supports spreading the revocation
- RSA helps recovery from leaked key.

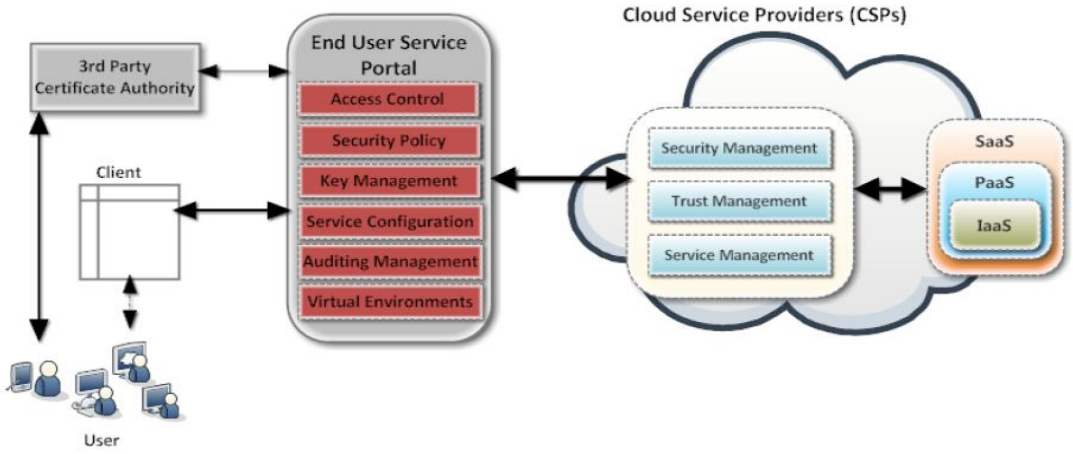

Fig.2 Security framework to keep track of traded data

The customized monitoring tool decrypts the encrypted packets of Internet Key Exchange version 2 only. All other packets like Internet Key Exchange version 1 and Encapsulation Security Payload are decrypted with the help of ISAKMP (Internet Security Association Key Management Protocol) protocol. The following fields of the ISAKMP protocol have been used for encryption and decryption of packets. Initially length of 16 hex characters has been created for Senders Security Protocol Index (SPI). Similarly, length of 16 hex characters has been created for Receivers SPI. The IKEv2 packets of sender to receiver have been encrypted / decrypted by using the key en key. Similarly, the IKEv2 packets of receiver to sender have been encrypted / decrypted by using the key dec_key. The Integrity Checksum for receiver to sender has been calculated by the key en_key. Similarly, the Integrity Checksum for sender to receiver has been calculated by the key dec_key.

Based on all the gaps of Literature survey this security model is constructed. User can be certificated by the 3rd party certificate authority, then can be issued token for service by End User Service Portal. After joining service portal, user can purchase and use cloud services which are provided by single service provider. End User Service Portal, which is composed access control, security policy, key management, service configuration, auditing management, and virtual environments, provides secure access control using Virtual Private Network (VPN) and cloud service managing and configuration.
The proposed framework overcomes the drawback of existing systems like manual configuration, AWS product restriction, and scalability & Automaticity issues.

RESULT

Customized standard algorithm can be developed to monitor owner's data being traded off from Service Provider and following outcomes are expected

- Secured customized monitoring system with encrypted data with the help of TLS
- Enhancement of the efficiency of the cloud transactions using Unicode for the storage of the data
- Evidence for keeping the track of traded data using the Log file

REFERENCES

A Freier, P. Karlton, and P. Kocher, \The SSL Protocol Version 3.0", March 4 1996, Internet Draft, work in progress. [Koc96] P. Kocher, personal communication, 1996
A Giannakou, L. Rilling, J. L. Pazat, and C. Morin, "Al-safe: A secure self adaptable application-level firewall for iaas clouds," in 2016 IEEE International Conference on Cloud Computing Technology and Science (CloudCom), pp. 383–390, Dec 2016
AL.Jeeva, Dr.V.Palanisamy And K.Kanagaram "Comparative Analysis Of Performance Efficiency And Security Measures Of Some Encryption Algorithms" International Journal Of Engineering Research And Applications (IJERA) ISSN: 2248-9622 Vol. 2, Issue 3, May-Jun 2012, Pp.3033-3037.
Amazon CloudWatch https://aws.amazon.com/cloudwatch/ Accessed 2018
FrédéricDesprez,EddyCaron,LuisRodero-Merino,Adrian Muresan,1820Auto-scaling,load balancing and monitoring in commercial and open-source clouds,in:CloudComputing:Methodology,System and Applications,CRC Press,2011
G. Devi , M. Pramod Kumar "Cloud Computing: A CRM Service Based on a Separate Encryption and Decryption using Blowfish algorithm" International Journal Of Computer Trends And Technology Volume 3 Issue 4, ISSN: 2231-2803,2012, pp. 592-596.
Maha TEBAA, Saïd EL HAJJI, Abdellatif EL GHAZI "Homomorphic Encryption Applied to the Cloud Computing Security", World Congress on Engineering Volume I, July 4 - 6, 2012, London, U.K. ISBN: 978-988-19251-3-8, ISSN: 2078-0958 (Print); ISSN: 2078- 0966 (Online).
Muhammad Faheem Mushtaq1 , Urooj Akram1 , Irfan Khan2 , SundasNaqeeb Khan1 , Asim Shahzad1 ,Arif Ullah1, "Cloud Computing Environment and Security Challenges", (IJACSA) International Journal of Advanced Computer Science and Applications, Vol. 8, No. 10, 2017
Neha Jain and Gurpreet Kaur 'Implementing DES Algorithm in Cloud for Data Security" VSRD International Journal of CS & IT Vol. 2 Issue 4, 2014, pp. 316-321.
Ronald L. Krutz and Russell Dean Vines, Cloud Security: A Comprehensive Guide to Secure Cloud Computing Wiley Publishing, Inc. Indianapolis, Indiana 2012.

CIVIL ENGINEERING, ENVIRONMENT & RELATED FIELDS

9th International Engineering Symposium - IES 2020
March 3-5, 2020, Kumamoto University, Japan

Effect of gravity column in seismic response of buildings with buckling restrained braces

Archana Rajan [1] and Katta Venkatramana [2]

1 *Former Mtech Student (Structural Engineering), Department of Civil Engineering, National Institute of Technology Karnataka, Surathkal, Mangalore 575025, India. email:archanarajan4@gmail.com*
2 *Professor, Department of Civil Engineering, National Institute of Technology Karnataka, Surathkal, Mangalore 575025, India. email:ven.nitk@gmail.com*

ABSTRACT: Buckling restrained braces (BRBs) are energy dissipating devices which are provided in steel frames to reduce the earthquake impact analysis damage. These braces consist of a slender core continuously supported over restraining members to resist axial buckling due to compression. These braces offer robust cyclic performance and significant cost saving compared to conventional bracing system which has asymmetrical hysteretic behavior in tension and compression. But over years of study it is found that they have certain shortcomings like large residual drift and high storey shear . Several researches have been carried out to find solution to the above problems, especially to control the residual drift which if exceeded by a particular limit, will require the complete demolition of the building. It is known that continuous stiffness can prevent or reduce the probability of buildings to develop drift concentrations or weak story mechanisms. If gravity columns are purposely made continuous and an adequate stiffness is assigned to the gravity columns, the performance of the building could be enhanced considerably. The present work explains the general behavior of buckling restrained braced frames by the analytical study carried out to study the effect of gravity column in BRBFs by varying the support condition of gravity column.

Keywords*: buckling restrained braces, residual drift, storey shear, gravity column.*

INTRODUCTION

Analysing the experiences from the past earthquakes and the structural damages give us enough reasons to develop earthquake resistant designs. Dissipation of seismic energy and inelastic performance can be achieved through various systems, the most common being Moment Resisting Frames (MRF) and Concentrically Braced Frames (CBF). MRFs develop ductility through flexure yielding of beams and shear yielding of column panel zones, but it has low elastic stiffness. These are susceptible to large displacements during severe earthquake motions, and special attention is required to limit damage and avoid problems associated with P- Δ effects. Compared to MRFs, CBFs are stiff and economical structural systems whose response is governed by inelastic deformation of braces. But performance of these frames in past earthquakes raises concerns about the energy dissipating and deformation capacity of this class of structures, especially the buckling of compression brace. The disadvantages of the CBF system can be overcome if the brace can yield during both tension and compression without buckling. A braced frame that incorporates this type of brace, i.e., buckling restrained brace (BRB).

The buckling-restrained braced frame system (BRBF) is similar to the special concentrically braced frame system in that seismic accelerations are resisted by a vertical truss composed of building-frame members and diagonal braces; the difference lies in the design and behaviour of the braces. Buckling-restrained braces are designed

to permit ductile yielding in both compression and tension. They are characterized by a full, stable hysteretic loop that is balanced between compression and tension, and by relatively low post-yield stiffness. Therefore, BRBF is a special class of CBF that precludes brace buckling.

CONCEPT OF BRB

Most of the BRBs developed to date are proprietary, but the concepts are similar.The brace is composed of a ductile steel core, which is designed to yield during both tension and compression Uang and Nakashima (2004). To preclude global buckling in compression, the steel core is first placed inside a steel casing (usually a hollow structure shape) before the casing is filled with mortar or concrete.Prior to casting mortar, an unbonding material or a very small air gap between the steel core and mortar is provided to minimize, or eliminate if possible, the transfer of axial force from steel core to mortar and the hollow structural section (HSS). The Poisson effect also causes the steel core to expand under compression; this requires that a small gap be provided between the steel core and mortar.

COMPONENTS OF BRB

Figure 1 shows an example of a BRB, which is composed of the following five components

1. Restrained yielding segment:

This steel segment can be rectangular or cruciform in cross section. Although it is common that a steel plate be surrounded in a casing, more than one plate can be used, if desired. Because this segment is designed to yield under cyclic loading, mild steel that exhibits high ductility is desirable. Alternatively, high-strength low-alloy steel has also been used. Also desirable are steel materials with a predictable yield strength with small variations. This latter property is essential for reliable capacity design of BRBFs.

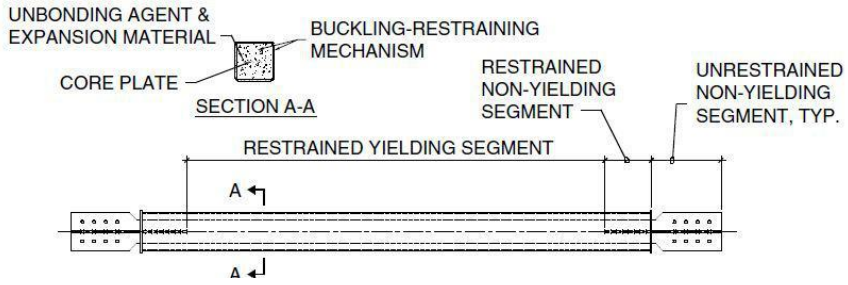

Fig 1. Components of buckling-restrained brace. Uang and Nakashima (2004)

2. Restrained non yielding segment:

This segment, which is surrounded by the casing and mortar, is usually an ex-tension of the restrained yielding segment but with an enlarged area to ensure elastic response. This can be achieved by widening the restrained yielding segment. (The transition in width needs to be smooth to avoid stress concentration.) It is also common that stiffeners be welded to increase the area in this region.

3. Unrestrained non-yielding segment:

This segment is usually an extension of the restrained non-yielding segment, except that it projects from the casing and mortar for connection to the frame. This segment is also called the steel core projection. It is common that this segment be designed as a bolted connection for field erection, but other connection de-signs such as a pin connection or a welded connection are also possible. Design considerations of this segment include (i) construction tolerance for ease of field erection and to facilitate the removal and (ii) local buckling prevention.

4. Unbonding agent and expansion material:

Inert material that can effectively minimize or eliminate the transfer of shear force between the restrained steel segment and mortar can be used; materials like rubber, polyethylene, silicon grease or mastic tape have been reported. The restrained yielding segment is expected to experience small-amplitude buckling in higher modes due to the presence of the restraining mechanism. The gap needs to be sufficiently large to allow for the expansion of the yielding steel core in compression. Otherwise the friction that is created by the bearing action between the expanding yielding steel and mortar would force the buckling restraining mechanism to carry some axial load. On the other hand, if the gap is too large the buckling amplitude and the associated curvature of the buckled steel-yielding segment can be large, which would reduce the low-cycle fatigue life of the yielding segment. In determining the design gap, the Poisson ratio in the elastic (0.3) and yielding (0.5) range needs to be considered. The design gap is also a function of the maximum design strain.

If a transition in width between the restrained yielding and non-yielding segments is used, a longitudinal gap in front of the widened non-yielding segment also needs to be provided to avoid direct bearing between the steel segment and the mortar. Such bearing action would, unexpectedly, increase the compressive capacity of the brace beyond the expected design strength, which is not desirable from the viewpoint of capacity design and also increases the possibility of an unbalanced load in case a chevron bracing configuration is used.

5.Buckling-restraining mechanism:

This mechanism is typically composed of mortar and steel casing (e.g., hollow structural shape). But BRBs that do not use mortar have also been proposed. Tremblay and Stiemer (1994) proposed the use of continuous columns as a backup stiffness to mitigate P-Delta effects in braced frames. The study used nonlinear dynamic analyses to investigate the influence of the continuous columns on the collapse of eight buildings that varied in height from two to twelve stories. The studied conditions were: columns with moment releases at the top and bottom of each floor (no continuous stiffness was provided) moment releases at the top and bottom of pairs of continuous stories, and continuous over the entire building height. The last case was analyzed using pinned connections at the base of the columns and was repeated for fixed connections at the base of the columns. The results showed that the worst case (more collapses occurred) was when columns had moment releases at each level (no continuity) and the best case was when the columns were continuous over the entire height and fixed at the base.Tagawa (2005) studied the continuous column effect on steel moment resisting frames when gravity columns are included in the analysis. Nonlinear static and dynamic analyses were performed using different buildings with and without the gravity columns. The results showed that the post-yield stiffness increased in pushover response and that interstory drift concentrations (large drifts in one story relative to an adjacent story) predicted by the dynamic analysis were reduced when the gravity columns are added.

DESCRIPTION AND MODELLING OF FRAMES

The analysis model was created in SAP2000 to evaluate and compare the influence of gravity column on the seismic response of buckling restrained braced frames. A brief description of the building and its site location will be presented, followed by other parameters required for the modelling and analysis of different framed buildings.

Building description

For the purpose of study, a 3-story steel structure of 11.88m in height as shown in figure is considered (Pandikkadavath, M.S. & Sahoo, D.R.2016)

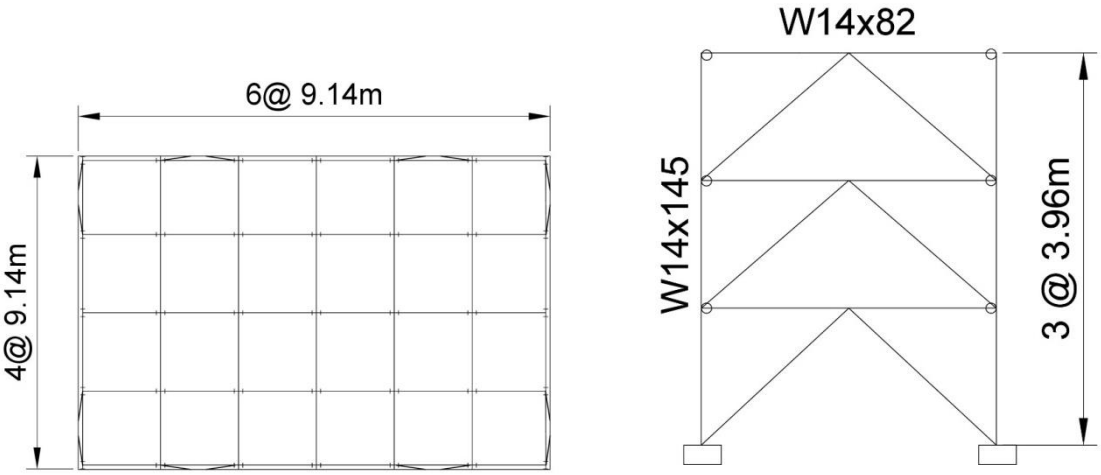

Fig.2 Plan of 3 storey building with BRBs and elevation of a BRBF

The building has four and six bays in the shorter and longer directions. The storey height is 3.96m and the width of each bay is 9.14m. The brace layout can be visualised in plan view with two braced bays in the principal directions placed symmetrically on the outer periphery of the building. All of the braces in the base model are a concentrically braced frame configuration, also known as a chevron brace, as shown in the elevation. One of the braced bays along the shorter direction is considered for the present study.
The building is assumed to be located at Downtown, Los Angeles with stiff soil of class D. The response reduction factor (R) is take as 8 for BRBF per the ASCE Standard 7-10. The design values for spectral acceleration for SDS 0.2s and SD1 1 s are 1.393 and 0.77g. The importance factor is taken as 1 for regular buildings. The seismic response coefficient or Base shear coefficient (Cs) was computed as 0.17. The approximate time period (Ta) for BRBF was calculated as 0.47s. The braces are designed for member forces obtained from critical load combination as per ASCE/SEI 7-10(2010). The values of fy and Ry are assumed as 248 MPa and 1.3, respectively. The value of ω and β are conservatively taken as 1.4 and 1.1. respectively (Sahoo and Chao,2010) . The values of fy and Ry for beams and columns are considered as 345MPa and 1.1 respectively. Columns are assumed to be perfectly as fixed to their bases. Table 1 summarises the braces section and structural sections used in beams and columns of braced frames.

Table 1 Section sizes of members used in braced frames

Storey	BRB (mm)	Beam (mm)	Column(mm)
3	60x36	W 14x82	W 14x145
2	100x36	W 14x82	W 14x145
1	125x36	W 14x82	W 14X145

NUMERICAL MODELLING OF FRAMES
To examine the seismic performance of BRBFs with gravity column nonlinear static pushover analysis and nonlinear time history analysis were carried out in SAP2000. Due

to symmetrical floor plan, lateral force resisting frames were modelled for only one side of the building. Floor masses are considered and are applied to columns at each storey and in the middle of the beams. All beam column connections are pinned. All bracing connections are idealized as pinned connections as they resist axial load only. To analyse the effect of gravity column, 4 different BRBFs with one and two braced bays with the base pinned or fixed were considered. The gravity column has been modelled as a leaning column attached to the braced frames by means of rigid link beams so that displacement of gravity column equals that of BRBF at each floor level. The gravity load in them was computed from total building weight and number of braced frames along a direction.
Beams and columns were modelled as standard frame elements with plastic hinge lumped at both ends. Both axial and moment rotation hinges were assigned to all beam and column elements in the BRBF assuming they would carry significant axial force with biaxial bending.

- 3VBRBF1- 3 story BRBF with 1 braced bay and gravity column with pinned base.
- 3VBRBF1-FX-3 story BRBF with 1 braced bay and gravity column with fixed base.
- 3VBRBF2-3 story BRBF with 2 braced bay and gravity column with pinned base.
- 3VBRBF2-FX-3 story BRBF with 2 braced bay and gravity column with fixed base.

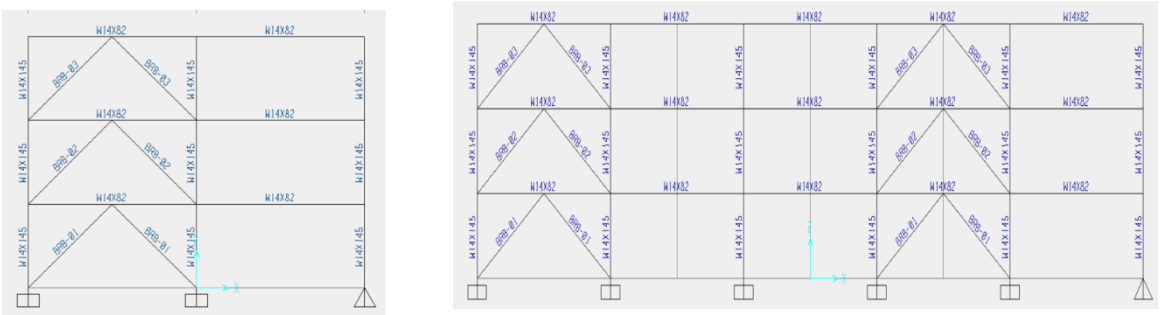

Fig.3 SAP model of 3VBRBF1 and 3VBRBF2

EARTHQUAKE GROUND MOTION RECORDS
The ground motions that were used in the previous research represent a suite of records for a hypothetical site in downtown Los Angeles with a probability of exceedance of 10% in 50 years. The 20 records used are from fault-parallel and fault-normal orientations of 10 recordings.
The selection of recordings was chosen based on the joint magnitude–distance probability for downtown Los Angeles, which included a magnitude 7 earthquake at less than 5 km away as well as a magnitude 7.5–8 earthquake at 50 km away. Most of the records in this suite are near-fault records; this type of record is chosen for this study because it tends to produce large residual deformations.

ANALYSIS RESULTS AND DISCUSSION

The structural analysis program SAP2000 was used to perform the nonlinear response history analyses. The main parameters studied are pushover curve, inter-storey drift response, residual drift response of the 4 BRBFs considered.

PUSHOVER CURVE
Though all frames showed yielding of braces at nearly same magnitude of base shear the peak lateral strength of BRBFs with the gravity column with fixed base is noted to be significantly higher than that of the frames with pinned base.

This shows that the fixed base BRBFs are stiffer than the pinned base BRBFs. BRBF with fixed base exhibited the post-yield strain hardening response without any degradation in the lateral strength and stiffness.

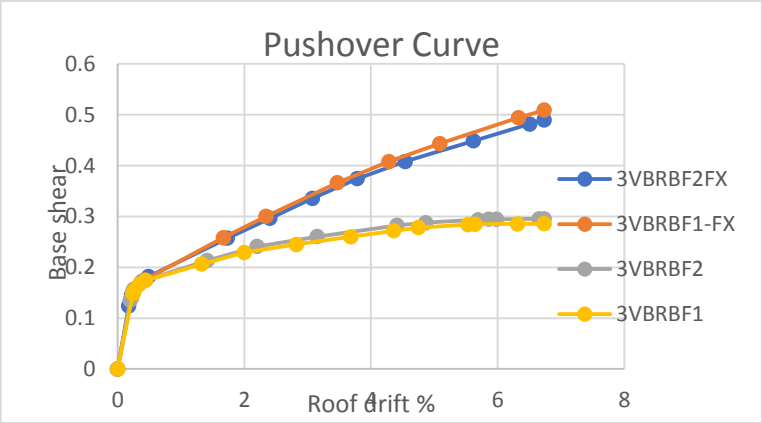

Fig.4 Pushover curve

INTERSTORY AND RESIDUAL DRIFT RESPONSE

Both peak inter-story drift(ISDR) and residual drift (RDR) response of braced frames are computed from the results of non-linear time history analyses for the selected ground motions. Two statistical values namely mean (AVG) and mean+standard deviation(AVG+SD) of peak RDR and ISDR response at each storey are computed from their peak values under each earthquake. The peak values of interstorey drift response is noted at the 3rd storey level. The peak values of ISDR are computed as 1.92%,2.05%,2.08% and 2.16% for 3VBRBF1,3VBRBF1-FX,3VBRBF2,3VBRBF2-FX respectively.

The figure shows the AVG and AVG+SD values of RDR response of all braced frames. 3VBRBF1 showed the maximum RDR response of all floors among all four frames. The maximum value of RDR of 0.24% is noted at the 2nd storey level. But the maximum RDR value of the other three frames are seen to be at the 3rd storey.

In order to compare the interstorey drift time history response of the braced frames LA17 ground motion is selected which corresponds to maximum RDR value in BRBFs as the value of RDR indicates the extent of damage in the BRBFs. The PGA value of LA17 ground motion is 0.57g. For the same excitation 2nd floor residual drift under LA17 ground motion is found to be 0.46%,0.09%,0.06% and 0.37% for 3VBRBF1,3VBRBF1-FX,3VBRBF2,3VBRBF2-FX respectively.

The primary reason for this larger story drift can be attributed to the relatively smaller story stiffness at the second story level as compared to the first story. The rigidity of columns at the first story columns of BRBFs due to the fixed bases increased the story stiffness that resulted in the smaller interstorey drifts at that level.

Fig 5: Interstorey drift response and residual drift response of the frames

CONCLUSION

This thesis presented a comparative study of the seismic performance of a conventional three story BRBFs, with varying support condition of gravity column. Nonlinear static pushover analyses and nonlinear time history analyses were carried out to compare the pushover curve, peak interstory drifts, residual drift response of the frames for 20 earthquake ground motions. The general conclusions drawn from the results of this study can be summarized

- Among the 4 frames considered the residual drifts in 3VBRBF1 was the highest and most critical of all the cases.
- 3VBRBF1 has very less base shear capacity as seen from the pushover curves
- Maximum value of residual drift in 3VBRBF1 (0.46%) was for LA17 ground motion.
- Results of BRBF with gravity column as fixed base suggests that providing continuous gravity column with fixed base can reduce considerable amount of drift in frames.
- So far studies have not been conducted in the effect of gravity column in

BRBFs, therefore further studies have to be done in taller buildings.

- Future studies on effect of stiffness of gravity columns should also be done.

REFERENCES

Pandikkadavath, M. S., & Sahoo, D. R. (2016). Analytical investigation on cyclic response of buckling-restrained braces with short yielding core segments. International Journal of Steel Structures, 16(4), 1273-1285.

Sahoo, D. R. and S.-H. Chao (2010). Performance-based plastic design method for buckling-restrained braced frames. Engineering Structures, 32(9), 2950–2958.

Tagawa, H. (2005). Towards an understanding of seismic response of 3D structures-stability & reliability. Doctor Thesis, Washington: University of Washington.

Tremblay, R., & Stiemer, S. F. (1994). Back-up stiffness for improving the stability of multi-storey braced frames under seismic loading. Proceedings of the 1994 SSRC Annual Technical Session, Bethlehem, Pa, 311-325.

Uang, C. M., & Nakashima, M. (2004). Steel buckling-restrained braced frames. In Earthquake engineering: From engineering seismology to performance-based engineering. CRC Press.

9th International Engineering Symposium - IES 2020
March 3-5, 2020, Kumamoto University, Japan

Some Studies on Embodied Energy & Cost of Tank-bed soil, Rice-husk-ash and Cement Based Geopolymer Adobes

Jyothi TK[1], Raghunath S[2] and **Jagadish KS[3]**

1 *Assistant Professor, Department of Civil Engineering, Government Engineering College, Doddamannina Gudde, Near Janapadaloka, B.M. Road, Ramanagara 562159, India. Email: jyothi271016@gmail.com*
2 *Professor, Department of Civil Engineering, BMS College of Engineering, India, Bengaluru 560019, India. Email: raghu.civ@bmsce.ac.in*
3 *Former Professor, Indian Institute of Science, India, Bengaluru 560012, India. Email:ksjagadish@gmail.com*

ABSTRACT: Load-bearing masonry has been and will continue to be the preferred choice of technology for construction of low-rise structures, especially houses. It is relatively easy to minimise the cost of construction in such structures since it is possible to dispense with expensive RC elements such as columns and beams. Further reduction in cost is by way of producing masonry units and mortar using locally available materials and cost-effective processes. This paper presents the results of the attempts made to stabilize tank-bed-soil (TBS), an abundantly available local material, using a combination of rice-husk -ash (RHA), Cement(C) and alkaline solution. Thus the blocks, produced through adobe process, is achieved through pozzolanic reaction and geopolymer reaction. The results have shown that it is indeed possible to produce TBS-RHA-C based geopolymer (GP) masonry units with adequate strength and with minimal effort in the form of adobes. It has been noticed from the cost and embodied energy(EE) computations that sodium silicate constituted to the bulk of the cost whilst sodium hydroxide contributed to the bulk of the embodied energy of the masonry units. However, the cost and energy per unit strength appears encouraging especially if the molarity of the alkaline solution is reduced.

Keywords: *Geopolymer adobes, embodied energy, tank-bed soil, rice-husk-ash, cement, cost*

INTRODUCTION

Embodied energy is defined as the summation of all the energy required to produce a product i.e. total energy spent to procure the raw materials, transport it, process it for the production of product, and manufacture the product. Generally quantification of embodied energy is done as a part of Life cycle Analysis (LCA). There are two types of LCA (1) involving embodied energy, operational energy and demolition energy, it is termed as 'cradle-to-grave' analysis. (2) 'cradle-to-gate' analysis is done to specify the embodied energy of building materials by aggregating all the energies up to the point of using them in a building. The embodied energy of different building materials obtained by such analysis by various researchers are presented in Table 1.

Table 1. Embodied energy of different building materials

Material	Unit	Energy (MJ/Unit)
Cement [Jagadish (2019)]	1 kg	3.6MJ
Lime [Satprem Maïni and Varun Thautam (2013)]	1 kg	5.63
Burnt brick [Satprem Maïni, and Varun Thautam (2013)]	1 Brick	4.25
Lime-pozzolana cement [Manjit Singh (2012)]	1 kg	2.5
NaOH [Tempest et al (2009)]	1 kg	20.5
Na_2SiO_3[Fawer et al (1999)]	1 kg	5.37

The embodied energy for different building blocks has been presented in table 2. These values are especially relevant for the materials used in and around Bengaluru, India.

Table 2. Embodied energy of building blocks [Surekha et al (2016)**]**

Material	Size per unit (mm)	Embodied Energy/Unit (MJ)
Brick	225 x 108 x 75	4.63-5.6
Stabilised Mud Block	230 x 190 x 100	2.85
Hollow Concrete Block	400 x 200 x 200	7.6
Hollow Clay Block	400 x 200 x 200	16.7
Cut Sandstone	450 x 230 x 150	7.55
Geopolymer masonry Block	230x105x75	4.74-6.5 [Jyothi et al (2017)]

PRESENT STUDY

In the present investigation, Geopolymer-based masonry units were cast and tested for various strength parameters. The dimensions of units were similar to the dimensions of table moulded bricks. The size of unit was 230 mm length, 105 mm breadth and 75 mm height with frog on one side. As per Bureau of Indian Standard specification IS1077-1992, the minimum wet compressive strength of bricks shall not be less than be 3.5 MPa. The mix proportions for the production of masonry units were selected based on the strength parameters of cubes studied during the development of the product. The mix proportions of cubes which gave wet compressive strength greater than 3.5 MPa were selected for the production of masonry units. Six samples were cast for each mix proportion. Following tests were carried out on TBS-RHA-C based masonry (i) Compressive strength of masonry units, (ii) Water absorption of masonry units. The results indicated that they could be used as an alternative for conventional masonry.
The various raw materials used for casting masonry units and their mix proportions selected for unit production have been tabulated in table 3. The concentration of the alkaline solution is also indicated.

Table 3. Details of raw materials and their mix proportions

Ingredients	TBS82-RHA10-C8	TBS72-RHA20-C8	TBS62-RHA30-C8	TBS52-RHA40-C8	TBS42-RHA50-C8
TBS	0.82	0.72	0.62	0.52	0.42
RHA	0.10	0.20	0.30	0.40	0.50
C	0.08	0.08	0.08	0.08	0.08
Alkaline Solution	"4 Molar Concentration(4M)"				

PRODUCTION OF GEOPOLYMER MASONRY UNITS

The pictorial representation of production of masonry units have been given in figure 1.

Figure 1. Pictorial representation of production of masonry units

The average compressive strength of all these units was well above the minimum strength of 3.5 MPa prescribed by IS1905-1987. The average water absorption values were well within the permissible limit of 20% as per IS1077-1992. Thus, it can be concluded that all the masonry units were suitable for low-rise, load-bearing masonry applications practiced in India. It would be interesting to compare the compressive strength of these units with that of typical table moulded bricks (TMB) available in south India. The comparison is presented in table 4.

Table 4. Compressive strength of GP masonry units compared with TMB

#	Type of geopolymer masonry unit	Alkaline solution(%) based on flow test and Molarity	Mean wet compressive strength (MPa)
1	TBS82-RHA10-C8	25% of the materials "4 molar concentration(4M)"	3.5
2	TBS72-RHA20-C8		4.2
3	TBS62-RHA30-C8		9.4
4	TBS52-RHA40-C8		9.2
5	TBS42-RHA50-C8		16.3
6	TMB[		6.0

EMBODIED ENERGY COMPUTATION

One of the methodologies to evaluate the influence of the materials on environment is by carrying out life cycle energy assessment (LCA). The prime step in this process is to calculate the embodied energy of the building products. There are a number of features that affect the embodied energy of building materials viz., availability and process of extraction of raw materials, geographic location, distance and mode of transportation to the processing site, type and efficiency of machinery used for processing and distance from which material is to be procured for construction.

The method adopted for embodied energy calculation, validity and accuracy of the data compiled plays a crucial role in LCA. There could be 'cradle-to-grave', 'cradle-to-site' or even 'cradle-to-gate' type of EE assessment depending upon the requirement. In the present study the end product i.e. the geopolymer masonry units are made at site using the adobe process; hence the cradle-to-site analysis has been carried out.

For the purpose of calculating embodied energy, the energy required for certain processes from the present study have been calculated based on the fuel/electrical energy related with the process. For some of the materials which have been procured, such as cement and alkaline solutions, the embodied energy from literature have been taken [Jagadish(2019), Tempest et al (2009), and Fawer et al(1999)].

The energy expended from the manual efforts, such as sieving, mixing, placing in the mould etc., has not been considered. Table 5 provides the depiction and calculation of the embodied energy of the ingredients of TBS-RHA-C based geopolymer masonry units.

Table 5. Embodied energy computation for production of TBS-RHA-C geopolymer masonry units

#	Process	Operation	Diesel / Electrical energy consumption	Energy (MJ/kg)
1	Excavation of TBS	Generally soil is excavated using diesel-operated excavators, which are typically operated over a shift of 8 hours per day. In 8 hours, the soil is excavated and loaded into a truck at the rate of 12 loads per hour for about 90 times into a truck of capacity 14.0 cum. Total output = 12x14 = 168 cum/hour	Diesel consumption per hour = 30 liters. Therefore, diesel required per cum = 30/168 = 0.178 lt/cum	Assuming bulk density of TBS is 1300 kg/m3 and [Fuel combustion energy for diesel is 35.8 MJ/lt [Satprem Maïni and Varun Thautam (2013)] 0.029 MJ/kg

	Transportation of TBS	Diesel required for transportation over a distance of approximately 50 km, at mileage of 5km/lt : 50/5= 10 liters	(Assuming a truck load is equivalent to 11.0 cum) 10/11 = 0.91 lt/cum	
	Total diesel required		1.087 lt/cum	
2	RHA	Energy for inter-grinding of 5 kg of RHA for 60 minutes in Ball mill. 375 Watt hour electrical energy is consumed	i.e. 375X12.44 = 1350/1000 = 4.665/5 kg = 0.93 MJ/kg.	0.93 MJ/kg
3	Cement	Energy for the production of Cement	-	3.6MJ/kg[Jagadish (2019)]
5	NaOH	Energy for the production of NaOH	-	20.5 MJ/kg [Tempest et al (2009)]
6	Na_2SiO_3	Energy for the production of Na_2SiO_3	-	5.36 MJ/kg [Fawer et al (1999)]

RESULTS AND DISCUSSIONS

The embodied energy of the four types of TBS-RHA-C based geopolymer masonry units of size 230 x 105 x 75 mm (i.e., the size of typical table-moulded bricks) has been presented in table 6. The table also provides the cost comparison and their respective compressive strength.

Table 6. Comparative analysis for TBS-RHA-C geopolymer masonry units and table moulded bricks

#	Samples	Avg. compressive strength (MPa)	EE (MJ/ unit)	EE per unit compressive strength (MJ/MPa)	Cost (INR/unit)	Cost per unit compressive strength (INR/MPa)
1	TBS82-RHA10-C8	3.5	4.87	1.39	13.63	3.89
2	TBS72-RHA20-C8	4.2	5.09	1.21	13.57	3.23
3	TBS62-RHA30-C8	9.4	5.3	0.56	13.51	1.43
4	TBS52-RHA40-C8	9.2	5.52	0.6	13.45	1.46
5	TBS42-RHA50-C8	16.3	5.74	0.35	13.38	0.82
6	TMB [Surekha, B et al (2016)]	6.0	4.25	0.71	6.0	1.0

It would be pertinent to look at the main contributors to EE and cost of each unit. Table 3 shows the quantity of the ingredient materials used in each of the 5 types of masonry units. The EE and cost of each material is also provided in table 6. It has to be noted that the EE and cost of grinding has also been included. The comparison clearly reveals that table moulded brick has the least EE amongst the six types of masonry units. The embodied energy of GP masonry units made with 82% TBS and 10%RHA and 8% C was the minimum (4.87 MJ/unit) among the remaining five and this is marginally more than that of the EE of TMB.

Although the EE values and cost of blocks made with rice-husk-ash is high it is due to the presence of alkaline solution and not due to rice-husk-ash. However, the addition of

these materials is not without any benefits. They have indeed contributed to the enhanced compressive strength. It would now be interesting to look at the EE benefits of TBS-RHA-C based GP units in terms of relative strength. The EE of each masonry unit is normalized with respect to its compressive strength and presented in Table 7. This comparison appears encouraging and clearly indicates that the blocks made by using TBS42-RHA50-C8 possess the least EE per unit compressive strength (0.35MJ/MPa), which is half of that of TMB.

Similarly, the cost of each masonry unit has been normalized with respect to its compressive strength. It can be observed that TBS42-RHA50-C8 (4M) bricks were comparable in cost to that of table-moulded bricks looked at from the units of cost per unit strength.

The graphical comparison of the EE of the five types of GP blocks is shown in fig 2. The comparison indicates that the bulk contributors are the alkaline materials, especially Na2SiO3. The major contributor for cost is also alkaline materials; again the bulk is from Na2SiO3. It can, hence, be concluded that any further improvements in the development of GP masonry units using TBS-RHA-C should have to keep the issue of energy and cost contribution of NaOH and Na2SiO3. This is possible by using alkaline solutions at lower concentration and reduced NaOH: Na2SiO3 ratio. Perhaps using locally available ingredients which possess reactive silica may lead to dispensing with the use of Na2SiO3 and thus contribute to energy and cost benefits. Further studies are being undertaken in this direction.

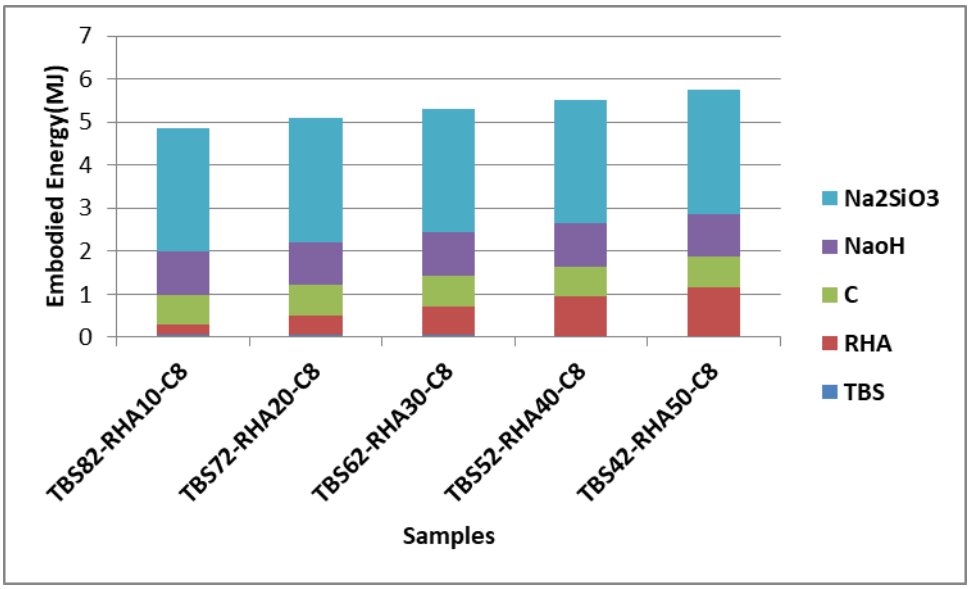

Figure 2. Embodied energy contribution material breakup

CONCLUDING REMARKS

The following are the highlights of embodied energy computations:

- The embodied energy of GP masonry units of TBS82-RHA10-C8 was the minimum among the five, which was 4.87 MJ/unit. This EE (embodied energy) value is comparable to that of similar-sized, table-moulded bricks of south India; however, the strength of remaining GP units was better than that of TMBs of south India. The EE values of the other GP units ranged from 5.09 to 5.74 MJ/unit.

- The cost comparison trends were also along similar lines as that of EE. All the masonry units were significantly expensive when compared to the cost of similar-sized TMBs. Again, the major contributors were NaOH and Na_2SiO_3. It is evident

that reducing molarity and ratio of NaOH: Na_2SiO_3 should to be the next steps in reaping the benefits of energy and cost.

- In terms of relative strength, embodied energy of each type of masonry unit per unit compressive strength was favorable when compared to that of table-moulded bricks of south India.
- It could be concluded that any further improvements in the development of GP masonry units using TBS-RHA-C should keep the issue of energy and cost contribution of NaOH and Na_2SiO_3.

REFERENCES

.

1. Fawer, Matthias et al (1999), Life cycle inventories for the production of sodium silicates, The International Journal of Life Cycle Assessment, Vol. 4, No.4, pp. 207-212.
2. IS: 1077-1992, (Reaffirmed 2007), Common Burnt Clay Building Bricks – Specification, Bureau of Indian Standards, New Delhi, India.
3. IS: 1905-1987. (Reaffirmed 2002), Indian Standard Code of Practice for Structural Use of Unreinforced Masonry. Bureau of Indian Standards, New Delhi, India, 3rd Edition, 1987.
4. Jagadish, KS(2019), Sustainable building Technologies, I K International Publishing House Pvt. Ltd
5. Jyothi, TK et al (2017), Embodied Energy & Cost Issues of Tank-bed-Lime based Geopolymer Adobes, Open Journal of Energy Efficiency[OJEE] VOL. 6, No.3, pp 1-12.
6. Manjit, Singh (2012), Energy and Environmental Concerns in Building Materials,National Conference on Emerging trends of energy conservation in buildings. Central Building Research Institute Roorkee, Uttrakhand, India.
7. Satprem Maïni, and Varun Thautam (2013), Embodied energy of various materials and technologies,Auroville Earth Institute, A Data Compilation, 2005, revised 2013.
8. Surekha, B et al (2016), Energy and Building Materials, International Journal of Civil Engineering [IJCE], VOL.5, No. 5, pp 13-24.
9. Tempest, et al (2009), Compressive strength and embodied energy optimization of fly ash-based geopolymer concrete, In World of Coal Ash (WOCA) Conference.

9th International Engineering Symposium - IES 2020
March 3-5, 2020, Kumamoto University, Japan

Crippling of Webs with Intermediate Bearing Stiffeners under Local Compressive Loads

Raghuvir Salkar [1], Abhishek Salkar [2]

1 *Proprietor, Kuvelkar Salkar Associates, A-2 Ramakant Apts., 18 June Road, Panaji Goa 403001. Email: salkar@ksa-india.com*
2 *Consulting Engineer, Kuvelkar Salkar Associates, A-2 Ramakant Apts., 18 June Road, Panaji Goa 403001. Email: a.salkar@ksa-india.com*

ABSTRACT:
Three design codes, namely, the Specifications for Structural Steel Buildings ANSI/AISC 360-10 (2010) from the U.S.A., Limit States Design of Steel Structures CSA S-16-01 (2006) from Canada, and Steel Structures AS 4100 (1998) from Australia were studied for design of bearing stiffeners. All three codes provide a similar design procedure for assessing the stiffened web strength, where stiffeners are full web depth stiffeners. No direct formula is available to calculate the stiffened web strength with partial depth stiffeners. This paper evaluates the above mentioned three design codes with respect to test results from the University of Maine and presents a formula for evaluating web crippling strength with partial depth bearing stiffeners.

Keywords*: web crippling, stiffened webs, transverse stiffeners, ultimate stiffened web capacity*

INTRODUCTION

Web crippling can occur in webs of rolled shapes and built-up beams and girders which are subjected to local concentrated compressive loads acting in the plane of the web. Such loads can occur either over supports or between supports of beams and girders. As a rule, design codes specify the use of web bearing stiffeners or web doubler plates when the design capacity of web is less than the local concentrated compressive load.

Experimental and analytical research was conducted by Salkar (1992) at the University of Maine, U.S.A. on the crippling strength and behavior of webs with back to back intermediate welded stiffeners. This paper presents highlights of that research and an evaluation of crippling strength of stiffened webs of rolled shapes with reference to provisions of AISC Specifications (2010), Canadian (CSA, 2006) and Australian (AS, 1998) codes, along with design recommendations. Fitted stiffeners have not been considered in this paper.

RESEARCH CONDUCTED AT UNIVERSITY OF MAINE

Salkar (1992) conducted research on intermediate load bearing stiffeners for rolled shapes which has been summarized below. The evaluation was done through experimental investigation as well as analytical work using finite element analysis. Three types of local compressive loading were considered:

i. Loading through roller on top flange as shown in Figure 1,
ii. Loading through patch plate on top flange as shown in Figure 2, and
iii. Loading through I-shaped beam on top flange as shown in Figure 3.

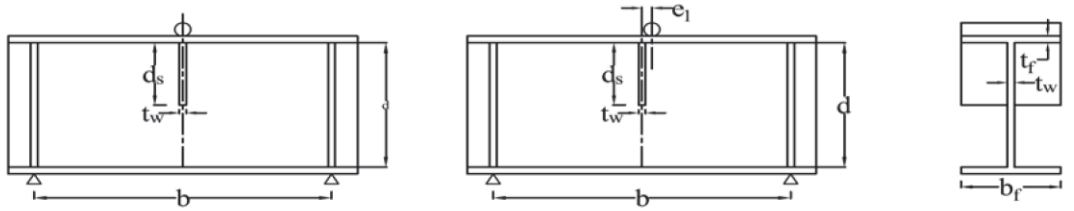

Figure 1: Loading through roller on top flange

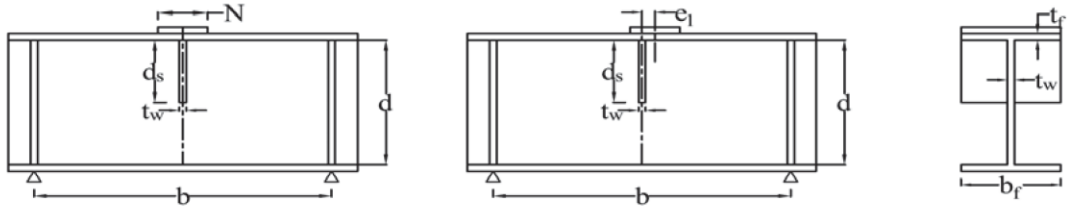

Figure 2: Loading through patch plate on top flange

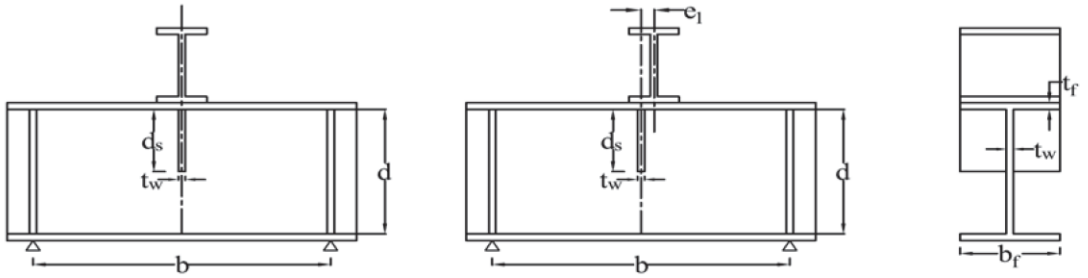

Figure 3: Loading through I- shaped beam on top flange

Experimental Investigation

As a part of experimental work, seventeen rolled beams (W16×26) were tested in a Baldwin Testing Machine, and various factors of stiffener thickness t_s, depth of stiffener d_s , eccentricity of load with respect to the plane of stiffeners e_1, and width of patch load N were considered as test parameters. Small values of eccentricity up to 0.5 inch, which can occur due to fabrication and construction tolerances, were considered. These 17 test results are summarized below in Table 1.

Modes of Failure

Three modes of failure described below, namely, web crippling below the stiffener, local stiffener crippling, and global stiffener crippling, were observed in the above 17 tests.

i. Failure mode 1 - Yielding in the web below the bottom of the stiffener with or without excessive yielding in the stiffener led to the web crippling failure mode and was seen in cases where the load was applied through a plate. It was also seen in the case of specimens with thick stiffener, under concentric loading through a roller.

ii. Failure mode 2 - Local stiffener crippling occurred in beams with thin to moderately thick half depth stiffener under concentric loading through a roller. It was also noted in all specimens subjected to eccentric roller loads.

iii. Failure mode 3 - Global stiffener crippling was found to occur in all specimens with deep stiffeners, subjected to concentric loads through a roller or an I-beam.

Table 1: Tests on webs with intermediate load bearing stiffeners

Sr.No	*tw*	*tf/tw*	*bf/tf*	d/t_w	*b/d*	*ts/tw*	d_s/d	*N/d*	e_1 *inch*	*Fyw*	F_{ys}	P_{tst}	Load Application Method
1	0.26	1.23	17.2	59.9	2.3	0.65	0.50	0.303	0	48	55	161	Patch plate
2	0.25	1.24	17.4	61.5	2.3	0.67	0.50	0	0.5	49	55	107	Roller
3	0.26	1.22	17.2	59.9	2.3	0.65	0.50	0.303	0.5	46	55	162	Patch plate
4	0.25	1.29	17.2	62.8	2.3	0.69	0.50	0	0	47	53	114	Roller
5	0.25	1.36	16.0	61.8	2.3	0.96	0.50	0.304	0	49	48	169	Patch plate
6	0.25	1.26	17.5	62.5	2.3	0.97	0.50	0	0.5	52	48	120	Roller
7	0.26	1.31	16.2	60.3	2.3	0.93	0.50	0.304	0.5	48	48	161	Patch plate
8	0.25	1.27	17.0	61.3	2.3	0.95	0.50	0	0	47	48	144	Roller
9	0.26	1.31	16.5	61.0	2.3	1.23	0.50	0.303	0	49	47	175	Patch plate
10	0.25	1.29	17.0	62.5	2.3	1.25	0.50	0	0.5	49	47	128	Roller
11	0.26	1.27	16.8	60.8	2.3	1.22	0.50	0	0	50	47	149	Roller
12	0.26	1.29	16.1	59.2	2.3	1.19	0.50	0	0	44	49	150	Roller
13	0.25	1.34	16.2	61.8	2.3	0.68	0.75	0	0	47	45	126	Roller
14	0.26	1.29	16.1	59.4	2.3	0.93	0.75	0	0	46	48	154	Roller
15	0.26	1.28	16.3	59.4	2.3	1.18	0.75	0	0	46	48	164	Roller
16	0.26	1.26	16.7	59.6	2.3	0.92	0.75	0	0.5	46	48	132	Roller
17	0.25	1.29	16.7	61.3	2.3	0.95	0.75	0.303	0	47	48	145	I section W4×13

Analytical Work - Finite Element Analysis (FEA)

A non-linear finite elemental analysis was carried out using the modified version of the program NONSAP. The original version was developed by Bathe, Wilson and Iding (1974) at the University of California, Berkeley, and the modifications were made by Du (1991), at the University of Maine. The main objectives of the analysis were:

- To obtain a better picture of the stiffened web behavior,
- To conduct a parametric study to determine the effect of various factors t_s , d_s , e_1 , and *N* on the stiffened web strength.

A three-dimensional 8 node iso-parametric doubly curved shell element was used to study web crippling. The finite element mesh used for the analysis was made up of 216 such elements and 705 nodes. The average value of the ratio of the test results to the failure loads predicted by the finite element analysis was 1.017. Further, as may be noted from Figure 4, 5 and 6 below, the finite element analysis was also able to accurately predict failure modes observed during experimental work.

The results of the parametric study were used along with the test results, to develop a formula to predict the stiffened web capacity P_u given by :

$$P_u = K(2d_s/d)^X + F_{ys}t_s b_s R \qquad (1)$$ where K is given by

$$K = 135t_w^2 (F_{yw}t_f / t_w)^{0.5}\{1+ 3(N/d)(t_f/ t_w)^{1.5} \} \qquad (2)$$

$$R = 2e_1\{(t_f/ t_w)^{0.5}(t_f/ t_s)^{0.5}/1.55 - 1\} + 1 \text{ ″ } 1 \qquad (3)$$ where X and b_s are given by

$X = 0.50\ (d/d_s)$ (4) and

b_s = twice the width of the front or back stiffener

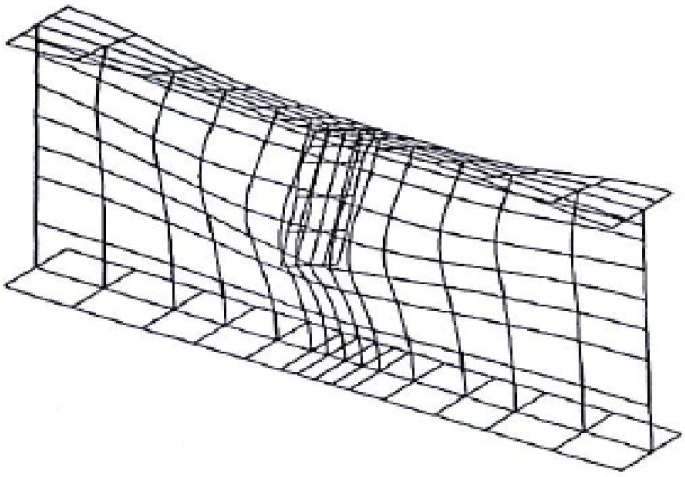

Figure 4: Failure Mode 1 - Web Crippling below Stiffener (thick half depth stiffener, concentric load through a roller)

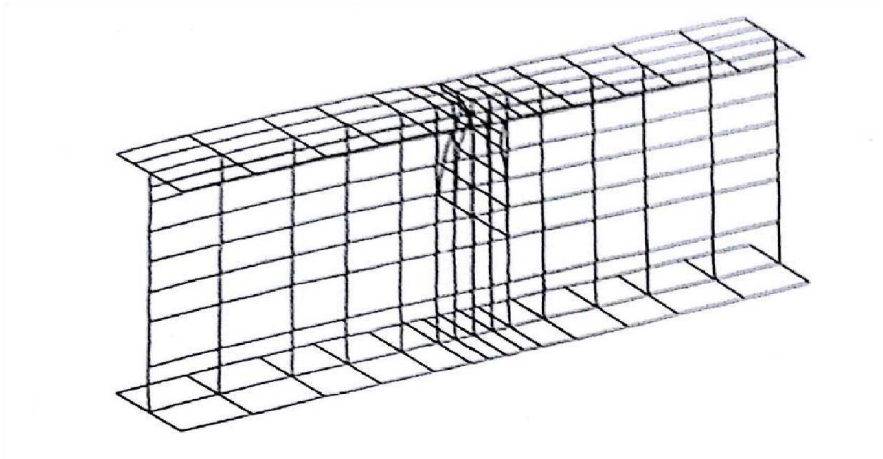

Figure 5: Failure Mode 2 - Local Stiffener Crippling (Thin half depth stiffener, concentric loading through a roller)

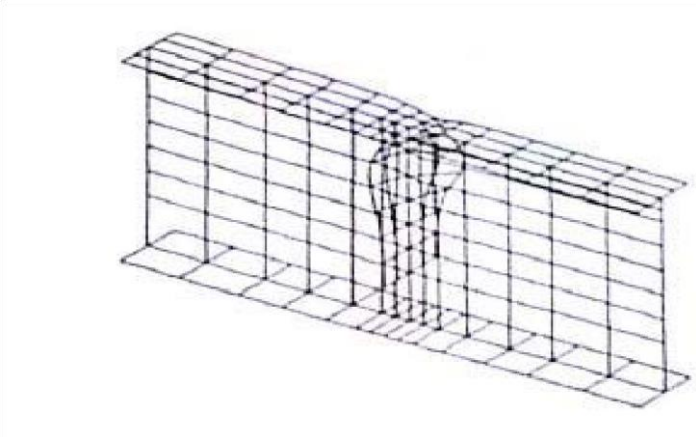

Figure 6: Failure Mode 3 - Global Stiffener Crippling (Three quarter depth stiffener, concentric loading through a roller)

DESIGN RECOMMENDATIONS

Equation (1) developed at the University of Maine was modified to Equation (5) below.

$$P_u = K + F_{ys} t_s b_s R \left(2d_s/d \right)^X \qquad (5)$$

The proposed formula is valid when *N/d* lies between 0 and 0.304, eccentricity of loading is smaller than or equal to 0.5 inch, the stiffener depth ranges from 0.5 to 0.75 times the web depth, and stiffener satisfies compactness criteria.

A comparison between the test results conducted at the University of Maine and the stiffened web strengths predicted by the AISC, CSA and AS design codes as well as the proposed formula is presented below in Table 2.

The average ratios of test results to the predicted failure loads were found to be 1.03 for both AISC and CSA, 1.39 for AS and 0.99 for the proposed formula. The coefficients of variation were found to be 0.13 for both AISC and CSA, 0.19 for AS and 0.05 for the proposed formula. Hence, it may be said that the proposed formula is able to predict stiffened web strength more accurately than the AISC, CSA and AS design codes. Further, these design codes do not have any provisions for evaluating crippling strength of webs with partial depth stiffeners and eccentric loading.

Table 2: Comparison of predicted values v/s test results

Sr No	Test Results	AISC Results (AISC)	Canadian Results (CSA)	Australian Results (AS)	Proposed Formula	Test/ AISC	Test/ CSA	Test/ AS	Test/ (Prop. Formula)
1	161	135	135	148	169	1.20	1.20	1.09	0.95
2	107	130	130	72	115	0.82	0.82	1.48	0.93
3	162	132	132	146	166	1.23	1.23	1.11	0.98
4	114	123	123	70	113	0.93	0.93	1.62	1.01
5	169	139	139	155	172	1.21	1.21	1.09	0.98
6	120	142	142	89	110	0.84	0.84	1.36	1.00
7	161	142	142	159	170	1.13	1.13	1.01	0.95
8	144	138	138	85	129	1.05	1.05	1.69	1.12
9	175	158	158	174.	192	1.11	1.11	1.01	0.91
10	128	154	154	103	126	0.83	0.83	1.23	1.02
11	149	161	161	106	150	0.93	0.93	1.41	0.99

12	150	157	157	102	149	0.96	0.96	1.47	1.01
13	126	115	115	66	122	1.10	1.10	1.92	1.04
14	154	141	141	86	151	1.09	1.09	1.79	1.02
15	164	157	157	102	172	1.04	1.04	1.61	0.95
16	132	140	140	85	137	0.94	0.94	1.56	0.96
17	145	137	137	115	147	1.06	1.06	1.26	0.99

The following design recommendations are made.

- It is recommended that webs shall be provided with minimum three-quarter depth web stiffeners, and the stiffener thickness be around 0.95 times the thickness of the web.
- It is recommended that Equation (5) be used for evaluating the stiffened web crippling strength.

CONCLUSIONS

The following conclusion was deducted from this study:

- The provisions given in AISC Specifications, CSA S-16-01 and AS 4100 for calculating the stiffened web strength needed to be re-examined in the light of the information provided here.
- On the basis of this research, Section J10.3 in the latest version of Specifications for Structural Steel Buildings ANSI/AISC 360-10 (2016) now states that a three-quarter depth stiffener or a doubler plate is needed to eliminate web local crippling.

REFERENCES

American Society of Steel Construction (2010). *Specification for Structural Steel Buildings*, *ANSI/AISC 360-10*, *Chapter J*, 16.1-128 - 16.2-139.
C. Du (1991). *Ph.D. Thesis, Dept. of Civil Engineering, University of Maine*.
J. Bathe, Wilson and Iding (1974). *Structural Engineering Laboratory, University of California, Berkeley*, *Report No. UCSESM 74-3*.
R. Salkar (1992). *Ph.D. Thesis, Dept. of Civil Engineering, University of Maine, Vol. 2, Chapter 5.* pp. 424-522.
Standards Australia (1998). *Steel Structures*, *AS 4100*, *Section 5*. pp. 65 - 70.
The Canadian Standards Association (2006). *Limit States Design of Steel Structures (update 3), CAN/CSA S-1601,Chapter 14*. pp. 43 - 44.

9th International Engineering Symposium - IES 2020
March 3-5, 2020, Kumamoto University, Japan

ACID BLUE 29 TEXTILE DYE DEGRADATION BY PHOTOCHEMICAL TREATMENT

Rekha H B[1] and **AKSHATHA[2]**

1 *Assistant Professor, Department of Civil Engineering, University Visveswaraya College of Engineering and Technology, Bangalore University, Bangalore 560056, Karnataka, India. email: rekhahb@gmail.com*
2 *Graduate Student, Department of Civil Engineering, University Visveswaraya College of Engineering and Technology, Bangalore University, Bangalore 560056 Karnataka, India. email: akshathagowda555@gmail.com*

ABSTRACT: The present investigation aims at laboratory scale batch treatment of textile dye solution by Photochemical Treatment using oxidizing agent such as H_2O_2 and TiO_2 in combination with UV. The effects of variation in the operating conditions such as pH, dosage of hydrogen peroxide and TiO_2 were considered for photochemical treatment. The pollutant used in this study is a commercial textile dye Acid Blue 29. The results of photochemical treatment for Acid Blue 29 using UV + H_2O_2 showed maximum color and COD removal of 95% and 64% at 50 minutes with 5ml H_2O_2 dosage, at pH3, whereas the removal of color and COD by TiO_2 was insignificant. Hence the study concluded that the photochemical oxidation in the presence of H_2O_2 is a promising pre-treatment process in treating textile wastewater.

Keywords**: **Acid Blue 29, Hydrogen peroxide, Titanium Di-Oxide, COD, Color.

INTRODUCTION

Textile industry plays an important role in the industrial development of India and is the second largest sector of Indian economy, next to agriculture. A large number of textile mills have mushroomed in India to meet the demand for fabric (H.Amin et al 2008). It is estimated that 100 to 200 liters of water is required for processing one kilogram of fabric. The Effluent from Textile industry is highly toxic containing chemicals like acids, alkalis, colors, high BOD/COD concentration, surfactants, soap and dispersing agents (AE Ghaly 2014). There are many structural varieties of dyes, such as: acidic, direct, disperse, azo, diazo, sulfur-based, reactive, basic, mordant, Vat and metal complexes. Many of them are designed to be chemically stable so that they are difficult to decolorize due to their complex structure and synthetic origin. The main challenges are the mineralization of dyes, organic compounds and toxicity of the wastewater generated by the textile industry. Many treatment alternatives have been reported in lab as well as full scale, including physical, chemical, biological, Advanced Oxidation Process (AOP) and a combination of them for efficient treatment of colored effluent (Aleboyeh et al 2005).
Advanced Oxidation Processes (AOPs) are defined as the processes which involve generation and use of powerful but relatively non-selective hydroxyl radicals in sufficient quantities to be able to oxidize majority of the complex chemicals present in the effluent water (Adel al-kdasi et al 2004). The main and short mechanism of AOPs can be defined in two steps: (a) the generation of hydroxyl radicals, (b) oxidative reaction of these radicals with molecules. AOPs can convert the dissolved organic pollutants to CO_2 and H_2O (Modirshahla et al 2007). Hydroxyl radicals ($OH^{\cdot}$) has the highest oxidation potential (Oxidation potential, *E*0: 2.8 eV vs normal hydrogen electrode (NHE)) after fluorine radical. Fluorine, the strongest oxidant (Oxidation potential, *E*0: 3.06 V) cannot be used for wastewater treatment because of its high toxicity (Galindo 1998). And use of AOP for

degradation of textile dye produces no toxic bearing sludge which is the major problem in other treatment methods. From these reasons, generation of hydroxyl radical including AOPs has gained the attention of most scientists and technology developers (Joanne M. Bell et al 2003).

The generation of highly effective hydroxyl radical might be possibly by the use of UV/H_2O_2, UV/TiO_2 and a number of other processes (Metcalf & Eddy 2003). Acid dyes which are water-soluble anionic dyes. And they are so-called because they are applied in presence of organic and inorganic acid in dyebath solutions (Mohamed A. Hassaan et al 2017). And they are available in different shades (Minghua Zhou et al 2007).Therefore the present study has taken up to determine the efficiency of UV/H_2O_2 and UV/TiO_2 in the degradation of Acid Blue 29 a textile dye at different initial pH of 3,5,7 and 9.

MATERIALS AND METHODS

Acid Blue 29 belongs to Vinyl sulphone group of azo class having CI -20460 has been considered for the study. The chemical structure of same has been shown in Figure 1. Table 1 shows the Characteristics of Acid Blue 29. Characteristics such as toxicity, recalcitrant nature and higher solubility in water are the main criteria behind the selection of Dyes (Abidin et al 2011). Dyes are supplied from local supplier (Trade Name: Novacron) and chemicals used for the analysis are of analytical grade.

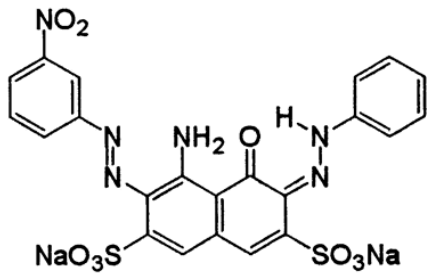

Fig. 1 Chemical Structure of Acid Blue 29

Textile Dye solution was prepared by dissolving accurately weighed 1g of Textile dye in one litre of distilled water. 500ml of 100mg/L concentration was used as a working volume for the study. The following treatment methods such as UV + H_2O_2 and UV + TiO_2 are adopted for the study to analyse the best suited method for color and COD removal for the Textile dye solution.

Table 1 Characteristics of Acid Blue 29

CHARACTERISTIC	DETAILS
Molecular Formula	$C_{22}H_{14}N_6Na_2O_9S_2$
C.I. Name	Acid Blue 29
Color Index No	C.I.20460
Applications	Silk, Wool, Cosmetics,
Molecular Weight	616.49 g/mol

For UV/H_2O_2 PROCESS, dye solution with 100mg/L concentration was added with different dosages of H_2O_2 like 1ml, 2ml, 3ml, 4ml,5ml and 6ml.

For **UV/TiO_2 process** different dosages of TiO_2 (98%purity) of 0.1gms, 0.2gms, 0.3gms, 0.4gms and 0.5gms are added to the working volume of 500ml solution. Once the initial pH of sample was adjusted to 3,5,7 and 9 by adding 1N H_2SO_4 and/or 1N NAOH solution, the samples are fed into UV reactor, and analyzed for color and COD removal by drawing the samples at regular intervals of 10 minutes at each pH

respectively for a period of 60 minutes. The study concludes with the optimum dosage of H_2O_2, TiO_2 and pH for the maximum removal of color and COD.

Analysis

The pH measurements were made by using Digital pH meter (Model: pH meter 335, Make: Systronics). Chemical Oxygen Demand was estimated by Closed Reflux Method by using COD digestor (Model: DRB 200, Make: HACH). The color of the dye solution was measured by using Double Beam Spectrophotometer (Model: Smart 2203, Make: Systronics). The wavelength (λmax) at maximum absorbance for Acid Blue 29 was recorded by using spectral scan. The percentage color and COD removal were calculated as follows.

$$Color\ Removal\ (\%) = \frac{(Abs)i - (Abs)t}{(Abs)i} x\ 100$$

Abs_i = Absorbance of the raw sample at λmax

Abs_t = Absorbance of the sample collected at regular time(t) interval

$$COD\ Removal\ (\%) = \frac{(COD)o - (COD)t}{(COD)o}\ x\ 100$$

COD_o: Initial COD of textile dye solution

COD_t: COD removal at regular time(t) interval of the textile dye solution

RESULTS AND DISCUSSION

The results of the experimental studies carried out for the different dosages of H_2O_2 and TiO_2 at initial pH of 3,5,7 and 9 are discussed below.

UV + H_2O_2

UV and H_2O_2 alone is quite ineffective in the treatment of textile wastewater at both alkaline and acidic pH, while under UV irradiation, H_2O_2 are photolysed to form two hydroxyl radicals (2OH•) which react with organic contaminants (Galindo 1998). Therefore, the experimental work has been conducted to study combined effect of UV and H_2O_2 on the degradation of the Acid Blue 29 with 100 mg/L dye concentration and at different solution pH of 3,5,7 and 9 respectively.

pH 3

From figure. 2, it is observed that, a maximum 49%, 53%, 57%, 59% and 64% of COD removal and 73%, 87%, 91%, 93% and 95% of color removal was achieved with 1mL, 2mL, 3mL, 4mL and 5mL dosage of H_2O_2 respectively at pH 3. The rate of decolorization and COD removal was maximum at 50 minutes with 5mL dosage of H_2O_2 then it remained constant. Hence 5mL of H_2O_2 dosage and 50 min of contact time is considered as favorable condition for maximum color and COD removal of 95% and 64%.

pH 5

From figure. 3, it is observed that, a maximum 20%, 25%, 33%, 42% and 56% of COD removal and 71%, 80%, 85%, 85% and 87% of color removal was achieved with 1mL, 2mL, 3mL, 4mL and 5mL dosage of H_2O_2 respectively at pH 5. The rate of decolorization and COD removal was maximum at 60 minutes with 5mL dosage of H_2O_2 then it remained constant. Hence 5mL of H_2O_2 dosage and 60 min of contact time is considered as favorable condition for maximum color and COD removal of 87% and 56%.

pH 7

From figure. 4, it is observed that, a maximum COD removal of 19%, 21%, 25%, 33%, 47% at 60min duration and 49% of COD removal at 50min duration and color removal of 31%, 45%, 52%, 59%, 71% at 60 min duration and 73% of color removal at 50min duration was achieved with 1mL, 2mL, 3mL, 4mL, 5mL and 6mL dosage of H_2O_2 respectively at pH 7. The rate of decolorization and COD removal was maximum at 50 minutes with 6mL dosage of H_2O_2 then it starts decreasing. Therefore, 6mL of H_2O_2 dosage and 50 min of contact time is considered as favorable condition for maximum color and COD removal of 73% and 49%.

pH 9

From figure. 5, it is observed that, a maximum COD removal of 19%, 20%, 24%, 33%, 45% at 60min duration and 45% of COD removal at 50min duration and color removal of 35%, 43%, 50%, 55%, 61% at 60min duration and 63% of color removal at 50min duration was achieved with 1mL, 2mL, 3mL, 4mL, 5mL and 6mL dosage of H_2O_2 respectively at pH 9 Hence 5mL of H_2O_2 dosage and 60 min of contact time is considered as favorable condition for maximum color and COD removal of 61% and 45%.

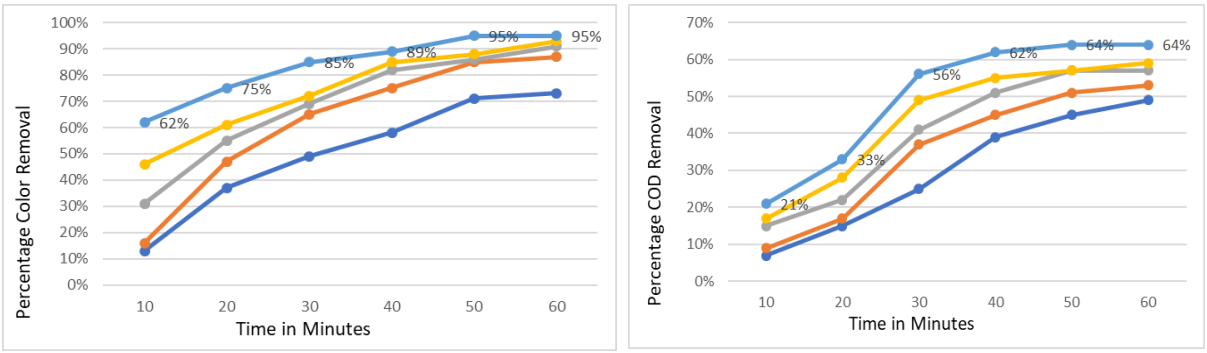

Fig.2 Percentage color and COD Removal of Acid Blue 29 with Various Dosages of H_2O_2 with UV at pH 3

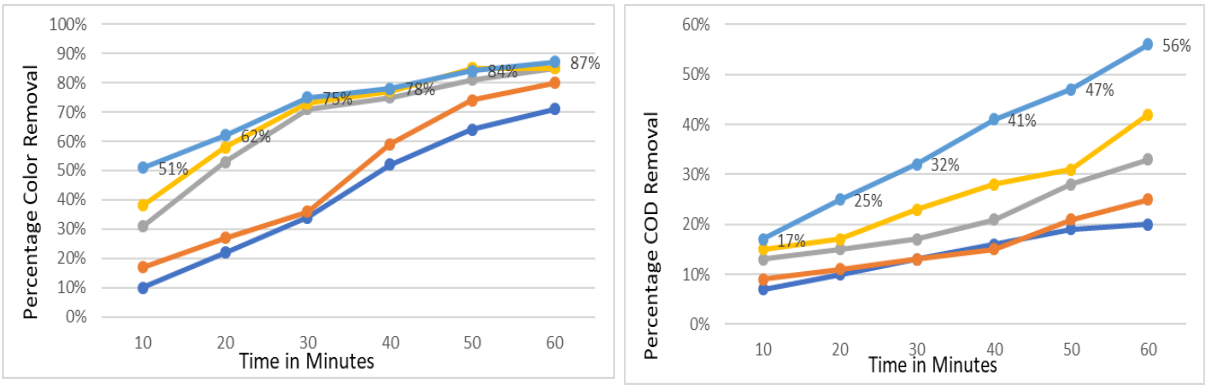

Fig.3 Percentage color and COD Removal of Acid Blue 29 with Various Dosages of H_2O_2 with UV at pH 5

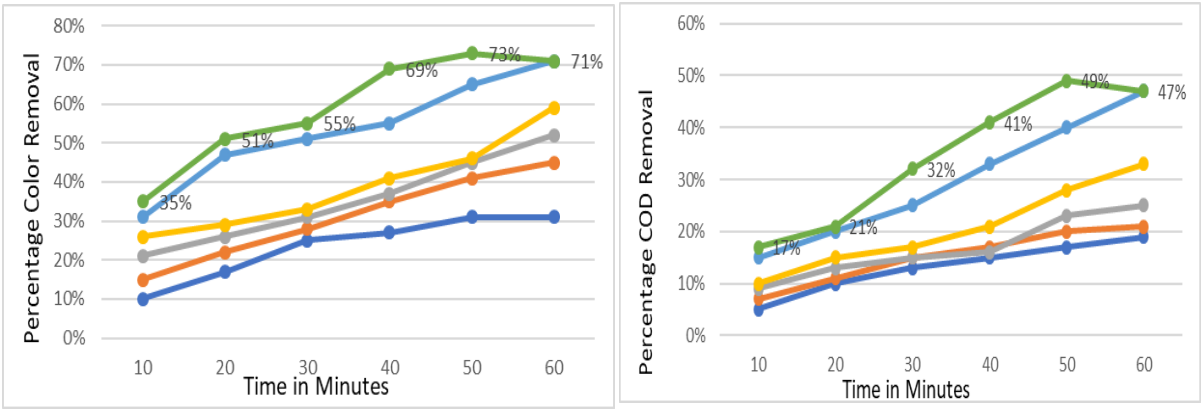

Fig.4 Percentage color and COD Removal of Acid Blue 29 with Various Dosages of H_2O_2 with UV at pH 7

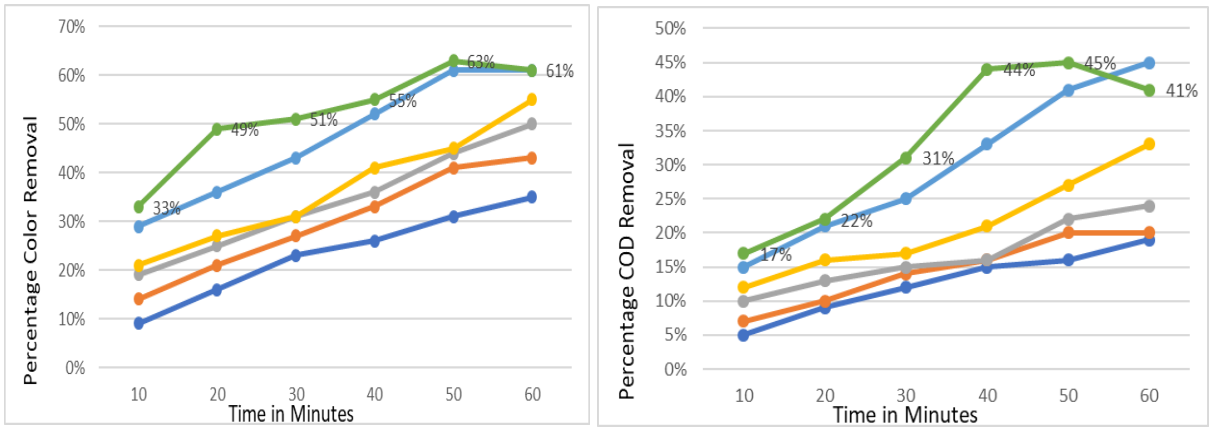

Fig.5 Percentage color and COD Removal of Acid Blue 29 with Various Dosages of H_2O_2 with UV at pH 9

Discussion

At pH 3 maximum color and COD removal of 95% and 64% was achieved at 50min duration with 5ml H_2O_2 dosage.

At pH 5 maximum color and COD removal of 87% and 56% was achieved at 60min duration with 5ml H_2O_2 dosage.

At pH 7 and 9 maximum color and COD removal of 73%, 9% and 63%, 45% was achieved at 50min duration with 6ml H_2O_2 dosage, after that it starts decreasing.

This may be due to H_2O_2 dosage, which plays a vital role in degradation process and removal efficiency increases as the H_2O_2 dosage increased, after which the efficiency starts to decrease or constant depending upon the type of dye and contact time. H_2O_2 in excess becomes a scavenger of hydroxyl radicals to form water and hydroperoxyl radicals (HO_2•), thus initiating other reactions that affect the oxidation process (Shashank S K et al 2011). Similar finding was reported from H. Amin et al,2008 that decolorization efficiency decreased from 90.69% to 82.3% when the dose was increased from 10cm^3 to 12cm^3.Hence study concludes that 50min contact time, 5mL H_2O_2 dosage at pH3 was optimum for the degradation of AB 29 Dye.

UV+TiO_2

The study shows the experimental work carried out to determine the combined effect of UV and TiO_2 on the degradation of Acid Blue 29 dye with 100 mg/L dye concentration and at different solution pH 3,5,7 and 9.

pH 3

From figure. 6, maximum of 67%, 61%, 55%, 51% and 45% of COD removal was observed with 0.1gm, 0.2gm, 0.3gm, 0.4gm and 0.5gm dosage of TiO_2 at pH 3 and Color removal was insignificant in all the cases. Therefore, contact time of 60min and TiO_2 dosage of 0.1gm is considered as Favourable dosage for maximum COD removal of 67%.

pH 5

From figure. 7, maximum of 59%, 55%, 53%, 49% and 41% of COD removal was observed with 0.1gm, 0.2gm, 0.3gm, 0.4gm and 0.5gm dosage of TiO_2 at pH 5 and Color removal was insignificant in all the cases. Therefore, contact time of 50min and TiO_2 dosage of 0.1gm is considered as favourable dosage for maximum COD removal of 59%.

pH 7

From figure. 8, maximum of 45%, 43%, 38%, 35% and 31% of COD removal was observed with 0.1gm, 0.2gm, 0.3gm, 0.4gm and 0.5gm dosage of TiO_2 at pH 7 and Color removal was insignificant in all the cases. Therefore, contact time of 40min and

TiO_2 dosage of 0.1gm is considered as favourable dosage for maximum COD removal of 45%.

pH 9

From figure. 9, maximum of 37%, 34%, 32%, 29% and 27% of COD removal was observed with 0.1gm, 0.2gm, 0.3gm, 0.4gm and 0.5gm dosage of TiO_2 at pH 9 and Color removal was insignificant in all the cases. Therefore, contact time of 60min and TiO_2 dosage of 0.1gm is considered as favourable dosage for maximum COD removal of 37%.

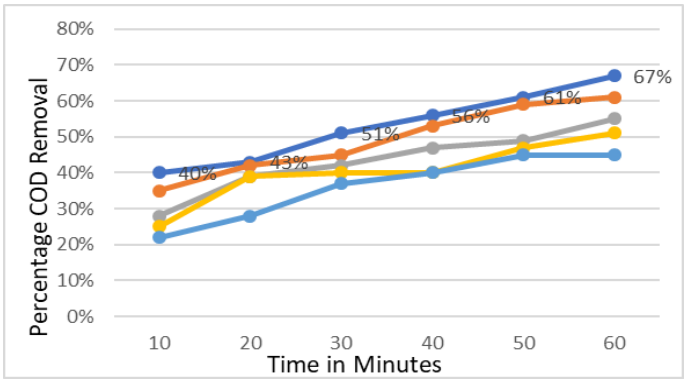

Fig.6 Percentage COD Removal at pH 3 by TiO_2

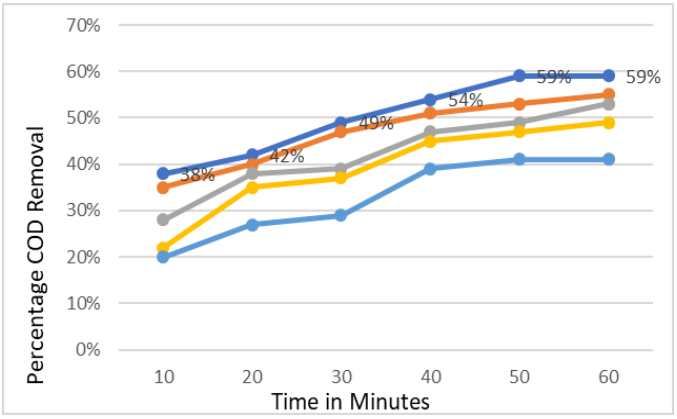

Fig.7 Percentage COD Removal at pH 5 by TiO_2

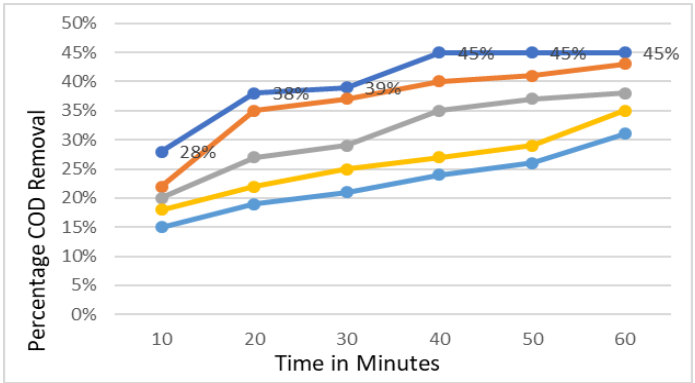

Fig.8 Percentage COD Removal at pH 7 by TiO_2

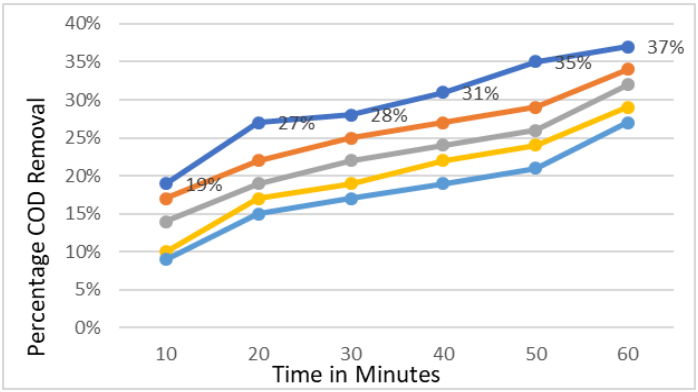

Fig.9 Percentage COD Removal at pH 9 by TiO_2

Discussion

At pH 3,5,7 and 9 the maximum COD removal achieved was 67%, 59%, 45% and 37% at 0.1 gm and at contact time of 50-60 minutes. This is due to fact that over the period of time, increase in TiO_2 dosage forms white precipitation leads to increase in color and COD. And the formation of precipitate depends on the contact time and dye composition (Sumathi Suresh 2005).

Hence the study concludes that pH 3 is considered as optimum condition for the maximum COD removal of 67% at 60min duration with 0.1gm TiO_2 dosage.

CONCLUSIONS

Advanced Oxidation process such as UV+H_2O_2 and UV+TiO_2 was used to degrade the Textile dyes such as Acid Blue 29 and each exhibit different removal characteristics in terms of color and COD removal for different treatment process.

For the selected dye, at pH 3 a maximum color and COD removal of 95% and 64% was achieved at 50min for 5ml H_2O_2 dosage, for UV + H_2O_2 process.

For UV + TiO_2, at pH 3 maximum COD removal of 67% was obtained at 60min for 0.1gm of TiO_2 dosage and shown insignificant color removal for the same dye. By comparing two different treatment process, UV + H_2O_2 was found to be most effective in degradation of Acid Blue 29 in terms of color and COD removal. Therefore, the study concludes that AOPs can be efficiently used as pretreatment technology for the degradation of the Textile dyes.

ACKNOWLEDGEMENTS

Authors would like to thank Vision Group on Science and Technology (VGST), Government of Karnataka, India for extending the financial support in carrying out this research work.

REFERENCES

1. AE Ghaly, R Ananthashankar, M Alhattab and VV Ramakrishnan (2014), "Production, Characterization and Treatment of Textile Effluents: A Critical Review", Department of Biological Engineering, Process Engineering and Applied Science, Dalhousie University Halifax, Nova Scotia, Canada.
2. Abidin, Z. A., Fahmi, M. R. and Rahmat, N. R (2011), "Characteristic of color and COD removal of azo dye by advanced oxidation process and biological treatment". International Conference on Biotechnology and Environment Management IPCBEE, vol. 18.
3. Adel al-kdasi, Azni idris, Katayon saed, Chuah teong guan (2004), "Treatment of textile wastewater by advanced oxidation processes – a review", University Putra Malaysia 454443400 UPM Serdang, Selangor, Malaysia.
4. A. Aleboyeh, Y. Moussa, H. Aleboyeh, (2005) "The effect of operational parameters on UV/H_2O_2 decolourisation of Acid Blue 74," Dyes and Pigments, vol. 66, pp. 129- 134.
5. C. Galindo and A. Kalt, (1998), "UV-H_2O_2 oxidation of mono azo dyes in aqueous media: a kinetic study, Dyes and Pigments", Vol 4, pp27-35.
6. Gohl, E. P. and Vilensky, L. D, (2005) "Textile Science". CBS Publishers &Distributors, New Delhi.
7. Joanne M. Bell, Carina Buckley, (2003), "Treatment of a textile dye in the anaerobic baffled reactor", Pollution Research Group, School of Chemical Engineering, University of Natal, Durban, 4041, South Africa.
8. Minghua Zhou, (2007), "Degradation of azo dye by three clean advanced oxidation processes: Wet oxidation, electrochemical oxidation and wet electrochemical oxidation—A comparative study" Dec, Electrochimica Acta 53(4):1902-1910
9. Mohamed A. Hassaan, Ahmed El Nemr, (2017), "Advanced Oxidation Processes for Textile Wastewater Treatment", Marine Environment Division, National Institute of Oceanography and Fisheries, Alexandria, Egypt.
10. Modirshahla N, Behnajady MA, Ghanbary F, (2007), "Decolorization and mineralization of C.I. Acid Yellow 23 by Fenton and photo-Fenton processes". Dye Pigm 2007; 73: 305-310.
11. Metcalf, Eddy, (2003), "Wastewater engineering treatment and reuse", Fourth Edition, McGraw- Hill, New York.
12. Shashank Singh Kalra, Satyam Mohan, Alok Sinha and Gurdeep Singh, (2011), "Advanced Oxidation Processes for Treatment of Textile and Dye Wastewater" A Review 2nd International Conference on Environmental Science and Development, IPCBEE vol.4 IACSIT Press, Singapore.
13. Sumathi Suresh**,** (2015), Treatment of Textile Dye Containing Effluents", Indian Institute of Technology Bombay.

9th International Engineering Symposium - IES 2020
March 3-5, 2020, Kumamoto University, Japan

LABORATORY PERFORMANCE STUDIES ON BITUMINOUS CONCRETE MIX WITH DIFFERENT FILLERS

Ranjith R[1], Rekha H B[2] and **Manjesh L[3]**

1 *Research scholar, Department of Civil Engineering, University Visveswaraya College of Engineering, Bangalore University, Bangalore 560056 Karnataka, India. email: ranjithgowda111@gmail.com*
2 *Associate Professor, Department of Civil Engineering, University Visveswaraya College of Engineering, Bangalore University, Bangalore 560056, Karnataka, India. email: rekhahb@gmail.com*
3 *Professor, Department of Civil Engineering, University Visveswaraya College of Engineering, Bangalore University, Bangalore 560056, Karnataka, India. email: manjeshl@yahoo.co.in*

ABSTRACT: In the present experimental studies, an attempt has been made to design the bituminous concrete mixes by Marshall method using both conventional (VG 30) and polymer modified bitumen (PMB 40) with two different fillers i.e., stone dust and Pond Ash and also laboratory performance studies like Indirect tensile strength, moisture susceptibility and fatigue tests by varying temperature from 10 to 60°C on both conventional bituminous concrete mix and polymer modified bituminous mix were carried out. Experimentally evidenced that polymer modified bituminous concrete (PMBC) mix with stone dust and Pond Ash as fillers showed higher Marshall stability when compared to conventional bituminous concrete (BC) mix and ITS decreases with increase in temperature. Further, the PMBC mixes showed higher indirect tensile strength compared to BC mixes. PMBC mix showed higher fatigue life than BC mix with stone dust and Pond Ash as fillers.

Keywords: - **Polymer modified bituminous concrete (PMBC),Bituminous Concrete(BC), Stone dust, Pond Ash, Marshal Stability, Indirect Tensile Strength (ITS), Temperature Sensitivity, Fatigue.**

INTRODUCTION

The fast development of urban communities as of late brought about a great deal of transportation. In tropical nations, the ordinary temperature in late spring will make the black-top material end up plainly gentler. Different materials, for example, concrete, lime, rock powder, stone clean and fine sand are typically utilized as filler in bituminous blends

The scope of the present study is to analyse the effect of two different fillers and the effect of temperature by carrying out experimental investigations such as Marshall test, indirect tensile test, tensile strength ratio and fatigue tests on bituminous concrete mixes using VG-30 and PMB 40 as binders.

In the laboratory, the fatigue response of bituminous concrete mixes with VG-30 and PMB 40 as binders and two different fillers (Stone dust and Pond Ash) have been studied using indirect tensile fatigue test. The test frequency has been set at 2 cycles per second (2Hz) with a rest period of 0.20 seconds. Tests were carried out at 10°C, 20°C, 30°C 40°C, 50°C and 60°C respectively.

The bituminous mix using PMB 40 as binders and Stone dust as fillers showed higher indirect tensile strength compared to PMBC mix with Pond Ash as fillers and bituminous mixes with VG-30 as binder using stone dust and Pond Ash as fillers. Bituminous concrete mix with PMB 40 as binder and stone dust as filler showed higher fatigue life compared to other bituminous mixes

The objectives of the present study

1. To design bituminous concrete mixes using VG-30 and PMB 40 as binders with grade II aggregate gradation by Marshall mix design method using stone dust and Pond Ash as fillers.
2. To compare the Marshall properties of conventional (VG-30) bituminous concrete (BC) mix and polymer modified bituminous concrete (PMBC) mix.
3. To determine the Indirect tensile strength (ITS) and Moisture susceptibility of bituminous concrete mix with VG-30 and PMB 40 as binders at six different temperatures viz., 10, 20,30,40,50 and 60°C respectively.
4. To determine the fatigue properties of conventional (VG-30) bituminous concrete (BC) mix and polymer modified bituminous concrete (PMBC) mix at six different temperatures viz., 10, 20,30,40,50 and 60°C respectively.

EXPERIMENTAL INVESTIGATION

A. Materials Used

- **Aggregates**

The aggregates were procured from a local quarry named Cauvery Asphalts at Bengaluru in the state of Karnataka, the test results are given in the Table 2.1, and Table 2.2 gives the recommended gradation limits by MoRT&H for BC Mix Grade II**.**

Table 1.1 Test results of aggregates

Aggregate Test	Test result	Requirements as per Table 500-18 of MORT&H (V Revision) Specifications
Aggregate impact value (%)	22.65	Max 24%
Los Angeles abrasion value (%)	25.90	Max 30%
Combined Index (%)	25.10	Max 30%
Water absorption (%)	0.38	Max 2%
Aggregate specific Gravity		
• Coarse aggregates	2.62	----
• Fine aggregates	2.64	----

- **Binder**

Bitumen acts as a binding agent to the aggregates, fines and stabilizers in bituminous mixtures. Binder provides durability to the mix. The characteristics of bitumen which affects the bituminous mixture behaviour are temperature susceptibility, visco-elasticity and aging. The behaviour of bitumen depends on temperature as well as on the time of loading. It exhibits both viscous as well as elastic properties at the normal pavement temperature. Though at low temperature it behaves like an elastic material and at high temperatures its behaviour is like a viscous fluid.

Table 1.2 VG-30 Binder Test results

Tests on Bitumen	Results	Requirements as per IS 73-2013
	VG 30	

Penetration at 25°C	**65**	Min 45
Softening point (Ring & Ball), °C	**52**	Min 47
Flash point, °C	**252**	Min 220
Ductility @27 °C, cm	**84**	Min 40
Specific gravity	**1.02**	Min 0.99

Table 3.3 Test Results of PMB 40 Binder

Particulars	**Results PMB 40**	**Requirements as per Table-2 of IRC SP-53-2010**
Penetration at 25°C, 100gm, 5 Seconds, 0.1mm	**39**	30-50
Softening point (Ring & Ball), °C	**68**	Min 60
Flash point, °C	**280**	Min 220
Specific gravity	**1.03**	Min 0.99
Elastic recovery @ 15^0C, %	**62**	Min 60
Separation (Difference in softening point ring ball), °C	**2**	Max 3
Thin Film Oven Test • Loss in mass, %	**0.8**	Max 1.0
• Increase in softening point, °C	**3**	Max 5
• Reduction in penetration of residue at 25^oC, %	**30.76**	Max 35
• Elastic recovery @ 25°C	**56**	Min 50

- **Filler**

Filler fills the voids between aggregate grains and improves the wearing capabilities of mix. It is stored and fed dry into the mix, during or after addition of binder. stone dust/slag dust/ hydrated lime/fly ash/ cement can be used as mineral filler. Also, fine aggregate below 75micron can be used as filler. For this observation stone dust and Pond Ash has been used as filler for both conventional bituminous concrete and polymer modified bituminous concrete mix. The filler also improves the binding property between the aggregate. Filler content of 2% is used in the present study.

- **Stone dust**

Stone dust is one of the conventional filler is used in bituminous concrete mix. Stone dust is obtained from the quarry whose size varies from 300 microns to 75 microns passing. In the study material passing 75 microns is considered as filler. The specific gravity of stone dust is shown in Table 3.4

➢ **Pond Ash**

The Pond Ash is a waste product from boilers, where the coal is burnt to heat the water for preparing the steam, which is a common process in most of coal based thermal power plants. It is mainly obtained from the wet disposal of fly ash. The Pond Ash is a mixture of fly ash and bottom ash, the Pond Ash being coarser and less pozzolonic and hence is not being accepted as pozzolona. Class C Pond Ash is used in the study. The specific gravity, chemical composition and hydrometer analysis of Pond Ash is shown in Table 3.4, 3.5 and 3.6 respectively. The particle size distribution is shown in Fig 3.1

Table 1.3 Specific Gravity of Fillers

Filler	Specific gravity
Stone dust	2.60
Pond Ash	2.16

Table 1.4 Chemical Composition of Pond Ash

Constituent	Pond Ash (%)
Silica (SiO2)	67.40
Alumina (Al2O3)	19.44
Iron Oxide (Fe2O3)	8.5
Calcium Oxide (CaO)	2.7
Magnesium Oxide (MgO)	0.45
Sulphur (SO3)	0.30
Loss of Ignition	3.46

ANALYSIS OF DATA

1. Marshall stability test

Marshall Stability Test was conducted on bituminous concrete mix (GR-II) withpond ash and stone dust as filler and VG-30 and PMB-40 as binder. To determine optimum bitumen content (OBC), Marshall Stability Value, Flow Value, Bulk density, Total Air voids, Voids in Mineral Aggregates and Voids Filled with Bitumen. The relationship of binder content v/s Marshall Properties and graphical comparison between pond ash and without FRP

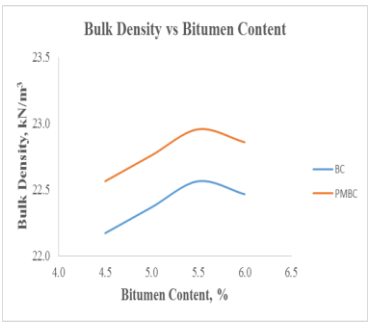

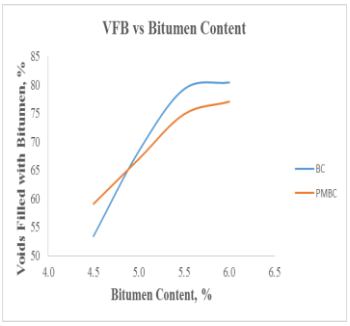

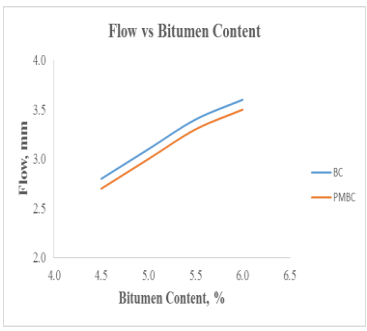

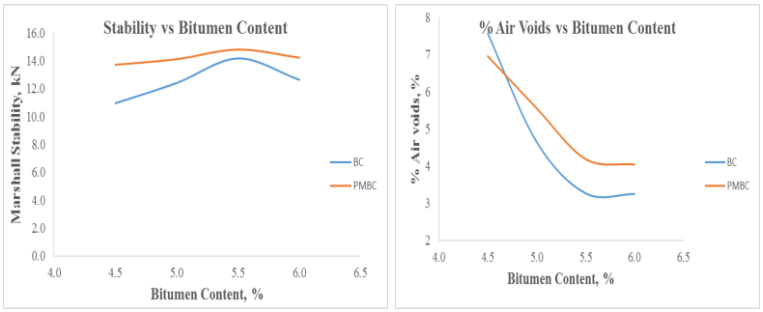

Figure:1 Comparison Between Marshall Properties of BC and PMBC Mixes with Stone dust as filler

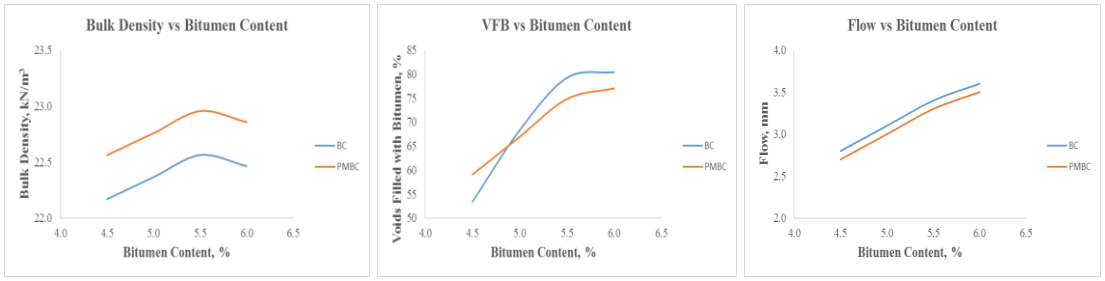

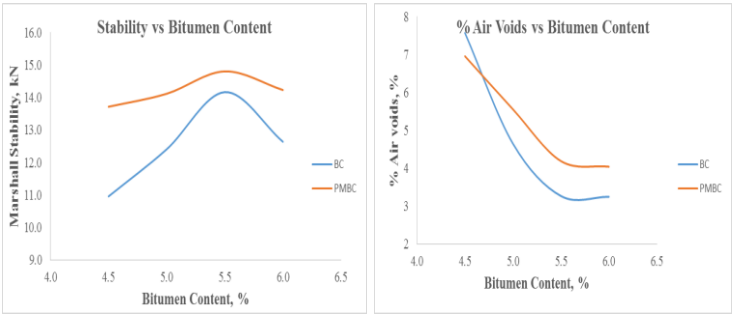

Figure:2 Comparison Between Marshall Properties of BC and PMBC Mixes with Pond Ash as filler

2. Indirect Tensile Strength

Indirect Tensile Strength Test is a pointer of quality and adherence against exhaustion, temperature breaking and rutting. Weakness life of the bituminous blend relies on upon ITS esteem. ITS value fills in as the reason for touching base at stress proportion for completing weakness tests. In this test, compressive load is applied through a vertical strip on Marshall Specimen. Because of the geometry of the specimen, tractable burdens are created and the specimen flops by part into two parts. The heap at failure is recorded and ITS is processed utilizing the condition.

$$S_x = (2 \times P) / (\pi \times D \times t)$$

Where, S_x = Horizontal tensile strength or tensile stress, N/mm2
P = Failure Load, N
D= Diameter of the specimen, mm T = Height of the specimen, mm

3. Tensile Strength Ratio (TSR)

Dampness harm in bituminous blends alludes to the loss of serviceability because of the nearness of dampness. The degree of dampness harm is known as the dampness defenselessness. The ITS test is an execution test which is regularly used to assess the dampness defenselessness of a bituminous blend. Rigidity proportion (TSR) is a measure of water affectability. It is the proportion of the rigidity of water

molded example, (ITS wet, 60°C, and 24 h) to the elasticity of unconditioned example (ITS dry) which is communicated as a rate. A higher TSR esteem normally shows that the blend will perform well with a decent imperviousness to dampness harm. The higher the TSR esteem, the lesser will be the quality lessening by the water drenching condition, or the more water- safe it will be. The Indirect Tensile Test is a standout amongst the most well known tests utilized for hot bituminous blend portrayal in assessing asphalt structures.

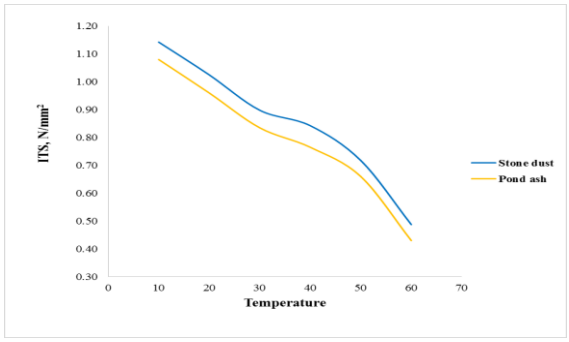

Figure:3 Variation in ITS of PMBC with temperature

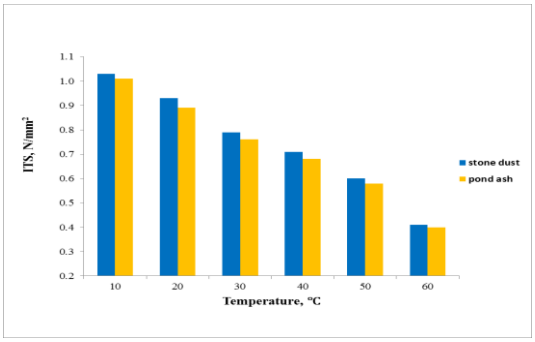

Figure:4 Bar chart showing variation in ITS of PMBC mix with temperature

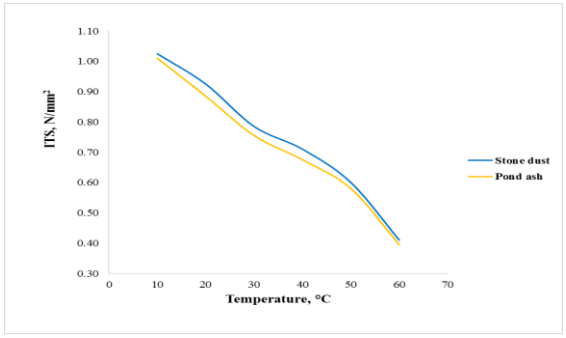

Figure:5 Variation in ITS of BC with temperature

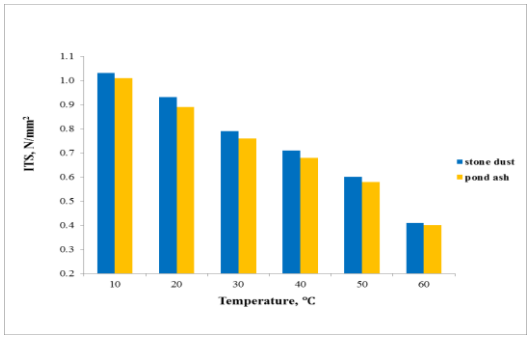

Figure:6 Bar chart showing variation in ITS of BC mix with temperature

4. Indirect Tensile Fatigue Test

The indirect tensile fatigue test was conducted to evaluate the fatigue life of bituminous concrete mixtures. The horizontal deformation during the indirect tension fatigue test is recorded as a function of load cycle. The test specimen is subjected to a different level of stress so that a regression analysis on a range of values allows the development of the fatigue relationship between the number of cycles at failure (N) and initial tensile strain (ε) on a log-log relationship**.**Fatigue life (N) of a specimen is number of cycles to failure for bituminous concrete mix.

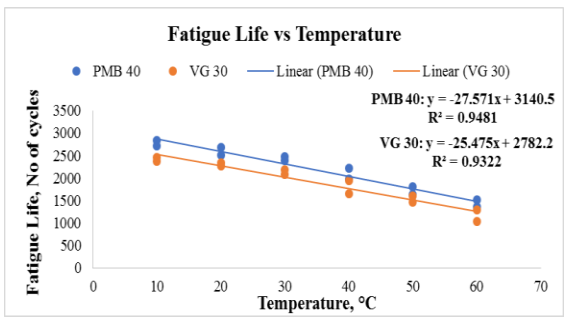

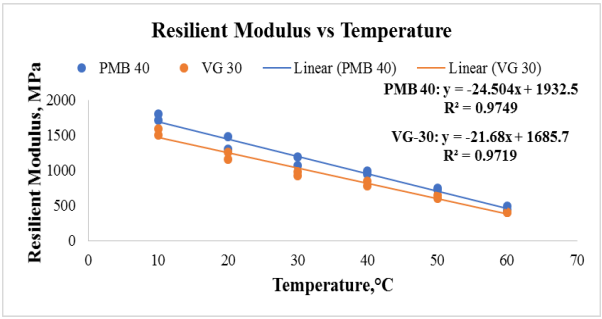

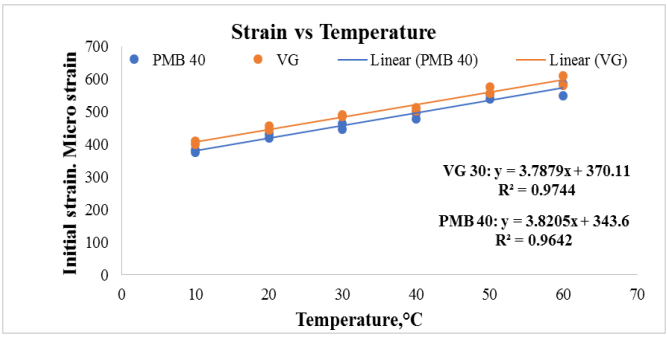

Figure:7 Relationship between fatigue life, resilient modulus and strain vs temperature at 30% stress level for PMBC and BC mixes using Stone dust as filler

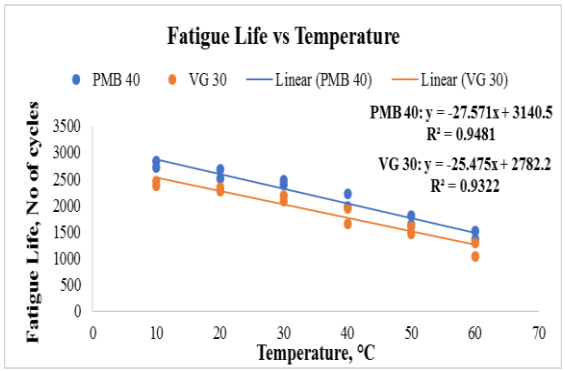

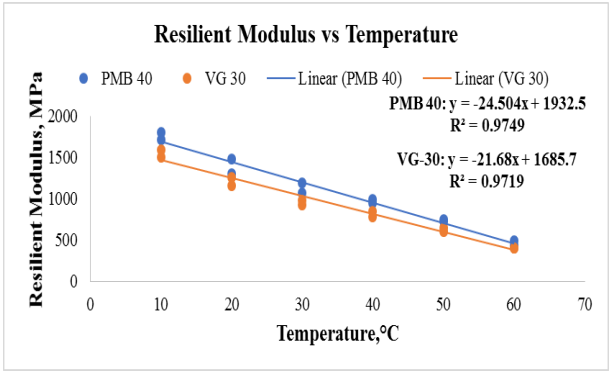

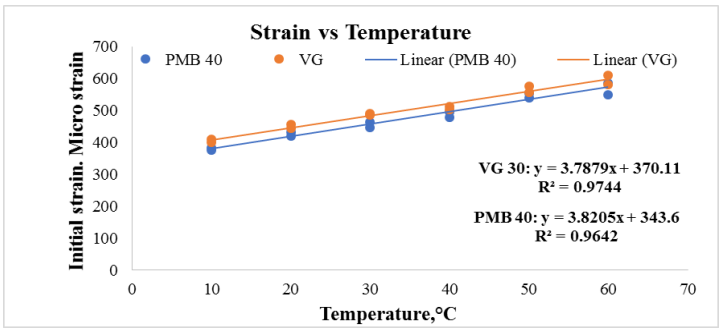

Figure:8 Relationship between fatigue life, resilient modulus and strain vs temperature at 30% stress level for PMBC and BC mixes using Pond Ash as filler

CONCLUSIONS

- The optimum bitumen content for PMBC mix with stone dust and pond as filler is higher when compared to BC mix with Stone dust and Pond Ash as fillers.
- The Marshall properties of PMBC mix is superior than BC mix with Stone dust and Pond Ash as filler.
- The ITS values of PMBC mix is higher than that of BC mix with Stone dust and Pond Ash as fillers, thus from ITS results it can be stated that PMBC mix performs better than conventional BC mix.
- PMBC mix are less temperature susceptible than BC mix with Stone dust and Pond Ash as fillers
- The fatigue life of PMBC mix with Stone dust and Pond Ash as fillers is higher than that of BC mix with Stone dust and Pond Ash as filler.

REFERENCES

1. **Awanti, S. S., Amarnath, M. S., and Veeraragavan, A., (2007),** "*Influence of Rest Periods on Fatigue Characteristics of SBS Polymer Modified Bituminous Concrete Mixtures*", International Journal of Pavement Engineering, Vol. 8 (3), pp. 177-186.
2. **Chetan M K and Sowmya N J (2015)** "*Utilization of Copper Slag in Polymer Modified Bituminous Concrete with A Stone Dust and Fly Ash as Filler*" International Journal for Research in Applied Science & Engineering Technology (IJRASET), Volume 3 Issue VI, ISSN: 2321-9653
3. **Debashish Kar, Mahabir Panda and Jyoti Prakash Giri (2014)** "*Influence of Fly-Ash as A Filler in Bituminous Mixes*" ARPN Journal of Engineering and Applied Sciences vol. 9, no. 6, ISSN 1819-6608
4. **Dipu Sutradhar, Mintu Miah, Golam Jilany Chowdhury and Mohd. Abdus Sobhan (2015)** "*Effect of Using Waste Material as Filler in Bituminous Mix Design*" American Journal of Civil Engineering, 3(3): 88-94, ISSN 2330-8729
5. **Durga Priyanka B, Ajay Kumar P.V, Dedeepya.K, Shabuddin.A and Krishna Rao.S (2014)** "*Use of Fly Ash as Mineral Filler for Bituminous Paving*" International Journal of Research in Engineering and Technology, Volume: 04 Special Issue: 01, ISSN 2319-1163
6. **Ravindra Tomar, Jain R K and Kostha M K (2013)** "*Effect of Fillers on Bituminous Paving Mixes*" International Journal of Engineering Research and Science & Technology, vol. 2, no. 4, ISSN 2319-5991
7. **Satyajeet Pradhan, Pragnanando Roy (2008)** "*Effect of fillers on Bituminous Paving Mixes*" NIT Rourkela
8. **Satyakumar M, Satheesh Chandran R. and Mahesh M.S (2013)** "*Influence of Mineral Fillers on The Properties of Hot Mix Asphalt*", International Journal of Civil Engineering and Technology (IJCIET), Volume 4, Issue 5.
9. **IRC SP 53-2010** "*Specifications for modified bitumen*" Indian road congress, New-Delhi.
10. **IS 73-2013** "*Specification for paving bitumen*" Bureau of Indian Standards, New Delhi.
11. **MORT&H "***Specifications for Road and Bridge Works***"- 2013**, Fifth Revision, Indian Roads Congress, New Delhi.
12. **IRC 111-2009, "***Specification for Dense Graded Bituminous Mixes",* Indian Road Congress, New-Delhi, India.
13. **ASTM D 6931 (2012), "***Indirect Tensile (IDT) Strength for bituminous mixtures"* American Society for Testing and Materials, Philadelphia, USA.
14. **ASTM D 4123-82 (1995),** *"Standard Test Method for Indirect Tension Test for Resilient Modulus of Bituminous Mixtures",* American Society for Testing and Materials, Philadelphia, USA.
15. **Khanna S.K., Justo C.E.G. and Veeraragavan A**, A Text Book on "*Highway Engineering*", Revised 10th Edition, Nem Chand & Bros., Roorkee, India, ISBN 978-81-85240-80-0.

9th International Engineering Symposium - IES 2020
March 3-5, 2020, Kumamoto University, Japan

IMPACT BEHAVIOUR OF RAILWAY PSC SLEEPER USING NANO BASED CARBON WITH FIBER REINFORCED CONCRETE

Sadath Ali Khan Zai [1], Guruswamy J [2] and Shashisankar A[3]

1 Professor, Department of Civil Engineering, UVCE, Bangalore University, Bangalore, Karnataka, India. email Id: drsakzaiuvce@gmail.com
2 Research Scholar, Jain University, Bangalore, Karnataka, India & Lecturer, Department of Civil Engineering, PVP Polytechnic, Dr.AIT Campus, Bangalore-56. email Id: guruhalasurkar@gmail.com
3. Professor and Head, Dept. of civil Engineering, AMC Engineering College, Bangalore, Karnataka,India. email Id: shashianant@gmail.com

ABSTRACT: This paper presents the studies on under repeated low-energy horizontal impact loading through experimental programs of Railway PSC sleepers integrated with next generation Nano based Carbon along with Fiber Reinforced Concrete. load-time variation, displacement-time history and energy absorption capacity were studied. Carbon nano tube, Carbon fibers, Polypropylene fibers integrated with High Performance Concrete using a design mix of M60 grade of concrete. Five different PSC test specimens were casted and tested viz. M60, M60+CNT, M60+CNT+PF, M60+CNT+CF, M60+CNT+PF+CF. Carbon Nanotubes were first dispersed in deionized water and surfactant using an ultrasonic mixer, then the CNTs, Carbon fibers, Polypropylene fibers were combined with concrete as per state-of -art techniques. It can be seen that the properties of concrete matrix used in PSC railway sleepers were enhanced with respect to energy absorption capacity and peak load.

Keywords: **Carbon Nanotubes(CNTs), Carbon fibers, Polypropylene fibers, load time history, displacement time history , energy absorption capacity, Impact load, Railway PSC sleepers.**

INTRODUCTION

INTRODUCTION

India is a land of diverse culture, and Railways play a key role in not only meeting the transport needs of the country. Indian Railways is the backbone of the country's transport infrastructure integrating market and connects communities all over the country. Indian Railways is the fourth largest railway networks in the world (after USA, China and Russia) with a rail network length of 67,368 kilometers (In 2017) and runs approximately 11,000 trains in a day. A major portion of the railway network in India is more than a century old. With the passage of time, this network is showing signs of ageing; but it still has to cater to the ever-increasing rail traffic. Not only the total number of trains plying on the network is rising, also the speed, the axle loads and the number of bogies attached to the trains is also increasing. All this calls for a thorough and fast modernization of the sprawling railway network through development of new design concepts and use of advanced materials.Prestressed Concrete (PSC) railway sleeper is an imperative component of ballasted railway tracks. The primary function of the railway sleeper is to transmit the wheel load to the ballast medium. The premature deterioration of railway sleepers is due to rail-seat deterioration, cracking and damaging

under different loading conditions and adverse environment conditions. The undetermined ultimate load capacity of track components has been under suspicion for some time, regardless of the fact that they are subjected to impact dynamics induced by wheel/rail interaction, irregularities, and so on along with the static loads. The key to damage-resistant concrete and long-life concrete structures, which has been known for a long time, lies in enhancing the tensile strength and fracture toughness of concrete material which is achieved by reinforcing fibers in concrete.

LITERATURE REVIEW

In general, the axle loading tends to physically behave like the dynamic impact pulses due to the continual moving ride over track irregularities and faster speeds .Concrete with strength of above 40 Mpa is generally termed as high strength concrete. Toughness and ductility properties of conventional concrete can be significantly improved by addition of fibers such as carbon and polypropylene fibers into conventional concrete(1,2,3). Impact is a dynamic phenomenon. The impact event can be classified into low velocity, intermediate velocity and high velocity regions. A combination of rigid target and flexible striker or rigid striker and flexible target can be used., impact problems can be classified as high energy impact loading problem or low energy repeated impact loading problems(12,13,14). The impact load was monitored and recorded by the dynamic load cell connected to the computer(4). the stiffness degradation of reinforced concrete beams under repeated low-energy impact load using Horizontal impact test on beam of size 100 X 200 X 2300mm with M40 concrete, Schrader's test device (as per ACI-544 committee) for impact test on concrete specimen 152mm dia and 62.5mm thick with M30 concrete matrix(5). PSC railway sleeper test specimen was placed on the base plate between four positioned lugs at the periphery, steel ball placed on top of the PSC railway sleeper test specimen and drop hammer was used to apply the impact load[6,11]. Impact behaviour of structural elements can be increased by using higher toughness and high absorbed capacity can be achieved by inclusion of fibers. It was observed that, the Load-Time history under impact loading is essentially triangular. The duration of the impact pulse remains as a constant, while the peak force reduces with increased number of impact blows for a given energy of impact loading[7,8,9,10]. Hence, the present experimental investigation aims at full understanding of the influence of cementitious materials such as GGBS, Silica Fumes, Carbon fibers, polypropylene fibers, Carbon Nanotubes by preparing PSC railway sleepers test specimens subjected to low velocity repeated impact loading to study load-time variation, displacement-time and energy absorption capacity.

EXPERIMENTAL PROCEDURE

A series of five PSC railway sleeper test specimens were casted as per IRS, T-39 . Cement (53-S conforming to IRS/T-40-1985), Multi wall Carbon nano tubes, fine aggregate (Zone II Grade), 20 mm down size coarse aggregate. Super plasticizer (AURACAST 270M) was added in the ratio of 0.4 liter per 100 kg of binder, 0.5% of carbon fiber, 900grams of polypropylene fiber for one bag of cement, 8% of Silica fume (as cement replacement) and 21.6 % GGBS were used. The mix ratio adopted is 1:1.061:2.499 with water binder ratio of 0.263 with characteristics strength of concrete 60 N/mm^2. Each set of PSC railway sleepers test specimens were subjected to impact loading. The hammer is 170 mm in diameter and 320 mm in length, which forms the main striking mass. The hammer attached with the load cell strikes the test specimen with an effective mass equal to mass of the hammer and the mass of the load cell. The effective weight of hammer together with load cell is 50 tons. The impact responses and repeated impact loads are monitored and stored during 1, 20, 40, 60, 80, 100, 120, 140, 160, 180, 200 and up to the failure of PSC railway sleepers test specimens were recorded load-time variation, displacement-time variation and energy absorption capacity were observed.

INSTRUMENTATION

The impact testing machine used in the present experimental investigation is of pendulum type instrumented horizontally impact testing machine as shown in Fig 1. The instrumented pendulum consists of steel impact hammer, which strikes the PSC railway sleepers test specimens horizontally at the mid span. The dimension of the hammer is 170 mm dia. and 320mm length, which is fitted with instrumented hammer head to record the dynamic responses. To record the different responses during impact loading. linear variable differential transformer (LVDT), Load cell are used and are as shown in Fig 2. The post processing of recorded data is carried out using a data acquisition system, which is equipped with MS Visual Basic 6.0 software.

TEST PROCEDURE

Pendulum Type Horizontal Impact Testing Machine is used for repeated low-energy impact loading test on PSC railway sleepers test specimens. The specimens were held rigidly between two rigid steel supports such that spherical steel hammer head attached with load cell can hit the PSC railway sleepers test specimen exactly at its mid-width and at center of span. The mechanical stopper arrangement behind the hammer is adjusted and kept at a known distance so as to get the desired height of fall of 1.0 m for a required energy level and the hammer is held back manually after every hit to avoid a second impact on the sleeper. The load cell attached to the striking hammer gives the load-time variations and displacement-time variations are recorded using LVDT for the following PSC railway sleepers test specimens viz: M60 (S1), M60+CNT (S2), M60+CNT+PF (S3), M60+CNT+CF (S4) and M60+CNT+PF+CF (S5)

Figure. 1 Pendulum Type Horizontal Impact Testing Machine

Figure.2 LVDT Instrumentation Used In Experiment

TEST RESULT

The experimental test results obtained for the dynamic response of PSC railway sleepers test specimens consists of responses like, load-time variation, displacement-time variation and energy absorption capacity.

1. Load-Time Variation

The load-time variation which has to be expressed in terms of pattern of variation in peak load and area under the load time curve. The peak load value and the duration of impact on the specimen is obtained at regular intervals using load cell attached to the impact hammer. Figure 3 shows the Load –Time variation for PSC sleeper test specimens obtained at first impact blows for M60 (S1), M60+CNT (S2), M60+CNT+PF (S3), M60+CNT+CF (S4) and M60+CNT+PF+CF (S5) respectively.

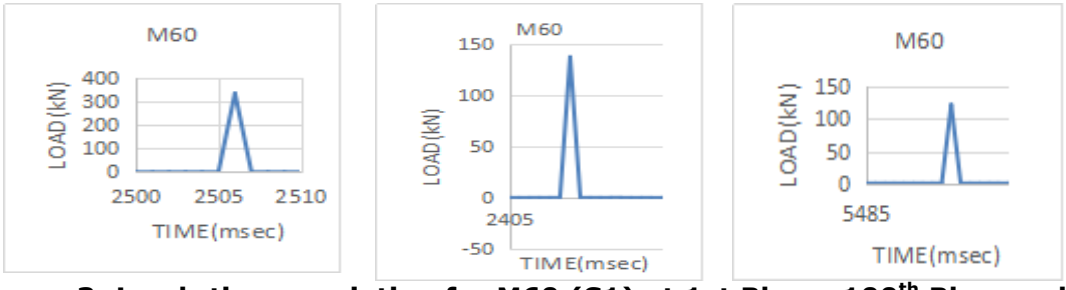

Figure 3: Load- times variation for M60 (S1) at 1st Blow , 100th Blow and Last Blow

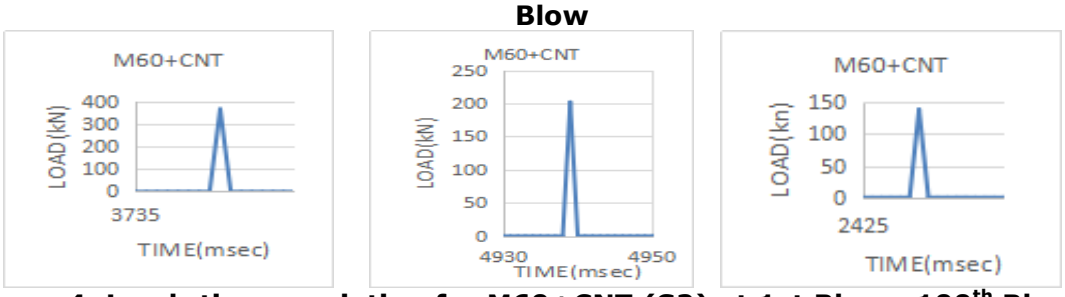

Figure 4: Load- times variation for M60+CNT (S2) at 1st Blow , 100th Blow and Last Blow

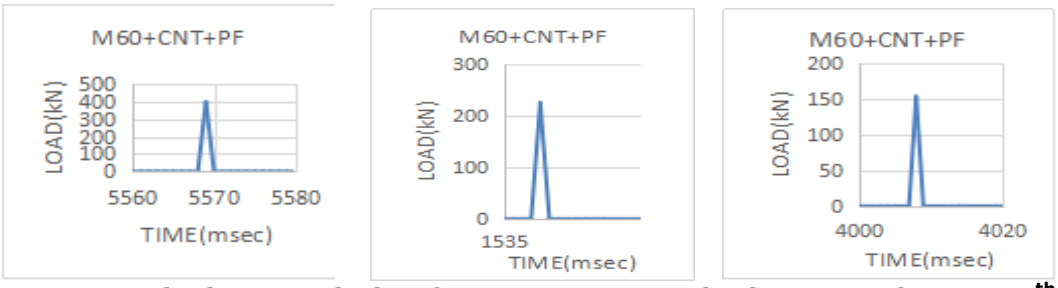

Figure 5: Load- times variation for M60+CNT+PF (S3) at 1st Blow , 100th Blow and Last Blow

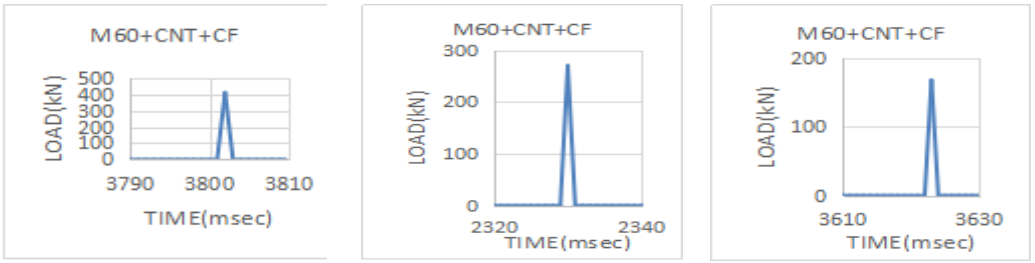

Figure 6: Load- times variation for M60+CNT+CF (S4) at 1st Blow , 100th Blow and Last Blow

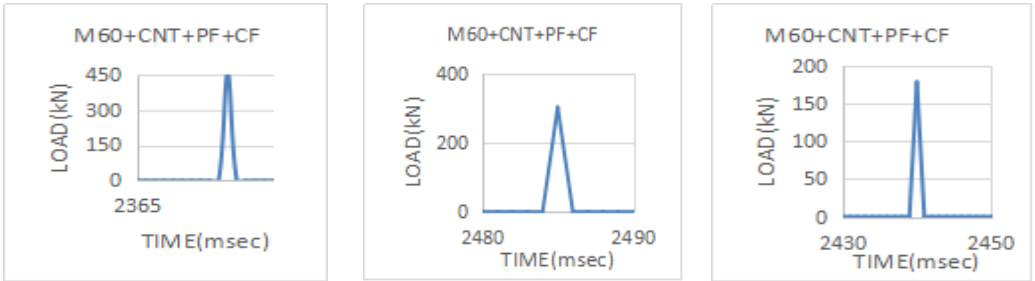

Figure 7: Load- times variation for M60+CNT+PF+CF (S5) at 1st Blow , 100th Blow and Last Blow

Figure 3 – 7 shows the peak load obtained for 1st ,100th and last impact blows for M60 (S1), M60+CNT (S2), M60+CNT+PF (S3), M60+CNT+CF (S4) and M60+CNT+PF+CF (S5), it can be seen that as number of impact blows increase peak load decreases. The highest peak load obtained for the M60+CNT+PF+CF (S5). 455.00 kN for 1st blow and 178.23 kN for last blow (200th blow) as compared to PSC railway sleepers test specimen (S1, S2, S3 and S4)

1.2 Variation of Peak Load with Number of Impact Blows

The variation of peak load with no of impact blows for psc railway sleepers test specimens M60 (S1), M60+CNT (S2), M60+CNT+PF (S3) ,M60+CNT+CF (S4) and M60+CNT+PF+CF (S5) are as shown in figure 8.

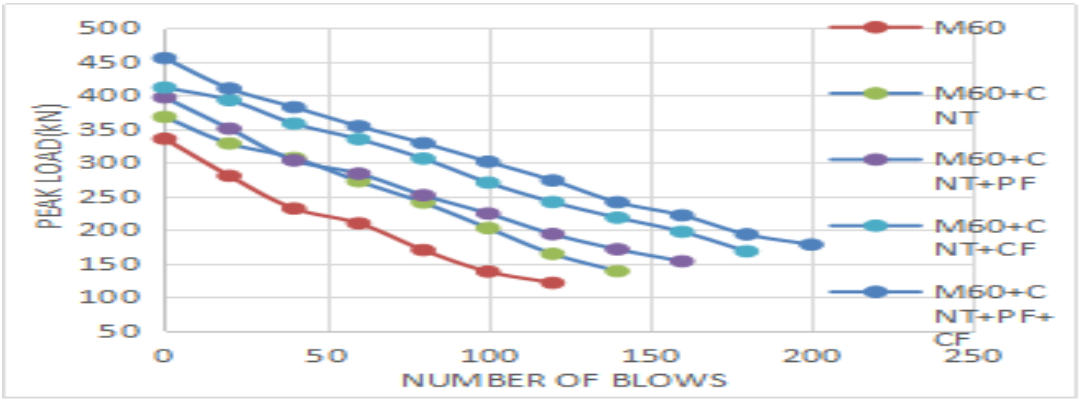

Figure 8: Variation of Peak Load v/s Number of blows for all test PSC railway sleeper specimens

From figure 8, it can be observed that the duration of impulse during each impact essentially remains a constant and load-time variation on all PSC railway sleepers test specimens for M60 (S1), M60+CNT (S2), M60+CNT+PF (S3), M60+CNT+CF (S4) and M60+CNT+PF+CF (S5). The shape of pulse is always triangle. Peak load is registered at the center of impulse. The time duration of pulse ranges from 25 to 30 millisecond based on test results. Hence, in this experiment the duration of pulse loading can be considered as 30 milisecond. Further the peak load indicated by the load cell reduces with increase in no. of impact blows

2 Displacement Time History

The displacement-time variations for the M60 (S1), M60+CNT (S2), M60+CNT+PF (S3), M60+CNT+CF (S4) and M60+CNT+PF+CF (S5) for different number of impact blows are recorded and are as shown in figure 13- 21 and table 2

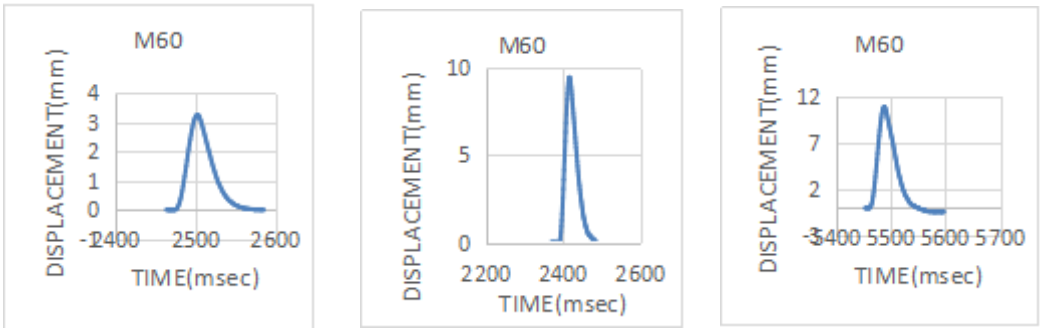

Figure 9 :Displacement variation for M60 (S1) at 1st Blow , 100th Blow and Last Blow

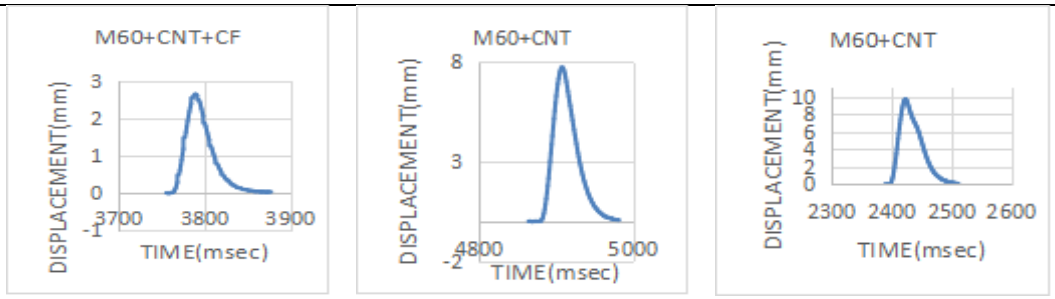

Figure 10 :Displacement variation for M60+CNT (S2) at 1st Blow , 100th Blow and Last Blow

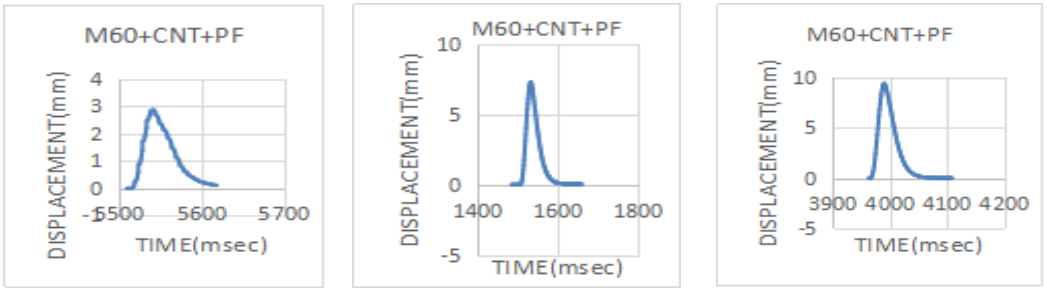

Figure 11 :Displacement variation for M60+CNT+PF (S3) at 1st Blow , 100th Blow and Last Blow

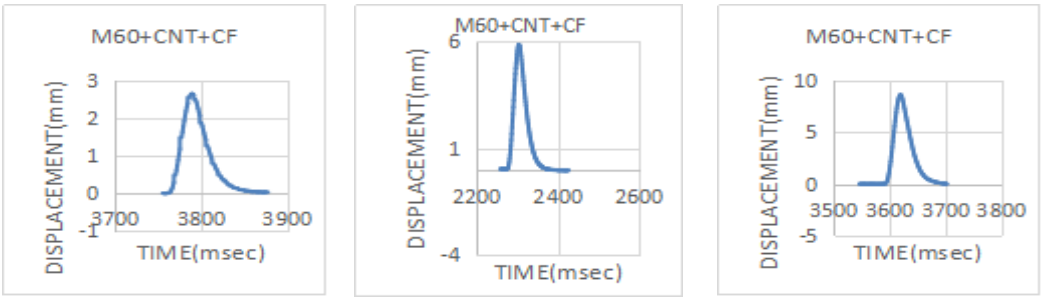

Figure 12 :Displacement variation for M60+CNT+CF (S4) at 1st Blow , 100th Blow and Last Blow

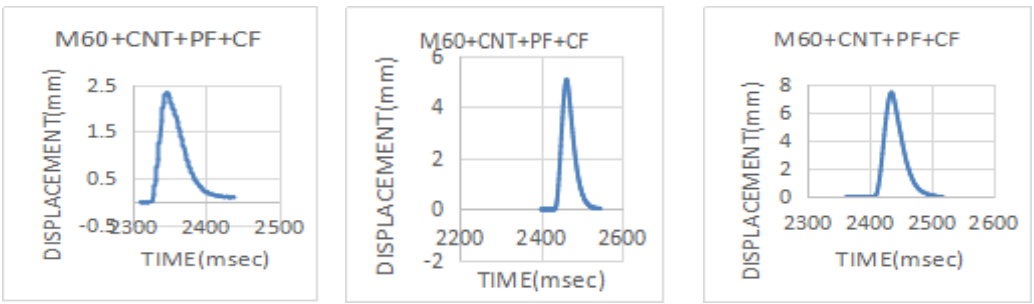

Figure 13 :Displacement variation for M60+CNT+PF+CF (S5) at 1st Blow , 100th Blow and Last Blow

Figure 9– 13 shows the displacement variation obtained for 1st ,100th and last impact blows for M60 (S1), M60+CNT (S2), M60+CNT+PF (S3), M60+CNT+CF (S4) and M60+CNT+PF+CF (S5). It can be seen that as number of impact blows increases displacement increases. The displacement obtained for the M60+CNT+PF+CF (S5) is 2.21mm at 1st blow and 7.26mm for last blow (200th blow). Whereas 3.12mm, 2.90mm, 2.69mm and 2.43mm for 1st blow obtained for other test specimens (S1, S2, S3 and S4).

3 Energy absorption capacity

During the low velocity repeated impact load on PSC railway sleepers test specimens, impact input energy (Eb_o = mgh) partly get absorbed by the dynamic behaviour of that element. This absorbed energy capacity gives its ability to sustain the dimensional integrity or internal resistance capacity during the low velocity impact experiment. The load-time variation data are used to calculate energy absorption capacity for M60 (S1), M60+CNT (S2), M60+CNT+PF (S3), M60+CNT+CF (S4) and M60+CNT+PF+CF (S5) are given in figures 22-26.

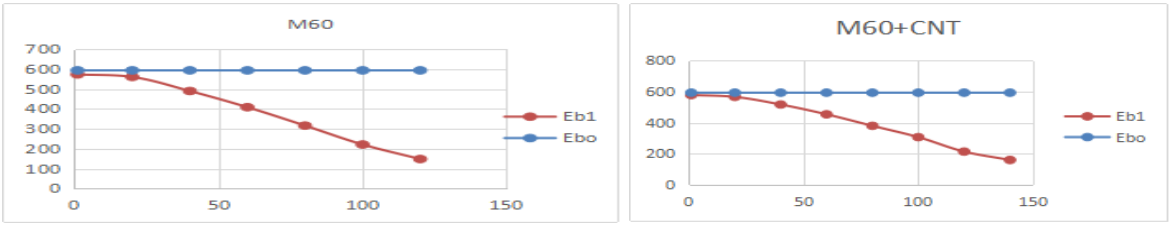

Figure 14: Variation of Energy (Ebo and Eb1) with increased number of blows for PSC sleeper test specimen M60 and M60+CNT

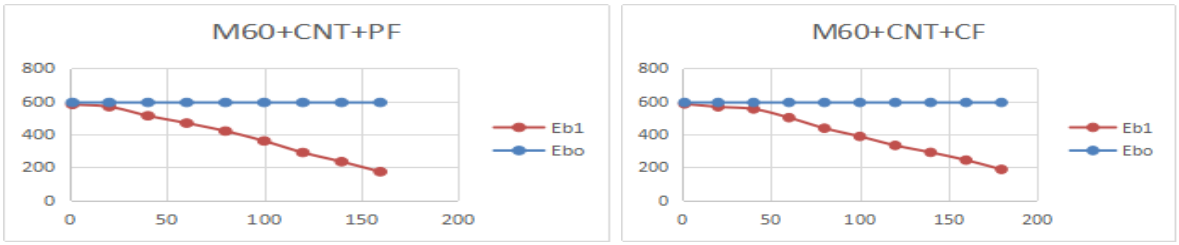

Figure 15: Variation of Energy (Ebo and Eb1) with increased number of blows for PSC sleeper test specimen M60+CNT+PF and M60+CNT+CF

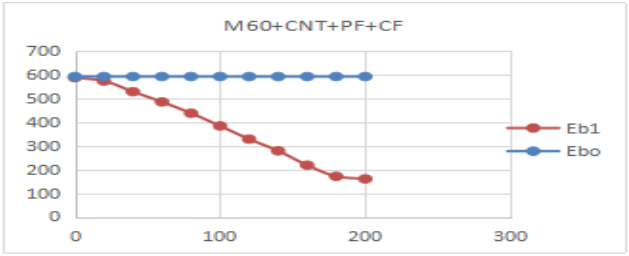

Figure 16: Variation of Energy (Ebo and Eb1) with increased number of blows for PSC sleeper test specimen M60+CNT+PF+CF

Figure 14-16 and table 3, shows the energy absorption capacity for PSC railway sleeper test specimen M60 (S1), M60+CNT (S2), M60+CNT+PF (S3), M60+CNT+CF (S4) and M60+CNT+PF+CF (S5). It is observed that the highest energy absorption capacity is obtained for M60+CNT+PF+CF (S5).

CONCLUSIONS

1. From the experimental results of load carrying capacity obtained for PSC railway sleeper test specimens for M60 (S1:Control), M60+CNT (S2), M60+CNT+PF (S3), M60+CNT+CF (S4) and M60+CNT+PF+CF (S5) are 335.34kN, 367.75kN, 396.75kN, 411.32kN and 455kN respectively. It is observed that load carrying capacity has been increased by 9.6%, 18.31%, 22.65%, and 35.68% for M60+CNT (S2), M60+CNT+PF (S3), M60+CNT+CF (S4) and M60+CNT+PF+CF (S5) with respect to M60 (S1:Control),. Hence it can be concluded that there is a significant increase of 35.68%, in the load carrying capacity for M60+CNT+PF+CF (S5) w.r.t M60 (S1:Control).

2. Displacement time records for M60 (S1:Control), M60+CNT (S2), M60+CNT+PF (S3), M60+CNT+CF (S4) and M60+CNT+PF+CF (S5) at different number of impact blows. The peak amplitude of the displacement increases with increase in number of impact blows., maximum displacement obtained for the last impact blows for, M60 (S1), M60+CNT (S2), M60+CNT+PF (S3), M60+CNT+CF (S4) and M60+CNT+PF+CF (S5) are 10.48mm, 9.70mm, 9.40mm, 8.62mm and 7.4mm respectively
3. The energy absorption capacity obtained for the test sleeper specimens of M60 (S1), is 573.04 Joules and whereas for the M60+CNT (S2)**,** M60+CNT+PF (S3), M60+CNT+CF (S4) and M60+CNT+PF+CF (S5) are 578.30 Joules, 581.63 Joules, 584.72 Joules and 589.13 Joules respectively. It is experimentally evident that M60+CNT+PF+CF (S5) gives highest energy absorption capacity as compared to the other PSC sleeper test specimens

REFERENCES

1. A. Sivakumar, V.M. Sounthararajan and S. Thirumurugan "Mechanical Performance of High Strength Concrete Matrix with Fibre Combinations", World Applied Sciences Journal 26 (1): 126-137, 2013 ISSN 1818-4952 2013 DOI: 10.5829,.2013.
2. A.M. Shende, A.M. Pande, M. Gulfam Pathan, 'Experimental Study on Steel Fiber Reinforced Concrete for M-40 Grade', ISSN:2319-1821 Volume 1, Issue 1 (September 2012), PP. 043-048.(NSC)
3. H.M.Somasekharaiah , Mahesh Sajjan , Nelson Mandela "A study on fiber reinforced high performance concrete using multiple mineral admixtures" IJRET: International Journal of Research in Engineering and Technology eISSN: 2319-1163 | pISSN: 2321-7308
4. Sakdirat Kaewunruen and Alex M. Remennikov. (2007), "Investigations of static and dynamic performance of railway PSC sleepers", SEM Annual Conference and Exposition on Experimental and Applied Mechanics., Spring_eld., Massachusetts
5. Rajagopalan N, Lakhmanan,Muthumani K, "Stiffness Degradation of reinforced concrete beam under repeated low energy impact loading" The Indian concrete journal, April, 1995,pp.227-234
6. Balasubramanian K, Bharathkumar B H, Gopalakrishnan S and Parameswaran V S, "Impact Resistance of steel Fiber reinforced concrete, The Indian concrete journal, May, 1996,pp.257-262.
7. Andreas, P. Christoforou, "Impact Dynamics and Damage in Composite Structures," Journal of Composite Structures, Vol.52, 2001, pp.181-188.
8. Choubey U.B., Uttamasha Gupta and Hitendra Dixit, "Residual strength of Reinforced concrete beams subjected to various impact energy levels" – Journal of structural engg,. Computation, Cape Town, South Africa, 231-237, 1995.
9. Hughes G. and Beeby A.W., "Investigation of the effect of impact loading on concrete beams" The structural Engineer, 45-52, 1982.
10. Indrajit Ray, A P Gupta & M Biswas, "Effect of Latex and Superplasticizer on Portland Cement Mortar in the Fresh State," Cement & Concrete Composites, Vol. 16, 1994, pp. 309-316
11. Lakshmanan, N., Srinivasulu, P., Muthumani, K., Sivarama Sarma, B., and Goplakrishnan, N., "Behavior of Fiber Reinforced Concrete Beams under Repeated Impact Loading," Proceedings of ASCE, Journal of Structural Engineering, Vol. 18, No. 1, April., 1991, pp. 21-30.
12. Li Bing, Park, R., and Tanaka, H., "Constitutive Behaviour of High Strength Concrete under Dynamic Loads," ACI Structural Journal, Vol. 97, N0. 4, Jul-Aug., 2000, pp. 619-629.
13. Shashikumara S.R , Sadath Ali Khan Zai , Muthumani K., and Munirudrappa N, "Residual Strength of SBR-Latex modified high strength concrete under repeated

9th International Engineering Symposium - IES 2020
March 3-5, 2020, Kumamoto University, Japan

Experimental Studies on Durability Characteristics of Next Generation Nano Based Carbon with Fiber Reinforced Concrete

Showkath Ali Khan Zai [1], Guruswamy J [2] and Shashishank A[3]

1 Guest Faculty, Department of Civil Engineering, UVCE, Bangalore University and Professor and Head (R&D), Islamiah Institute of technology,Bangalore, Karnataka, India and . email Id: showkathzai@gmail.com
2 Research Scholar, Jain University, Bangalore, Karnataka, India & Lecturer, Department of Civil Engineering, PVP Polytechnic, Dr.AIT Campus, Bangalore-56. email Id: guruhalasurkar@gmail.com
3. Professor and Head, Dept. of civil Engineering, AMC Engineering College, Bangalore, Karnataka,India. email Id: shashianant@gmail.com

Abstract- This paper presents the detailed experimental studies on Durability characteristics on carbon nanotubes concrete modified with carbon and polypropylene fiber integrated with High performance concrete (HPC) of grade M60, which reviews advancement in the field of fiber reinforced cementitious composites. Cement concrete is a great source for the construction of buildings, bridges, dams and infrastructures etc., because of its high compressive strength but it has resistance to limited tensile and flexural strength. Thus, for improving its properties, cement concrete is reinforced with fibers, carbon nanotubes (CNTs) and polypropylene fibers. CNT reinforced cement concrete enhances tensile and flexural strength in comparison to fiber reinforced cement composite materials. Though significant research has not been done in this area over the past decade, but more challenges are need to be addressed. For durability tests Acid attack, Sulphate attack and Water absorption are performed as per the specifications of ASTM. The test specimen consists of M-60, M-60+CNT, M-60+CNT+PF, M-60+CNT+CF, M-60+CNT+PF+CF concrete matrices. The present experimental results have shown that there is an improvement in durability properties in concrete by incorporating carbon fiber, Carbon Nano Tubes and polypropylene fiber. It has been recognized as a finer reinforcement which can reduce water absorption and increase acid and sulphate attack resistance of concrete matrices. The results proved that the durability has improved for M60+CNT+PF+CF in comparison with other concrete matrices.

key words: High Performance Concrete (HPC), Carbon Nanotubes (CNTs), Carbon fibers, Polypropylene fibers.

1.0INTRODUCTION

Concrete is the requisite engineering material used in most of the structural engineering. Its vogue as the basic building material in construction is because of its economy, strength, durability, and the ease with which it can be produced at the site. Durability in concrete is an important characteristic to assure serviceability, long life and cost effectiveness. However, over the past several years, structural deterioration has become a critical issue. A more economical approach is to prevent deterioration and avoid the resulting high cost of the rehabilitation and replacement with durable concrete. The solution for the durability characteristics is to improve the resistance to acid attack,

sulphate attack and water absorption. The key to damage-resistant concrete and long-life concrete structures, which has been known for a long time lies in enhancing the strength and durability of concrete material which is achieved by reinforcing fibers in concrete by incorporating carbon fiber, Carbon Nano Tubes, polypropylene fibers.

2.0 LITERATURE REVIEW

Durability is a major concern for concrete structures exposed to aggressive environments. When Reinforced concrete structures are exposed to harsh environments, deterioration of concrete will occur due to many reasons like chloride attack, sulphate attack, acid attack and corrosion of reinforcement [11,13,17] etc. The rate of deterioration of concrete subjected to chemical attack depends not only upon the nature of chemicals but also upon the permeability of concrete and passivating effects of the reaction products [1,10,15]. Fibers are used to increase the strength and durability aspects of the concrete structures. Carbon fibers also offer an economical benefit as they are readily available as a waste product from the aerospace industry and offers 2 to 5 times more rigidity than the other fibers. Carbon fibers possess many potential benefits over other fibers, including a higher strength, higher modulus of elasticity, and increased durability [16,18]. Addition of fibers to the concrete enhances properties of the ductility, tensile strength, flexural strength. Furthermore, adding fibers reduces the possibility of spalling and scabbing failures, prevents crack propagation, and extends the softening region in the concrete matrix [7,12]. The use of fly ash and silica fume is becoming more common because they improve concrete durability and strength, especially where high early age curing temperatures occur [9]. From the literature survey it is found that the progress in the area of CNT, Carbon fiber with integration of HPC has been fairly low, partly due to the high material cost and partly to lack of experimental data for new composite. Hence, in the present experimental investigation an attempt has been made to use CNTs, Polypropelene fibers, Carbon fibers to integrate with high performance concrete on durability characteristics in particular acid attack, sulphate attack and water absorption.

3.0EXPERIMENTAL PROGRAM

The present experimental program was designed to investigate the durability characteristics on carbon nanotubes concrete modified with carbon and polypropylene fiber integrated with High performance concrete (HPC) of grade M60.The experimental studies include casting, curing and testing of sixty (45) number of cube specimens having sizes 150 mm and 100 mm respectively. All the test specimens are cured for 28 days. Acid attack test as per ASTM C 267-01(2012), sulphate attack test as per ASTM C 452-02(2002) and water absorption test as per ASTM C 642(2006) were conducted. The five different concrete matrices considered in present experimental investigations are viz., (i) M- 60 (M-60 Grade of concrete, control mix), (ii) M-60+CNT (Carbon Nano Tubes combined with M-60 Grade of concrete), (iii) M-60+CNT+PF (Carbon Nano Tubes and Polypropylene Fibers combined with M-60 Grade of concrete), (iv) M-60+CNT+CF (Carbon Nano Tubes and Carbon Fibers combined with M-60 Grade of concrete), (v) M-60+CNT+PF+CF (Carbon Nano Tubes, Carbon Fibers and Polypropylene Fibers combined with M-60 Grade of concrete). Three cube specimens of size 150 mm each, for acid attack, sulphate attack tests and 100 mm cube for water absorption were used.

3.1 MATERIALS

In present experimental investigation, Special Grade Portland cement (53-S) conforming to IRS-T-40-1985 was used. Physical properties of cement were conducted in accordance with the Indian standards confirming to IS-12269:1987. Manufacture sand (M-sand), Crushed angular coarse aggregate of size 20 mm and 10mm has been used. The tests on the fine aggregate were conducted in accordance with IS 2386 Part 1 to Part 4-1964 (Reaffirmed-2002) and confirmed Zone-II for requirement as per IRS T-39 Specifications. The tests on the coarse aggregate were conducted in accordance with IS 2386 Part 1 to Part 4-1963 (Reaffirmed-2002). Auracast 270M as Super Plasticizer (chemical admixture), Silica fumes supplied by Elkem India Pvt. Ltd, Navi Mumbai and

Ground Granulated Blast Furnace Slag (GGBFS) supplied by Nuvoco Vistas Corporation Limited, (formerly Lafarge India Ltd.), Bangalore as mineral admixtures. Polypropylene fibers (Recron 3S) supplied by Ranka Udyog, Pvt, Ltd, Bangalore. Carbon fibres of 6mm chopped length supplied by M/s Baseer Fibers Private Limited, Bengaluru, CNTs supplied by Sigma-Aldrich and ordinary potable water were used. Mix design is carried as per ACI 211.4R-93 method and the mix proportions for Next Generation Nano Based Carbon with Fiber Reinforced Concrete matrix was arrived after trail mixes and their compressive strength for M-60, M-60+CNT, M-60+CNT+PF, M-60+CNT+CF, M-60+CNT+PF+CF are tabulated in table 1.

Table 1: Compressive strength for 7,15& 28 days

Properties	Age	M60	M60+CNT	M60+CNT+PF	M60+CNT+CF	M60+CNT+PF+CF
	(Days)	(N/mm^2)	(N/mm^2)	(N/mm^2)	(N/mm^2)	(N/mm^2)
Compressive strength	7	**39.60**	**40.20**	**40.80**	**41.40**	**42.00**
	15	**60.12**	**60.94**	**61.55**	**62.98**	**65.22**
	28	**67.53**	**69.47**	**70.31**	**72.15**	**74.90**

3.1.1. Dispersion of CNTs

The CNT is allotrope of carbon with multiwall. It has to be breakdown by ultrasonication for dispersion through state of art method. The dispersion of CNTs has been done at AZYME BIOSCIENCE PVT. LTD. BANGALORE, first the required water, surfactant and CNTs are measured and then mixed together. In order to ensure a well-dispersed solution, an ultrasonic mixer is used, which can deliver up to 500 watts at 20 kHz. An ultrasonic mixer is a device that uses a high frequency driver to transmit acoustical energy throughout a liquid medium. The energy in the shock waves are extremely high and significantly accelerates chemical reactions and breaks the clumps and agglomerations of particles. To reduce the chances of breaking the nanofilaments, CNTS are mixed for 20 minutes.

3.2 MIX PROPORTIONS

The concrete mix having a compressive strength of 60 N/mm^2 was aimed in the present research investigation, the design mix proportion was obtained by **ACI 211.4R-93 Method** of mix design for high strength concrete. Based on the same, the mix proportions arrived are tabulated in table 2. The Polypropylene fibre, carbon fiber, Auracast 270M, Silica Fumes, GGBS and CNT's were included in this mix proportion as per the predetermined optimum percentages subject to the required workability. 8% of Silica Fumes is replaced by weight of cement, 21.6% of GGBS as replaced by weight of cement, 0.125% of carbon nano tube (CNT) has been replaced by weight of cement, 900gm/cubic meter of volume of concrete of polypropylene fibres, 0.5% of volume of concrete of carbon fibers and 0.4% of Super plasticizer by weight of cement were included into the concrete mix in the present investigation.

Table 2: Mix proportions for different concrete matrices

Mix	cement	Fine aggregate	Coarse aggregate	w/b	water	Carbon fibre	Polypropylene fibre	Super plasticizer	GGBS	Silica fumes	CNT
Specimens	(kg/m³)	(kg/m³)	(kg/m³)		(kg/m³)	(kg/m³)	(kg/m³)	(litres/m³)	(kg/m³)	(kg/m³)	(litres/m³)
M60	450	477.69	1124.64	0.26	168.15	-	-	2.02	138.2	51.15	-
M60+CNT	450	477.69	1124.64	0.26	168.15	-	-	2.02	138.2	51.15	0.63
M60+CNT+ PF	450	477.69	1124.64	0.26	168.15	-	0.9	2.02	138.2	51.15	0.63
M60+CNT+ CF	450	477.69	1124.64	0.26	168.15	8.8	-	2.02	138.2	51.15	0.63
M60+CNT+ PF+CF	450	477.69	1124.64	0.26	168.15	8.8	0.9	2.02	138.2	51.15	0.63

4.0 METHODOLOGY OF TEST

The experimental test program includes the following tests as per German standard and ASTM specifications different concrete matrices.

4.1 Acid attack test: Acid attack test was carried out as per ASTM C 267-01 (2012) method, which consists of cube specimens of size 150 mm were casted and cured for 28 days. The initial weight of test specimens and compressive strength were taken. Then after 28 days of water curing again the test specimen subjected to extended curing by adding calculated amount of 5% of concentrated Sulphuric acid by weight to the curing water. After 56 days (28 days water curing+28 days acid solution) then specimens are taken out from acid solution and outer surfaces are cleaned properly. The final weight, visual appearance and compressive strength were determined. The resistance to acid attack is obtained from differences in weight and the compressive strength before and after the acid attack test.

4.2 Sulphate attack test: Sulphate attack test was carried out as per ASTM C 452-02 (2002) method, which consists of cube specimens of size 150 mm were casted and cured for 28 days. The initial weight of test specimens and compressive strength were taken. Then after 28 days of water curing again the test specimen subjected to extended curing by adding calculated amount of 5% of sodium sulphate by weight to the curing water. After 56 days (28 days water curing+28 days base solution) then specimens are taken out from base solution and outer surfaces are cleaned properly. The final weight, visual appearance and compressive strength were determined. The resistance to sulphate attack is obtained from differences in weight and the compressive strength before and after the sulphate attack test. Figure 1 shows specimens curing in 5% H_2SO_4 and 5% Na_2SO_4.

Figure 1: Specimens curing in 5% H_2SO_4 (acid attack test) and 5% Na_2SO_4(sulphate attack test)

4.3 Water absorption test: Water absorption test was conducted as per ASTM C 642 (2006) specifications. It employs a cube specimen of 100 mm size and cured for 28 days. Determine the mass of test specimen and dry in an oven at a temperature of

100^0 to 110^0 C for not less than 24 hours. After removing each test specimen from the oven, allow it to cool in dry air (preferably in desiccator) to a temperature of 20 to 25^0 C and determine the mass A. Determination of final surface dry mass B after immersion in water at approximately 21^0 C for not less than 48hours. Percentage of Water absorption =[(B-A)/A]x100.

5.0 RESULTS AND DISCUSSIONS

The experimental values obtained for Water permeability, acid attack test, sulphate attack and water absorption test in the present investigation are tabulated in following tables and corresponding graphs.

5.1 Results for Acid attack test

In the present experimental investigation, the Acid Attack test employs for a hardened concrete cube specimen (28 days cured in water) of 150 mm size were immersed in 5% of concentration Sulphuric Acid solution for a period of 28 days in acid solution. The result of final weight and compressive strength after 56 days of total immersion are tabulated in table no 3, 4 and figure 2, 3 and 4.

Figure 2: Compression test under progress after total immersion of 56 days

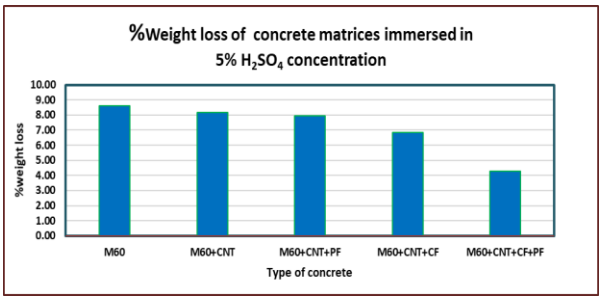

Figure 3: Percentage weight loss of test specimens after immersed in 5% H_2SO_4 solution

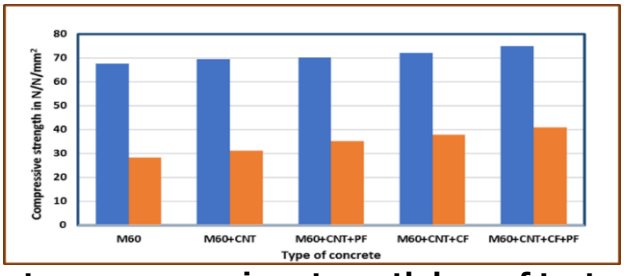

Figure 4: Percentage compressive strength loss of test specimens after immersed in 5% H_2SO_4 solution

figures 3 shows the % weight loss of different test specimens viz M-60, M-60+CNT, M-60+CNT+PF, M-60+CNT+CF, M60+CNT+PF+CF are 8.61%, 8.19%, 7.96%, 6.85% and 4.27% respectively**.** It is can be seen that the reduction in weight is lowest in case of M60+CNT+PF+CF test specimen as compared to other test specimens under consideration.

figures 4 shows the results of % loss in compressive strength of various test specimens after immersed in 5% H_2SO_4 for M-60, M-60+CNT, M60+CNT+PF, M60+CNT+CF, M60+CNT+PF+CF are 58.21%, 55.22%, 50.06%, 47.65% and 45.41% respectively**.** It is found that the reduction in compressive strength is lowest in case of M60+CNT+PF+CF test specimen as compared to other test specimens under consideration.

5.2 Results of Sulphate Attack Test

In the present experimental investigation, the sulphate Attack test employs a hardened concrete cube specimen of 150 mm size (28 days cured in water) and subsequently same test specimen was immersed in 5% of sodium sulphate solution for a period of 28 days in base solution. The results of final weight and compressive strength after 56 days of total immersion (water + base solution) are tabulated in table no 5 and 6 and figure 5, 6 and 7 respectively.

Figure 5: Compression test under progress

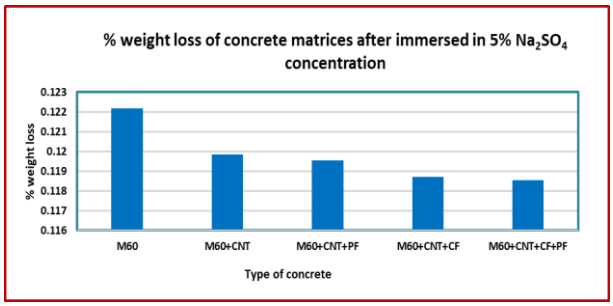

Figure 6: Percentage weight loss of concrete matrices after immersed in 5% Na_2SO_4 solution

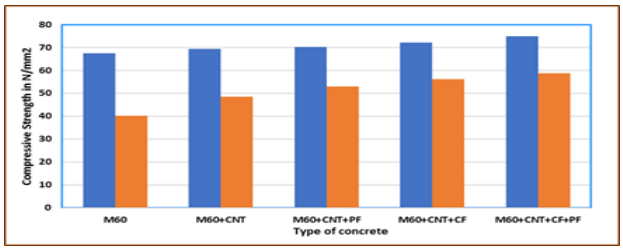

Figure 7: Compressive Strength before and after immersion in 5% Na_2SO_4 solution

Figure 6 shows the results of % weight loss due to sulphate attack on various test specimens viz: M-60, M-60+CNT, M-60+CNT+PF, M-60+CNT+CF, M60+CNT+PF+CF are 0.1222%, 0.1198%, 0.1195%, 0.1187% and 0.1186% respectively. It is can be seen that the reduction in weight is lowest for M60+CNT+PF+CF test specimen and followed by M-60, M-60+CNT, M-60+CNT+PF, M-60+CNT+CF.

Figures 7shows the results of % loss in compressive strength of various test specimens after immersed in 5% Na_2SO_4 for M-60, M-60+CNT, M-60+CNT+PF, M-60+CNT+CF, M60+CNT+PF+CF are 40.44%, 30.27%, 24.79% ,22.18% and 21.68 % respectively**.** From the experimental results it can be seen that reduction in compressive strength is lower in case of M60+CNT+PF+CF test specimens as compared to other test specimens under consideration.

5.3 Water absorption test

The Water absorption test for concrete employs a cube specimen of 100 mm size and cured for 28 days. The experimental obtained water absorption values for M-60, M-60+CNT, M-60+CNT+PF, M-60+CNT+CF, M-60+CNT+PF+CF test specimens are tabulated in Table 7.

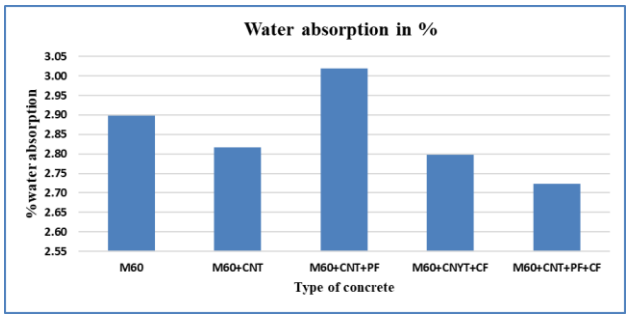

Figure 8: Water absorption of different concrete matrices

From Figure 8, the obtained water absorption values for M-60, M-60+CNT, M60+CNT+PF, M60+CNT+CF, M60+CNT+PF+CF test specimens are 2.90 %, 2.82 %, 3.02%, 2.80%, 2.72 % respectively. It can be seen that the variation in water absorption is from 2.72% to 3.02%. Whereas in case of M-60+CNT+PF+CF the % water absorption is least as compared to the other test specimens.

6.0 CONCLUSION

Based on the experimental investigation results the following conclusions are drawn.

(1) A number of variables can cause changes in the physical and durability properties of concrete. These include the composition of concrete mix, type of aggregate and their size and shape, admixtures and addition of fibers and other supplimentary reinforcing materials.
(2) For acid attack test, the percentage weight loss of M-60, M-60+CNT, M-60+CNT+PF, M-60+CNT+CF and M-60+CNT+CF+PF test specimens are 8.61%, 8.19%, 7.96%, 6.85% and 4.27% respectively. And percentage strength loss are 58.21%, 55.22%, 50.06%, 47.65% and 45.41% respectively. Percentage weight loss and strength loss are least in case of M60+CNT+PF+CF test specimen in comparison with other test specimens.

(3) For sulphate attack test, the percentage weight loss of test specimens viz: M-60, M-60+CNT, M-60+CNT+PF,M60+CNT+CF, M60+CNT+PF+CF are 0.1222%, 0.1198%, 0.1195%, 0.1187% and 0.1186% respectively. The percentage loss in compressive strength are 40.44%, 30.27%, 24.79%, 22.18% and 21.68 % respectively**.** Percentage reduction in weight and compressive strength is lower in case of M60+CNT+PF+CF test specimen as compared to other test specimens.

(4) The percentage of water absorption capacity for M-60, M-60+CNT, M-60+CNT+PF, M-60+CNT+CF, M-60+CNT+PF+CF are 2.90%, 2.82%, 3.02%, 2.80% and 2.72%. It can be seen that the variation in water absorption is from 2.72% to 3.02%. Whereas in case of M-60+CNT+PF+CF the % water absorption is least as compared to other test specimens.

7.0 REFERANCES

1. A. Jayaranjini and B. Vidivelli, "Durability properties of high Performance concrete using industrial byproducts", ARPN Journal of Engineering and Applied Sciences, VOL. 11, NO. 7, APRIL 2016.
2. ACI 211.4R-93 Method of mix design for high strength concrete.
3. ASTM C 267-01(2012), Specification for acid attack test.
4. ASTM C 452-02(2002), Specification for sulphate attack test.
5. ASTM C 642(2006), Specification for water absorption test.
6. B. Naresh Goud and K. Nagaraj, "Characteristics of High-Performance Concrete Using Metakaolin", International Journal of Innovative Research in Science, Engineering and Technology, Vol. 6, Issue 8, August 2017.
7. Biswajit Jena, Asha Patel, 2016. Study of the Mechanical properties and Microstructure of Chopped Carbon Fibre Reinforced Self-Compacting Concrete. International Journal of Civil Engineering and Technology, p. 223–232.
8. C. Vijayaprabha, D. brindha and a. Siva, "Durability performance of copper slag concrete admixed with polypropylene fiber", Journal of Structural Engineering Vol. 43, no. 6, february - March 2017.
9. Chitlange, M. R. Bang, R. S. Pajgade, P. S. "Strength appraisal of artificial sand as a fine aggregate in steel fibre reinforced concrete (SFRC)" ARPN Journal of Engineering and Applied sciences, vol 5, NO 10, October 2010, pp 34-38.
10. Dr. B. Vidivelli and T. Subbulakshmi, "Experimental Study on Durability Characteristics of High-Performance Concrete Incorporating with Silica Fume, Bottom Ash & Steel Slag Aggregate", The International Journal of Engineering and Science (IJES), Volume 5, Issue 6, June 2016.
11. Dr.Jadhao Pradip D, Shelorkar Ajay P, "Determination of durability of Metakaolin Blend High Grade Concrete by using Water Permeability Test", IOSR Journal of Mechanical and Civil Engineering (IOSR-JMCE) e-ISSN: 2278-1684 Volume 5, Issue 2 (Jan. - Feb. 2013).
12. Hawra Alradhawi, "Experimental Investigation of use Polypropylene Fibers in Self-Compacting Concrete", International Journal of Engineering Trends and Technology (IJETT) – Volume 57 Number 1 - March 2018.
13. I. B. Muhit, S. S. Ahmed, M. M. Amin and M. T. Raihan, "Effects of Silica Fume and Fly Ash as Partial Replacement of Cement on Water Permeability and Strength of High-Performance Concrete", Proc. of Int. Conf. on Advances in Civil Engineering, AETACE, April 2013.
14. IS: 456-2000 Code of practice for plain and reinforced concrete, bureau of Indian standards.
15. M Vijaya Sekhar Reddy, I V Ramana Reddy, K Madan Mohan Reddy and C M Ravi Kumar, "Durability aspects of standard concrete", International Journal of structural and civil engineering Research",2013.

9th International Engineering Symposium - IES 2020
March 3-5, 2020, Kumamoto University, Japan

BIOMEDICAL WASTE MANAGEMENT

PAVITHRA. S[1] and THARA S SHETTY[2]

1 *Formerly master course student, Department of P.G studies in Commerce, BESANT EVENING COLLEGE, MANGALURU 575003, India email: spavithra.rsb@gmail.com*

2 *Assistant Professor, Department of P.G studies in Commerce, BESANT EVENING COLLEGE, MANGALURU 575003, India*

INTRODUCTION

Medical care is vital for our life and health, but the waste generated from medical activities represents a real problem of living nature and human world. Improper management of waste generated in health care facilities causes a direct health impact on the community, the health care workers and on the environment Every day, relatively large amount of potentially infectious and hazardous waste are generated in the health care hospitals and facilities around the world. Indiscriminate disposal of Biomedical Waste Management (BMW) or hospital waste and exposure to such waste possess serious threat to environment and to human health that requires specific treatment and management prior to its final disposal.

Medical waste is unwanted biological products that are highly infectious in nature. It has to be disposed properly otherwise it poses a health and environmental danger. Medical waste is found in hospitals, laboratories, research centers, tattoo parlours, etc. Medical waste is broadly classified as infectious waste and bio-hazardous waste, and can easily spread any disease virally and can even pose a danger to life.

Biomedical waste is defined as the waste which is generated during the diagnosis, treatment or immunization of human beings or animals or in research activities pertaining thereto, or in the production of testing of biological. Biomedical waste consists of solids, liquids, sharps and laboratory waste that are potentially infectious or dangerous and are considered bio-waste. It must be properly managed to protect the general public, especially healthcare and sanitation workers who are regularly exposed to biomedical waste as an occupational hazard. Proper handling, treatment and disposal of biomedical waste are important elements of healthcare infection control programme.

Biomedical waste is distinct from normal trash or general waste, and differs from other types of hazardous waste, such as chemical, radioactive, universal or industrial waste. Medical facilities generate waste hazardous chemicals and radioactive materials. While such wastes are normally not infectious, they require proper disposal. Some wastes are considered multi-hazardous, such as tissue samples preserved in formalin.

The Government of India (notification, 1998) specifies that Hospital Waste Management is a part of hospital hygiene and maintenance activities. This involves management of range of activities, which are mainly engineering functions, such as collection, transportation, operation or treatment of processing systems, and disposal of wastes.

One of India's major achievements has been to change the attitudes of the operators of health care facilities to incorporate good Health Care Waste management practices in their daily operations and to purchase on-site waste management services from the private sector. (Bekir Onursal, 2003)

World Health Organization states that 85% of hospital wastes are actually non-hazardous, whereas 10% are infectious and 5% are non-infectious but they are included in hazardous wastes. About 15% to 35% of Hospital waste is regulated as infectious waste. This range is dependent on the total amount of waste generated (Glenn and Garwal, 1999).

Training constitutes a basic concept in human resource development. It is concerned with developing a particular skill to a desired standard by instruction and practice. Training is a highly useful tool that can bring an employee into a position where they can do their job correctly, effectively, and conscientiously. Training is the act of increasing the knowledge and skill of an employee for doing a particular job.

All hospital personnel, including senior medical doctors, should be convinced of the need for a comprehensive health-care waste management policy and the related training, and of its value for the health and safety of all. This should ensure their collaboration in the implementation of such a policy.

A policy for the management of health-care waste cannot be effective unless it is applied carefully, consistently, and universally. Training health-care personnel in implementing the policy is thus critical if a waste management programme is to be successful. The overall aim of training is to develop awareness of the health, safety, and environmental issues relating to health-care waste, and how these can affect employees in their daily work. It should highlight the roles and responsibilities of health-care personnel in the overall management programme. Health and safety at the workplace and environmental awareness are the responsibility of all and in the interests of all.

OBJECTIVES

- To study the need of proper Waste management system in hospitals.
- To study the working conditions and health related issues of the employees who are involved in waste management.
- To know about training patterns provided to the employees.
- To study the human resource required for waste management.
- To study how waste management personnel kept abreast of themselves about advances in Waste Management.
- To know about the new ways of scientific safe and cost effective waste management.
- To know the overall expenses incurred for waste management in the hospital.

NEED FOR THE STUDY

A lot has been said over the years regarding the health and hygiene in hospitals, but one thing that is over looked time and again is hospital-acquired infections. As such, one of the most important tools in hospital hygiene is hospital bins.
Hospital bins are a great source of dirt that gets accumulated over a period of time if not emptied timeously. They house a great deal of waste that can contain bacteria, which may further reduce the levels of hygiene in patients. They also contain bodily fluids and other waste products that, if stringent measures are not followed, will cause numerous problems for staff and patients.

The management of medical waste in hospitals poses a major health problem, inviting serious health implications. When visiting health care facilities, patients should not become more ill than they already are, hence it is vitally important to ensure patient safety by keeping the health centre clean and environmentally sound. Waste collection service providers also have to be looked at meticulously. Due to all such problems it is found necessary to carry on the study on waste management system.

RESEARCH DESIGN

It is a descriptive research. The study is based on both primary data and secondary data. The major sources of information were primary a comprehensive questionnaire was first designed so as to obtain relevant and precise information regarding working condition and health related issues of the employees. The collected data has been analyzed with the help of various statistical tools. Suggestions were given at the end on the basis of findings made. Secondary data was collected from various Journals, books and websites.

I. DESIGN IMPLIMENTATION

Serial No: Age:
Gender: Marital status:
Qualification: Years of experience:

1) Does the hospital have a waste management committee?
   a) Yes b) No

2) Is the segregation done as per biomedical waste rules?
   a) Yes b) No

3) Is the training given on health related issues for the employees?
   a) Yes b) No

4) Are proper protective devices used by waste handlers?
   a) Yes b) No

5) The commonist problem of the employee include
   a) Back ache b) Leg pain c) Head ache d)Hand pain

6) In case of needle stick injury what is the first type of approach
   a) Wash the hand in running water b) Squeeze c) Ignore d) Suck the finger

7) Which of the following is not a Personal Protection Equipment?
   a) Glove b) Facemask c) Boots d) Soap

8) Do you have waste management team or strategy monitoring and supervising waste management plans being followed?
   a) Yes b) No
9) Is there any segregation procedure at the point of generation of waste or before disposal?
   a) Yes b) No
10) Is the collected waste stored differently and out of the hospital campus?
   a) Yes b) No

11) Where is the medical waste treated?
   a) Onsite b) Offsite

12) On what basis does the hospital dispose bio medical waste?
   a) Daily b) Alternate days c) Weekly

13) Does the hospital dis- infect bio medical waste like plastic, rubber items, sharps before it is sent for final disposal?
   a) Yes b) No

14) Did you or any of the staff injure while handling bio medical waste?
   a) Yes b) No

15) Do you think that the present system of sharps management is easy and safe?
   a) Yes b) No

If No why _____

16) Where is the segregated waste kept for disposal?
   a) In coloured plastic with bar code and labels
   b) In cans with bar code and labels
   c) In coloured bags/ containers with bar codes and labels

II. CONCEPTUAL FRAMEWORK

The biomedical waste (BMW) management requires its categorization as a first step. The BMW Rules classify the BMW into following categories.

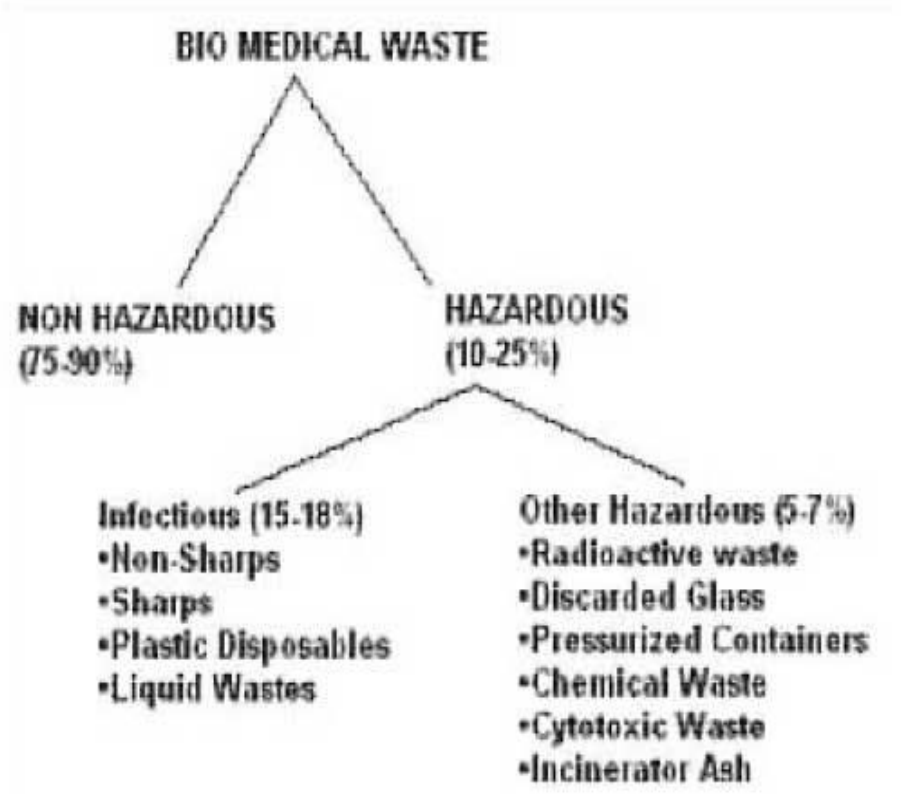

Fig. 1

Biomedical wastes categories and their segregation, collection, treatment; processing and disposal options are shown below:

CATEGORIES OF BIOMEDICAL WASTE SCHEDULE – I			
CATEGORY	**TYPE OF WASTE**	**TYPE OF BAG OR CONTAINER TO BE USED**	**TREATMENT AND DISPOSAL OPTION**
Yellow	Human tissues, organs, body parts and fetus below the viability period (as per the Medical Termination of Pregnancy Act 1971, amended from time to time).	Yellow coloured non-chlorinated plastic bags	Incineration or Plasma Pyrolysis or deep burial*
	Animal Anatomical Waste : Experimental animal carcasses, body parts, organs, tissues, including the waste generated from animals used in experiments or testing in veterinary hospitals or colleges or animal houses.		
	Soiled Waste: Items contaminated with blood, body fluids like dressings, plaster casts, cotton swabs and bags containing residual or discarded blood and blood components.		Incineration or Plasma Pyrolysis or deep burial* In absence of above facilities, autoclaving or micro-waving/ hydroclaving followed by shredding or mutilation or combination of sterilization and shredding. Treated waste to be sent for energy recovery.
	Expired or Discarded Medicines: Pharmaceutical waste like antibiotics, cytotoxic drugs including all items contaminated with cytotoxic drugs along with glass or plastic ampoules, vials etc.	Yellow coloured non-chlorinated plastic bags or containers	Expired cytotoxic drugs and items contaminated with cytotoxic drugs to be returned back to the manufacturer or supplier for incineration at temperature >1200 ^{0} C or to common bio - medical waste treatment facility or hazardous waste treatment, storage and disposal facility for incineration at >1200 ^{0} C Or Encapsulation or Plasma Pyrolysis at >1200 ^{0} C All other discarded medicines shall be either sent back to manufacturer or disposed by incineration.

	Chemical Waste: Chemicals used in production of biological and used or discarded disinfectants.	Yellow coloured containers or non-chlorinated plastic bags	Disposed of by incineration or Plasma Pyrolysis or Encapsulation in hazardous waste treatment, storage and disposal facility.
	Chemical Liquid Waste : Liquid waste generated due to use of chemicals in production of biological and used or discarded disinfectants, Silver X - ray film developing liquid, discarded Formalin, infected secretions, aspirated body fluids , liquid from laboratories an d floor washings, cleaning, house - keeping and disinfecting activities etc.	Separate collection system leading to effluent treatment system	After resource recovery, the chemical liquid waste shall be pre - treated before mixing with other wastewater. The combined discharge shall conform to the discharge norms given in Schedule - III.
	Discarded linen, mattresses, beddings contaminated with blood or body fluid.	Non-chlorinated yellow plastic bags or suitable packing material	Non - chlorinated chemical disinfection followed by incineration or Plasma Pyrolysis or for energy recovery. In absence of above facilities, shredding or mutilation or combination of sterilization and shredding. Treated waste to be sent for energy recovery or incineration or Plasma Pyrolysis.
	Microbiology, Biotechnology and other clinical laboratory waste: Blood bags, Laboratory cultures, stocks or specimens of micro - organisms, live or attenuated vaccines, human and animal cell cultures used in research, industrial laboratories, production of biological, residual toxins, dishes and devices used for cultures.	Autoclave safe plastic bags or containers	Pre - treat to sterilize with non - chlorinated chemicals on - site as per National AIDS Control Organization or World Health Organization guidelines thereafter for Incineration.
Red	Contaminated Waste (Recyclable) or wastes generated from disposable items such as tubing, bottles, intravenous tubes and sets, catheters, urine bags, syringes (without needles and fixed	Red coloured non-chlorinated plastic bags or containers	Autoclaving or micro - waving/ hydroclaving followed by shredding or mutilation or combination of sterilization and shredding. Treated waste to be sent to registered or authorized recyclers or for energy recovery or

	needle syringes) and vaccutainers with their needles cut) and gloves.		plastics to diesel or fuel oil or for road making, whichever is possible. Plastic waste should not be sent to landfill sites.
White (Translucent)	**Waste sharps including Metals**: Needles, syringes with fixed needles, needles from needle tip cutter or burner, scalpels, blades, or any other contaminated sharp object that may cause puncture and cuts. This includes both used, discarded and contaminated metal sharps	Puncture proof, Leak proof, tamper proof containers	Autoclaving or Dry Heat Sterilization followed by shredding or mutilation or encapsulation in metal container or cement concrete; combination of shredding cum autoclaving; and sent for final disposal to iron foundries (having consent to operate from the State Pollution Control Board s or Pollution Control Committee s) or sanitary landfill or designated concrete waste sharp pit.
Blue	**Glassware:** Broken or discarded and contaminated glass including medicine vials and ampoules except those contaminated with cytotoxic wastes Metallic Body Implants	Cardboard boxes with blue colored marking	Disinfection (by soaking the washed glass waste after cleaning with detergent and Sodium Hypochlorite treatment) or through autoclaving or microwaving or hydroclaving and then sent for recycling.

* Disposal by deep burial is permitted only in rural or remote areas where there is no access to common bio - medical waste treatment facility. This will be carried out with prior approval from the prescribed authority and as per the Standards specified in Schedule - III. The deep burial facility shall be located as per the provisions and guidelines issued by Central Pollution Control Board from time to time.

SCHEDULE IV

Part A

LABEL FOR BIO-MEDICAL WASTE CONTAINERS or BAGS

BIOHAZARD SYMBOL

CYTOTOXIC HAZARDSYMBOL

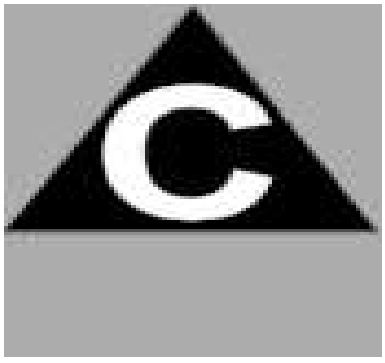

Part B

LABEL FOR TRANSPORTING BIO-MEDICAL WASTE BAGS OR CONTAINERS

Day.....

. Month.....

Year.....

Date of generation.....

Waste category Number.....

Waste quantity……

Sender's Name and Address Receiver's Name and Address:

Phone Number.....

Fax Number.....

Contact Person.....

Receiver's Name and Address:

Phone Number.....

Fax Number.....

Contact Person.....

In case of emergency please contact:

Name and Address:

Phone Number.....

Note: Label shall be non-washable and prominently visible.

III. SUMMARY OF FINDINGS

Findings of the study based on survey data are as follows:

- It is observed that majority that is 84% of the respondents were female and 16% were male respondents.
- In the study, majority that is 34% of the respondents were belonging to the age group of 40-50 years and only 3% belonged to the age group less than 20years.
- It is very clear that majority that is 54% of the respondents are just high school passed and 9% are uneducated.
- In the study it is observed that majority that is 80% of the respondents are married and 20% are unmarried.
- It is observed that majority that is 73% of the respondents are experienced between 0-20 years and 27% between 20-40years.
- It is found that there is a waste management committee in the hospital and majority that is 99% of the respondents are aware it.
- It is very clear that all respondents are aware that waste is segregated as per biomedical waste rules. They are also aware that they are given training on health related issues. And also given with proper Personal Protective Equipments.

- Majority that is 39% of the respondents undergo back ache due to work and 3% respondents undergo head ache and hand pain.
- Majority that is 89% of the respondents of them are aware that the first approach towards needle stick injury is to wash hands in the running water.
- Majority that is 92% of the respondents of them are aware that soap is not a Personal Protective Equipment.
- It is observed that all respondents follow waste management team or strategy monitoring and supervising waste management plans.
- Majority that is 96% of the respondents are aware that waste is segregated at the point of generation.
- It is observed that all the respondents are aware that the waste is stored separately in the hospital campus.
- Majority that is 99% of the respondents of them are aware that waste treated offsite and not onsite.
- It very clear from the respondents that the hospital disposes the waste every day.
- Majority that is 97% of the respondents of them are aware those hazardous wastes like sharps is disinfected before disposal.
- Majority that is 86% of the respondents of them have not been injured while handling biomedical waste.
- It is clear that all respondents are happy with the present system of handling sharps and also it is observed that all the respondents take the waste for disposal in coloured containers with bar code and label.
- The overall expense incurred in waste management is Rs. 1440000 per year.
- It is also observed that human resource of various levels is also indulged in biomedical waste management.
- It is found that 133 Nursing staffs, 22 Technicians and 45 General workers are already trained.
- It is found that new ways of scientific, safe and cost effective waste management system is followed in hospital that is by eradicating white bins and introducing cans for disposal of needles.

IV. CONCLUSION AND SCOPE FOR FUTURE DIRECTIONS

Medical wastes should be classified according to their source, typology and risk factors associated with their handling, storage and ultimate disposal. The segregation of waste at source is the key step and reduction, reuse and recycling should be considered in proper perspectives. We need to consider innovative and radical measures to clean up the distressing picture of lack of civic concern on the part of hospitals and slackness in government implementation of bare minimum of rules, as waste generation particularly biomedical waste imposes increasing direct and indirect costs on society. The challenge before us, therefore, is to scientifically manage growing quantities of biomedical waste that go beyond past practices. If we want to protect our environment and health of community we must sensitize ourselves to this important issue not only in the interest of health managers but also in the interest of community.

The findings of this study suggest that a training programme increases the knowledge as well as the sense of responsibility resulting in change in attitude and practices. Budget support, allocation of resources and technical guidance is required to implement an effective and sustainable hospital waste management system. Hence all the biomedical waste carrying personnel should be trained and properly supervised, thus helping in the efficiency of waste segregation.

REFERENCES

[1] www.rguhs.ac.in/cdc/onlinecdc/uploads/05_N036_23739.doc

[2] http://www.infrastructurene.ws/2012/07/12/the-importance-of-medical-waste-bins-in-hospitals/

[3] http://vikaspedia.in/energy/environment/waste-management/bio-medical-waste-management/what-is-bio-medical-waste

[4] http://www.cwejournal.org/vol7no1/need-of-biomedical-waste-management-system-in-hospitals-an-emerging-issue-a-review/

[5] https://www.cabdirect.org/cabdirect/abstract/20143055911

[6] www.iwma.in/BMW%20Rules,%202016.pdf

[7] www.who.int/water_sanitation_health/medicalwaste/159to166.pdf

[8] http://www.yourarticlelibrary.com

[9] www.rguhs.ac.in/cdc/onlinecdc/uploads/05_N036_23739.doc

[10] http://www.infrastructurene.ws/2012/07/12/the-importance-of-medical-waste-bins-in-hospitals/

[11] http://vikaspedia.in/energy/environment/waste-management/bio-medical-waste-management/what-is-bio-medical-waste

[12] http://www.cwejournal.org/vol7no1/need-of-biomedical-waste-management-system-in-hospitals-an-emerging-issue-a-review/

[13] https://www.cabdirect.org/cabdirect/abstract/20143055911